THE ELASTIC BEHAVIOR OF A BALANCED FOUR-BAR LINKAGE WITH AN OVERHANGING ROCKER: THEORY AND EXPERIMENT

by

WALTER G. JANDRASITS

A dissertation submitted to the Graduate Faculty in Engineering in partial fulfillment of the requirements for the degree of Doctor of Philosophy, The City University of New York.

1975

This manuscript has been read and accepted for the Graduate Faculty in Engineering in satisfaction of the dissertation requirement for the degree of Doctor of Philosphy.

1/23/75
date

Gerard G. Lowen
Chairman of Examining Committee

1/29/75
date

Jacques E. Beweniste
Executive Officer

Prof. G. G. Lowen (Chairman)

Prof. C. B. Anderson

Prof. S. B. Menkes

Prof. C. M. Tchen

Supervisory Committee

The City University of New York

ACKNOWLEDGEMENTS

First and foremost, I wish to express my deep appreciation to my advisor, Professor Gerard G. Lowen. I am truly indebted to him for his guidance, inspiration, encouragement and assistance throughout the course of my work and the preparation of this dissertation. His enthusiasum and boundless energy were significant factors in making this research possible.

I would also like to thank the members of my guidance committee, as well as Professors F. R. E. Crossley and Ming L. Pei, who served as examiners, for their interest. In addition, I am indebted to the staff of the City College Computation Center for their cooperation and for the extensive use of their facilities.

The financial support received from a City College Teaching Fellowship, a NASA Traineeship and a City University Dissertation Fellowship is gratefully acknowledged.

Finally, I owe a very special debt of gratitude to my wife, Gail, and my daughter, Lisa Ann, whose great love, understanding, encouragement and help made this work possible.

TABLE OF CONTENTS

NOMENCLATURE

A_j = cross-sectional area of j-th link

$A(\varphi_1)$ = periodic function in $B(\varphi_1)$

$\mathcal{A}$ = coefficient in characterisitc equation

a_j = pivot-to-pivot dimension of j-th link

$B(\varphi_1)$ = periodic coefficient in Hill's equation

b, b_3 = pivot-to-endmass dimension of arbitrary link and link 3, respectively

b_0, b_{cn}, b_{sn} = Fourier coefficients of $B(\varphi_1)$

C_i = i-th constant containing mechanism parameters

C_{D2m}, C_{D3m} = viscous damping coefficients for links 2 and 3, respectively

$D_i(x,t)$ = i-th coefficient in partial differential equation of motion for coupler link

d = pivot-to-counterweight dimension of arbitrary link

E_j = modulus of elasticity of j-th link

$F_m(t)$, $\hat{F}_m(\varphi_1)$, $\mathcal{F}(\varphi_1)$ = forcing functions of Hill's equations

f_0, f_{cn}, f_{sn} = Fourier coefficients of forcing function in Hill's equation

f_i = i-th constraint equation

$G_i(x,t)$ = i-th coefficient in partial differential equation of motion for rocker link

$H_{mn}(t)$, $\hat{H}_{mn}(\varphi_1)$ = periodic coefficients in Hill's equation

I_j = area moment of inertia of cross-section of j-th link

J_{2c} = mass moment of inertia of link 2 about its center of mass

J_{3D} = mass moment of inertia of link 3 with respect to pivot D

J_M = mass moment of inertia of endmass about its center of mass

J_{m^*} = mass moment of inertia of counterweight about its center of mass

L = total length of rocker link

M_2 = total mass of link 2

M = mass of endmass

m^* = mass of counterweight

p_0, p_{cn}, p_{sn} = Fourier coefficients of particular solution of Hill's equation

$\ddot{R}_{xj}$, $\ddot{R}_{yj}$ = x and y components of acceleration of a point on centroidal locus of j-th link, respectively

$\bar{r}_p$ = position vector to an arbitrary point P on a link

r_M = distance to center of mass of endmass from end of overhang

r^* = radius of counterweight

T = total kinetic energy of the mechanism

T_e = kinetic energy of arbitrary elastic link

U = strain energy of an arbitrary link

u_j = foreshortening of j-th link

V_n = shape function of link associated with n-th mode

γ_m = value of orthogonality condition

v_j = transverse deflection of j-th link

x_j, y_j, z_j = body-fixed coordinates of j-th link

$\ddot{\alpha}_j$, $\ddot{\beta}_j$ = x and y components of acceleration of a point on x_j-axis, respectively

β_n = n-th complex Fourier coefficient in expansion of $B(\varphi_1)$

Δ = damping parameter

δ = variational operator

ϵ = maximum transverse bending strain

$\Phi(\varphi_1)$ = 2π-periodic function associated with Floquet solution

φ_j = angular position of j-th link taken with respect to ground when mechanism has rigid links

φ_{ej} = angular position of x_j-axis on j-th link taken with respect to ground when mechanism has elastic links

Λ = ratio of natural frequency of link to input speed, squared

λ_i, λ_n = i-th Lagrange multiplier; n-th eigenvalue, respectively

μ_j, μ = mass per unit length of j-th link; characteristic exponent, respectively

ω_m = m-th natural frequency of rocker link

Π = total potential energy of the mechanism

ρ_j, ρ = mass density of j-th link; root of characteristic equation, respectively

ξ = dummy variable for x

ζ = damping ratio

ABSTRACT

The theoretical and experimental transverse vibrational behavior of the elastic rocker link of a four-bar linkage is presented. The rocker link contains a counterweight and its overhanging portion carries an endmass, while the crank and coupler links are assumed to be rigid.

The partial differential equations of motion for the elastic link are derived by a systems' approach utilizing Hamilton's principle with auxiliary conditions. This technique makes it unnecessary to treat each link, and the pin forces acting on it, separately during analysis.

The solution for the deflections is based on the method of Kantorovich. The space portion of this solution consists of a prescribed set of shape functions, derived from the free vibration problem associated with the rocker link, which satisfy the geometric boundary conditions. The remaining time portion of the solution is obtained from nonhomogeneous Hill-type differential equations. The analysis of these Hill's equations furnishes stability criteria as well as the resonance conditions for the link. Also, it is shown that for the particular shape function assumed, three modes of the solution form are necessary in order to sufficiently describe the strain response of the link. The particular solution is used to show that the response at the resonance locations differs dramatically from that away from resonance, and it is found that this difference disappears with sufficient damping. This finding may be useful in controlling noise and fatigue.

The theory is applied to a specific mechanism and the numerical results are compared to those of a corresponding experiment. The experiment confirmed both the qualitative as well as the quantitative findings of the theoretical analysis.

LIST OF TABLES

LIST OF FIGURES

LIST OF FIGURES

LIST OF FIGURES

I. INTRODUCTION

With the demand for ever increasing productivity it has become clear that rigid body analysis of machines may become insufficient for the full prediction of their performance. The elastic deformations of the machine components, which are due to increases in speeds and loads, cause inaccuracies of position in addition to fatigue failures and noise, and thus sharply limit the potential of the machines involved.

The main thrust of the present work is the analytical and experimental investigation of the response of the elastic rocker link of the four-bar linkage shown in Figure 1.1. (The crank and coupler links are assumed to be rigid.) The rocker link contains a counterweight and the overhanging portion carries an endmass. This particular configuration was chosen because a biological shaker mechanism [25](*) of similar construction has been known to fail at relatively low speeds.

The first part of this dissertation shows a novel systems' approach for the derivation of the differential equations and the associated natural boundary conditions for several links of an elastic mechanism. This is accomplished with the help of Hamilton's principle with auxiliary conditions. These auxiliary conditions, which describe the foreshortening of the links as well as the changes in the mechanism angles due to

---

(*) Numbers in brackets designate references at the end of the dissertation.

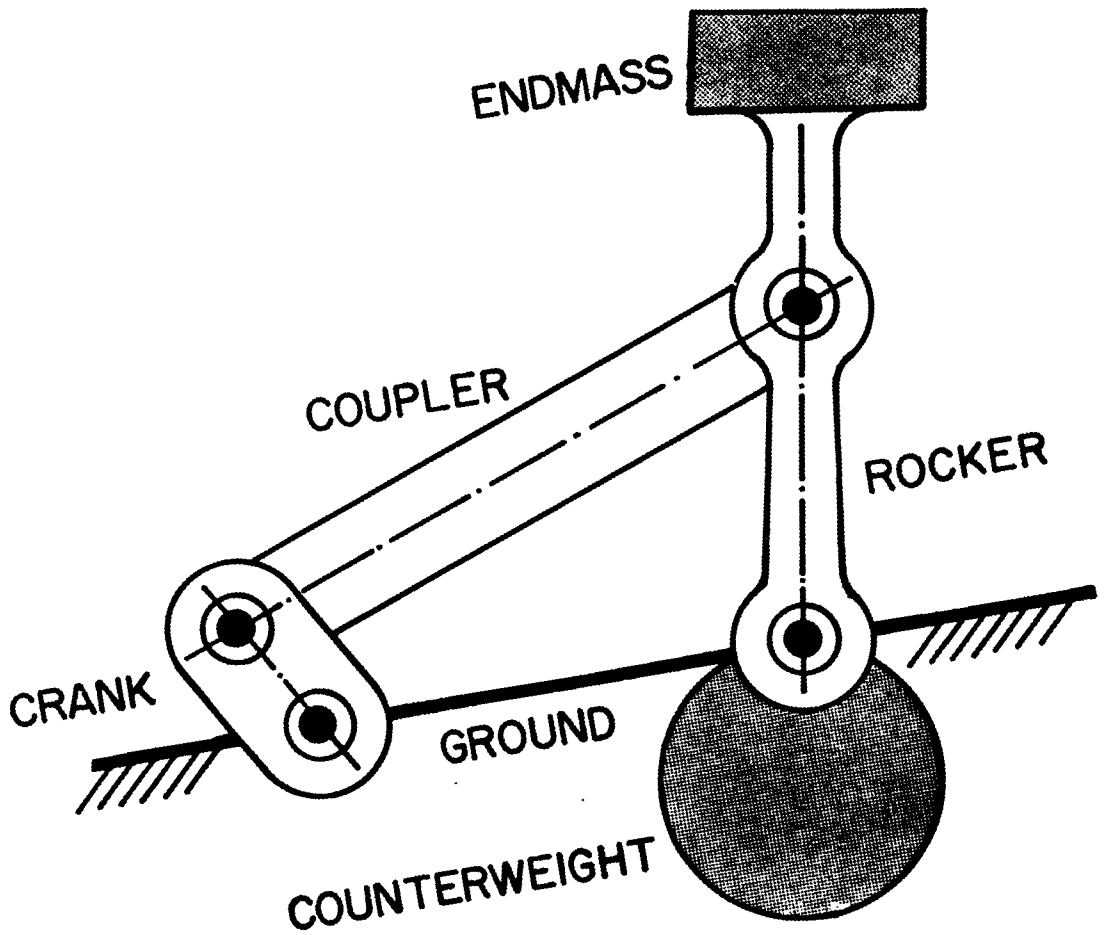

FIGURE I.I: MECHANISM WITH COUNTERWEIGHT AND ENDMASS

this foreshortening, may be incorporated into the variational integral either with the help of Lagrange multipliers or by direct substitution. Both of these approaches makes it unnecessary to treat each link as a free body. Secondly, the general derivations are reduced to the case of the elastic rocker above, and the now linearized partial differential equations are solved with the aid of the method of Kantorovich. The space portions of this solution are an assumed set of shape functions satisfying the geometric boundary conditions, while the remaining time portions are solutions of nonhomgeneous Hill-type differential equations. The analysis of these Hill's equations furnishes the mechanism input speeds for which the deflections of the link may become unstable as well as those speeds for which resonant vibrations occur. With the partcular shape function chosen, it was found that several modes of the total solution form are necessary to fully describe the response.

Finally, an experiment confirmed the responses predicted by the theoretical analysis. The generally excellent agreement between theory and experiment assures the usefulness of the chosen analytical approach.

The present state of the art in the field of elastic mechanism behavior is discussed below. Section II gives a more detailed outline of this investigation and summarizes its results.

Background

The state of the art of the dynamic behavior of mechanisms containing links with distributed mass and elasticity, as of 1971, was reviewed by G. G. Lowen and the present author [21], as well as A. G. Erdman and G. N. Sandor [11]. Since that time, additional contributions were made by the following researchers:

R. C. Winfrey [33] combined kinematic analysis with the structural dynamics stiffness technique to determine the response of a mechanism with elastic links.

Using a mathematical model based on the stiffness method, R. M. Alexander and K. L. Lawrence [1,2,3] compared numerical strain values for a four-bar linkage with experimentally determined ones.

Several investigators have extended the flexibility method of Structural Mechanics for the analysis and synthesis of the motion of mechanisms with elastic links. Amongst these are: A. G. Erdman, G. N. Sandor and R. G. Oakberg [10], I. Imam, G. N. Sandor and S. N. Kramer [15], I. Imam and G. N. Sandor [16,17], as well as J. Chakraborty and A. K. Khare [7].

J. P. Sadler and G. N. Sandor [27,28] employed lumped parameter models for simulating the elastic links of a mechanism. Further, J. P. Sadler [29] compared the results of this method for a four-bar linkage with the experimental data previously obtained by R. M. Alexander and K. L. Lawrence [1,2,3].

S. C. Chu and K. C. Pan [8] investigated the nonlinear longitudinal and transverse vibrations of the connecting rod of a slider-crank mechanism.

II. OUTLINE OF INVESTIGATION AND SUMMARY OF RESULTS

The following outlines the analytical as well as the experimental portions of this investigation, and gives a summary of the principal conclusions which may be formed.

A. Theory

1. Differential Equations of Motion

The theoretical portion of this work begins with the derivation of the equations of motion for the elastic rocker and coupler links of the mechanism shown in Figure 2.1. There are overhangs at both ends of the rocker, which carry a counterweight and endmass respectively. The rigid crank is subject to a time dependent angular velocity and the damping mechanism in the elastic links is assumed to be viscous.

The partial differential equations of motion for both elastic links are derived by a systems' approach which is believed to be novel as applied to an elastic mechanism problem. It starts from Hamilton's integral(*) with auxiliary conditions, and makes it unnecessary to treat each link, and the forces acting on it, separately during analysis. Some of these auxiliary conditions describe the foreshortening of the link portions due to bending, while the remaining ones are elastic mechanism loop equations which describe the changes in mechanism angles due to the above foreshortening. The constraint equations are

---

(*) The allowable elastic deformations are those associated with the Euler-Bernoulli theory.

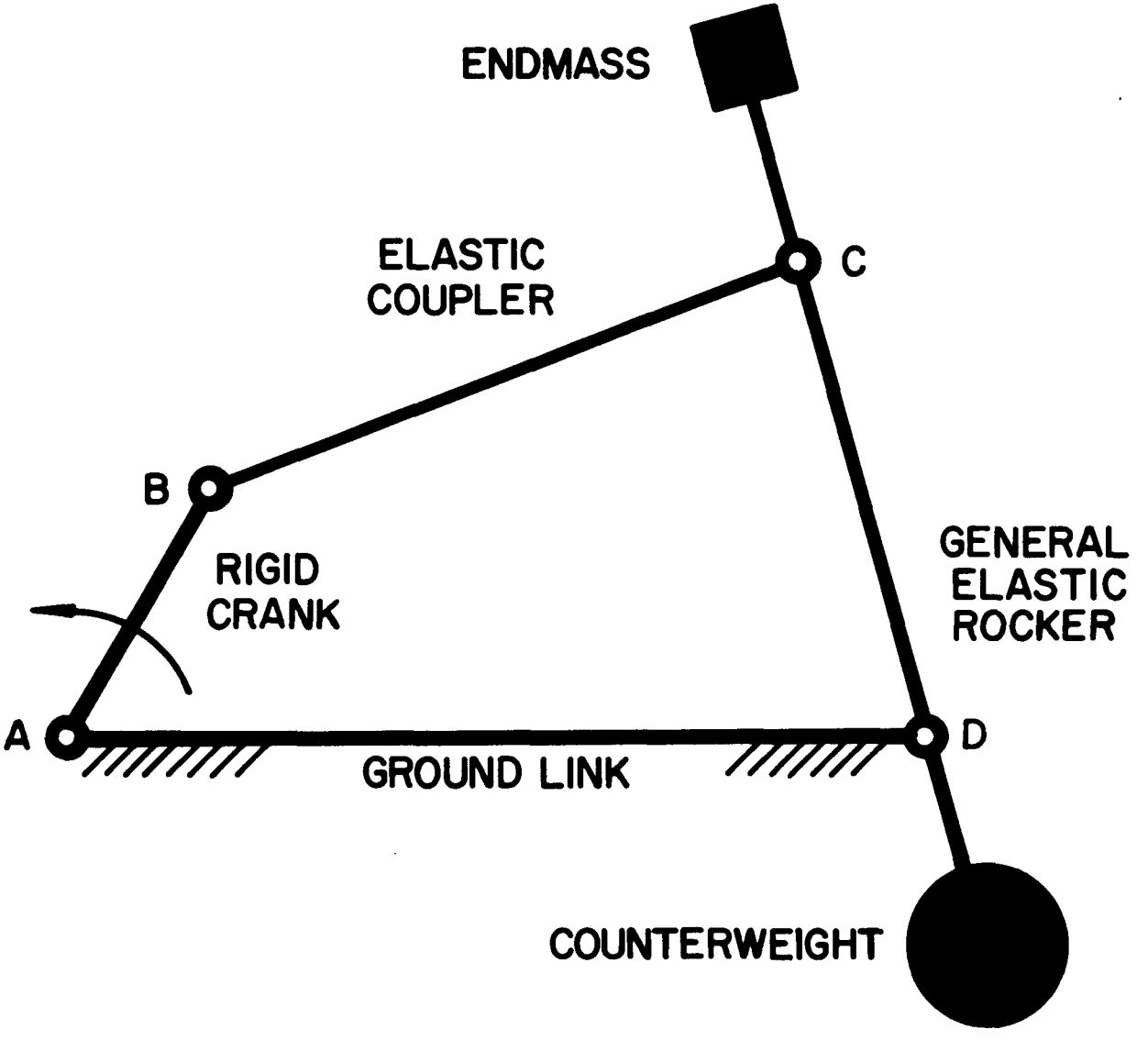

FIGURE 2.1: MECHANISM WITH ELASTIC COUPLER AND ROCKER LINKS

incorporated into Hamilton's integral by way of the method of Lagrange multipliers.

The machinery of the Calculus of Variations furnishes the partial integro-differential equations for each link together with the associated dynamic boundary conditions as well as expressions for the Lagrange multipliers.

The subsequent linearization and replacement of the elastic angles by their rigid body counterparts, which furnish more tractable expressions, are well justified by the experiment performed on a somewhat simplified rocker configuration. It is of interest to note that the linearized equations of motion of the two links are only "parametrically coupled". This means that the expressions associated with each link contain only the parameters of the other link, but not its deflection. This work may be found in Section III, with much of the background material done in Appendices A, B and C.

2. Response of Elastic Rocker Link with Overhang, Endmass and Counterweight

The principal topic of this dissertation is the analysis of the elastic rocker link of the mechanism shown in Figure 2.2. Here the counterweight of the rocker is tangent to pivot D and the coupler is considered rigid. Again, the crank is also rigid but is now driven with constant input angular velocity. Section IV deals with this portion of the effort and is supported by Appendices D to I.

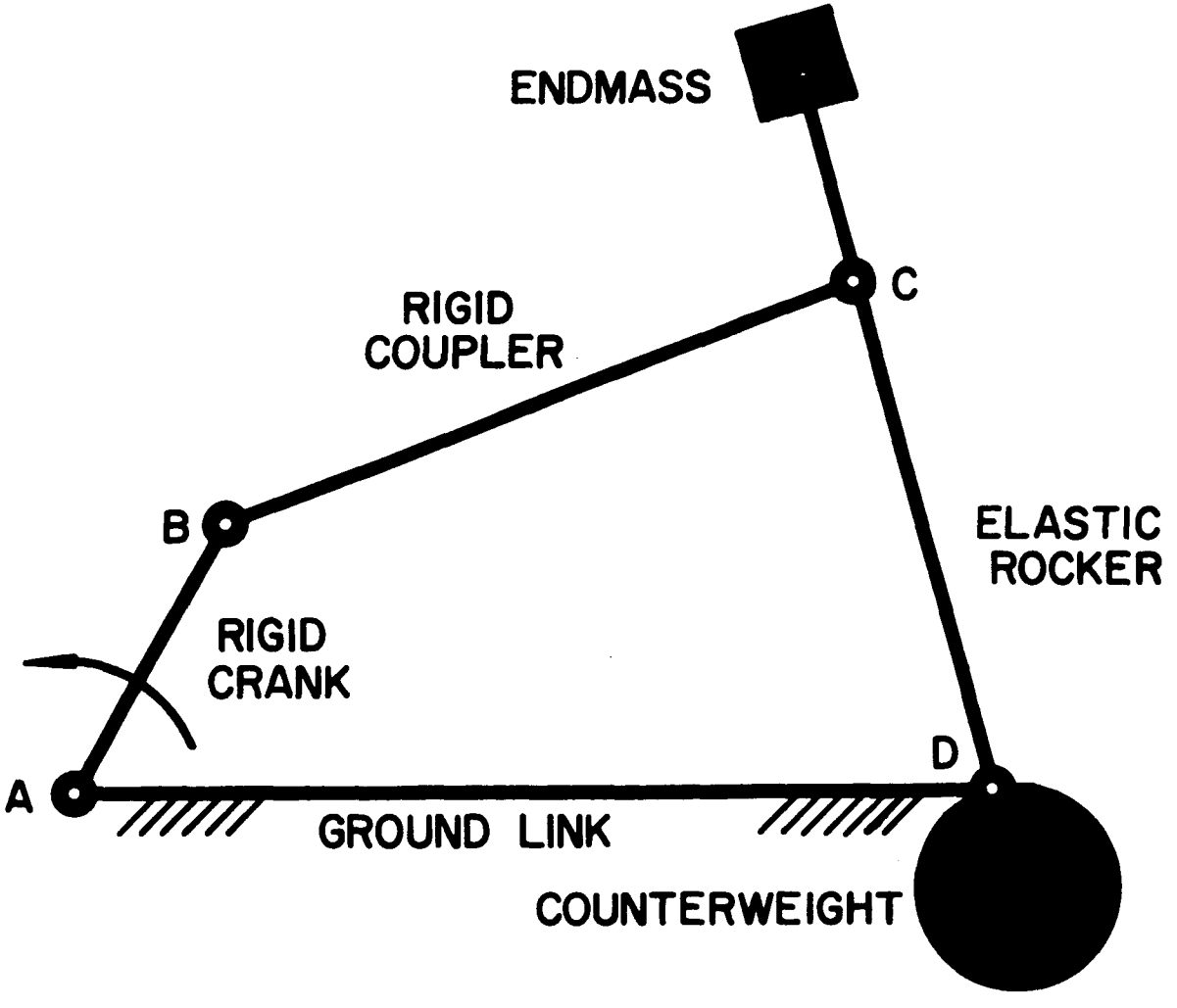

FIGURE 2.2: SHAKER MECHANISM WITH ELASTIC ROCKER LINK

While the differential equations of motion for the rocker link only can be obtained by the appropriate reduction of the results of Section III, an alternate derivation is also given. It again uses a systems' approach without the need for free body diagrams. The variations of the constraint equations are now incorporated by direct substitution, rather than by the method of Lagrange multipliers. The process of linearization and replacement of elastic angles is identical to that of Section III.

The solution of the problem is based on the method of Kantorovich. This requires the assumption of a solution form which is represented by an infinite series of space-time function products, where the space or shape function components must represent a complete set of functions which should satisfy the geometric boundary conditions.(*)

The resulting solution form is substituted into the variational integral associated with the linearized and simplified partial differential equation. This leads to an infinite set of coupled, nonhomogeneous Hill-type differential equations in the time portion of the solution.

For use in subsequent analysis, the theory associated with the solution of homogeneous and nonhomogeneous Hill's equations is reviewed.

(*) The shape function (subproblem) used here is that resulting from the associated free vibration problem.

The multitude of physical parameters present makes it impossible to present the solution in non-dimensional form.

B. Example and Confirming Experiment

The theory developed in Section IV is applied to a specific mechanism in Section V and the numerical results are compared to those of a corresponding experiment. All comparisons are made in terms of strain.

The example mechanism was designed in such a way that sufficiently large strains could be obtained at relatively low input rpm. (The strains are compared at the midpoints of the rocker and the overhang.)

The numerical portion of the example considers the following:

1. A numerical solution of the coupled Hill's equations by way of a fourth order Runge-Kutta technique indicates that for the chosen shape function, at least three modes of the solution form are required for an adequate description of the response.(*) It is further shown that the results are not influenced to any degree when the equations are uncoupled and solved separately.

2. The influence of the initial conditions on the transient response is examined for certain on and off-resonance conditions. The results of this portion of the investigation form the basis for the conclusion that the response in the experiment can be fully described by the particular solution.

(*) It is not known how many modes other possible shape functions would have required for a good description of the response.

3. A stability analysis is performed and it is shown that within the operating range of the mechanism, and beyond, there are neither 2π nor 4π-periodic instabilities as long as the damping ratio is larger than zero.

The stability analysis also furnishes the resonance locations, which are associated with the 2π-periodic instability points of the undamped system.

4. The particular solution is determined for the three modes necessary, and it is shown that, for sufficiently small values of the damping ratio ζ, the response at the resonance locations differs dramatically from that for locations off resonance. Further, it became clear that this difference in response disappears for values of the damping ratio ζ larger than approximately 0.034. This finding should be most useful towards the better control of fatigue and noise.

The experimental mechanism was operated between 110 and 200 rpm, and the following conclusions can be reported:

1. The strain throughout the operating range never grows without bound, and therefore there are no 2π or 4π-periodic instabilities. This confirms the results of the stability analysis. Further, even though one could observe some bearing impacts, all transient phenomena are of exceedingly small magnitude. Thus, the particular solution furnishes a very good description of the response.

2. The dramatic difference between on-resonance and off-resonance response found in the analysis is confirmed by the experiment.

The amplification of the higher harmonics of the first mode response, corresponding to the associated 2π-periodic instability boundaries, was clearly observable at the predicted input speeds.

3. A quantitative comparison between the experimental and numerical results indicates good agreement on and off-resonance.

C. Discussion of Results

Section VI discusses the results of this investigation and attempts to put analytical and experimental results into the proper focus.

III. DERIVATION OF EQUATIONS OF MOTION FOR MECHANISM CONTAINING TWO ELASTIC LINKS

This section gives the derivation of the linearized partial differential equations and boundary conditions which describe the elastic behavior of a four-bar linkage consisting of an elastic coupler and rocker (see Figure 3.1). The rocker contains two overhangs as well as an endmass and a counterweight.

The derivation starts, in Section A, from Hamilton's principle with auxiliary conditions, where the auxiliary conditions have their origin both in the elastic loop equation of the mechanism as well as in the elastic constraints of the individual links. Sections B, C and D define the kinetic and potential energy of the system together with their variations. Section E defines the constraint equations and their variations. Appendices A, B and C contain the bulk of the work, i.e. the substitution into Hamilton's integral, and the determination of the Euler-Lagrange equations, the Lagrange multipliers and the boundary conditions. The resulting set of partial integro-differential equations are subsequently linearized in Part F of this section.

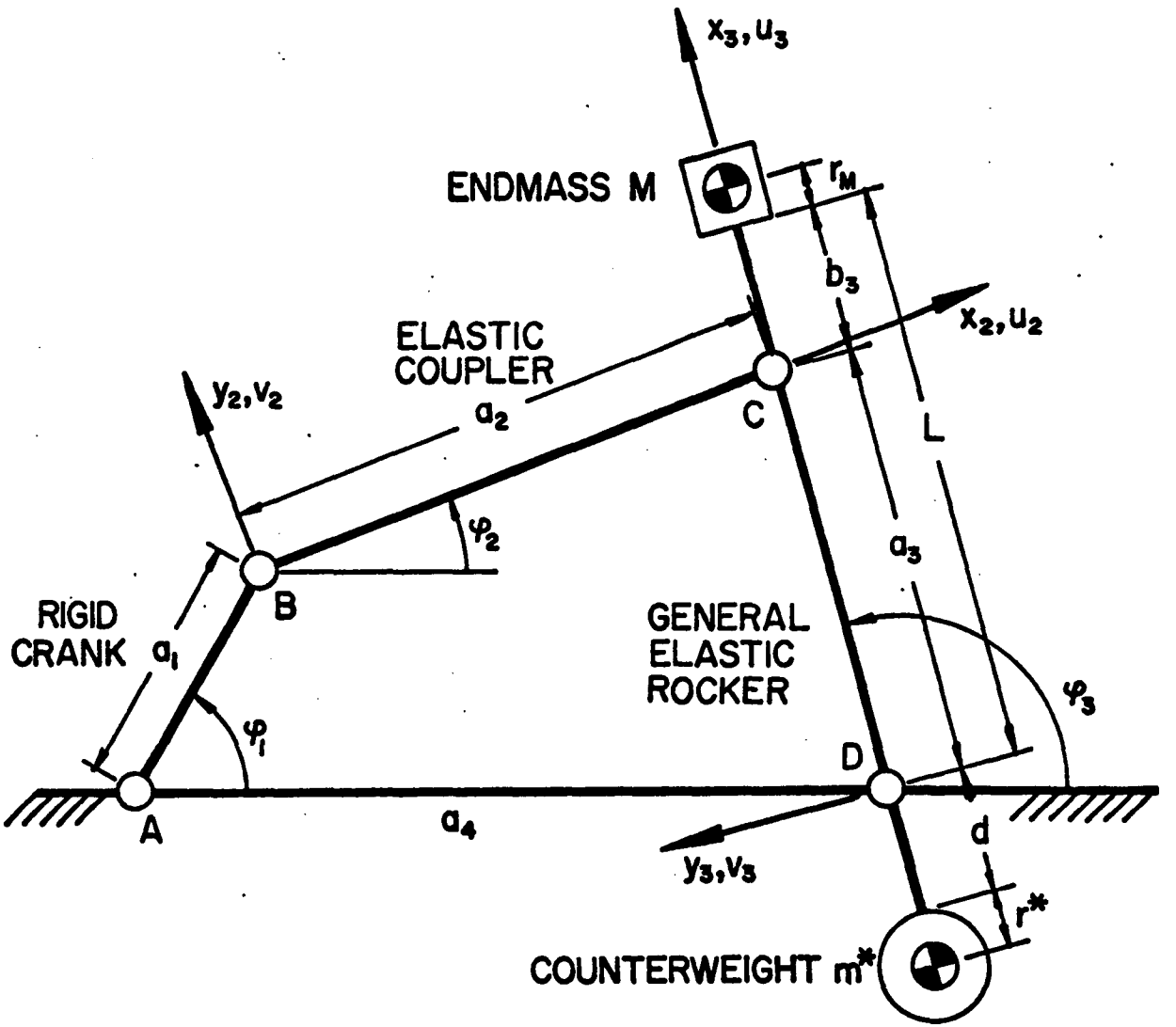

FIGURE 3.1: GENERAL ELASTIC MECHANISM

A. Hamilton's Principle

Hamilton's principle with auxiliary conditions, in the absence of external forces and damping(*), becomes:

$$\delta\int_{t_0}^{t_1}\left[(T-\Pi)+\sum_{i=1}^{k}\int\lambda_i f_i\,dx_2+\sum_{i=k+1}^{m}\int\lambda_i f_i\,dx_3+\sum_{i=m+1}^{n}\lambda_i f_i\right]dt=0, \qquad (3.1)$$

where

T = total kinetic energy of the mechanism,

Π = total potential energy of the mechanism,

λ_i = i-th Lagrange multiplier,

f_i = i-th constraint equation.

The second and third terms in the above refer to constraint conditions which, in addition to time, are functions of x_2 and x_3 respectively (link constraints). The constraint conditions in the fourth term are only functions of time (mechanism constraints).

(*) Damping will only be included in the final linearized differential equation.

B. Method of Variation of Kinetic Energy Integral

Because of the complexity of the velocity terms in the kinetic energy, it has been found convenient to employ the following alternate formulation of Hamilton's equation which uses acceleration terms. For further convenience, elastic and rigid body components are kept separate.

The variation of the integral of the kinetic energy, T_e, of an elastic link is defined as:

$$\delta\int_{t_0}^{t_1} T_e\,dt = \int_{t_0}^{t_1}\delta\,\frac{1}{2}\int_{\alpha_1}^{\alpha_2}\int_A \rho\,\dot{\bar{r}}_P\cdot\dot{\bar{r}}_P\,dA\,dx\,dt$$

$$= \int_{t_0}^{t_1}\int_{\alpha_1}^{\alpha_2}\int_A \rho\,\dot{\bar{r}}_P\cdot\delta\dot{\bar{r}}_P\,dA\,dx\,dt, \qquad (3.2)$$

where

$\dot{\bar{r}}_P$ = the velocity of an arbitrary point P on the elastic link,

ρ = the mass density of the link material,

A = the cross-sectional area of the link,

$\left.\begin{matrix}\alpha_2\\ \alpha_1\end{matrix}\right\}$ = the limits of integration of the independent variable x.

Integration by parts of equation (3.2) in the variable t as well as the use of the requirement of Hamilton's principle that

$$\delta\bar{r}_P\Big|_{t_0,t_1} = 0, \qquad (3.3)$$

leads to the more advantageous form:

$$\delta\int_{t_0}^{t_1} T_e\,dt = -\int_{t_0}^{t_1}\int_{\alpha_1}^{\alpha_2}\int_{A} \rho\,\ddot{\bar{r}}_P\cdot\delta\bar{r}_P\,dA\,dx\,dt, \qquad (3.4)$$

where

$\ddot{\bar{r}}_P$ = the acceleration of an arbitrary point P on the elastic link (see equation (A.21)),

$\delta\bar{r}_P$ = the virtual displacement of an arbitrary point P on the elastic link (see equation (B.2)).

The variation of the integral pertaining to the kinetic energy, T_r, of the rigid body masses, such as the counterweight may be transformed in a similar manner:

$$\delta\int_{t_0}^{t_1} T_r\,dt = \int_{t_0}^{t_1}\delta\left[\frac{1}{2}m\dot{\bar{r}}_m\cdot\dot{\bar{r}}_m + \frac{1}{2}J_m\dot{\bar{\theta}}_m\cdot\dot{\bar{\theta}}_m\right]dt$$

$$= \int_{t_0}^{t_1}\left[m\dot{\bar{r}}_m\cdot\delta\dot{\bar{r}}_m + J_m\dot{\bar{\theta}}_m\cdot\delta\dot{\bar{\theta}}_m\right]dt, \qquad (3.5)$$

where

m = mass of the rigid body,

$\dot{\bar{r}}_m$ = velocity of the center of mass of the rigid body,

J_m = mass moment of inertia with respect to the center of mass of the rigid body,

$\dot{\bar{\theta}}_m$ = total angular velocity of the mass (see equations (A.18) and (A.19)).

Integration by parts of equation (3.5) and letting

$$\delta\bar{\theta}_m\Big|_{t_0,t_1} = 0 \qquad (3.6)$$

leads again to the more desirable form:

$$\delta \int_{t_0}^{t_1} T_r \, dt = - \int_{t_0}^{t_1} m \, \bar{\ddot{r}}_m \cdot \delta \bar{r}_m \, dt - \int_{t_0}^{t_1} J_m \, \bar{\ddot{\theta}}_m \cdot \overline{\delta \theta}_m \, dt \, . \tag{3.7}$$

C. Kinetic Energy of the System and its Variation

The total kinetic energy of the mechanism system consists of:

$$T = T_1 + T_2 + T_3 + T_{m*} + T_M \tag{3.8}$$

where

T_1 = kinetic energy of the crank,

T_2 = kinetic energy of the coupler,

T_3 = kinetic energy of the rocker,

T_{m*} = kinetic energy of the rocker counterweight,

T_M = kinetic energy of the rocker endmass.

Variation of the various components of the kinetic energy, according to equations (3.4) and (3.7) leads to:

$$\delta\int_{t_o}^{t_1} T_2\,dt = -\int_{t_o}^{t_1}\int_{o}^{a_2}\int_{A_2} \rho_2\,\ddot{\bar{r}}_{P_2}\cdot\delta\bar{r}_{P_2}\,dA_2\,dx_2\,dt\,, \tag{3.9}$$

$$\delta\int_{t_o}^{t_1} T_3\,dt = -\int_{t_o}^{t_1}\int_{-d}^{L}\int_{A_3} \rho_3\,\ddot{\bar{r}}_{P_3}\cdot\delta\bar{r}_{P_3}\,dA_3\,dx_3\,dt\,, \tag{3.10}$$

$$\delta\int_{t_o}^{t_1} T_{m^*}\,dt = -\int_{t_o}^{t_1} m^*\,\ddot{\bar{r}}_{m^*}\cdot\delta\bar{r}_{m^*}\,dt - \int_{t_o}^{t_1} J_{m^*}\,\ddot{\bar{\theta}}_{m^*}\cdot\delta\bar{\theta}_{m^*}\,dt\,, \tag{3.11}$$

$$\delta\int_{t_o}^{t_1} T_M\,dt = -\int_{t_o}^{t_1} M\,\ddot{\bar{r}}_M\cdot\delta\bar{r}_M\,dt - \int_{t_o}^{t_1} J_M\,\ddot{\bar{\theta}}_M\cdot\delta\bar{\theta}_M\,dt\,. \tag{3.12}$$

Note that

$$\delta \int_{t_0}^{t_1} T_1 \, dt = 0, \tag{3.13}$$

since the motion of the crank is prescribed at all times and therefore $\delta \bar{r}_{P1}$, the virtual displacement, vanishes.

D. Potential Energy of the System and its Variation

The potential energy of the mechanism system is composed entirely of the strain energies of the elastic links.

The variation of the integral of the strain energy U of an elastic link is generally defined as:

$$\delta\int_{t_0}^{t_1} U\,dt = \int_{t_0}^{t_1}\delta\,\frac{1}{2}\int_{\alpha_1}^{\alpha_2} EI\left(\frac{\partial^2 v}{\partial x^2}\right)^2 dx\,dt$$

$$= \int_{t_0}^{t_1}\int_{\alpha_1}^{\alpha_2} EI\,\frac{\partial^2 v}{\partial x^2}\,\delta\left(\frac{\partial^2 v}{\partial x^2}\right) dx\,dt\,, \qquad (3.14)$$

where

EI = the modulus of rigidity of the link,
which is assumed constant.

The limits of integration α_1 and α_2 are now set by those portions of the beam over which the moment function does not change. For link 2, there is a single moment function for $0 \le x_2 \le a_2$. For link 3, the moment is expressed by three different functions, i.e. one each between $-d \le x_3 \le 0^-$, $0 \le x_3 \le a_3$, and $a_3^+ \le x_3 \le L$.

The appropriate formulations of equation (3.14) for links 2 and 3 are integrated by parts twice. One obtains for link 2:

$$\delta\int_{t_0}^{t_1} U_2\,dt = \int_{t_0}^{t_1}\left\{\int_0^{a_2} E_2 I_2\,\frac{\partial^4 v_2}{\partial x_2^4}\,\delta v_2\,dx_2\right.$$

$$\left. + \left[E_2 I_2\,\frac{\partial^2 v_2}{\partial x_2^2}\,\delta\frac{\partial v_2}{\partial x_2} - E_2 I_2\,\frac{\partial^3 v_2}{\partial x_2^3}\,\delta v_2\right]_0^{a_2}\right\} dt\,. \qquad (3.15)$$

For link 3, one finds:

$$\delta \int_{t_0}^{t_1} U_3 \, dt = \int_{t_0}^{t_1} \left\{ \int_{-d}^{0} E_3 I_3 \frac{\partial^4 v_3}{\partial x_3^4} \delta v_3 \, dx_3 + \int_{0}^{a_3} E_3 I_3 \frac{\partial^4 v_3}{\partial x_3^4} \delta v_3 \, dx_3 \right.$$

$$+ \int_{a_3}^{L} E_3 I_3 \frac{\partial^4 v_3}{\partial x_3^4} \delta v_3 \, dx_3 + \left[E_3 I_3 \frac{\partial^2 v_3}{\partial x_3^2} \delta \frac{\partial v_3}{\partial x_3} - E_3 I_3 \frac{\partial^3 v_3}{\partial x_3^3} \delta v_3 \right]_{-d}^{0^-}$$

$$\left. + \left[E_3 I_3 \frac{\partial^2 v_3}{\partial x_3^2} \delta \frac{\partial v_3}{\partial x_3} - E_3 I_3 \frac{\partial^3 v_3}{\partial x_3^3} \delta v_3 \right]_{0}^{a_3} + \left[E_3 I_3 \frac{\partial^2 v_3}{\partial x_3^2} \delta \frac{\partial v_3}{\partial x_3} - E_3 I_3 \frac{\partial^3 v_3}{\partial x_3^3} \delta v_3 \right]_{a_3}^{L} \right\} dt. \tag{3.16}$$

E. Constraint Equations and their Variations

For the method used in the present work, it is necessary to define elastic link constraints as well as elastic mechanism constraints.

1. Elastic Link Constraints

As a result of the foreshortening described by equation (A.2), six elastic link constraint equations arise.

For an arbitrary point on link 2:

$$f_1 = u_2 + \frac{1}{2}\int_0^{x_2}\left(\frac{\partial \tilde{v}_2}{\partial \xi_2}\right)^2 d\xi_2 = 0. \qquad (3.17)$$

For an arbitrary point on link 3:

$$f_2 = u_3 + \frac{1}{2}\int_0^{x_3}\left(\frac{\partial \tilde{v}_3}{\partial \xi_3}\right)^2 d\xi_3 = 0. \qquad (3.18)$$

For point C located either on links 2 or 3, one finds:

$$f_3 = u_2(a_2) + \frac{1}{2}\int_0^{a_2}\left(\frac{\partial v_2}{\partial x_2}\right)^2 dx_2 = 0, \qquad (3.19)$$

$$f_4 = u_3(a_3) + \frac{1}{2}\int_0^{a_3}\left(\frac{\partial v_3}{\partial x_3}\right)^2 dx_3 = 0. \qquad (3.20)$$

For $x_3 = -d$ and $x_3 = L$ respectively:

$$f_5 = u_3(-d) + \frac{1}{2}\int_0^{-d}\left(\frac{\partial v_3}{\partial x_3}\right)^2 dx_3 = 0, \qquad (3.21)$$

$$f_6 = u_3(L) + \frac{1}{2}\int_0^{L}\left(\frac{\partial v_3}{\partial x_3}\right)^2 dx_3 = 0. \qquad (3.22)$$

2. Elastic Mechanism Constraints (Elastic Loop Equation)

Figure 3.2 shows the elastically deformed mechanism with a rigid crank. The body fixed x-axes connect the pivot points of the foreshortened elastic links. The interrelationships between φ_{2e}, φ_{3e}, $u_2(a_2)$ and $u_3(a_3)$ are determined by way of the elastic loop equation:

$$\overline{AB} + \overline{BC} = \overline{AD} + \overline{DC} \tag{3.23}$$

where

$$\left.\begin{aligned} |\overline{AB}| &= a_1 \\ |\overline{BC}| &= a_2 + u_2(a_2) \\ |\overline{AD}| &= a_3 + u_3(a_3) \\ |\overline{DC}| &= a_4. \end{aligned}\right\} \tag{3.24}$$

The component form of equation (3.23) furnishes two additional constraint equations:

$$\begin{aligned} f_7 = {} & a_1 \cos\varphi_1 + (a_2 + u_2(a_2)) \cos\varphi_{2e} - a_4 \\ & - (a_3 + u_3(a_3)) \cos\varphi_{3e} = 0, \end{aligned} \tag{3.25}$$

$$\begin{aligned} f_8 = {} & a_1 \sin\varphi_1 + (a_2 + u_2(a_2)) \sin\varphi_{2e} \\ & - (a_3 + u_3(a_3)) \sin\varphi_{3e} = 0. \end{aligned} \tag{3.26}$$

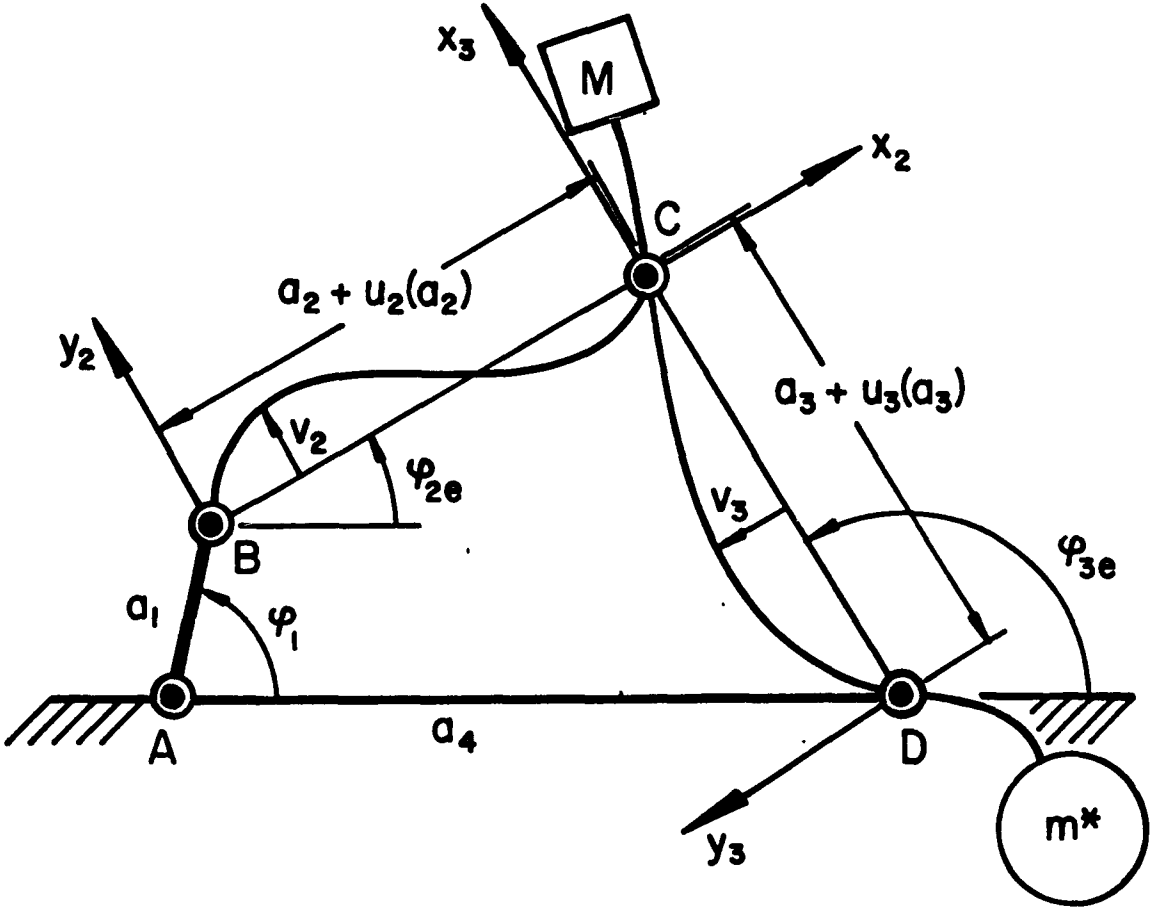

FIGURE 3.2: MECHANISM IN ARBITRARY CONFIGURATION

3. Variation of the Constraint Equations

The variations of the eight constraint equations are obtained in the following manner from equations (3.17) to (3.22), (3.25) and (3.26). Thus for f_1:

$$\delta f_1 = \delta u_2 + \int_0^{x_2} \frac{\partial \tilde{v}_2}{\partial \xi_{32}} \, \delta\left(\frac{\partial \tilde{v}_2}{\partial \xi_{32}}\right) d\xi_{32} = 0 , \tag{3.27}$$

where $\tilde{v}_2 = v_2(\xi_2, t)$. After integration by parts, the above becomes:

$$\delta f_1 = \delta u_2 + \left[\frac{\partial v_2}{\partial x_2} \, \delta v_2\right]_0^{x_2} - \int_0^{x_2} \frac{\partial^2 \tilde{v}_2}{\partial \xi_{32}^2} \, \delta \tilde{v}_2 \, d\xi_{32} = 0 . \tag{3.28}$$

In a similar manner, one obtains:

$$\delta f_2 = \delta u_3 + \left[\frac{\partial v_3}{\partial x_3} \, \delta v_3\right]_0^{x_3} - \int_0^{x_3} \frac{\partial^2 \tilde{v}_3}{\partial \xi_{33}^2} \, \delta \tilde{v}_3 \, d\xi_{33} = 0 . \tag{3.29}$$

where whenever $a_3^+ \le x_3 \le L$, the integration consists of two parts with limits from 0 to a_3 and from a_3^+ to x_3.

$$\delta f_3 = \delta u_2(a_2) + \left[\frac{\partial v_2}{\partial x_2} \, \delta v_2\right]_0^{a_2} - \int_0^{a_2} \frac{\partial^2 v_2}{\partial x_2^2} \, \delta v_2 \, dx_2 = 0 . \tag{3.30}$$

$$\delta f_4 = \delta u_3(a_3) + \left[\frac{\partial v_3}{\partial x_3} \, \delta v_3\right]_0^{a_3} - \int_0^{a_3} \frac{\partial^2 v_3}{\partial x_3^2} \, \delta v_3 \, dx_3 = 0 . \tag{3.31}$$

$$\delta f_5 = \delta u_3(-d) + \left[\frac{\partial v_3}{\partial x_3} \, \delta v_3\right]_0^{-d} - \int_0^{-d} \frac{\partial^2 v_3}{\partial x_3^2} \, \delta v_3 \, dx_3 = 0 . \tag{3.32}$$

$$\delta f_6 = \delta u_3(L) + \left[\frac{\partial v_3}{\partial x_3}\,\delta v_3\right]_0^L - \int_0^{a_3} \frac{\partial^2 v_3}{\partial x_3^2}\,\delta v_3\, dx_3$$

$$- \int_{a_3}^{L} \frac{\partial^2 v_3}{\partial x_3^2}\,\delta v_3\, dx_3 = 0. \qquad (3.33)$$

In the above, the integration is performed in two steps since the moment function changes at $x_3 = a_3$. Further,

$$\delta f_7 = \cos\varphi_{2e}\,\delta u_2(a_2) - (a_2 + u_2(a_2))\sin\varphi_{2e}\,\delta\varphi_{2e}$$

$$- \cos\varphi_{3e}\,\delta u_3(a_3) + (a_3 + u_3(a_3))\sin\varphi_{3e}\,\delta\varphi_{3e} = 0. \qquad (3.34)$$

$$\delta f_8 = \sin\varphi_{2e}\,\delta u_2(a_2) + (a_2 + u_2(a_2))\cos\varphi_{2e}\,\delta\varphi_{2e}$$

$$- \sin\varphi_{3e}\,\delta u_3(a_3) - (a_3 + u_3(a_3))\cos\varphi_{3e}\,\delta\varphi_{3e} = 0. \qquad (3.35)$$

F. Linearized Equations of Motion and Boundary Conditions for Two Elastic Links
Inclusion of Viscous Damping

Appendix C shows the derivation of the partial differential equations of motion for both links, together with the determination of the associated boundary conditions and the Lagrange multipliers starting from equation (3.1).

While the recognition of the existence of the variations $\delta\varphi_{2e}$ and $\delta\varphi_{3e}$ of the elastic angles and their determination from the elastic mechanism constraints is essential to the success of the method used, the angles φ_{2e} and φ_{3e} themselves, as well as their derivatives, may be approximated by their rigid body expressions. Since this simplification is employed the determination of these quantities in terms of $v_2(x_2,t)$ and $v_3(x_3,t)$ is only outlined (see end of Appendix C-5). Further, the physical significance of the Lagrange multipliers is not considered.

The resulting partial integro-differential equations, (C.51), (C.57), (C.59) and (C.61), and boundary conditions, equations (C.53) to (C.56) and (C.63) to (C.74), contain numerous non-linear terms as well as the elastic angles φ_{2e} and φ_{3e}.

All non-linear terms are now removed, and because of the small deflections involved, the elastic angles are approximated by the rigid body ones(*):

$$\varphi_{2e}(t) \approx \varphi_2(t)$$

(*) The elastic mechanism constraints, equations (3.25) and (3.26), become the constraint equations for a rigid mechanism when the effects of $u_2(a_2)$ and $u_3(a_3)$ are neglected.

and

$$\varphi_{3e}(t) \approx \varphi_3(t).$$

To account for viscous damping in both links, the terms $C_{D2}\partial v_2/\partial t$ and $C_{D3}\partial v_3/\partial t$ are now introduced. (It was felt that this approach was preferable to including a corresponding work term in Hamilton's integral.)

The linearized equation of motion for the coupler is given by:

$$E_2 I_2 \frac{\partial^4 v_2}{\partial x_2^4} - \rho_2 I_2 \frac{\partial^4 v_2}{\partial x_2^2 \partial t^2} + D_1(x_2,t)\frac{\partial^2 v_2}{\partial x_2^2} + \mu_2 \frac{\partial^2 v_2}{\partial t^2} + D_2(x_2,t)\frac{\partial v_2}{\partial x_2} + C_{D2}\frac{\partial v_2}{\partial t} - \mu_2 \dot{\varphi}_2^2 v_2 + D_3(x_2,t) = 0. \quad (3.36)$$

The associated geometric and natural boundary conditions are:

$$v_2(0,t) = 0, \quad (3.37)$$

$$v_2(a_2,t) = 0, \quad (3.38)$$

$$E_2 I_2 \frac{\partial^2 v_2(0,t)}{\partial x_2^2} = 0, \quad (3.39)$$

$$E_2 I_2 \frac{\partial^2 v_2(a_2,t)}{\partial x_2^2} = 0, \quad (3.40)$$

The linearized equations of motion for the rocker sections are given by:

Section 1: $-d \le x_3 \le 0^-$

$$E_3 I_3 \frac{\partial^4 v_3}{\partial x_3^4} - \rho_3 I_3 \frac{\partial^4 v_3}{\partial x_3^2 \partial t^2} + G_0(x_3,t)\frac{\partial^2 v_3}{\partial x_3^2} + \mu_3 \frac{\partial^2 v_3}{\partial t^2} + G_2(x_3,t)\frac{\partial v_3}{\partial x_3} + C_{D3}\frac{\partial v_3}{\partial t} - \mu_3 \dot{\varphi}_3^2 v_3 + G_3(x_3,t) = 0. \quad (3.41)$$

Section 2: $0 \le x_3 \le a_3$

$$E_3 I_3 \frac{\partial^4 v_3}{\partial x_3^4} - \rho_3 I_3 \frac{\partial^4 v_3}{\partial x_3^2 \partial t^2} + G_1(x_3,t)\frac{\partial^2 v_3}{\partial x_3^2} + \mu_3 \frac{\partial^2 v_3}{\partial t^2} + G_2(x_3,t)\frac{\partial v_3}{\partial x_3} + C_{D3}\frac{\partial v_3}{\partial t} - \mu_3 \dot{\varphi}_3^2 v_3 + G_3(x_3,t) = 0. \quad (3.42)$$

Section 3: $a_3^+ \le x_3 \le L$

$$E_3 I_3 \frac{\partial^4 v_3}{\partial x_3^4} - \rho_3 I_3 \frac{\partial^4 v_3}{\partial x_3^2 \partial t^2} + G_4(x_3,t)\frac{\partial^2 v_3}{\partial x_3^2} + \mu_3 \frac{\partial^2 v_3}{\partial t^2} + G_2(x_3,t)\frac{\partial v_3}{\partial x_3} + C_{D3}\frac{\partial v_3}{\partial t} - \mu_3 \dot{\varphi}_3^2 v_3 + G_3(x_3,t) = 0. \quad (3.43)$$

The associated geometric boundary conditions are:

$$v_3(0^-,t) = 0, \quad (3.44)$$

$$v_3(0,t) = 0, \quad (3.45)$$

$$\frac{\partial v_3(0^-,t)}{\partial x_3} = \frac{\partial v_3(0,t)}{\partial x_3}, \quad (3.46)$$

$$v_3(a_3,t) = 0 \quad (3.47)$$

$$v_3(a_3^+,t) = 0, \tag{3.48}$$

$$\frac{\partial v_3(a_3,t)}{\partial x_3} = \frac{\partial v_3(a_3^+,t)}{\partial x_3}, \tag{3.49}$$

while the dynamic boundary conditions become:

$$-E_3I_3\frac{\partial^2 v_3(-d,t)}{\partial x_3^2} + (J_{m^*} + m^*r^{*2})\frac{\partial^3 v_3(-d,t)}{\partial x_3\partial t^2} - m^*r^*\frac{\partial^2 v_3(-d,t)}{\partial t^2}$$

$$-m^*r^*\ddot{\alpha}_3(-d)\frac{\partial v_3(-d,t)}{\partial x_3} + m^*r^*\dot{\varphi}_3^2 v_3(-d,t) - m^*r^*\ddot{\beta}_3(-d)$$

$$+ (J_{m^*} + m^*r^{*2})\ddot{\varphi}_3 = 0, \tag{3.50}$$

$$E_3I_3\frac{\partial^3 v_3(-d,t)}{\partial x_3^3} - (m^*r^* + \rho_3I_3)\frac{\partial^3 v_3(-d,t)}{\partial x_3\partial t^2} + m^*\frac{\partial^2 v_3(-d,t)}{\partial t^2}$$

$$-m^*\ddot{\alpha}_3(-d)\frac{\partial v_3(-d,t)}{\partial x_3} - m^*\dot{\varphi}_3^2 v_3(-d,t) + m^*\ddot{\beta}_3(-d) - (m^*r^* + \rho_3I_3)\ddot{\varphi}_3 = 0, \tag{3.51}$$

$$E_3I_3\frac{\partial^2 v_3(0^-,t)}{\partial x_3^2} = E_3I_3\frac{\partial^2 v_3(0,t)}{\partial x_3^2}, \tag{3.52}$$

$$E_3I_3\frac{\partial^2 v_3(a_3,t)}{\partial x_3^2} = E_3I_3\frac{\partial^2 v_3(a_3^+,t)}{\partial x_3^2}, \tag{3.53}$$

$$E_3I_3\frac{\partial^2 v_3(L,t)}{\partial x_3^2} + (J_M + Mr_M^2)\frac{\partial^3 v_3(L,t)}{\partial x_3\partial t^2} + Mr_M\frac{\partial^2 v_3(L,t)}{\partial t^2} - Mr_M\ddot{\alpha}_3(L)\frac{\partial v_3(L,t)}{\partial x_3}$$

$$-Mr_M\dot{\varphi}_3^2 v_3(L,t) + Mr_M\ddot{\beta}_3(L) + (J_M + Mr_M^2)\ddot{\varphi}_3 = 0, \tag{3.54}$$

$$-E_3I_3\frac{\partial^3 v_3(L,t)}{\partial x_3^3} + (Mr_M + \rho_3I_3)\frac{\partial^3 v_3(L,t)}{\partial x_3\partial t^2} + M\frac{\partial^2 v_3(L,t)}{\partial t^2} - M\ddot{\alpha}_3(L)\frac{\partial v_3(L,t)}{\partial x_3}$$

$$-M\dot{\varphi}_3^2 v_3(L,t) + M\ddot{\beta}_3(L) + (Mr_M + \rho_3I_3)\ddot{\varphi}_3 = 0. \tag{3.55}$$

Further, the following definitions hold for the above equations(*):

$$D_1(x_2,t) = \int_{x_2}^{a_2} \mu_2 \ddot{\alpha}_2(\xi_2)\, d\xi_2 - \frac{\cot(\varphi_3-\varphi_2)}{a_2}\int_0^{a_2}\left[\mu_2 x_2 \ddot{\beta}_2(x_2) + \rho_2 I_2 \ddot{\varphi}_2\right] dx_2$$

$$- \frac{\csc(\varphi_3-\varphi_2)}{a_3}\left\{\int_{-d}^{L}\left[\mu_3 x_3 \ddot{\beta}_3(x_3) + \rho_3 I_3 \ddot{\varphi}_3\right] dx_3 - m^*(d+r^*)\ddot{\beta}_3(-d) + m^* r^* d\,\ddot{\varphi}_3\right.$$

$$\left. + (J_{m^*} + m^* r^{*2})\ddot{\varphi}_3 + M(L+r_M)\ddot{\beta}_3(L) + M r_M L \ddot{\varphi}_3 + (J_M + M r_M^2)\ddot{\varphi}_3\right\}, \tag{3.56}$$

$$D_2(x_2,t) = -\mu_2 \ddot{\alpha}_2 \quad , \tag{3.57}$$

$$D_3(x_2,t) = \mu_2 \ddot{\beta}_2 \quad , \tag{3.58}$$

$$G_0(x_3,t) = \int_{x_3}^{-d} \mu_3 \ddot{\alpha}_3(\xi_3)\, d\xi_3 - m^* \ddot{\alpha}_3(-d) - m^* r^* \dot{\varphi}_3^2 , \tag{3.59}$$

$$G_1(x_3,t) = \int_{x_3}^{L} \mu_3 \ddot{\alpha}_3(\xi_3)\, d\xi_3 + \frac{\csc(\varphi_3-\varphi_2)}{a_2}\int_0^{a_2}\left[\mu_2 x_2 \ddot{\beta}_2(x_2) + \rho_2 I_2 \ddot{\varphi}_2\right] dx_2$$

$$+ \frac{\cot(\varphi_3-\varphi_2)}{a_3}\left\{\int_{-d}^{L}\left[\mu_3 x_3 \ddot{\beta}_3(x_3) + \rho_3 I_3 \ddot{\varphi}_3\right] dx_3 - m^*(d+r^*)\ddot{\beta}_3(-d)\right.$$

$$+ m^* r^* d\,\ddot{\varphi}_3 + (J_{m^*} + m^* r^{*2})\ddot{\varphi}_3 + M(L+r_M)\ddot{\beta}_3(L) + M r_M L \ddot{\varphi}_3$$

$$\left. + (J_M + M r_M^2)\ddot{\varphi}_3\right\} + M\ddot{\alpha}_3(L) - M r_M \dot{\varphi}_3^2 , \tag{3.60}$$

(*) The integrals in these definitions are only functions of the rigid body kinematic terms, and may be evaluated after substitution.

$$G_2(x_3,t) = -\mu_3 \ddot{\alpha}_3 \quad , \tag{3.61}$$

$$G_3(x_3,t) = \mu_3 \ddot{\beta}_3 \quad , \tag{3.62}$$

$$G_4(x_3,t) = \int_{x_3}^{L} \mu_3 \ddot{\alpha}_3(\xi_3) d\xi_3 + M\ddot{\alpha}_3(L) - Mr_M \dot{\varphi}_3^2 \quad . \tag{3.63}$$

Note that while the coupler and rocker differential equations are uncoupled in the $v_n(x_n,t)$, they are "coupled parametrically", i.e. the deflection of one link depends very much on the mass properties of the adjacent link. It is of further interest to observe that the coefficients $D_i(x_2,t)$ and $G_i(x_3,t)$ in these expressions are 2π-periodic because of their mechanism origin.

IV. RESPONSE OF ELASTIC ROCKER LINK WITH OVERHANG, ENDMASS AND COUNTERWEIGHT

This section concerns itself with the main problem of this dissertation, i.e. the solution method for the elastic response of a counterweighted rocker with overhang and endmass in a four-bar linkage with a rigid crank and coupler (see Figure 4.1).

The governing differential equations and boundary conditions may be obtained, after some simplification, from the previous section or by an alternate derivation, given in Appendices D and E.

The solution of the problem is based on the method of Kantorovich. It requires the assumption of a solution form which is represented by an infinite series of space-time function products, where the space or shape function components must be chosen as a complete set of functions which should satisfy the geometric boundary conditions.(*)

The resulting solution form is substituted into the variational integral associated with the linearized and simplified partial differential equation. This leads to an infinite set of coupled, nonhomogeneous Hill-type differential equations in the time portion of the solution. The details of this procedure are outlined in Sections B to E with the bulk of the work in Appendices F and G.

(*) The shape function (subproblem) used here is that resulting from the associated free vibration problem.

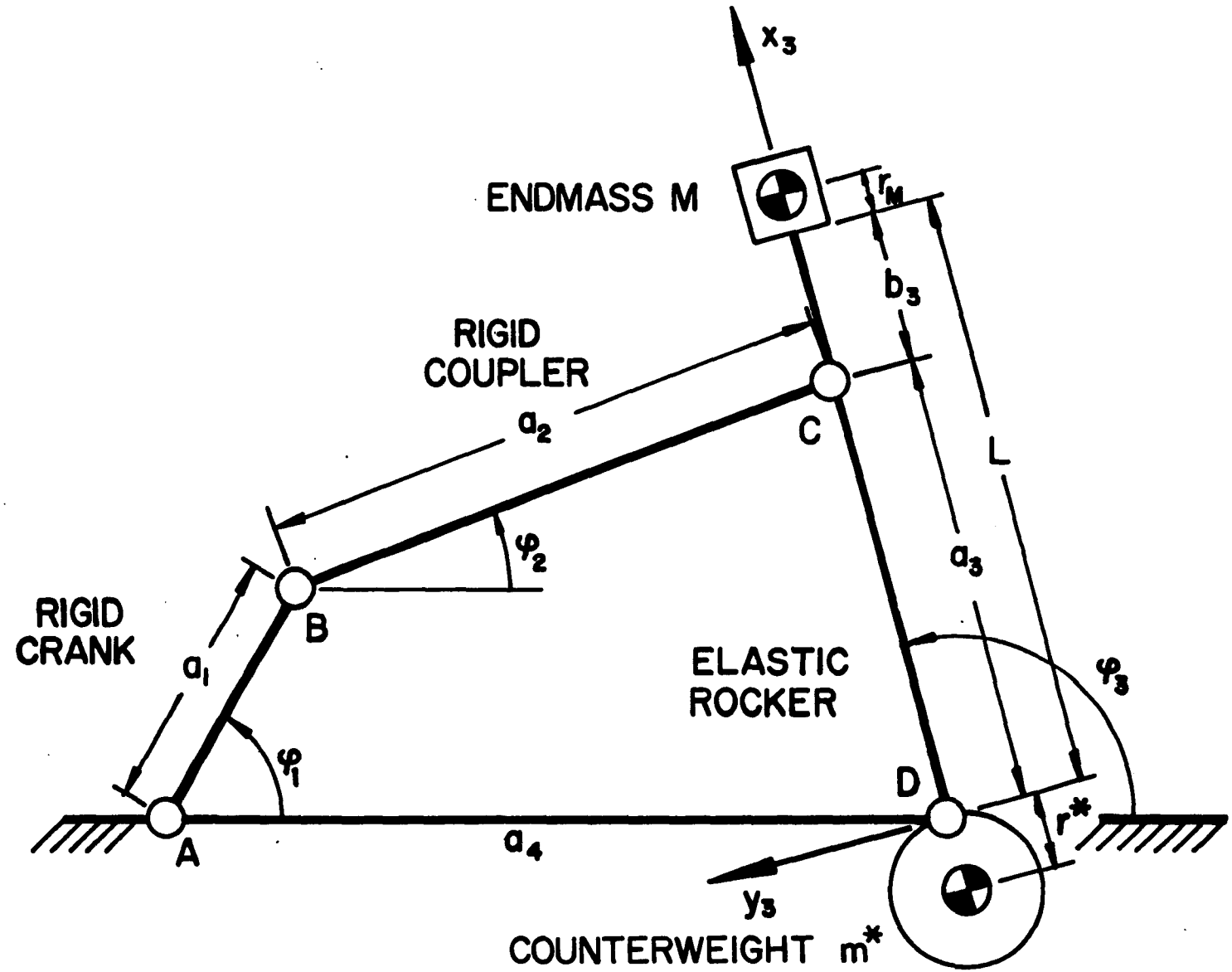

FIGURE 4.1: FOUR-BAR LINKAGE WITH ELASTIC ROCKER

Sections E and F together with Appendix H discuss stability questions associated with the homogeneous portion of the Hill-type differential equations as well as the particular solution and the associated resonance locations, which are necessary for the complete solution of the problem.

A. Linearized Differential Equations and Boundary Conditions

The linearized equations for the shaker mechanism, where only the rocker is considered elastic, may be obtained from the results of the last section. The presence of the rigid coupler is accounted for by the omission of equations (3.36) through (3.40), while the equation of motion of the elastic rocker, which contains an endmass and a counterweight, is supplied by equations (3.41) through (3.55). The fact that the counterweight is tangent to the pivot at point D is accounted for by letting d become zero.

Appendix D gives an alternate derivation for this case. Instead of using the Lagrange multiplier method to account for the constraint equations, the variations δu_3, $\delta \Phi_{2e}$ and $\delta \Phi_{3e}$, which are functions of $v_3(x_3,t)$, are used directly in Hamilton's equation. Subsequently, Hamilton's integral is simplified by approximating the elastic angles φ_{2e} and φ_{3e} by their rigid body counterparts (see also discussion in Section III-F), and by dropping all non-linear terms. The resulting expression (equation (D.10)), into which damping terms have been introduced in the manner shown in Section III-F, forms the basis for the linearized differential equations and boundary conditions below, as well as for the solution by the method of Kantorovich, (see Section IV-B).

For $0 \le x_3 \le a_3$:

$$C_1 \frac{\partial^4 v_3}{\partial x_3^4} + G_1(x_3,t) \frac{\partial^2 v_3}{\partial x_3^2} + C_2 \frac{\partial^2 v_3}{\partial t^2} + G_2(x_3,t) \frac{\partial v_3}{\partial x_3} + C_{D_3} \frac{\partial v_3}{\partial t}$$

$$- C_5 G_5(t) v_3 + G_3(x_3,t) = 0 . \tag{4.1}$$

For $a_3^+ \le x_3 \le L$:

$$C_1 \frac{\partial^4 v_3}{\partial x_3^4} + G_4(x_3,t) \frac{\partial^2 v_3}{\partial x_3^2} + C_2 \frac{\partial^2 v_3}{\partial t^2} + G_2(x_3,t) \frac{\partial v_3}{\partial x_3} + C_{D_3} \frac{\partial v_3}{\partial t}$$

$$- C_5 G_5(t) v_3 + G_3(x_3,t) = 0. \tag{4.2}$$

The geometric boundary conditions are given by:

$$v_3(0,t) = 0 , \tag{4.3}$$

$$v_3(a_3,t) = 0 , \tag{4.4}$$

$$v_3(a_3^+,t) = 0 , \tag{4.5}$$

$$\frac{\partial v_3(a_3,t)}{\partial x_3} = \frac{\partial v_3(a_3^+,t)}{\partial x_3} . \tag{4.6}$$

The dynamic boundary conditions are given by:

$$-C_1 \frac{\partial^2 v_3(0,t)}{\partial x_3^2} + C_3 \frac{\partial^3 v_3(0,t)}{\partial x_3 \partial t^2} + C_3 G_6(t) = 0 , \tag{4.7}$$

$$C_1 \left[\frac{\partial^2 v_3(a_3,t)}{\partial x_3^2} - \frac{\partial^2 v_3(a_3^+,t)}{\partial x_3^2} \right] = 0 , \tag{4.8}$$

$$C_1 \frac{\partial^2 v_3(L,t)}{\partial x_3^2} + C_4 \frac{\partial^3 v_3(L,t)}{\partial x_3 \partial t^2} + C_5 \frac{\partial^2 v_3(L,t)}{\partial t^2} + C_6 G_5(t) \frac{\partial v_3(L,t)}{\partial x_3}$$

$$- C_5 G_5(t) v_3(L,t) + C_9 G_6(t) = 0 , \tag{4.9}$$

$$-C_1\frac{\partial^3 v_3(L,t)}{\partial x_3^3}+C_5\frac{\partial^3 v_3(L,t)}{\partial x_3\partial t^2}+C_7\frac{\partial^2 v_3(L,t)}{\partial t^2}+C_8G_5(t)\frac{\partial v_3(L,t)}{\partial x_3}$$

$$-C_7G_5(t)v_3(L,t)+C_{10}G_6(t)=0\ , \tag{4.10}$$

where

$$\left.\begin{aligned} C_1 &= E_3I_3 & C_6 &= Mr_ML\\ C_2 &= \mu_3 & C_7 &= M\\ C_3 &= J_m^*+m^*r^{*2}=J^* & C_8 &= ML\\ C_4 &= J_M+Mr_M^2=\tilde{J} & C_9 &= \tilde{J}+Mr_ML=C_4+C_6\\ C_5 &= Mr_M & C_{10} &= ML+Mr_M=C_5+C_8 \end{aligned}\right\} \tag{4.11}$$

C_{D3} = coefficient of damping, (4.12)

$$G_1(x_3,t)=-\frac{\mu_3}{2}(L^2-x_3^2)\dot{\varphi}_3^2+\frac{\csc(\varphi_3-\varphi_2)}{a_2}\left[\frac{M_2a_2}{2}\left(-\dot{\varphi}_1^2a_1\sin(\varphi_1-\varphi_2)\right.\right.$$

$$\left.+\ddot{\varphi}_1a_1\cos(\varphi_1-\varphi_2)+\frac{a_2}{2}\ddot{\varphi}_2\right)+J_{2C}\ddot{\varphi}_2\Bigg]+\ddot{\varphi}_3\frac{\cot(\varphi_3-\varphi_2)}{a_3}\left(J_{3D}+J^*\right.$$

$$\left.+J_M+M(L+r_M)^2\right)-M(L+r_M)\dot{\varphi}_3^2\ , \tag{4.13}$$

$$G_2(x_3,t)=\mu_3x_3\dot{\varphi}_3^2\ , \tag{4.14}$$

$$G_3(x_3,t)=\mu_3x_3\ddot{\varphi}_3\ , \tag{4.15}$$

$$G_4(x_3,t)=-\frac{\mu_3}{2}(L^2-x_3^2)\dot{\varphi}_3^2-M(L+r_M)\dot{\varphi}_3^2\ , \tag{4.16}$$

$$G_5(t) = \dot{\varphi}_3^2 \ , \tag{4.17}$$

$$G_6(t) = \ddot{\varphi}_3 \ . \tag{4.18}$$

B. Solution Method

A number of authors [13, 24, 26] have shown that differential equations of the type represented by equations (4.1) and (4.2), which contain periodic coefficients, may be solved approximately using the method of L.V. Kantorovich by letting

$$v_3(x_3,t) = \sum_{n}^{\infty} V_n(x_3)\, q_n(t). \qquad (4.19)$$

To this end, shape functions $V_n(x_3)$, which form a complete set and satisfy the geometric boundary conditions, equations (4.3) through (4.6), must be determined from a suitable subproblem. Substitution of equation (4.19) and its derivatives into the Hamilton's integral (D.10), results in a set of nonhomogeneous Hill-type differential equations in $q_n(t)$ after suitable integrations and application of the Fundamental Lemma.

C. Subproblem

The shape function $V_n(x_3)$, which is associated with the free vibration problem of the simply supported beam with overhang, endmass and counterweight shown in Figure 4.2, satisfies the geometric boundary conditions, equations (4.3) through (4.6).

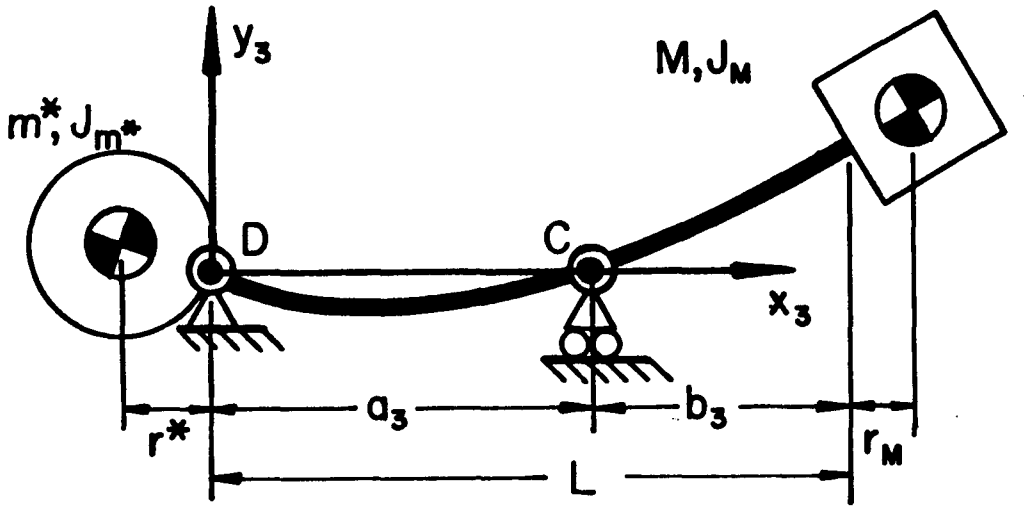

Figure 4.2 Subproblem

This particular subproblem was chosen in preference to one without endmass and counterweight, which also satisfies the geometric boundary conditions, because it was hoped that it would produce the best approximation with a minimum number of modes. In the absence of an exact solution, or the comparisons of various shape functions with an experiment, no real quality judgements can be made.

The subproblem has been solved in Appendix F:

Equation (F.29) gives the shape function $V_n(x_3)$ for $0 \leq x_3 \leq a_3$ while (F.32) furnishes the expression for $a_3^+ \leq x_3 \leq L$. Equation (F.43) represents the

characteristic equation for the determination of the eigenvalues, while equation (F.53) gives the associated orthogonality condition.

D. Determination of Hill-Type Differential Equations by Method of Kantorovich

The infinite set of coupled nonhomogeneous Hill's equations describing the time portion $q_n(t)$ of the solution form are derived in Appendix G. Equation (G.5) gives:

$$\ddot{q}_m + \frac{C_{D3m}}{\mathcal{N}_m} \sum_n \mathcal{J}_{1(m,n)} \dot{q}_n + (\omega_m^2 - G_5(t)) q_m + \frac{1}{\mathcal{N}_m} \sum_n H_{mn}(t) q_n = \frac{F_m(t)}{\mathcal{N}_m} , \tag{4.20}$$

for m = 1,2,3,... . The damping constant C_{D3m}, associated with each natural frequency ω_m, may be expressed in terms of its relationship to critical damping by:

$$C_{D3m} = 2\mu_3 \omega_m \zeta , \tag{4.21}$$

where

μ_3 = mass per unit length of the rocker link,

ζ = damping ratio.

Further, in equation (4.20):

$\mathcal{N}_m$ = the orthogonality condition as defined by equation (F.53),

$$\mathcal{J}_{1(m,n)} = \int_0^{a_3} V_m V_n \, dx_3 + \int_{a_3}^{L} V_m V_n \, dx_3 , \tag{4.22}$$

$$H_{mn}(t) = \int_0^{a_3} G_1(x_3,t) V_m V_n'' \, dx_3 + \int_{a_3}^{L} G_4(x_3,t) V_m V_n \, dx_3 + \int_0^{a_3} G_2(x_3,t) V_m V_n' \, dx_3 + \int_{a_3}^{L} G_2(x_3,t) V_m V_n' \, dx_3 + G_5(t) \left[C_9 V_m'(L) V_n'(L) + C_{10} V_m(L) V_n'(L) + C_5 V_m'(0) V_n'(0) \right] , \tag{4.23}$$

$$F_m(t) = -\int_0^{a_3} G_3(x_3,t) V_m dx_3 - \int_{a_3}^{L} G_3(x_3,t) V_m dx_3 - G_6(t)\left[C_3 V_m'(0) + C_9 V_m'(L) + C_{10} V_m(L)\right] . \tag{4.24}$$

In order to introduce the frequency ratio

$$\Lambda = \left(\frac{\omega}{\dot{\varphi}_1}\right)^2 \tag{4.25}$$

where $\dot{\varphi}_1$ represents the <u>constant</u> input angular velocity, into equation (4.20), the following change of variable is made, i.e. one lets:

$$\frac{dq}{dt} = \dot{\varphi}_1 \frac{dq}{d\varphi_1} , \tag{4.26a}$$

and

$$\frac{d^2q}{dt^2} = \dot{\varphi}_1^2 \frac{d^2q}{d\varphi_1^2} . \tag{4.26b}$$

Further, since $G_5(t)$, $H_{mn}(t)$ and $F_m(t)$ are functions of $\dot{\varphi}_1^2$, one may write:

$$G_5(t) = \dot{\varphi}_1^2 \hat{G}_5(\varphi_1) , \tag{4.27}$$

$$H_{mn}(t) = \dot{\varphi}_1^2 \hat{H}_{mn}(\varphi_1) , \tag{4.28}$$

and

$$F_m(t) = \dot{\varphi}_1^2 \hat{F}_m(\varphi_1) , \tag{4.29}$$

where

$$\hat{H}_{mn}(\varphi_1) = \frac{\dot{\varphi}_3^2}{\dot{\varphi}_1^2}\left[-\frac{C_2}{2} J_{2(m,n)} - C_{10} J_{3(m,n)} + C_2 J_{4(m,n)} + C_9 V_m'(L) V_n'(L) + C_{10} V_m(L) V_n'(L) + C_3 V_m'(0) V_n'(0)\right] + \left[\csc(\varphi_3-\varphi_2) \frac{\ddot{\varphi}_2}{\dot{\varphi}_1^2} \frac{J_{2B}}{a_2} - \frac{\sin(\varphi_1-\varphi_2)}{\sin(\varphi_3-\varphi_2)} \frac{M_2 a_1}{2} + \frac{\ddot{\varphi}_3}{\dot{\varphi}_1^2} \cot(\varphi_3-\varphi_2)\left(\frac{J_{3D} + C_3 + C_4 + 2C_6 + C_7 L^2}{a_3}\right)\right] J_{5(m,n)} , \tag{4.30}$$

with

$$\mathcal{I}_{2(m,n)} = \int_0^{a_3} (L^2 - x_3^2) V_m V_n'' dx_3 + \int_{a_3}^{L} (L^2 - x_3^2) V_m V_n'' dx_3, \quad (4.31)$$

$$\mathcal{I}_{3(m,n)} = \int_0^{a_3} V_m V_n'' dx_3 + \int_{a_3}^{L} V_m V_n'' dx_3 , \quad (4.32)$$

$$\mathcal{I}_{4(m,n)} = \int_0^{a_3} x_3 V_m V_n' dx_3 + \int_{a_3}^{L} x_3 V_m V_n' dx_3 , \quad (4.33)$$

$$\mathcal{I}_{5(m,n)} = \int_0^{a_3} V_m V_n'' dx_3 , \quad (4.34)$$

and

$$\hat{F}_m(\varphi_1) = -\frac{\ddot{\varphi}_3}{\dot{\varphi}_1^2}\left[C_2 \mathcal{I}_{6(m)} + C_3 V_m'(0) + C_9 V_m'(L) + C_{10} V_m(L)\right], \quad (4.35)$$

where

$$\mathcal{I}_{6(m)} = \int_0^{a_3} x_3 V_m dx_3 + \int_{a_3}^{L} x_3 V_m dx_3 . \quad (4.36)$$

Finally, equations (4.20) become:

$$\frac{d^2 q_m}{d\varphi_1^2} + \frac{C_{D3m}}{\gamma_m \dot{\varphi}_1} \sum_n \mathcal{I}_{1(m,n)} \frac{dq_n}{d\varphi_1} + \left(\frac{\omega_m^2}{\dot{\varphi}_1^2} - \hat{G}_5(\varphi_1)\right) q_m + \frac{1}{\gamma_m} \sum_n \hat{H}_{mn}(\varphi_1) q_n = \frac{\hat{F}_m(\varphi_1)}{\gamma_m} , \quad (4.37)$$

for m = 1,2,3,... .

E. Final Form of Solution

Determination of Bending Strain

After q_n is expressed as a function of φ_1, as shown in the previous section, the total solution according to equation (4.19) becomes:

$$V_3(x_3,\varphi_1) = \sum_{n}^{\infty} V_n(x_3) q_n(\varphi_1). \tag{4.38}$$

From the above, the maximum bending strain $\epsilon(x_3,\varphi_1)$ at any point x_3 on the rocker link is obtained according to:

$$\epsilon(x_3,\varphi_1) = \frac{M(x_3,\varphi_1)\, y_{max}}{E_3 I_3}, \tag{4.39}$$

where

$M(x_3,\varphi_1)$ = bending moment,

y_{max} = distance to extreme fiber.

The bending moment is given, from elementary stress theory with the help of equation (4.38), by:

$$M(x_3,\varphi_1) = -E_3 I_3 \sum_{n} \frac{\partial^2 V_n(x_3)}{\partial x_3^2} q_n(\varphi_1). \tag{4.40}$$

Substitution of equation (4.40) into (4.39) leads to the expression for the strain:

$$\epsilon(x_3,\varphi_1) = -y_{max} \sum_{n} \frac{\partial^2 V_n(x_3)}{\partial x_3^2} q_n(\varphi_1). \tag{4.41}$$

F. Solution of Hill-Type Differential Equations

The following section shows that because coupling between the infinite sets of Hill's equations was found to be weak, it is possible to treat the Hill's equation associated with each mode separately.

It also briefly outlines the review of the solution theory for Hill's equations given in Appendix H. There, it is shown how the homogeneous portion of the differential equation is used to determine the regions of instability of the system. In addition, it is pointed out that the steady-state response becomes unbounded for certain values of the parameter Λ. These "resonance locations" are associated with certain stability boundaries.

1. Decoupling of Equations

When doing the example problem shown in Section V, as well as one with a more realistic cross-section size, it became clear that the uncoupling of the infinite set of Hill's equations does not introduce great inaccuracy. Similar conclusions were drawn by H. Houben [13] in connection with a related mechanism problem.

When equations (4.37) are uncoupled, they are of the form:

$$\frac{d^2 q_m}{d\varphi_1^2} + \Delta_m \frac{dq_m}{d\varphi_1} + B_m(\varphi_1)\, q_m = \frac{\hat{F}_m(\varphi_1)}{N_m} , \qquad (4.42)$$

for $m = 1,2,3,\ldots$, where now

$$\Delta_m = \frac{C_{D3m}\, J_1(m,n)}{\dot{\varphi}_1\, N_m} , \qquad (4.43)$$

$$B_m(\varphi_1) = \Lambda_m + A_m(\varphi_1) \tag{4.44}$$

$$\Lambda_m = \left(\frac{\omega_m}{\dot{\varphi}_1}\right)^2 \tag{4.45}$$

and $A_m(\varphi_1)$ originates from the appropriate combination of the terms $\hat{G}_5(\varphi_1)$ and $\hat{H}_{mm}(\varphi_1)$, i.e.

$$A_m(\varphi_1) = \frac{\dot{\varphi}_3^2}{\dot{\varphi}_1^2}\left(-1 + \frac{1}{V_m}\left[\mu_3\left(J_{4(m,m)} - \frac{J_{2(m,m)}}{2}\right) + M(L+r_M)\left(V_m(L)V_m'(L) - J_{3(m,m)}\right)\right.\right.$$

$$\left.\left. + (\tilde{J} + Mr_M L)V_m'(L)V_m'(L) + J^* V_m'(0)V_m'(0)\right]\right) + \left[\frac{\ddot{\varphi}_2}{\dot{\varphi}_1^2 \sin(\varphi_3-\varphi_2)}\,\frac{J_{2\beta}}{a_2}\right.$$

$$\left. - \frac{\sin(\varphi_1-\varphi_2)}{\sin(\varphi_3-\varphi_2)}\,\frac{M_2 a_1}{2} + \frac{\ddot{\varphi}_3}{\dot{\varphi}_1^2}\cot(\varphi_3-\varphi_2)\left(\frac{J_{3D} + J^* + J_M + M(L+r_M)^2}{a_3}\right)\right]\frac{J_{5(m,m)}}{V_m}. \tag{4.46}$$

The terms $J_{i(m,m)}$, and V_m and $F_m(\varphi_1)$ are obtained from the appropriate expressions in the previous section.

2. Stability of Homogeneous Hill's Equations

The solution to a Hill's equation of the type of equation (4.42), i.e.

$$\frac{d^2q}{d\varphi_1^2} + \Delta\frac{dq}{d\varphi_1} + (\Lambda + A(\varphi_1))q = 0, \tag{4.47}$$

is stable or unstable depending upon the combination of Λ, Δ and various mechanism parameters contained in $A(\varphi_1)$. Specific combinations of the above furnish stability boundaries which separate stable from unstable regions.

a) Stability Boundaries for Undamped System

The 2π-periodic boundaries are found from the solution of the eigenvalue problem in $(-\Lambda)$ of a finite segment of the following Hill's determinant (see equation (H.21)):

$$\begin{vmatrix} \cdot & \cdot & \cdot & \cdot & \cdot & \cdot & \cdot \\ \cdot & -4+\beta_0+\Lambda & \beta_{-1} & \beta_{-2} & \beta_{-3} & \beta_{-4} & \cdot \\ \cdot & \beta_1 & -1+\beta_0+\Lambda & \beta_{-1} & \beta_{-2} & \beta_{-3} & \cdot \\ \cdot & \beta_2 & \beta_1 & \beta_0+\Lambda & \beta_{-1} & \beta_{-2} & \cdot \\ \cdot & \beta_3 & \beta_2 & \beta_1 & -1+\beta_0+\Lambda & \beta_{-1} & \cdot \\ \cdot & \beta_4 & \beta_3 & \beta_2 & \beta_1 & -4+\beta_0+\Lambda & \cdot \\ \cdot & \cdot & \cdot & \cdot & \cdot & \cdot & \cdot \end{vmatrix} = 0. \qquad (4.48)$$

The β's represent the coefficients of the Fourier expansion of $A(\varphi_1)$, (see equation (H.17)), which contain all the mechanism parameters.

Similarly, the 4π-periodic boundaries are found, according to equation (H.21), from the solution of the eigenvalue problem in $(-\Lambda)$ given by the following determinantal equation:

$$
\begin{vmatrix}
\cdot & \cdot & \cdot & \cdot & \cdot & \cdot & \cdot & \cdot \\
\cdot & -\frac{25}{4}+\beta_0+\Lambda & \beta_{-1} & \beta_{-2} & \beta_{-3} & \beta_{-4} & \beta_{-5} & \cdot \\
\cdot & \beta_1 & -\frac{9}{4}+\beta_0+\Lambda & \beta_{-1} & \beta_{-2} & \beta_{-3} & \beta_{-4} & \cdot \\
\cdot & \beta_2 & \beta_1 & -\frac{1}{4}+\beta_0+\Lambda & \beta_{-1} & \beta_{-2} & \beta_{-3} & \cdot \\
\cdot & \beta_3 & \beta_2 & \beta_1 & -\frac{1}{4}+\beta_0+\Lambda & \beta_{-1} & \beta_{-2} & \cdot \\
\cdot & \beta_4 & \beta_3 & \beta_2 & \beta_1 & -\frac{9}{4}+\beta_0+\Lambda & \beta_{-1} & \cdot \\
\cdot & \beta_5 & \beta_4 & \beta_3 & \beta_2 & \beta_1 & -\frac{25}{4}+\beta_0+\Lambda & \cdot \\
\cdot & \cdot & \cdot & \cdot & \cdot & \cdot & \cdot & \cdot
\end{vmatrix} = 0. \qquad (4.49)
$$

The solution of these eigenvalue problems for various combinations of mechanism parameters permits the fashioning of a "Strutt-chart [30]", which indicates stable and unstable regions. This is facilitated by Haupt's theorem [30], which states that regions between consecutive boundaries of similar periodicity are unstable, while those between boundaries of different periodicity are stable.

b) Stability Boundaries for Damped System

Section 1c of Appendix H shows how the damped homogeneous Hill's equation

$$\frac{d^2q}{d\varphi_1^2} + \Delta \frac{dq}{d\varphi_1} + B(\varphi_1)q = 0 \qquad (4.50)$$

may be transformed into an undamped one of the type:

$$\frac{d^2z}{d\varphi_1^2} + \left(\Lambda - \frac{\Delta^2}{4} + A(\varphi_1)\right)z = 0 \qquad (4.51)$$

by means of the substitution

$$q(\varphi_1) = e^{-\frac{\Delta}{2}\varphi_1} z(\varphi_1). \qquad (4.52)$$

In the above,

$$z(\varphi_1) = e^{\mu\varphi_1}\Phi(\varphi_1) \qquad (4.53)$$

represents the Floquet solution to Hill's equation, where μ is the characteristic exponent and $\Phi(\varphi_1)$ is a 2π-periodic function.

This transformation allows one to determine the stability of the solution for $q(\varphi_1)$ by way of the Hill's

determinant associated with $z(\varphi_1)$. Appendix H shows how the 2π and 4π-periodic stability boundaries of $q(\varphi_1)$ are determined by the eigenvalue problem of equation (H.34) with

$$\mu = \frac{\Delta}{2} \tag{4.54}$$

and

$$\mu = \frac{\Delta}{2} + \frac{1}{2} i \tag{4.55}$$

respectively.

This approach leads to difficulties when applied to the case of a mechanism where Δ is not a systems' constant in the usual sense, but is a function of the input angular velocity $\dot{\varphi}_1$. Since, according to equations (4.21) and (4.43),

$$\Delta = r \frac{\omega}{\dot{\varphi}_1} = r\sqrt{\Lambda} , \tag{4.56}$$

where

$$r = \frac{2 \mu_3 \xi J_1}{\nu} , \tag{4.57}$$

the Hill's determinant (H.34) associated with the 2π-periodic stability boundaries has, according to equations (4.54) and (4.56), the form:

$$\begin{vmatrix}
\cdot & \cdot & \cdot & \cdot & \cdot & \cdot & \cdot \\
\cdot & -4+\beta_0-2ri\sqrt{\Lambda}+\Lambda & \beta_{-1} & \beta_{-2} & \beta_{-3} & \beta_{-4} & \cdot \\
\cdot & \beta_1 & -1+\beta_0-ri\sqrt{\Lambda}+\Lambda & \beta_{-1} & \beta_{-2} & \beta_{-3} & \cdot \\
\cdot & \beta_2 & \beta_1 & \beta_0+\Lambda & \beta_{-1} & \beta_{-2} & \cdot \\
\cdot & \beta_3 & \beta_2 & \beta_1 & -1+\beta_0+ri\sqrt{\Lambda}+\Lambda & \beta_{-1} & \cdot \\
\cdot & \beta_4 & \beta_3 & \beta_2 & \beta_1 & -4+\beta_0+2ri\sqrt{\Lambda}+\Lambda & \cdot \\
\cdot & \cdot & \cdot & \cdot & \cdot & \cdot & \cdot
\end{vmatrix} = 0. \qquad (4.58)$$

The presence of the row-dependent coefficient in front of $\sqrt{\Lambda}$, in the term association with the main diagonal in each row, makes it impossible to solve this determinantal expression for Λ in the usual manner of an eigenvalue problem. Thus, it becomes necessary to devise a different means of solving for the stability boundaries of the damped Hill's equation.

Section 1 of Appendix H indicates a numerical method by which the characteristic exponent of the solution to a Hill's equation may be found when all systems' parameters are known. If this technique is applied to equation (4.51), one may determine the 2π and 4π-periodic stability boundaries of $q(\varphi_1)$ by searching for those values of Λ which lead to the values of the characteristic exponents given in equations (4.54) and (4.55).

Specifically, μ is determined from the characteristic equation:

$$\rho^2 - \Delta\rho + 1 = 0, \tag{4.59}$$

where

$$\rho_{1,2} = e^{2\pi\mu_{1,2}}, \tag{4.60}$$

and therefore

$$\mu_{1,2} = \frac{\ln \rho_{1,2}}{2\pi} \tag{4.61}$$

(see equation (H.6)).

The constant Δ is obtained from

$$\Delta = z_1(2\pi) + \frac{dz_2(2\pi)}{d\varphi_1}, \tag{4.62}$$

where $z_1(\varphi_1)$ and $z_2(\varphi_1)$ represent two linearly independent solutions to equation (4.51) which satisfy the initial conditions:

$$\left.\begin{aligned} z_1(0) &= 1, \quad \frac{dz_1(0)}{d\varphi_1} = 0, \\ z_2(0) &= 0, \quad \frac{dz_2(0)}{d\varphi_1} = 1. \end{aligned}\right\} \tag{4.63}$$

3. Particular Solution in Stable Regions and Resonance Condition

a) Solution Method

G. Kotowski [19] has shown by means of Variation of Parameters that the form of the particular solution of an equation of the type of (4.42), at all points in the stable regions, is a 2π-periodic Fourier series:

$$q_p(\varphi_1) = \frac{p_0}{2} + \sum_{m}^{\infty} \left(p_{cm} \cos m\varphi_1 + p_{sm} \sin m\varphi_1 \right). \tag{4.64}$$

Section 2a of Appendix H shows that when the functions $B(\varphi_1)$ and $\mathfrak{F}(\varphi_1) = \hat{F}_m(\varphi_1)/\mathfrak{N}_m$ are expressed in terms of the Fourier series (H.39) and (H.43) respectively, the coefficients in equation (4.64) can be determined from the infinite set of nonhomogeneous algebraic equations (see equation (H.53)):

$$\mathbb{B}\,\mathbb{P} = \mathbf{F}. \tag{4.65}$$

The coefficient matrix $\mathbb{B}$ and the column vectors $\mathbb{P}$ and $\mathbf{F}$ are defined according to equation (H.54) as follows:

$$
\begin{bmatrix}
\cdot & \cdot & \cdot & \cdot & \cdot & \cdot & \cdot & \cdot \\
\cdot & -9+\frac{b_0+b_{c6}}{2}+\Lambda & \frac{b_{c1}+b_{c5}}{2} & \frac{b_{c2}+b_{c4}}{2} & \frac{b_{c3}}{2} & \frac{b_{s4}-b_{s2}}{2} & \frac{b_{s5}-b_{s1}}{2} & 3\Delta+\frac{b_{s6}}{2} \\
\cdot & \frac{b_{c1}+b_{c5}}{2} & -4+\frac{b_0+b_{c4}}{2}+\Lambda & \frac{b_{c1}+b_{c3}}{2} & \frac{b_{c2}}{2} & \frac{b_{s3}-b_{s1}}{2} & 2\Delta+\frac{b_{s4}}{2} & \frac{b_{s1}+b_{s5}}{2} \\
\cdot & \frac{b_{c2}+b_{c4}}{2} & \frac{b_{c1}+b_{c3}}{2} & -1+\frac{b_0+b_{c2}}{2}+\Lambda & \frac{b_{c1}}{2} & \Delta+\frac{b_{s2}}{2} & \frac{b_{s1}+b_{s3}}{2} & \frac{b_{s2}+b_{s4}}{2} \\
\cdot & b_{c3} & b_{c2} & b_{c1} & b_0+\Lambda & b_{s1} & b_{s2} & b_{s3} \\
\cdot & \frac{b_{s4}-b_{s2}}{2} & \frac{b_{s3}-b_{s1}}{2} & -\Delta+\frac{b_{s2}}{2} & \frac{b_{s1}}{2} & -1+\frac{b_0+b_{c2}}{2}+\Lambda & \frac{b_{c1}-b_{c3}}{2} & \frac{b_{c2}-b_{c4}}{2} \\
\cdot & \frac{b_{s5}-b_{s1}}{2} & -\Delta 2+\frac{b_{s4}}{2} & \frac{b_{s1}+b_{s3}}{2} & \frac{b_{s2}}{2} & \frac{b_{c1}-b_{c3}}{2} & -4+\frac{b_0-b_{c4}}{2}+\Lambda & \frac{b_{c1}-b_{c5}}{2} \\
\cdot & -3\Delta+\frac{b_{s6}}{2} & \frac{b_{s5}+b_{s1}}{2} & \frac{b_{s4}-b_{s2}}{2} & \frac{b_{s3}}{2} & \frac{b_{c2}-b_{c4}}{2} & \frac{b_{c1}-b_{c5}}{2} & -9+\frac{b_0-b_{c6}}{2}+\Lambda \\
\cdot & \cdot & \cdot & \cdot & \cdot & \cdot & \cdot & \cdot
\end{bmatrix}
\begin{bmatrix} \cdot \\ p_{c3} \\ p_{c2} \\ p_{c1} \\ p_0 \\ p_{s1} \\ p_{s2} \\ p_{s3} \\ \cdot \end{bmatrix}
=
\begin{bmatrix} \cdot \\ f_{c3} \\ f_{c2} \\ f_{c1} \\ f_0 \\ f_{s1} \\ f_{s2} \\ f_{s3} \\ \cdot \end{bmatrix}
$$

(4.66)

In the above, b_0, b_{cm}, b_{sm} and f_0, f_{cm}, f_{sm} are the Fourier coefficients associated with $B(\varphi_1)$ and $\mathcal{F}(\varphi_1)$ respectively.

For a solution of a finite number of coefficients p_0, p_{cm}, p_{sm}, the infinite set of equations is reduced to a finite one by choosing a finite coefficient matrix $\mathbb{B}$ symmetrical in rows and columns with respect to the central element $\Lambda + \frac{b_0}{2}$. The resulting finite set of nonhomogeneous equations can then be solved by an appropriate numerical scheme.

b) Resonance Locations

Whenever the determinant of the coefficient matrix $\mathbb{B}$ of equation (4.65) vanishes, a condition of resonance occurs, i.e. the Fourier coefficients of equation (4.64) become unbounded. This occurs for those parameter combinations which correspond to the 2π-periodic stability boundaries of any mode of damped or undamped systems.

The above can be demonstrated by considering the first terms in equations (H.10) and (H.32) which show that a solution, for the undamped as well as the damped homogeneous systems respectively, is of 2π-periodic form at the 2π-periodic stability boundaries. Because of this, the Hill's determinant at any of the 2π-periodic stability boundaries is identical with the determinant of the coefficient matrix $\mathbb{B}$ at those locations.(*)

(*) While the Hill's determinant in equation (4.48) has been obtained in a different manner than the coefficient matrix $\mathbb{B}$ of equation (4.65), it could also have been derived by using a sine-cosine series, of the type of equation (H.38), for the $q_h(\varphi_1)$ involved.

Therefore, the values of Λ which locate the 2π-periodic stability boundaries also determine the positions of resonance.

G. Kotowski [19] has shown that all the coefficents of equation (4.64) increase somewhat in the vicinity of the stability boundaries when compared to locations further removed. The coefficients of that Fourier term, which is associated with a frequency equal to the natural frequency of the system, grows most under these circumstances. This selectivity of amplification was found by Kotowski to be most pronounced near those resonance locations associated with the larger values of Λ.

The present investigation has shown that this selective amplification of the coefficients associated with the Fourier terms corresponding to the natural frequency also occurs in locations which are completely stable due to damping, but contained a point-type 2π-periodic instability region when the system was undamped. (See Section V-G.)

V. EXAMPLE: APPLICATION OF THEORY AND COMPARISON WITH EXPERIMENT

A. Introduction

The theory of this dissertation is now applied to a specific example mechanism and the numerical results are compared with those of a corresponding experiment. Figure 5.1 shows the example mechanism and Table 5.1 lists dimensions and materials.

The in-line four-bar linkage consists of a relatively stiff aluminum coupler and a very thin, flexible brass rocker link with a counterweight m* and endmass M. The nature of the crank, which in the experimental setup was combined with a flywheel, is unimportant, since this link does not contribute in any way to the behavior of the rocker.

In order to avoid problems with existing equipment, it was decided to keep the range of mechanism speeds below 210 rpm. This decision necessitated the use of the very thin rocker link in order to obtain sufficiently large strains.

The specific choice of counterweight and endmass sizes was influenced by the need to keep the maximum deflections low enough not to violate small deflection theory at the higher speeds.

Two positions on the positive side (inside) of the rocker link are used to compare experiment to theory. These are

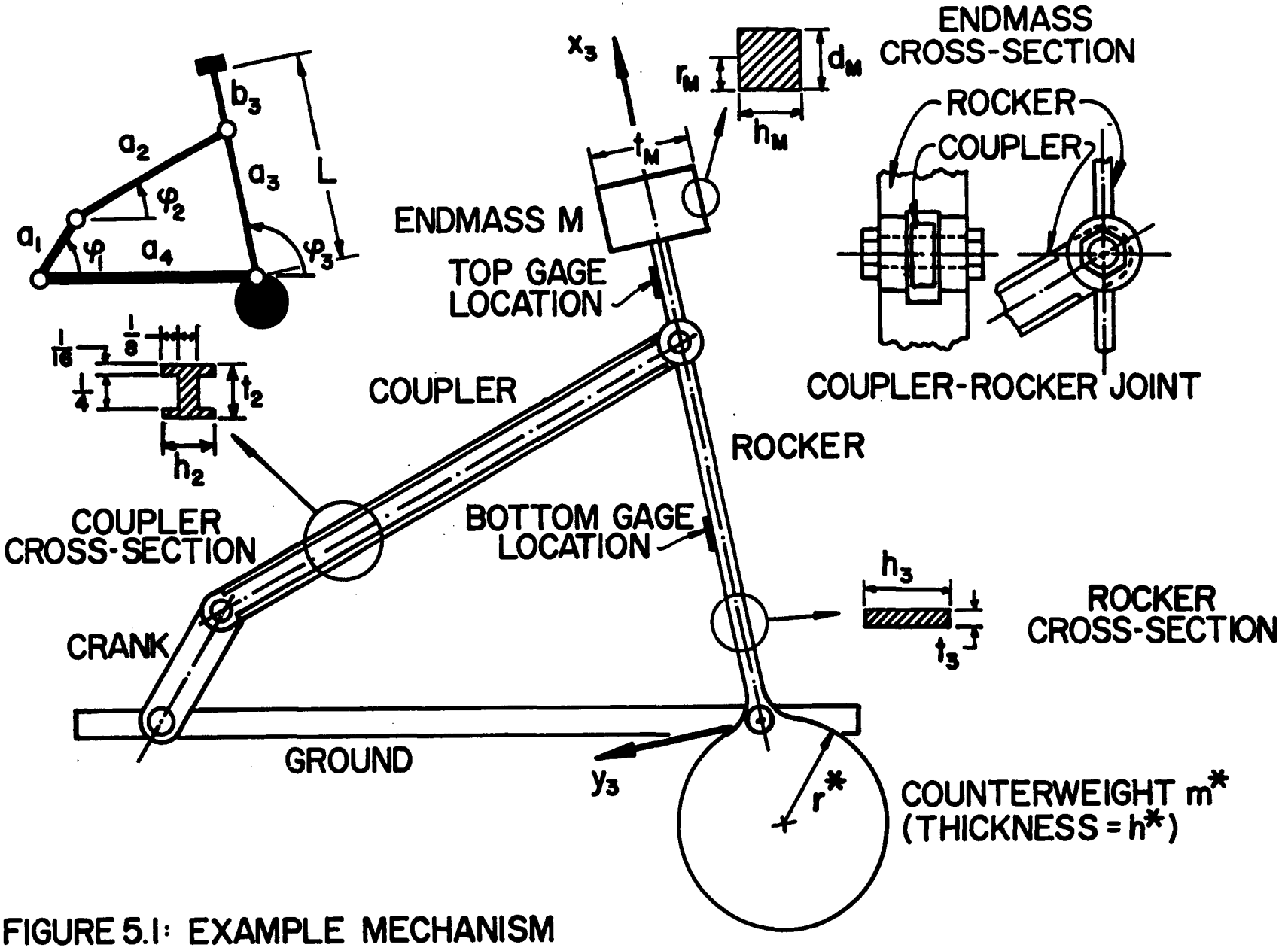

FIGURE 5.1: EXAMPLE MECHANISM

Link Lengths	Coupler (Aluminum)	Rocker (Brass)	Endmass (Brass)	Counterweight (Aluminum)
$a_1 = 1.640$ in	$E_2 = 1.0 \times 10^7$ psi	$E_3 = 15.5 \times 10^6$ psi	$r_M = 0.375$ in	$\rho^* = 0.259 \times 10^{-3} \frac{\text{lb-sec}^2}{\text{in}^4}$
$a_2 = 17.500$ in	$\rho_2 = 0.259 \times 10^{-3} \frac{\text{lb-sec}^2}{\text{in}^4}$	$\rho_3 = 0.776 \times 10^{-3} \frac{\text{lb-sec}^2}{\text{in}^4}$	$t_M = 1.067$ in	$r^* = 1.362$ in
$a_3 = 9.840$ in	$t_2 = 0.375$ in	$t_3 = 0.067$ in	$h_M = 0.750$ in	$t^* = 0.687$ in
$a_4 = 16.410$ in	$h_2 = 0.375$ in (+)	$h_3 = 0.687$ in	$d_M = 0.750$ in	$m^* = 0.104 \times 10^{-2} \frac{\text{lb-sec}^2}{\text{in}}$ (++)
$b_3 = 2.000$ in	$M_2 = 0.360 \times 10^{-3} \frac{\text{lb-sec}^2}{\text{in}}$	$M_3 = 0.422 \times 10^{-3} \frac{\text{lb-sec}^2}{\text{in}}$	$M = 0.466 \times 10^{-3} \frac{\text{lb-sec}^2}{\text{in}}$	
$L = 11.840$ in				

(+) See Figure 5.1 for detail.

(++) Accounts for manner of fixity to link.

Table 5.1 Example Mechanism Data

called top gage and bottom gage locations and are at $x_3 = 10.965$ in. and $x_3 = 4.920$ in. respectively, (see Figure 5.1).

The following summarizes the contents of this section and the results of the example:

Section B: The eigenvalues and shape functions of the rocker link are determined.

Section C: Coupled and uncoupled equations are given, and their numerical solutions are discussed.

Section D: The results of the numerical solution of coupled and uncoupled Hill's equations are compared and it is shown that uncoupling has little influence on the accuracy of the results. It is further found that at least three modes are required for an adequate description of the response.

Section E: The influence of the initial conditions is discussed, and the transient response on-resonance is compared with that off-resonance. The results of this section are later used to show that the experimental response is fully described by the particular solution.

Section F: A stability analysis is performed and it is shown that within the operating range of the mechanism there are neither 2π nor

4π-periodic instabilities as long as the damping ratio is larger than zero. The stability analysis also furnishes the resonance locations.

Section G: The particular solution is given for all three modes and it is shown that for sufficiently small values of ζ, the response on resonance differs dramatically from that off resonance. It is further demonstrated that this difference in response disappears for values of ζ larger than 0.034.

Section H: 1. The experiment confirms the absence of instabilities within the operating range, and clearly shows the difference between the steady-state responses on and off resonance.

2. A quantitative comparison between experimental and numerical results indicates good agreement, on and off resonance, throughout the operating range.

B. Eigenvalues and Shape Functions of Rocker Link

The first three eigenvalues of the sub-problem are obtained according to equation (F.47).(*) Subsequently, the associated eigenfunctions are determined with the help of equations (F.29) and (F.32). In addition, the second derivatives of the shape functions are found for the determination of the strain (according to equation (4.41)). Table 5.2 lists the above for the experimental mechanism.

(*) RTMI Routine, IBM System/360 Scientific Subroutine Package, (360A-CM-03X) Version III.

$0 \le x_3 \le a_3$:

$$V_n(x_3) = \sin\lambda_n x_3 + \Gamma_{1n}\sinh\lambda_n x_3 + \Gamma_{2n}(\cos\lambda_n x_3 - \cosh\lambda_n x_3)$$

$$V_n''(x_3) = \lambda_n^2\left(-\sin\lambda_n x_3 + \Gamma_{1n}\sinh\lambda_n x_3 - \Gamma_{2n}(\cos\lambda_n x_3 + \cosh\lambda_n x_3)\right)$$

$a_3^+ \le x_3 \le L$:

$$V_n(x_3) = \Gamma_{5n}\left[\sin\lambda_n(x_3-a_3) + \Gamma_{3n}\sinh\lambda_n(x_3-a_3) + \Gamma_{4n}\left(\cosh\lambda_n(x_3-a_3) - \cos\lambda_n(x_3-a_3)\right)\right]$$

$$V_n''(x_3) = \lambda_n^2\Gamma_{5n}\left[-\sin\lambda_n(x_3-a_3) + \Gamma_{3n}\sinh\lambda_n(x_3-a_3) + \Gamma_{4n}\left(\cosh\lambda_n(x_3-a_3) + \cos\lambda_n(x_3-a_3)\right)\right]$$

n	λ_n	ω_n (rpm)	Γ_{1n}	Γ_{2n}	Γ_{3n}	Γ_{4n}	Γ_{5n}
1	0.211	1159.3	0.408	0.546	-0.252	0.314	-1.943
2	0.279	2021.9	-140.1	-124.2	-0.606	0.535	-214.9
3	0.473	5815.4	-1.303	-1.320	-1.936	1.773	0.518

Table 5.2 Eigenvalues and Shape Functions of Rocker Link

C. Coupled and Uncoupled Hill's Equations: Discussion of Numerical Solution

The relative magnitudes of the strains due to the first three modes of the solution indicate that at least this number of modes is necessary for a meaningful description (see Table 5.4 and Figure 5.7). Accordingly, the first three Hill's equations must be solved for the $q_n(\varphi_1)$.

When the coupling between the equations is maintained, equation (4.37) becomes:

$$\frac{d^2q_1}{d\varphi_1^2} + \frac{C_{D31}}{\dot{\varphi}_1^2\gamma_1}\left[\mathcal{J}_{1(1,1)}\frac{dq_1}{d\varphi_1} + \mathcal{J}_{1(1,2)}\frac{dq_2}{d\varphi_1} + \mathcal{J}_{1(1,3)}\frac{dq_3}{d\varphi_1}\right] + \left[\frac{\omega_1^2}{\dot{\varphi}_1^2} - \hat{G}_5(\varphi_1) + \frac{\hat{H}_{11}(\varphi_1)}{\gamma_1}\right]q_1$$

$$+ \frac{\hat{H}_{12}(\varphi_1)}{\gamma_1}q_2 + \frac{\hat{H}_{13}(\varphi_1)}{\gamma_1}q_3 = \frac{\hat{F}_1(\varphi_1)}{\gamma_1}, \qquad (5.1)$$

$$\frac{d^2q_2}{d\varphi_1^2} + \frac{C_{D32}}{\dot{\varphi}_1^2\gamma_2}\left[\mathcal{J}_{1(2,1)}\frac{dq_1}{d\varphi_1} + \mathcal{J}_{1(2,2)}\frac{dq_2}{d\varphi_1} + \mathcal{J}_{1(2,3)}\frac{dq_3}{d\varphi_1}\right] + \frac{\hat{H}_{21}(\varphi_1)}{\gamma_2}q_1$$

$$+ \left[\frac{\omega_2^2}{\dot{\varphi}_1^2} - \hat{G}_5(\varphi_1) + \frac{\hat{H}_{22}(\varphi_1)}{\gamma_2}\right]q_2 + \frac{\hat{H}_{23}(\varphi_1)}{\gamma_2}q_3 = \frac{\hat{F}_2(\varphi_1)}{\gamma_2}, \qquad (5.2)$$

$$\frac{d^2q_3}{d\varphi_1^2} + \frac{C_{D33}}{\dot{\varphi}_1^2\gamma_3}\left[\mathcal{J}_{1(3,1)}\frac{dq_1}{d\varphi_1} + \mathcal{J}_{1(3,2)}\frac{dq_2}{d\varphi_1} + \mathcal{J}_{1(3,3)}\frac{dq_3}{d\varphi_1}\right] + \frac{\hat{H}_{31}(\varphi_1)}{\gamma_3}$$

$$+ \frac{\hat{H}_{32}(\varphi_1)}{\gamma_3}q_2 + \left[\frac{\omega_3^2}{\dot{\varphi}_1^2} - \hat{G}_5(\varphi_1) + \frac{\hat{H}_{33}(\varphi_1)}{\gamma_3}\right]q_3 = \frac{\hat{F}_3(\varphi_1)}{\gamma_3}. \qquad (5.3)$$

The constants γ_m, $\mathcal{J}_{1(m,n)}$, $\mathcal{J}_{2(m,n)}$,..., and $\mathcal{J}_{6(m)}$, together with their equations of origin are listed in Table 5.3.

The functions $\hat{G}_5(\varphi_1)$, $\hat{H}_{mn}(\varphi_1)$ and $\hat{F}_m(\varphi_1)$ are generated according to equations (4.27), (4.30) and (4.35) as part of the numerical solution of the differential equations. The associated kinematic expressions are listed in Appendix I.

When the coupling between the first three modes is neglected, equations (5.1), (5.2) and (5.3) take the form:

$$\frac{d^2q_1}{d\varphi_1^2} + \frac{C_{D31}\mathcal{J}_{1(1,1)}}{\dot{\varphi}_1\gamma_1}\frac{dq_1}{d\varphi_1} + \left[\frac{\omega_1^2}{\dot{\varphi}_1^2} - \hat{G}_5(\varphi_1) + \frac{\hat{H}_{11}(\varphi_1)}{\gamma_1}\right]q_1 = \frac{\hat{F}_1(\varphi_1)}{\gamma_1}, \qquad (5.4)$$

$$\frac{d^2q_2}{d\varphi_1^2} + \frac{C_{D32}\mathcal{J}_{1(2,2)}}{\dot{\varphi}_1\gamma_2}\frac{dq_2}{d\varphi_1} + \left[\frac{\omega_2^2}{\dot{\varphi}_1^2} - \hat{G}_5(\varphi_1) + \frac{\hat{H}_{22}(\varphi_1)}{\gamma_2}\right]q_2 = \frac{\hat{F}_2(\varphi_1)}{\gamma_2}, \qquad (5.5)$$

$$\frac{d^2q_3}{d\varphi_1^2} + \frac{C_{D33}\mathcal{J}_{1(3,3)}}{\dot{\varphi}_1\gamma_3}\frac{dq_3}{d\varphi_1} + \left[\frac{\omega_3^2}{\dot{\varphi}_1^2} - \hat{G}_5(\varphi_1) + \frac{\hat{H}_{33}(\varphi_1)}{\gamma_3}\right]q_3 = \frac{\hat{F}_3(\varphi_1)}{\gamma_3}. \qquad (5.6)$$

The applicable constants γ_m, $\mathcal{J}_{1(m,m)}$, $\mathcal{J}_{2(m,m)}$,..., and $\mathcal{J}_{6(m)}$ may again be taken from Table 5.3. The remaining functions $\hat{G}_5(\varphi_1)$, $\hat{H}_{mm}(\varphi_1)$ and $\hat{F}_m(\varphi_1)$ are again generated by the solution program.

γ_m: From Equation (F.53)		
m = 1	m = 2	m = 3
0.712×10^{-3}	0.865×10^{1}	0.584×10^{3}

$\mathcal{I}_{1(m,n)}$: From Equation (4.22)			
m \ n	1	2	3
1	0.342×10^{1}	-0.534×10^{2}	0.638×10^{1}
2	-0.534×10^{2}	0.994×10^{4}	-0.146×10^{3}
3	0.638×10^{1}	-0.146×10^{3}	0.138×10^{2}

$\mathcal{I}_{2(m,n)}$: From Equation (4.31)			
m \ n	1	2	3
1	-0.352×10^{2}	0.197×10^{4}	-0.709×10^{2}
2	0.126×10^{4}	-0.256×10^{6}	-0.900×10^{2}
3	-0.682×10^{2}	0.189×10^{4}	-0.197×10^{3}

$\mathcal{I}_{3(m,n)}$: From Equation (4.32)			
m \ n	1	2	3
1	-0.304	0.137×10^{2}	-0.754
2	0.993×10^{1}	-0.169×10^{4}	-0.778×10^{1}
3	-0.623	0.521×10^{1}	-0.177×10^{1}

$\mathcal{I}_{4(m,n)}$: From Equation (4.33)			
m \ n	1	2	3
1	0.112×10^{1}	0.504×10^{3}	-0.446×10^{1}
2	0.146×10^{3}	0.266×10^{5}	-0.486×10^{3}
3	-0.313×10^{1}	0.505×10^{3}	-0.676×10^{1}

$\mathcal{I}_{5(m,n)}$: From Equation (4.34)			
m \ n	1	2	3
1	-0.320	0.839×10^{1}	-0.625
2	0.839×10^{1}	-0.219×10^{4}	0.460×10^{1}
3	-0.625	0.460×10^{1}	-0.175×10^{1}

$\mathcal{I}_{6(m)}$: From Equation (4.36)		
m = 1	m = 2	m = 3
0.174×10^{2}	-0.911×10^{3}	0.507×10^{2}

Table 5.3 Values of Integrals
(Truncated computer results.)

The value of C_{D3m} (m = 1,2,3), according to equation (4.21), depends on the value selected for the damping ratio ζ.

Choosing the initial conditions for the numerical solution of the coupled or uncoupled equations presents a certain difficulty. Since the differential equations are only valid for $\ddot{\varphi}_1 = 0$, i.e. once the mechanism has come up to speed, there must be a definite value of $dq_n(\varphi_1)/d\varphi_1$ associated with each value of $q_n(\varphi_1)$. Initial conditions which do not exactly conform to the above will cause a considerable deviation from the experimental results until the resulting transients are damped out.

The following initial conditions were used:

$$\left.\begin{aligned} q_n(\varphi_{1s}) &= 0 \\ \frac{dq_n(\varphi_{1s})}{d\varphi_1} &= 0 \end{aligned}\right\}, \qquad (5.7)$$

and it was found that the transients could be minimized by choosing that starting angle φ_{1s} for which $\ddot{\varphi}_3$ was zero. This corresponds to $\varphi_{1s} = 115^{\circ}$. (See Figure 5.5.)

Both the coupled set and the uncoupled set of equations are solved using a fourth order Runge-Kutta(*) routine, with a step size of $\pi/720$ to increment the input angle φ_1.

Once the $q_n(\varphi_1)$ have been obtained in this manner, the deflection may be determined with the help of equation (4.38) and the strains by (4.41).

(*) RKGS Routine, IBM System/360 Scientific Subroutine Package, (360A-CM-03X) Version III.

D. Comparison of Results of Coupled and Uncoupled Hill's Equations

For the range of input angular velocities considered, the influence of coupling appears to be very small since the numerical solution of the uncoupled Hill's equations differs only very little from that of the coupled ones.

This result is demonstrated in Tables 5.4 and 5.5 for the nominal speeds of 193.3(*) and 160.0 rpm respectively. The numerical solutions for various strain values for the bottom gage and top gage locations are compared for the "first" and fortieth cycle of operation when the computation has been initiated at $\varphi_{1s} = 115^{\circ}$ in the cycle preceeding the "first". (Recall that the bottom gage is at $x_3 = 4.920$ in. and the top gage at $x_3 = 10.965$ in. .)

For all cases, $\zeta = 0.0025$. Table 5.4 shows mode by mode as well as total strain comparisons, while Table 5.5 compares only the total strain.

Note that the maximum differences for any given mode are between 0.3 and 0.6 μ in./in. .

(*) Actually 195.415 rpm. This accurate definition of rpm is necessary at resonance locations in order to observe the associated amplification of the higher harmonics. A few rpm difference was found between the resonance locations predicted by Runge-Kutta and those by the particular solution (and the stability analysis).

φ_1	Mode(1)		Mode(2)		Mode(3)		Total	
Degrees	C	UC	C	UC	C	UC	C	UC
0	59.0	59.2	- 9.0	- 9.0	-10.4	-10.7	39.6	39.4
10	71.0	71.3	-10.5	-10.5	-11.3	-11.8	49.2	48.9
20	71.9	72.2	- 9.9	- 9.9	-11.6	-12.2	50.4	50.0
30	63.8	64.1	-10.0	-10.0	-11.6	-12.1	42.3	42.0
40	54.6	54.9	-10.5	-10.6	-11.3	-11.6	32.8	32.6
50	50.3	50.4	- 9.0	- 9.1	-10.6	-10.9	30.7	30.5
60	49.8	50.0	- 7.1	- 7.1	- 9.3	- 9.5	33.4	33.3
70	46.9	47.0	- 6.7	- 6.7	- 7.6	- 7.8	32.6	32.5
80	36.4	36.5	- 5.6	- 5.6	- 5.8	- 5.8	25.0	25.0
90	20.1	20.1	- 3.0	- 3.0	- 4.0	- 4.1	13.0	13.0
100	5.2	5.2	- 1.7	- 1.7	- 2.5	- 2.5	0.9	0.9
110	- 2.3	- 2.3	- 1.4	- 1.4	- 1.0	- 1.0	- 4.7	- 4.7
120	- 3.2	- 3.3	0.6	0.6	0.6	0.6	- 2.0	- 2.1
130	- 4.7	- 4.7	2.6	2.6	2.3	2.2	0.2	0.2
140	-12.5	-12.5	2.7	2.7	3.8	3.8	- 6.0	- 6.0
150	-25.7	-25.7	3.5	3.5	5.1	5.0	-17.2	-17.2
160	-37.3	-37.3	5.5	5.5	6.0	5.8	-25.9	-26.0
170	-41.2	-41.2	6.0	6.0	6.7	6.6	-28.5	-28.6
180	-38.2	-38.1	5.6	5.6	7.5	7.4	-25.1	-25.1
190	-34.9	-34.9	6.9	6.9	8.3	8.2	-19.8	-19.8
200	-37.7	-37.6	7.9	7.9	8.9	8.8	-20.9	-21.0
210	-46.0	-45.9	7.1	7.1	9.1	9.0	-29.8	-29.8
220	-53.0	-52.9	7.0	7.0	9.1	8.9	-36.9	-37.0
230	-52.5	-52.4	8.1	8.1	8.9	8.8	-35.4	-35.5
240	-44.7	-44.7	7.6	7.6	8.8	8.7	-28.4	-28.4
250	-36.3	-36.3	6.3	6.3	8.6	8.5	-21.5	-21.5
260	-33.6	-33.5	6.6	6.6	8.0	7.9	-18.9	-19.0
270	-36.2	-36.1	6.5	6.5	7.1	7.0	-22.5	-22.6
280	-37.3	-37.3	4.5	4.5	5.8	5.7	-27.0	-27.0
290	-30.3	-30.3	3.2	3.2	4.3	4.2	-22.7	-22.8
300	-15.0	-15.0	2.9	2.9	2.6	2.6	- 9.5	- 9.5
310	2.1	2.0	0.8	0.8	0.7	0.7	3.5	3.5
320	14.2	14.2	- 2.1	- 2.1	- 1.5	- 1.5	10.6	10.6
330	20.7	20.7	- 3.2	- 3.2	- 4.0	- 4.0	13.5	13.5
340	27.2	27.2	- 4.8	- 4.8	- 6.5	- 6.6	15.9	15.9
350	39.0	39.1	- 7.7	- 7.7	- 8.6	- 8.8	22.6	22.6
360	55.5	55.7	- 9.2	- 9.3	-10.1	-10.5	36.1	36.0

C = Coupled; UC = Uncoupled

Table 5.4a Bottom Gage Strain in "First" Cycle (μ inches/inch).

193.3 rpm; $\varphi_{1s} = 115^{\circ}$; $\zeta = 0.0025$.

φ_1	Mode(1)		Mode(2)		Mode(3)		Total	
Degrees	C	UC	C	UC	C	UC	C	UC
0	25.3	25.4	42.6	42.7	7.5	7.7	75.4	75.9
10	30.5	30.6	49.5	49.6	8.2	8.5	88.1	88.8
20	30.9	31.0	46.6	46.7	8.4	8.8	85.8	86.5
30	27.4	27.5	47.0	47.1	8.4	8.7	82.8	83.4
40	23.5	23.6	49.8	49.8	8.2	8.4	81.4	81.8
50	21.6	21.7	42.7	42.7	7.6	7.8	71.9	72.2
60	21.4	21.4	33.4	33.4	6.7	6.9	61.5	61.7
70	20.2	20.2	31.6	31.7	5.5	5.6	57.3	57.5
80	15.6	15.7	26.5	26.5	4.2	4.2	46.3	46.4
90	8.6	8.6	14.1	14.2	2.9	2.9	25.7	25.7
100	2.2	2.2	8.2	8.2	1.8	1.8	12.2	12.2
110	- 1.0	- 0.9	6.5	6.5	0.7	0.7	6.3	6.3
120	- 1.4	- 1.4	- 2.9	- 2.9	- 0.4	- 0.4	- 4.7	- 4.8
130	- 2.0	- 2.0	-12.3	-12.3	- 1.6	- 1.6	-15.9	-15.9
140	- 5.4	- 5.3	-12.8	-12.8	- 2.8	- 2.7	-20.9	-20.8
150	-11.0	-11.0	-16.4	-16.3	- 3.6	- 3.6	-31.0	-30.9
160	-16.0	-16.0	-26.0	-26.0	- 4.3	- 4.2	-46.3	-46.2
170	-17.7	-17.7	-28.3	-28.3	- 4.8	- 4.8	-50.8	-50.7
180	-16.4	-16.4	-26.5	-26.5	- 5.4	- 5.3	-48.3	-48.2
190	-15.0	-15.0	-32.4	-32.4	- 6.0	- 5.9	-53.4	-53.3
200	-16.2	-16.2	-37.2	-37.2	- 6.4	- 6.3	-59.8	-59.7
210	-19.7	-19.7	-33.4	-33.3	- 6.6	- 6.5	-59.7	-59.5
220	-22.8	-22.7	-33.1	-33.0	- 6.5	- 6.4	-62.4	-62.2
230	-22.5	-22.5	-38.3	-38.3	- 6.4	- 6.3	-67.3	-67.1
240	-19.2	-19.2	-35.8	-35.8	- 6.3	- 6.2	-61.3	-61.2
250	-15.6	-15.6	-29.7	-29.7	- 6.2	- 6.1	-51.5	-51.4
260	-14.4	-14.4	-31.2	-31.2	- 5.8	- 5.7	-51.5	-51.4
270	-15.5	-15.5	-30.7	-30.7	- 5.1	- 5.1	-51.4	-51.3
280	-16.0	-16.0	-21.2	-21.2	- 4.2	- 4.1	-41.4	-41.3
290	-13.0	-13.0	-15.3	-15.3	- 3.1	- 3.0	-31.4	-31.4
300	- 6.4	- 6.5	-13.8	-13.8	- 1.9	- 1.9	-22.1	-22.1
310	0.9	0.9	- 3.6	- 3.6	- 0.5	- 0.5	- 3.2	- 3.2
320	6.1	6.1	9.8	9.8	1.1	1.1	17.0	17.0
330	8.9	8.9	15.3	15.3	2.9	2.9	27.1	27.1
340	11.7	11.7	22.5	22.6	4.7	4.8	38.9	39.0
350	16.8	16.8	36.5	36.6	6.2	6.4	59.5	59.8
360	23.8	23.9	43.6	43.7	7.3	7.6	74.8	75.2
C = Coupled; UC = Uncoupled								

Table 5.4b Top Gage Strain in "First" Cycle (μ inches/inch).

193.3 rpm; $\varphi_{1s} = 115^{\circ}$; $\zeta = 0.0025$.

φ_1	Mode(1)		Mode(2)		Mode(3)		Total	
Degrees	C	UC	C	UC	C	UC	C	UC
0	50.9	50.8	- 9.7	- 9.7	-10.6	-10.9	30.7	30.3
10	65.1	65.3	- 9.8	- 9.9	-11.5	-12.0	43.8	43.6
20	74.9	75.5	-10.0	-10.0	-11.8	-12.4	53.0	53.1
30	73.2	73.8	-10.7	-10.8	-11.7	-12.2	50.8	50.8
40	60.8	61.1	- 9.8	- 9.9	-11.1	-11.6	39.9	39.7
50	46.3	46.2	- 8.2	- 8.2	-10.2	-10.4	28.0	27.6
60	38.2	37.9	- 7.6	- 7.6	- 8.9	- 9.0	21.8	21.3
70	37.3	37.3	- 6.7	- 6.7	- 7.3	- 7.4	23.3	23.2
80	36.4	36.8	- 4.4	- 4.4	- 5.6	- 5.7	26.4	26.7
90	28.0	28.4	- 2.9	- 2.9	- 3.9	- 3.9	21.2	21.6
100	11.7	11.7	- 2.3	- 2.3	- 2.2	- 2.2	7.1	7.2
110	- 5.1	- 5.4	- 0.6	- 0.6	- 0.5	- 0.6	- 6.3	- 6.6
120	-13.9	-14.3	1.4	1.4	1.0	1.0	-11.5	-11.9
130	-13.8	-13.9	1.9	1.9	2.5	2.4	- 9.4	- 9.5
140	-12.1	-11.8	2.7	2.7	3.8	3.8	- 5.7	- 5.4
150	-17.0	-16.6	4.5	4.5	5.0	4.9	- 7.5	- 7.2
160	-29.6	-29.5	5.4	5.4	6.1	6.0	-18.2	-18.2
170	-42.7	-42.9	5.3	5.3	7.0	6.9	-30.4	-30.8
180	-47.8	-48.1	6.3	6.3	7.7	7.6	-33.8	-34.2
190	-43.6	-43.6	7.4	7.4	8.3	8.2	-27.9	-28.0
200	-37.1	-36.8	7.1	7.0	8.7	8.6	-21.3	-21.1
210	-36.9	-36.4	7.0	6.9	9.0	8.9	-20.9	-20.6
220	-44.4	-44.2	7.9	7.9	9.1	9.0	-27.4	-27.3
230	-52.9	-53.1	7.8	7.8	9.1	9.0	-36.0	-36.3
240	-53.7	-54.0	6.8	6.8	8.9	8.7	-38.0	-38.4
250	-44.9	-45.0	6.9	6.9	8.5	8.4	-29.5	-29.7
260	-33.3	-33.0	7.1	7.1	7.8	7.8	-18.4	-18.2
270	-27.2	-26.8	5.6	5.6	7.0	6.9	-14.6	-14.3
280	-28.5	-28.3	4.5	4.5	5.9	5.8	-18.1	-18.1
290	-30.3	-30.6	4.2	4.2	4.5	4.4	-21.7	-22.0
300	-24.0	-24.4	2.6	2.6	2.7	2.7	-18.7	-19.1
310	- 7.2	- 7.3	0.1	0.1	0.7	0.7	- 6.4	- 6.5
320	13.4	13.6	- 1.3	- 1.3	- 1.6	- 1.6	10.5	10.8
330	28.6	29.0	- 2.7	- 2.7	- 3.9	- 3.9	22.0	22.3
340	35.4	35.6	- 5.5	- 5.5	- 6.2	- 6.3	23.7	23.7
350	38.8	38.7	- 7.6	- 7.6	- 8.3	- 8.5	22.9	22.6
360	46.3	46.1	- 8.2	- 8.3	-10.1	-10.3	28.0	27.6

C = Coupled; UC = Uncoupled

Table 5.4c Bottom Gage Strain in Fortieth Cycle (μ inches/inch). 193.3 rpm; $\varphi_{1s} = 115^{\circ}$; $\zeta = 0.0025$.

φ_1	Mode(1)		Mode(2)		Mode(3)		Total	
Degrees	C	UC	C	UC	C	UC	C	UC
0	21.9	21.8	45.7	45.8	7.6	7.8	75.2	75.5
10	27.9	28.1	46.1	46.2	8.3	8.6	82.3	82.9
20	32.2	32.4	47.2	47.4	8.5	8.9	87.9	88.8
30	31.4	31.7	50.7	50.8	8.4	8.8	90.5	91.3
40	26.1	26.2	46.5	46.6	8.0	8.3	80.7	81.2
50	19.9	19.8	38.6	38.6	7.3	7.5	65.8	66.0
60	16.4	16.3	35.8	35.9	6.4	6.5	58.6	58.6
70	16.0	16.0	31.5	31.6	5.3	5.3	52.8	52.9
80	15.7	15.8	20.8	20.8	4.1	4.1	40.5	40.7
90	12.0	12.2	13.6	13.6	2.8	2.8	28.5	28.7
100	5.0	5.0	11.0	11.0	1.6	1.6	17.5	17.6
110	- 2.2	- 2.3	2.8	2.8	0.4	0.4	1.0	0.9
120	- 6.0	- 6.1	- 6.6	- 6.6	- 0.7	- 0.7	-13.3	-13.5
130	- 5.9	- 6.0	- 9.1	- 9.2	- 1.8	- 1.8	-16.9	-16.9
140	- 5.2	- 5.1	-12.5	-12.5	- 2.7	- 2.7	-20.5	-20.3
150	- 7.3	- 7.1	-21.2	-21.2	- 3.6	- 3.6	-32.1	-31.9
160	-12.7	-12.7	-25.3	-25.3	- 4.4	- 4.3	-42.4	-42.3
170	-18.3	-18.4	-24.8	-24.8	- 5.1	- 5.0	-48.2	-48.2
180	-20.5	-20.7	-29.6	-29.6	- 5.6	- 5.5	-55.7	-55.8
190	-18.7	-18.7	-35.0	-35.0	- 6.0	- 5.9	-59.7	-59.6
200	-15.9	-15.8	-33.3	-33.3	- 6.3	- 6.2	-55.5	-55.3
210	-15.8	-15.6	-32.8	-32.8	- 6.5	- 6.4	-55.1	-54.9
220	-19.1	-19.0	-37.4	-37.4	- 6.6	- 6.5	-63.0	-62.8
230	-22.7	-22.8	-36.8	-36.8	- 6.6	- 6.5	-66.1	-66.1
240	-23.1	-23.2	-32.1	-32.1	- 6.4	- 6.3	-61.6	-61.6
250	-19.3	-19.3	-32.8	-32.8	- 6.1	- 6.0	-58.2	-58.1
260	-14.3	-14.2	-33.3	-33.3	- 5.7	- 5.6	-53.3	-53.1
270	-11.7	-11.5	-26.5	-26.5	- 5.1	- 5.0	-43.3	-43.0
280	-12.2	-12.2	-21.0	-21.0	- 4.3	- 4.2	-37.5	-37.4
290	-13.0	-13.1	-19.7	-19.6	- 3.2	- 3.2	-35.9	-36.0
300	-10.3	-10.5	-12.2	-12.2	- 2.0	- 2.0	-24.4	-24.6
310	- 3.1	- 3.2	- 0.4	- 0.5	- 0.5	- 0.5	- 4.0	- 4.1
320	5.7	5.8	6.0	6.0	1.1	1.1	12.9	13.0
330	12.3	12.5	12.9	12.9	2.8	2.8	28.0	28.2
340	15.2	15.3	26.1	26.2	4.5	4.6	45.8	46.0
350	16.7	16.6	35.8	35.8	6.0	6.1	58.4	58.6
360	19.9	19.8	38.9	39.0	7.2	7.4	66.1	66.3

C = Coupled; UC = Uncoupled

Table 5.4d Top Gage Strain in Fortieth Cycle (μ inches/inch).

193.3 rpm; $\varphi_{1s} = 115^{\circ}$; $\zeta = 0.0025$.

φ_1	Bottom Gage		Top Gage	
Degrees	C	UC	C	UC
0	23.1	23.0	46.7	46.9
10	30.8	30.6	55.1	55.4
20	31.8	31.7	60.3	60.6
30	27.6	27.5	54.8	55.1
40	22.6	22.5	52.4	52.6
50	22.5	22.4	50.1	50.2
60	24.6	24.6	42.4	42.5
70	20.4	20.4	37.5	37.6
80	11.7	11.7	27.9	27.9
90	5.4	5.4	15.7	15.7
100	3.8	3.9	12.0	12.0
110	5.1	5.1	5.6	5.6
120	1.9	2.0	- 3.9	- 3.9
130	- 6.7	- 6.7	- 9.4	- 9.4
140	-12.0	-12.0	-18.6	-18.6
150	-11.3	-11.3	-24.1	-24.0
160	- 9.7	- 9.7	-23.8	-23.7
170	-11.5	-11.5	-30.8	-30.7
180	-18.0	-18.0	-36.4	-36.4
190	-22.4	-22.4	-37.5	-37.4
200	-19.3	-19.4	-41.3	-41.2
210	-15.7	-15.7	-39.6	-39.5
220	-17.0	-17.0	-38.5	-38.4
230	-21.1	-21.1	-43.8	-43.7
240	-23.3	-23.4	-41.8	-41.7
250	-19.3	-19.3	-37.6	-37.5
260	-13.0	-13.0	-36.1	-36.1
270	-12.7	-12.8	-29.9	-29.9
280	-15.3	-15.3	-27.1	-27.1
290	-13.8	-13.8	-24.1	-24.1
300	- 7.1	- 7.1	-11.3	-11.3
310	1.9	1.9	- 1.4	- 1.4
320	6.2	6.2	7.0	7.0
330	6.2	6.2	19.4	19.4
340	10.5	10.5	27.6	27.7
350	19.7	19.7	38.8	38.9
360	27.6	27.5	52.0	52.2

C = Coupled; UC = Uncoupled

Table 5.5a Total "First" Cycle Strain (μinches/inch).
160.0 rpm; $\varphi_{1s} = 115^{\circ}$; $\zeta = 0.0025$.

φ_1	Bottom Gage		Top Gage	
Degrees	C	UC	C	UC
0	27.0	26.9	49.7	49.9
10	29.1	29.0	56.9	57.2
20	28.0	27.9	57.4	57.7
30	26.3	26.2	54.4	54.6
40	25.3	25.2	54.1	54.3
50	25.0	24.9	48.5	48.6
60	21.8	21.8	41.0	41.1
70	15.4	15.3	34.9	35.0
80	10.5	10.5	24.5	24.5
90	7.9	8.0	17.0	17.0
100	5.9	6.0	12.1	12.1
110	2.8	2.8	2.2	2.2
120	- 2.9	- 2.9	- 5.2	- 5.2
130	- 7.7	- 7.7	-10.9	-10.9
140	- 8.6	- 8.6	-18.8	-18.8
150	- 9.3	- 9.3	-21.9	-21.9
160	-11.9	-11.9	-26.0	-26.0
170	-15.5	-15.6	-33.4	-33.3
180	-18.8	-18.8	-35.3	-35.2
190	-18.5	-18.5	-37.3	-37.3
200	-16.9	-16.9	-40.3	-40.2
210	-18.2	-18.3	-39.3	-39.2
220	-20.5	-20.6	-41.7	-41.6
230	-21.3	-21.3	-43.2	-43.2
240	-19.7	-19.8	-39.2	-39.1
250	-16.6	-16.6	-38.1	-38.0
250	-15.6	-15.6	-36.1	-36.1
270	-16.6	-16.6	-31.1	-31.0
280	-14.8	-14.8	-28.6	-28.5
290	-10.2	-10.2	-21.2	-21.2
300	- 4.9	- 4.9	-10.7	-10.7
310	- 0.6	- 0.6	- 4.0	- 4.1
320	2.0	2.0	6.4	6.4
330	6.4	6.4	18.3	18.3
340	14.2	14.2	27.8	27.8
350	21.1	21.0	40.5	40.6
360	24.8	24.7	49.1	49.3
C = Coupled; UC = Uncoupled				

Table 5.5b Total Fortieth Cycle Strain (μinches/inch). 160.0 rpm; $\varphi_{1s} = 115^{\circ}$; $\zeta = 0.0025$.

E. Determination of Strain Response by Numerical Solution of Uncoupled Equations: Transient and Steady State Behavior

A comparison of the transient and steady state responses of the uncoupled Hill's equations, as obtained by a numerical solution, is necessary in order to arrive at an appropriate interpretation of the experimental results. To this end, this section shows with Figures 5.2 to 5.4 the influence of the initial conditions on the transient response of the system as well as the dramatic difference in the steady state response on and off-resonance.(*)

The off-resonance location chosen is 190 rpm, while the on-resonance location is nominally 193.3 rpm, which corresponds to the "sixth"(**) resonance associated with the first mode. Where appropriate, the responses of the bottom and top gage locations are each compared with their particular solutions (see Section V-G) since it took too many cycles to converge to a steady state with the value of $\zeta = 0.0025$ used. (Larger, but less realistic values of the damping ratio cause a more rapid convergence to the steady state.)

(*) The term resonance refers to an amplification of the particular solution which occurs at specific input speeds. These speeds are associated with the undamped 2π-periodic stability boundaries (see Section V-F-1 below). For the mechanism and speed range considered, these speeds are whole numbered fractions of each natural frequency of the link.

(**) The "first" resonance location corresponds to the natural frequency itself. 193.3 rpm corresponds to "one-sixth" of the first mode natural frequency of 1159.3 rpm (see Table 5.2).

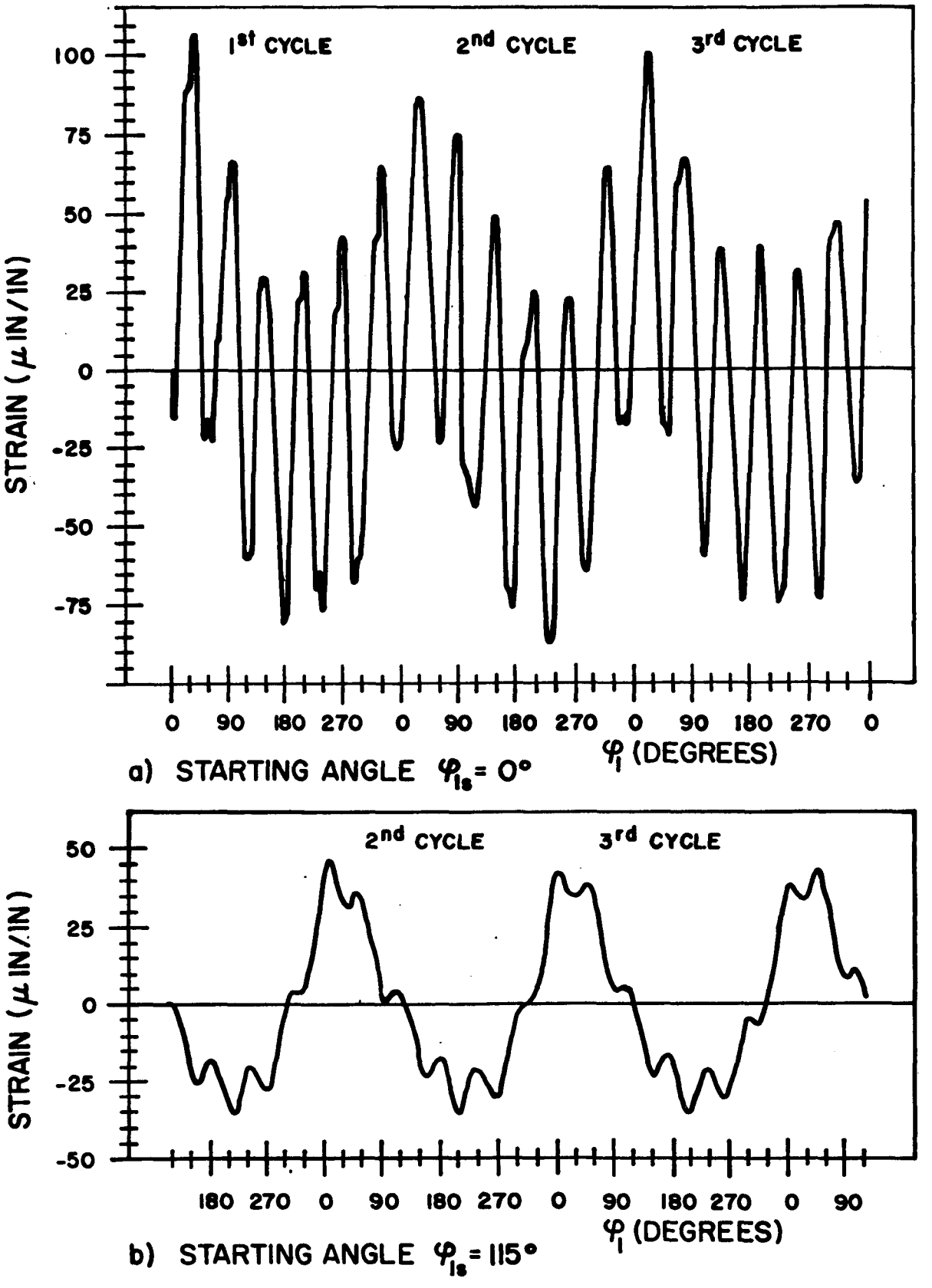

FIGURE 5.2: INFLUENCE OF INITIAL CONDITIONS ON TOTAL RESPONSE. BOTTOM GAGE LOCATION, 190 RPM. (ζ=0.0025)

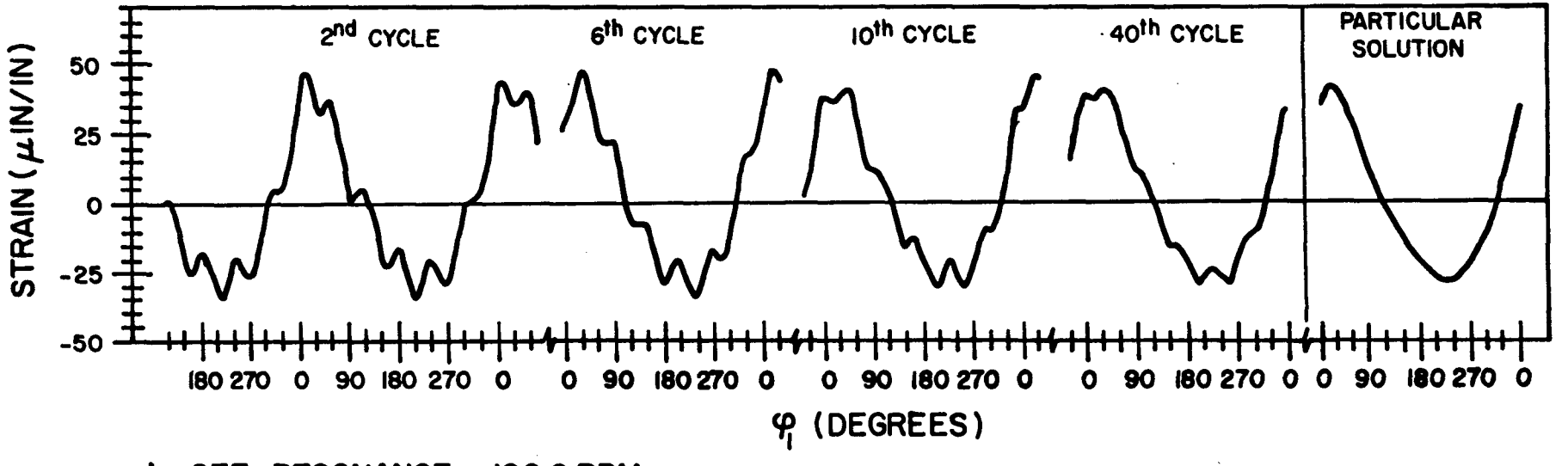

a) OFF RESONANCE: 190.0 RPM

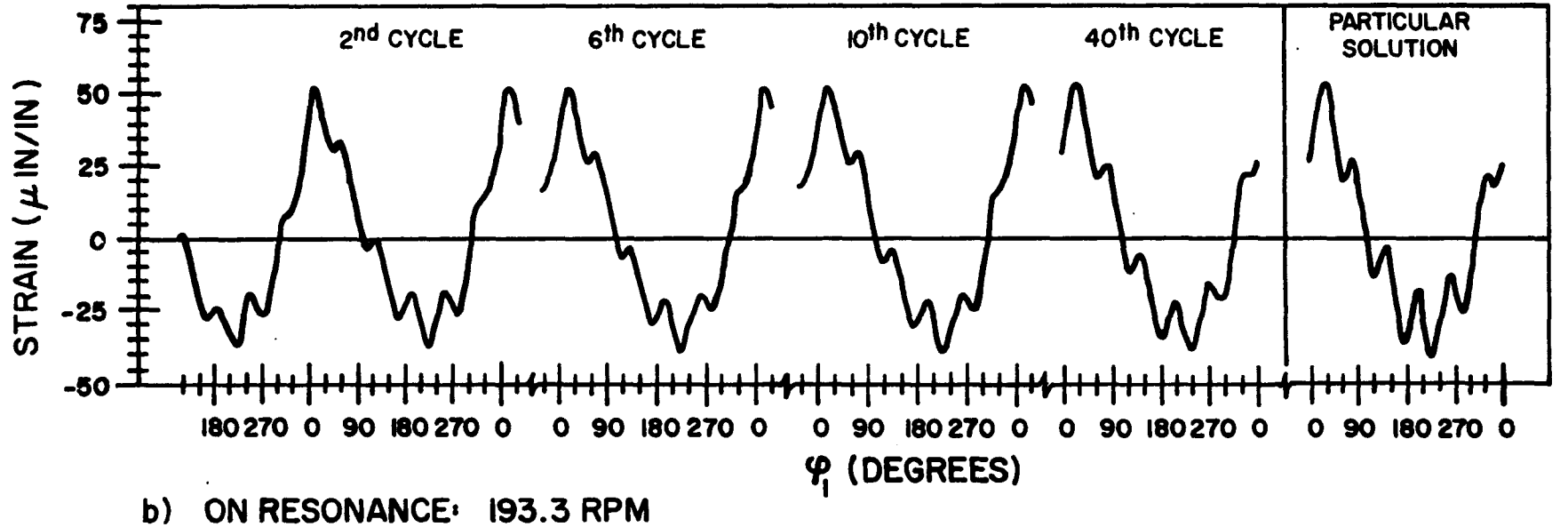

b) ON RESONANCE: 193.3 RPM

FIGURE 5.3: COMPARISON OF RESPONSES ON AND OFF RESONANCE
BOTTOM GAGE LOCATION: $\varphi_{is} = 115°$ ($\zeta = 0.0025$)

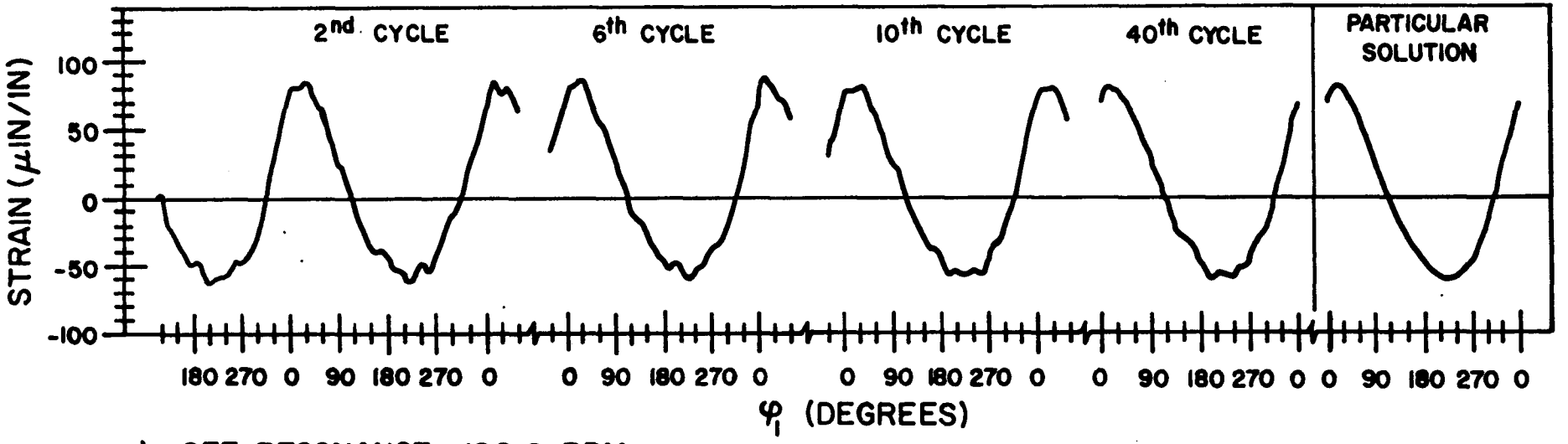

a) OFF RESONANCE: 190.0 RPM

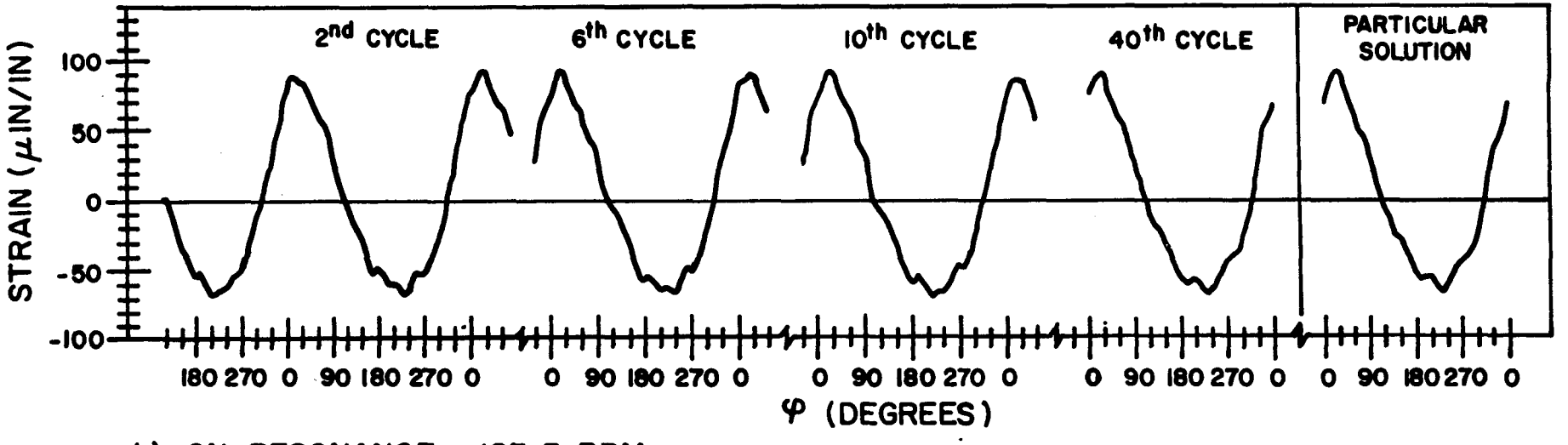

b) ON RESONANCE: 193.3 RPM

FIGURE 5.4: COMPARISON OF RESPONSES ON AND OFF RESONANCE
TOP GAGE LOCATION: $\varphi_{ls} = 115°$ ($\zeta = 0.0025$)

Discussion of Figures 5.2 to 5.4

a) Figure 5.2 shows that the strain amplitude during the early cycles is greatly influenced by the starting angle φ_{1s}. This may be explained with the help of Figure 5.5, which gives the ratio $\ddot{\varphi}_3/\dot{\varphi}_1^2$ as a function of the input angle φ_1. While the value of $\ddot{\varphi}_3$ is near a maximum at $\varphi_1 = 0^\circ$, it vanishes near 115°. Thus, for $\varphi_{1s} = 115^\circ$, the forcing terms in the differential equation are more gradually applied when the solution is started. (See also discussion in Section V-C.)

b) The shape of the solution at resonance (193.3 rpm nominal) is quite different from that off-resonance (190.0 rpm), both early and late in the course of operation. This is shown by Figure 5.3, which gives the response of the bottom gage location for a starting angle $\varphi_{1s} = 115^\circ$. For the resonance location, the contribution of the complementary solution, which is 2π-periodic there, is, as long as it exists, always in phase with the 2π-periodic particular portion of the solution. Off resonance the contribution of the complementary portion is not 2π-periodic and therefore, appears as a travelling wave on top of the fundamental frequency of the particular solution. This difference is illustrated by the appearance of the second, sixth, tenth and fortieth cycles of both types of responses. (For details on homogeneous solution see Appendix H.) Once the contribution of the complementary portion has been damped out, the solution at the resonance position reflects the presence of an amplified higher harmonic of the particular solution. Off the resonance position the wave

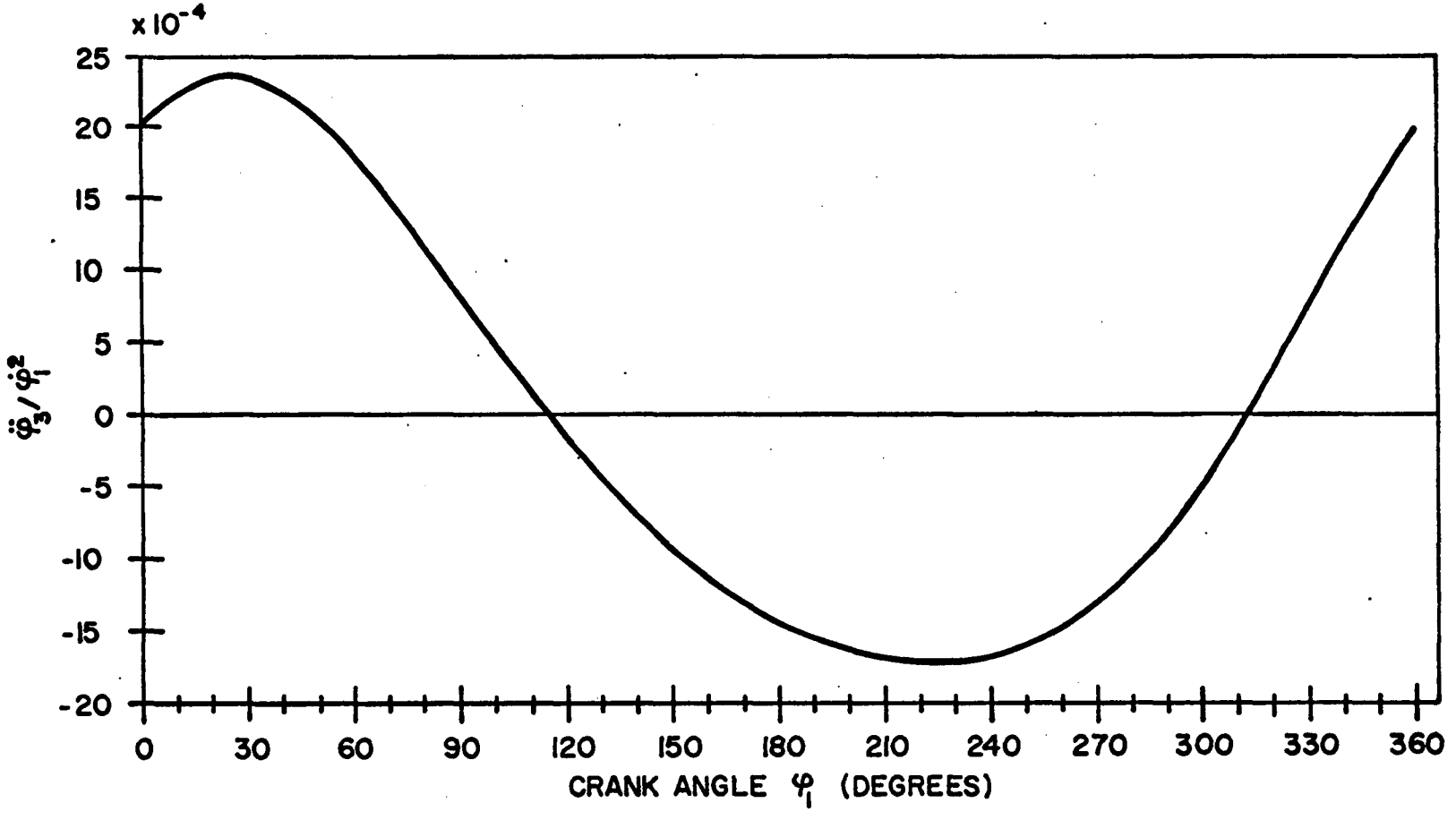

FIGURE 5.5: DIMENSIONLESS ANGULAR ACCELERATION OF ROCKER

only shows the first harmonic of the response which corresponds to the input angular velocity of the mechanism.

Figure 5.4 shows that the resonance phenomena are less pronounced for the top gage location. This occurs because the contribution of the second mode is greater here than that of the first mode. (At the bottom gage location the first mode prevails, see Section V-G.)

c) The in-phase condition of the complementary and particular portions of the solution at resonance seems to cause a more rapid convergence to the steady state.

It should be noted that in searching for resonance locations, i.e.the 2π-periodic boundaries of the first mode, by numerically solving equation (5.4) alone, it was found that they were a few rpm removed from those predicted by the stability analysis (see Section V-F). These locations were found by letting $\zeta = 0$ and looking for those rpm for which the amplitude of $q_1(\varphi_1)$ increased without bound. Very detailed searches with small increments in rpm were necessary. The "running away" of $q_1(\varphi_1)$ (i.e., the monotonically increasing peak to peak amplitudes) occured at a very slow rate.

F. Stability Analysis

The following represents a stability analysis of the first three uncoupled modes of the rocker link.

1. Stability Analysis of Undamped Equations

The 2π and 4π-periodic stability boundaries, for each of the undamped, homogeneous portions of the differential equations (5.4), (5.5) and (5.6), may be found by solving the eigenvalue problems indicated by equations (4.48) and (4.49) respectively.

The size of the matrix selected depends on the number of stability boundaries desired. Increasing the matrix size increases the number of stability boundaries associated with ever larger values of Λ. (Recall that the larger Λ, the lower the corresponding input speed of the mechanism.) Of course, increasing the matrix size also increases the numerical accuracy of the eigenvalues.

A (21x21) matrix was used for locating the 2π-periodic boundaries, and a (20x20) matrix for the 4π-periodic boundaries. This allows the exploration of the 2π-periodic stability boundaries for values of Λ up to approximately 100, and 4π-periodic stability boundaries for values of Λ up to approximately 90 (see Table 5.7). It confines the investigation to speeds larger than 116 rpm for the first mode, 202 rpm for the second mode, and 581 rpm for the third. (In an engineering problem where such a limitation prevents attaining necessary information, larger matrices must be chosen.)

The periodic coefficients in equations (5.4), (5.5)

and (5.6) are expressed in terms of complex Fourier series according to equation (H.17).(*) Table 5.6 lists the values of the complex β_n ($n = 0, \pm1, \pm2, \ldots, \pm20$) of each of the three modes. A complex QR-algorithm is used to solve the eigenvalue problems.

Table 5.7 serves as an example for the values of Λ and corresponding values of rpm associated with the 2π and 4π-periodic boundaries of the first mode respectively. It may be seen that some of the instability regions have a finite width while most others are only points.(**) Amongst the 2π-periodic regions, for example there is one of finite width between $\Lambda = 0.85$ and $\Lambda = 1.13$. The two values $\Lambda = 99.98$ represent a double root, and with that only an instability point. The negative value of Λ which appears in the table is a valid mathematical result, but has no physical meaning in mechanism problems and is therefore neglected.

To obtain the input angular velocity $\dot{\varphi}_1$ corresponding to a particular value of Λ, one makes use of equation (4.45), i.e.

$$\dot{\varphi}_1 = \frac{\omega}{\sqrt{\Lambda}}, \tag{5.8}$$

where ω represents the natural frequency of the mode under investigation.

(*) The results were determined numerically.

(**) In a larger stability chart, where some mechanism parameters are varied, this would reflect itself as one point of an instability line [30].

n	$\beta_n = a + bi = (a,b)$		
	Mode 1	Mode 2	Mode 3
0	(0.218865E-01, 0.0)	(0.282563E-01, 0.0)	(-0.552500E-01, 0.0)
1	(-0.164123E 00, 0.829161E-01)	(-0.911746E-01, 0.466088E-01)	(-0.111250E 01, 0.555128E 00)
2	(-0.804970E-01, 0.862225E-01)	(-0.483130E-01, 0.558943E-01)	(-0.500177E 00, 0.483326E 00)
3	(-0.155191E-01, 0.166948E-01)	(-0.912660E-02, 0.107204E-01)	(-0.988036E-01, 0.948758E-01)
4	(-0.318492E-02, 0.279665E-02)	(-0.188301E-02, 0.179137E-02)	(-0.201506E-01, 0.159498E-01)
5	(-0.548302E-03, 0.416531E-03)	(-0.324169E-03, 0.266078E-03)	(-0.346907E-02, 0.238474E-02)
6	(-0.905652E-04, 0.584969E-04)	(-0.535980E-04, 0.373315E-04)	(-0.572321E-03, 0.335364E-03)
7	(-0.141270E-04, 0.773835E-05)	(-0.835982E-05, 0.495252E-05)	(-0.892842E-04, 0.441864E-04)
8	(-0.216517E-05, 0.920027E-06)	(-0.128284E-05, 0.611441E-06)	(-0.136643E-04, 0.496722E-05)
9	(-0.319456E-06, 0.155738E-07)	(-0.199290E-06, 0.327208E-07)	(-0.188939E-05,-0.198861E-06)
10	(-0.679975E-07,-0.263817E-06)	(-0.547217E-07,-0.146908E-06)	(-0.246566E-06,-0.178383E-05)
	$\beta_n = 0$ for $n > 10$: $\beta_{-n} = \overline{\beta}_n$ (complex conjugate).		

Table 5.6 Complex Fourier Coefficients

2π Boundary Points			4π Boundary Points		
Λ	$\omega_1/\dot{\Phi}_1$	Corresponding rpm	Λ	$\omega_1/\dot{\Phi}_1$	Corresponding rpm
-0.08		imaginary	0.04	0.202	5747.16
0.85	0.922	1257.14	0.36	0.601	1927.30
1.13	1.283	1089.33	2.20	1.483	781.76
3.97	1.994	581.46	2.29	1.512	766.77
4.00	1.999	579.93	6.23	2.496	464.44
8.98	2.997	386.85	6.23	2.497	464.29
8.98	2.997	386.83	12.23	3.497	331.49
15.98	3.997	290.01	12.23	3.497	331.49
15.98	3.997	290.00	20.23	4.498	257.75
24.98	4.998	231.96	20.23	4.498	257.75
24.98	4.998	231.95	30.23	5.498	210.85
35.98	5.998	193.27	30.23	5.498	210.85
35.98	5.998	193.27	42.23	6.498	178.40
48.98	6.998	165.65	42.23	6.498	178.40
48.98	6.998	165.65	56.23	7.499	154.60
63.98	7.999	144.93	56.23	7.499	154.60
63.98	7.999	144.93	72.23	8.499	136.41
80.98	8.999	128.83	72.23	8.499	136.41
80.98	8.999	128.83	90.23	9.499	122.04
99.98	9.999	115.94	90.23	9.499	122.04
99.98	9.999	115.94			

Table 5.7 2π and 4π-Periodic Stability Boundaries

Similar to the condition found in a "Strutt-Chart" for the Mathieu equation, whenever a 2π-periodic instability region is given by a point, the value of $\dot{\varphi}_1$ is near a whole numbered fraction of the natural frequency $\omega_1 = 1159.3$ rpm. (See appropriate $\omega_1/\dot{\varphi}_1$ column in Table 5.7.)

Figure 5.6 presents the results of the stability analysis for all modes in the form of a graph for a speed range of 116 to 800 rpm. While 250 rpm represents a practical upper limit for this type of link, the above data are extended beyond that speed for the sake of the information they convey. Note especially the increasing width of the instability regions (in the first mode) as the rpm increase. A point type region is indicated by the letter P.

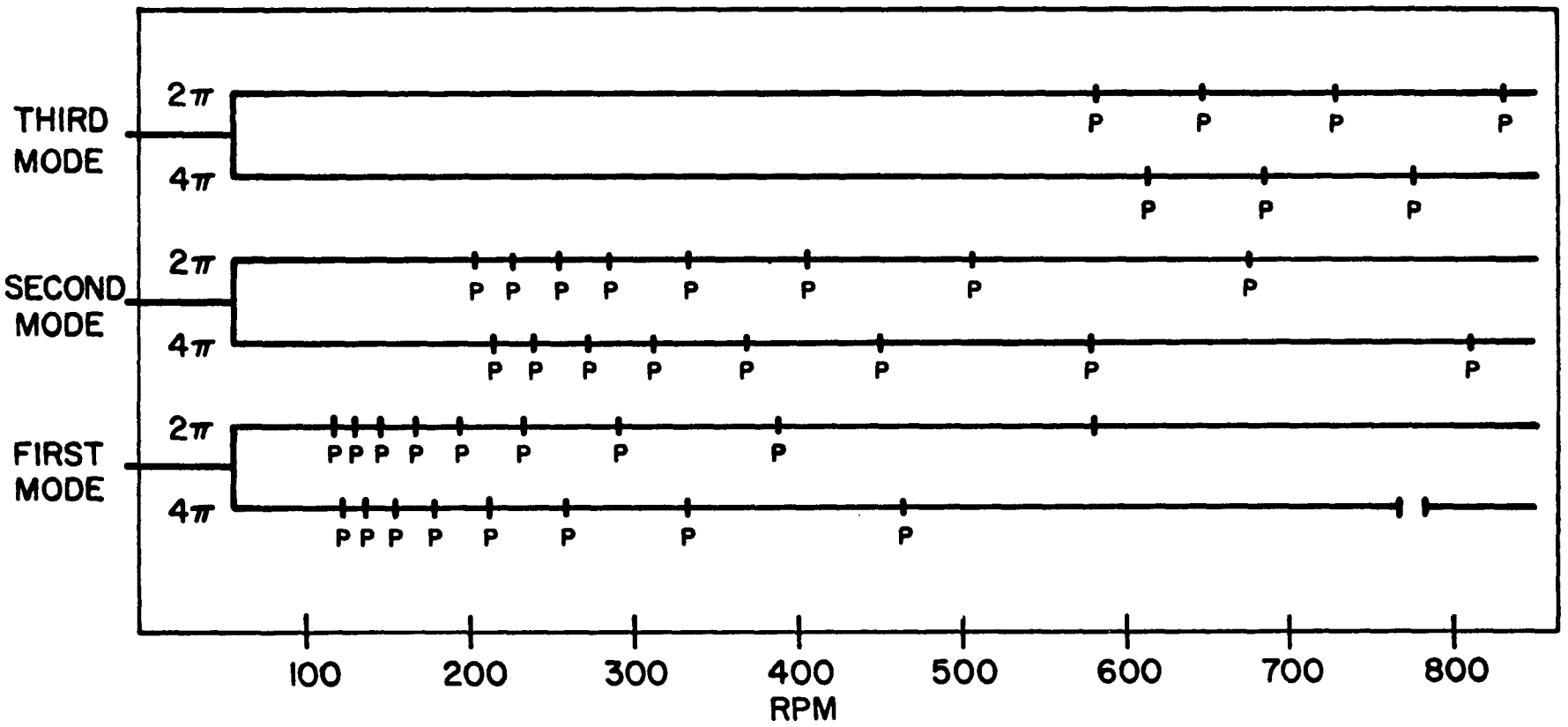

FIGURE 5.6: STABILITY BOUNDARIES

2. Stability Analysis of Damped Equations

The determination of the stability boundaries in the presence of damping will now be considered. It is shown that if an instability region of the undamped system is represented by a point, or more generally by a line, then damping removes the instability no matter how small ζ. If an instability region of the undamped system has finite width, the method discussed in Section IV-F-2b is used to obtain the stability boundaries corresponding to a given value of ζ.

Since the instability regions of all modes within the operating range of the mechanism are only points when damping is disregarded, the actual mechanism is completely stable for those speeds.

a) Instability Region is a Point in Undamped System

Equation (4.52) or equation (H.23) of Appendix H shows that the response of a damped Hill's equation is given by

$$q(\varphi_1) = e^{-\frac{\Delta}{2}\varphi_1} z(\varphi_1) . \qquad (5.9)$$

It is further indicated in the same Appendix that a damped system can only then become unstable if

$$Re(\mu) > \frac{\Delta}{2} \qquad (5.10)$$

in the characterisitc exponent μ associated with $z(\varphi_1)$.

Table H.1 shows that the above can only happen when the 2π or 4π-periodic instability regions of a Hill's equation such as $z(\varphi_1)$ have a finite width. (In the stable regions $Re(\mu) = 0$.) It will now be proven that $z(\varphi_1)$ can only contain

point-type regions, where $Re(\mu) = 0$, whenever the associated undamped system has point-type regions. Under these circumstances, equation (5.9) will be stable regardless of the magnitude Δ, or rather that of the damping ratio ζ.

The Hill's equation in $z(\varphi_1)$, i.e. equation (4.51) or equation (H.24), with the eigenvalue $\bar{\Lambda}$, is of the same form as the undamped Hill's equation (H.1) in $q(\varphi_1)$. Since it also contains the same periodic function $A(\varphi_1)$ as the undamped equation, its eigenvalues $\bar{\Lambda}$ are identical to those of the undamped equation. Thus, whenever the undamped system has eigenvalues which indicate a point-type region, the same type of instability is found in the $z(\varphi_1)$ system. This of course means that $Re(\mu) = 0$.

Accordingly, stability prevails in the first mode of the damped system up to 580 rpm, since the undamped first mode exhibits only instability points up to that speed (see Figure 5.6). The second and third modes are stable up to even higher speeds.

b) Instability Region Has Finite Width in Undamped System

While the 4π-periodic undamped instability region of of the first mode which occurs between 766 and 781 rpm is considerably above the practical operating range of the mechanism, it serves to illustrate the reduction of the width of such a region for a comparatively large ζ such as 0.034.

The method associated with the characteristic equation (4.59) is used to solve for the characteristic exponents $\mu_{1,2}$

of the equation in $z(\varphi_1)$. Subsequently, that speed is determined for which the total exponent $(Re(\mu) - \Delta/2)$ vanishes. Table 5.8 lists the values of Ω, $Re(\mu)$, $Imag(\mu)$, $\Delta/2$ and $(+Re(\mu) - \Delta/2)$ for a range of speeds from 766.92 to 780.00 rpm. Since $(+Re(\mu) - \Delta/2)$ is zero at approximately 769.62 and 779.29 rpm, these values represent the damped stability boundaries of this particular region.

3. Combination Resonances [14]

Combination resonances are instabilities, additional to the type described above, which arise in coupled Hill's equations. These types of instabilities were not investigated by the author because their presence was not detected in the experiment for the input speed range considered.

RPM	$\mathcal{A}$	+ Re(μ)	+ Imag(μ)	$\Delta/2$	+ Re(μ) - $\Delta/2$
766.92	-1.99850	0.000000	0.4938	0.00880	-0.8799×10^{-2}
767.59	-1.99998	0.000000	0.4992	0.00879	-0.8791×10^{-2}
768.27	-2.00131	0.005752	0.5000	0.00879	-0.3032×10^{-2}
768.94	-2.00251	0.007978	0.5000	0.00878	-0.7981×10^{-3}
769.62	-2.00357	0.009501	0.5000	0.00877	0.7323×10^{-3}
770.30	-2.00450	0.010670	0.5000	0.00876	0.1913×10^{-2}
770.98	-2.00530	0.011580	0.5000	0.00876	0.2827×10^{-2}
771.66	-2.00593	0.012250	0.5000	0.00875	0.3504×10^{-2}
772.35	-2.00643	0.012760	0.5000	0.00874	0.4020×10^{-2}
773.03	-2.00680	0.013120	0.5000	0.00873	0.4387×10^{-2}
773.72	-2.00701	0.013320	0.5000	0.00872	0.4602×10^{-2}
774.41	-2.00709	0.013390	0.5000	0.00872	0.4679×10^{-2}
775.10	-2.00702	0.013330	0.5000	0.00871	0.4621×10^{-2}
775.80	-2.00680	0.013120	0.5000	0.00870	0.4423×10^{-2}
776.49	-2.00646	0.012790	0.5000	0.00869	0.4099×10^{-2}
777.19	-2.00595	0.012280	0.5000	0.00869	0.3953×10^{-2}
777.89	-2.00533	0.011610	0.5000	0.00868	0.2936×10^{-2}
778.59	-2.00453	0.010710	0.5000	0.00867	0.2047×10^{-2}
779.29	-2.00358	0.009523	0.5000	0.00866	0.8641×10^{-3}
780.00	-2.00252	0.007981	0.5000	0.00865	-0.6706×10^{-3}

Table 5.8 Effect of Damping on 4π-Periodic Instability Region

G. Steady State Strain

The present section examines the steady state strain response between 140 and 205 rpm. This range includes resonance locations of the first mode at 144.93, 165.65 and 193.27 rpm. In addition the effect of damping is considered throughout the operating range.

The total strain response is obtained by superposing the particular solutions of each of the three uncoupled modes.

1. Determination of the Coefficients of the Particular Solution

The coefficients of the particular solution $q_{pn}(\varphi_1)$ are obtained with the help of equation (4.66). As described in Section IV-G-2b, the resonance locations of the particular solution for damped and undamped systems are associated with the 2π-periodic stability boundaries.

To find the response at a certain resonance location of a given mode, the number of simultaneous equations included in equation (4.66) must be such that the coefficient matrix $\mathbb{B}$ is large enough to include the value of Λ associated with the corresponding 2π-periodic boundary. (See Section V-F-1, Stability Analysis of Undamped Equations.) Again, parallel to the stability analysis, a system of twenty-one simultaneous equations was used. This allows the exploration of speeds as low as 116 rpm, with sufficient accuracy.

In equation (4.66), the Fourier coefficients of $B(\varphi_1)$ in the matrix $\mathbf{B}$ and the Fourier coefficients of $\mathcal{F}(\varphi_1)$ in the column vector $\mathbf{F}$ are independent of input speed (see equations (H.39) and (H.43)). The parameters Λ and Δ depend on input speed and ζ respectively. Tables 5.9 and 5.10 list the values of the above Fourier coefficients for each of the three modes. The values of the coefficients with subscripts greater than ten are taken to be zero.

A Gauss elimination(*) scheme was used for the determination of the coefficients p_0, p_{cm}, p_{sm}, $(m = 1,2,\ldots,10)$, of the particular solutions of the three modes considered.

(*) GELG, DGELG Routines, IBM System/360 Scientific Subroutine Package, (360A-CM-03X) Version III.

n	Mode 1		Mode 2		Mode 3	
	b_{cn}	b_{sn}	b_{cn}	b_{sn}	b_{cn}	b_{sn}
0	0.437718E-01	0.0	0.565126E-01	0.0	-0.110503E 00	0.0
1	-0.328253E 00	-0.165835E 00	-0.182352E 00	-0.932191E-01	-0.222503E 01	-0.111026E 01
2	-0.160993E 00	-0.172450E 00	-0.966251E-01	-0.111791E 00	-0.100034E 01	-0.966673E 00
3	-0.310383E-01	-0.333907E-01	-0.182533E-01	-0.214406E-01	-0.197606E 00	-0.189747E 00
4	-0.637028E-02	-0.559254E-02	-0.376605E-02	-0.358190E-02	-0.403003E-01	-0.318875E-01
5	-0.109685E-02	-0.831897E-03	-0.648210E-03	-0.531578E-03	-0.693696E-02	-0.476510E-02
6	-0.181126E-03	-0.116194E-03	-0.107083E-03	-0.742037E-04	-0.114373E-02	-0.671151E-03
7	-0.281461E-04	-0.148396E-04	-0.166118E-04	-0.982494E-05	-0.177813E-03	-0.896705E-04
8	-0.422618E-05	-0.125116E-05	-0.247594E-05	-0.136393E-05	-0.268085E-04	-0.118539E-04
9	-0.500406E-06	0.361638E-06	-0.303564E-06	-0.206244E-06	-0.328228E-05	-0.162415E-05
10	-0.521751E-07	0.671771E-06	-0.640330E-07	0.446840E-07	-0.341509E-06	0.127269E-05

Note: $b_{c0} = b_0$

Table 5.9 Fourier Coefficients of $B(\varphi_1)$

n	Mode 1		Mode 2		Mode 3	
	f_{cn}	f_{sn}	f_{cn}	f_{sn}	f_{cn}	f_{sn}
0	0.865276E-05	0.0	-0.446898E-07	0.0	0.802062E-05	0.0
1	0.692638E 00	0.457545E 00	0.115388E-01	0.762228E-02	-0.728089E 00	-0.480964E 00
2	-0.110237E 00	-0.914518E-01	-0.183643E-02	-0.152345E-02	-0.115879E 00	-0.961310E-01
3	0.239073E-01	0.137077E-01	0.398261E-03	0.228305E-03	-0.251307E-01	-0.144094E-01
4	-0.372052E-02	-0.182511E-02	-0.619759E-04	-0.303756E-04	-0.391094E-02	-0.191847E-02
5	0.581553E-03	0.226420E-03	0.967899E-05	0.376414E-05	-0.611264E-03	-0.238053E-03
6	-0.844157E-04	-0.258028E-04	-0.139842E-05	-0.436009E-06	-0.886383E-04	-0.270102E-04
7	0.121437E-04	0.196347E-05	0.197657E-06	0.478654E-07	-0.128078E-04	-0.207225E-05
8	-0.171585E-05	-0.836233E-06	-0.234936E-07	-0.630811E-08	-0.186644E-05	-0.853785E-06
9	-0.154154E-07	-0.989236E-06	-0.340917E-08	0.394198E-09	-0.379455E-07	0.110941E-05
10	-0.355739E-07	-0.141972E-05	-0.385384E-08	-0.712241E-08	-0.830057E-08	0.150140E-05

Note: $f_{c0} = f_0$

Table 5.10 Fourier Coefficients of $\mathcal{F}(\varphi_1)$

2. Typical Response Off-Resonance (190.0 rpm)

Table 5.11 lists the coefficients p_0, p_{cm}, and p_{sm}, (m = 1,2,...,10), for the non-resonant input speed of 190.0 rpm (with ω_1 = 1159.3 rpm, Λ_1 = 37.23) and a damping ratio ζ = 0.0025 for each of the first three modes.

These results are first used, with the help of equation (4.41), to show once more (as was already done in Section V-E) that the contributions of at least three modes are necessary for the determination of the total bending strain. Figure 5.7 gives the superposed strain along the rocker link for various combinations of modes at $\varphi_1 = 21.6^\circ$. At this angle the global maximum strain is reached at x_3 = 9.84 in. for two of the mode combinations. The figure clearly points out that the first mode alone is insufficient to approximate the actual response.

Figure 5.8 gives the magnitude of the bending strain at both the bottom and top gage locations for one cycle. Both figures indicate by their particular shape the prevalence of the fundamental harmonic of $q_n(\varphi_1)$ of all the modes involved. This can also be seen in the rapidly diminishing magnitudes of the coefficients of the higher harmonics of all modes in Table 5.11.

	Mode 1		Mode 2		Mode 3	
n	p_{cn}	p_{sn}	p_{cn}	p_{sn}	p_{cn}	p_{sn}
0	0.254645E-03		0.250472E-06		-0.270153E-05	
1	0.192079E-01	0.126477E-01	0.102877E-03	0.679192E-04	-0.778945E-03	-0.514263E-03
2	0.340107E-02	0.286694E-02	0.168829E-04	0.140478E-04	-0.125014E-03	-0.104200E-03
3	0.879006E-03	0.607912E-03	0.384297E-05	0.229676E-05	-0.273542E-04	-0.164281E-04
4	0.186828E-03	0.143483E-03	0.642785E-06	0.350764E-06	-0.431870E-05	-0.238006E-05
5	0.548406E-04	0.487034E-04	0.111748E-06	0.540876E-07	-0.692100E-06	-0.339868E-06
6	0.801672E-04	0.100490E-03	0.187836E-07	0.863687E-08	-0.104122E-06	-0.478121E-07
7	-0.175387E-05	-0.413208E-05	0.329089E-08	0.149720E-08	-0.158127E-07	-0.599716E-08
8	-0.136405E-07	-0.652511E-06	0.541487E-09	0.320516E-09	-0.244505E-08	0.279279E-09
9	-0.521183E-10	-0.454320E-07	-0.857753E-10	0.666610E-10	-0.109371E-09	0.117343E-08
10	-0.123412E-08	0.148823E-07	-0.280866E-09	-0.512677E-09	-0.261940E-10	0.177459E-08

Note: $p_{c0} = p_0$

Table 5.11 Fourier Coefficients of Particular Solution at 190.0 rpm. ($\zeta = 0.0025$)

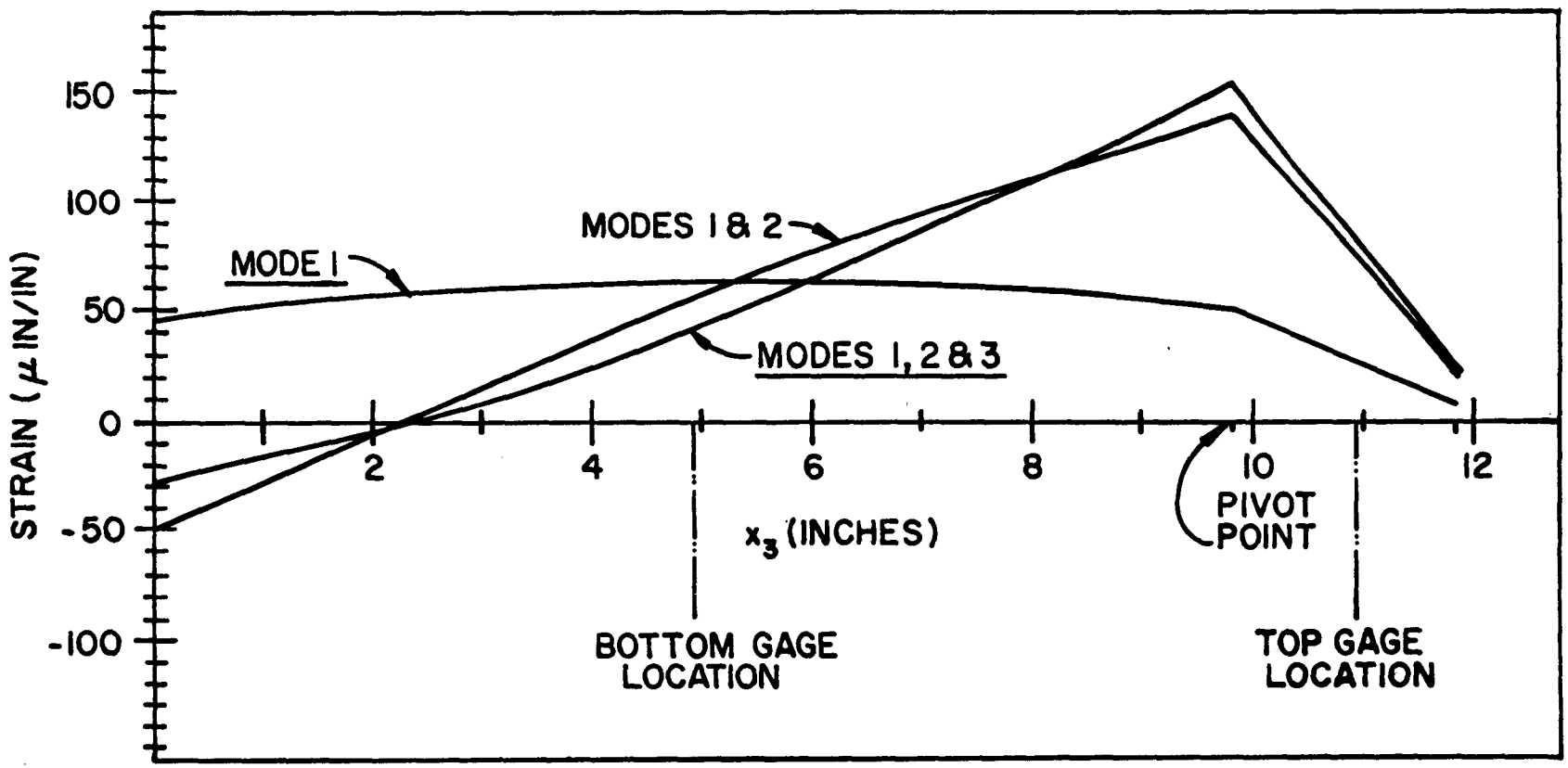

FIGURE 5.7: EFFECT OF SUPERPOSITION OF MODES
PARTICULAR SOLUTION: 190 RPM (ζ=0.0025)

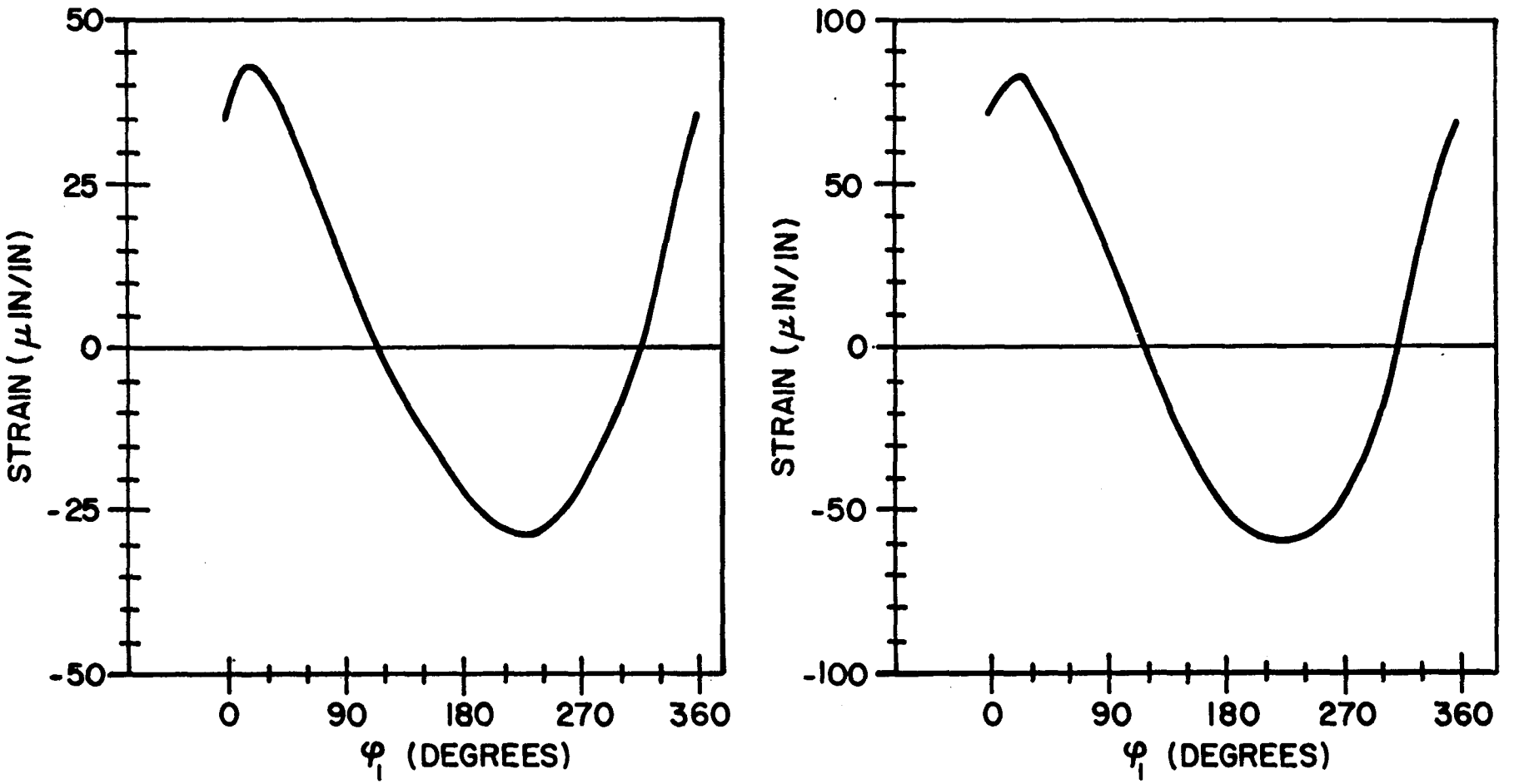

FIGURE 5.8: BENDING STRAIN AT 190.0 RPM (ζ=0.0025)

3. Typical Response On Resonance (193.27 rpm)

When the system operates at a resonance location corresponding to the first mode, the response of the first mode becomes dramatically different from that associated with a non-resonant speed. To illustrate this point, 193.27 rpm was chosen. With the natural frequency of the first mode at 1159.3 rpm, 193.27 rpm becomes the sixth subharmonic of the natural frequency, and one expects the sixth harmonic of 193.27 rpm, i.e. 1159.3 rpm, to be amplified considerably in the particular solution. Table 5.12 lists the coefficients p_0, p_{cm}, p_{sm}, ($m = 1,2,\ldots,10$), for all three modes of the particular solution for a damping ratio $\zeta = 0.0025$. Figure 5.9 shows the strain response at bottom gage and top gage locations for a complete cycle. Note, especially for the bottom gage location, the superposed wave due to the sixth harmonic. This portion of the response is less pronounced at the top gage location because of the greater influence of the second mode (see also numerical solution in Section E).

When comparing Table 5.11, which corresponds to 190.0 rpm, and Table 5.12, which corresponds to 193.27 rpm, it is to be noted that all but the coefficients of the sixth harmonic and those near the sixth harmonic of the first mode, are essentially the same, with those at 193.27 rpm slightly larger due to the higher speed.

It should be mentioned at this point that it was much easier to find the resonance effect in the experiment than in

	Mode 1		Mode 2		Mode 3	
n	p_{cn}	p_{sn}	p_{cn}	p_{sn}	p_{cn}	p_{sn}
0	0.273091E-03		0.268305E-06		-0.289300E-05	
1	0.198974E-01	0.131002E-01	0.106485E-03	0.702993E-04	-0.806054E-03	-0.532146E-03
2	0.353716E-02	0.298409E-02	0.174939E-04	0.145577E-04	-0.129402E-03	-0.107875E-03
3	0.920819E-03	0.645882E-03	0.398919E-05	0.238754E-05	-0.283233E-04	-0.170364E-04
4	0.195895E-03	0.187316E-03	0.669128E-06	0.366463E-06	-0.447392E-05	-0.247493E-05
5	0.220730E-04	0.136491E-03	0.116854E-06	0.569633E-07	-0.717585E-06	-0.354895E-06
6	-0.419911E-02	0.337125E-02	0.197813E-07	0.920492E-08	-0.108087E-06	-0.502050E-07
7	0.737734E-04	-0.182583E-04	0.350610E-08	0.162391E-08	-0.164411E-07	-0.635650E-08
8	0.219399E-04	0.294768E-05	0.589059E-09	0.356466E-09	-0.254688E-08	0.262474E-09
9	0.246086E-05	0.235593E-06	-0.969462E-10	0.782046E-10	-0.115735E-09	0.121322E-08
10	0.304801E-06	-0.163832E-07	-0.392732E-09	-0.716609E-09	-0.277442E-10	0.184303E-08

Note: $p_{c0} = p_0$

Table 5.12 Fourier Coefficients of Particular Solution at 193.27 rpm. ($\zeta = 0.0025$)

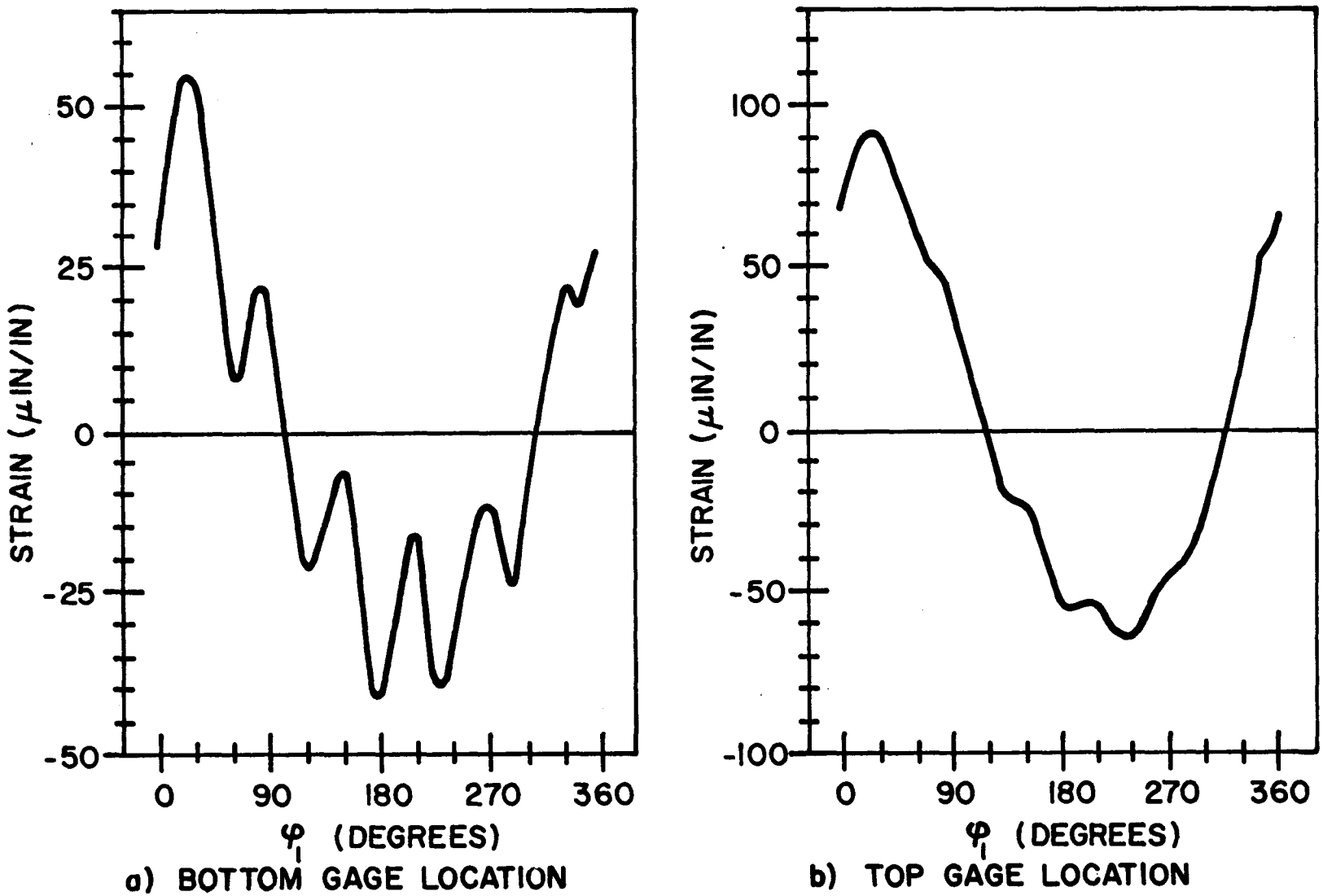

FIGURE 5.9: BENDING STRAIN AT 193.27 RPM (ζ=0.0025)

the computation. The region of speeds for which certain Fourier coefficients increase is very narrow. At 193.27 rpm, it spans 0.5 rpm.

4. Influence of Damping on Response

Figure 5.10 gives maximum bottom gage point strains for a traverse of input speeds from 140 to 205 rpm for damping ratios $\zeta = 0.00015$ and $\zeta = 0.0025$ (which have been found to be typical in the experiment, see Section V-H). It shows that the response is very sensitive to the choice of damping ratio at all resonant speeds, and essentially unaffected by it off-resonance.

The degree to which damping influences the response at a resonant speed is illustrated in Figure 5.11 for 193.27 rpm (bottom gage location). The magnitudes of the Fourier coefficients of the sixth harmonic of the first mode are plotted on a logarithmic scale as a function of the damping ratio ζ, for $0.00015 \leq \zeta \leq 0.034$. As the damping ratio increases, the amplitude of the superposed wave becomes smaller and smaller. For $\zeta = 0.034$, which could possibly be obtained by the introduction of damping tape, the response at resonance does not differ in shape from that off resonance. It is believed that the above observation may be helpful in noise abatement.

As stated previously, in searching for the "exact" resonance locations it was necessary to use very small increments in rpm. At 165.65 rpm and 144.93 rpm, one had to use "double precision" in order to observe the amplification of the higher

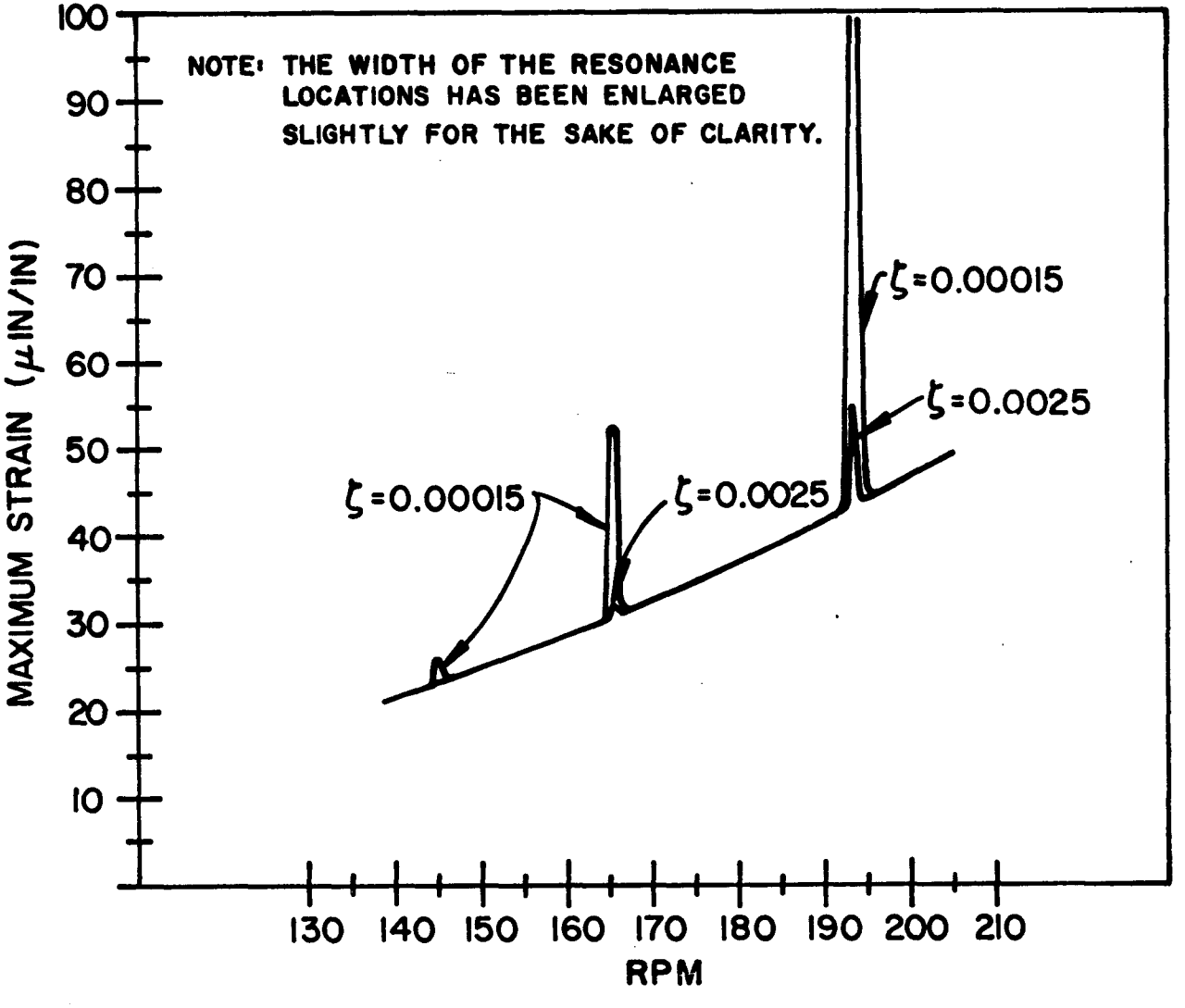

FIGURE 5.10: MAXIMUM BOTTOM GAGE POINT STRAINS

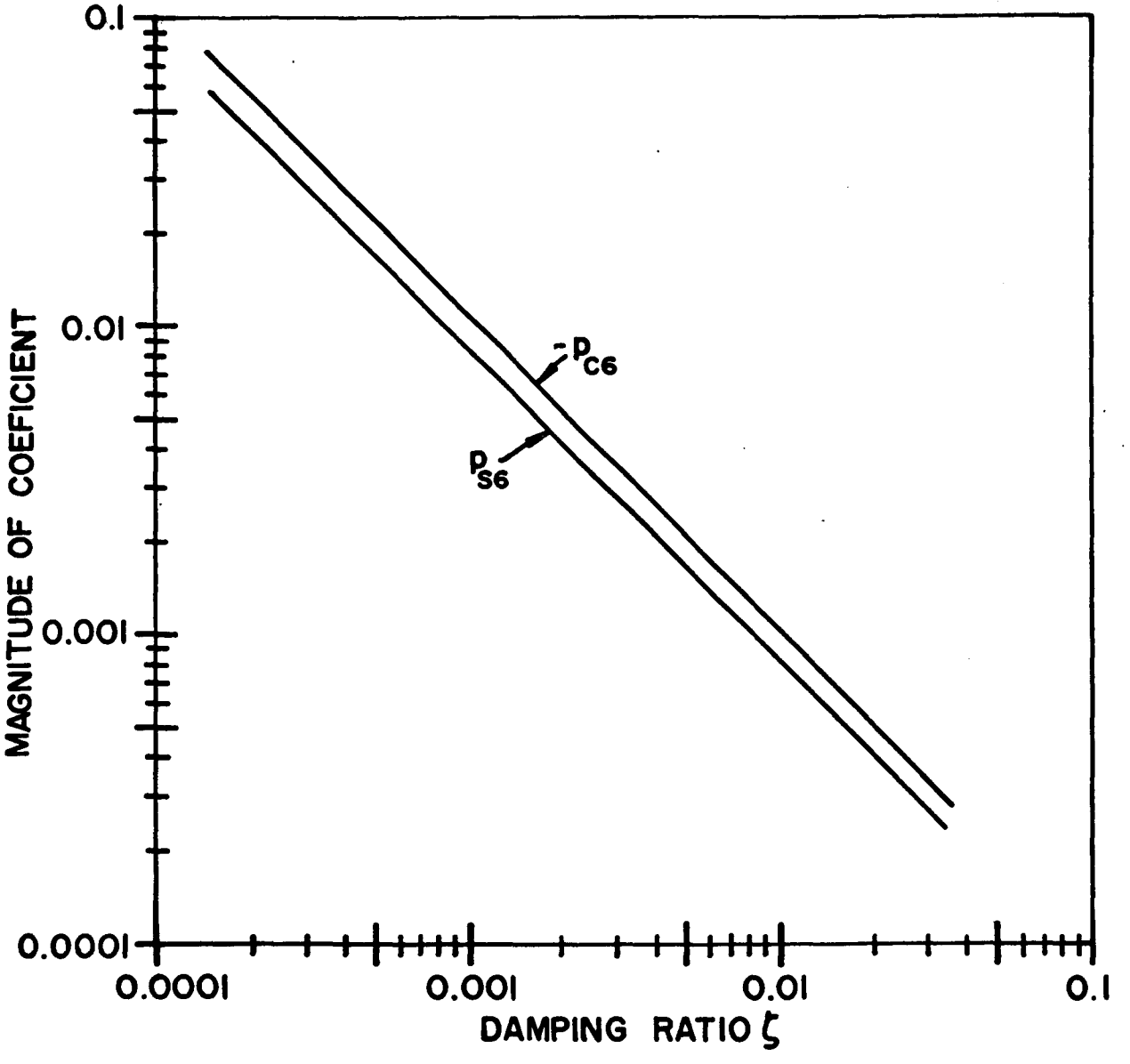

FIGURE 5.11: EFFECT OF DAMPING ON FIRST MODE FOURIER COEFFICIENTS $-p_{c6}$ AND p_{s6} AT 193.27 RPM

H. Experiment

1. Description of Experimental Setup

The essential dimensions of the experimental mechanism have been described in Section V-A . Figure 5.12a shows a photograph of the mechanism. Figure 5.12b gives a schematic of the complete experimental setup and Table 5.13 lists its individual components.

The SR-4 350 Ω foil strain gages were attached as accurately as possible at the "bottom gage" and "top gage" locations, which are $x_3 = 4.920$ in. and $x_3 = 10.965$ in. respectively.(*) Figure 5.1 shows that these gages were attached to the outer side of the rocker only. (The use of only one strain gage per location does not allow for the exclusion of the axial strain component. This omission was felt to be justified because the relative magnitude of the axial strain is quite small. In addition, the link was not overloaded with wires.) The strain gages were connected to a d.c. bridge circuit in the amplifier of the oscilloscope. The output of the amplifier could also be fed into a strip recorder.

The mechanism was directly driven by a variable speed 1/6 hp d.c. motor and its speed was monitored by a generator with a 60 cycle/revolution a.c. output. This output was

---

(*) The strain gages were attached to the outside of the link. The strain traces were inverted by the oscilloscope to make their signs conform to those corresponding to points on the inside of the link for which the computations were made.

harmonics. It may very well be necessary to use larger sets of simultaneous equations to explore such low speed resonance locations more accurately.

FIGURE 5.12a EXPERIMENTAL MECHANISM MODEL

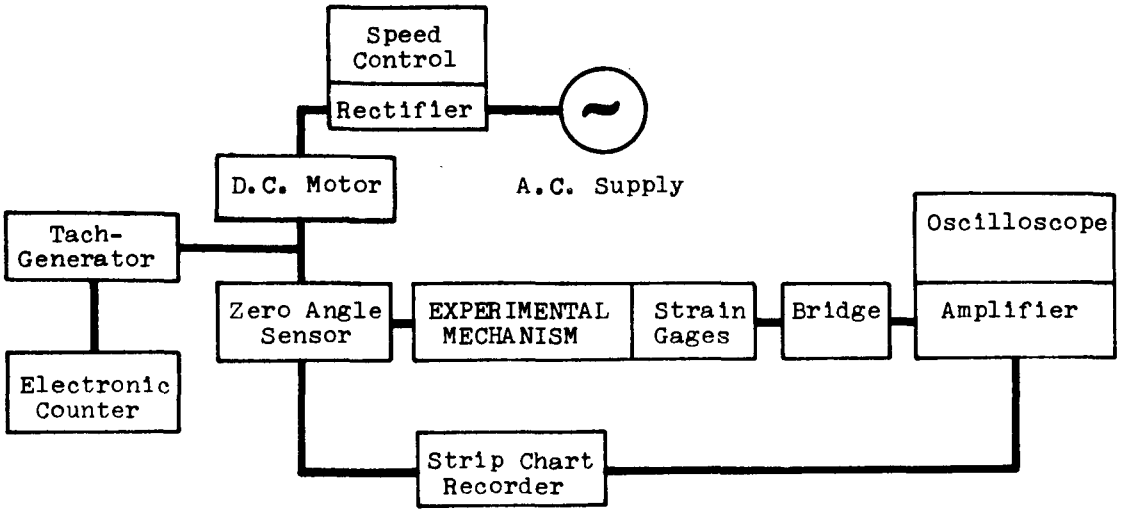

FIGURE 5.12b SCHEMATIC OF EXPERIMENTAL SETUP

Motor	Westinghouse D.C. Type FK, 1/6 HP
Motor Speed Control	Boston Gear Radiotrol 1/3 HP Motor Speed Control
Strain Gages	BLH SR-4 350 ohm foil gages
Oscilloscope	Tektronix Types 564B and 565 Type 3A10 Transducer Amplifier with Strain Gage Adapter
Electronic Counter	Hewlett-Packard Model 5326A Timer-Counter
Tachometer Generator	Hewlett-Packard Model 508A, 60 cycles/revolution
Photoelectric Cycle Timing	MTI Instruments Division Fotonic Sensor, Model KD-38
Chart Recorder	Hewlett-Packard

Table 5.13 Equipment Used in Experiment

converted into mechanism rpm with the help of an electronic counter.

The zero position of the input crank, i.e. $\varphi_1 = 0^o$, was determined with the help of a photo-electric transducer. A reflecting tape attached to the flywheel transmitted a light signal whenever $\varphi_1 = 0^o$. The associated electrical pulse was fed into the strip recorder for correlation with the strain gage output. Figure 5.13 shows a typical strip record containing both strain response (uncorrected) and zero input angle signal.

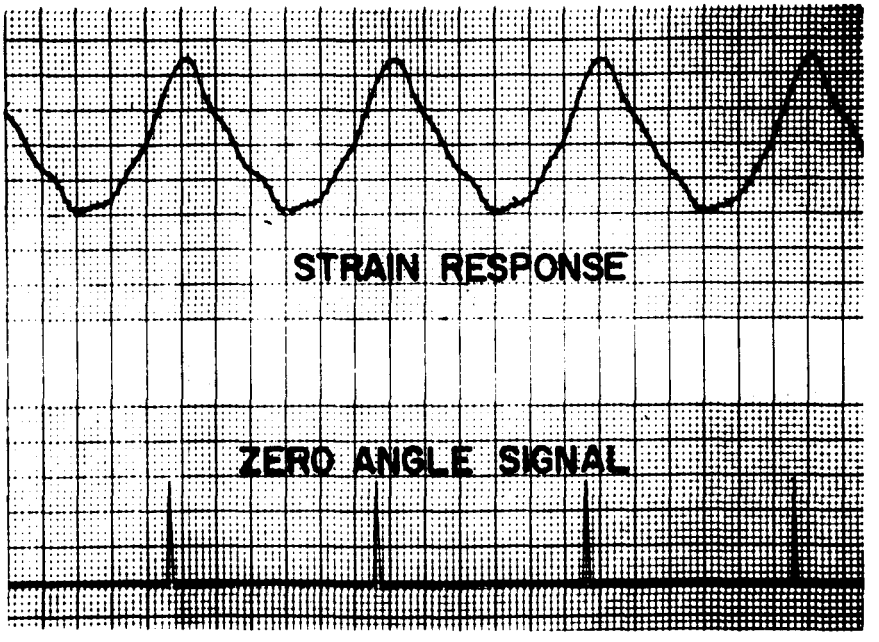

BOTTOM GAGE LOCATION (201 RPM)
VERTICAL SCALE: 25 μIN/IN/DIV
CHART SPEED: 100 MM/SEC

FIGURE 5.13: STRIP RECORDING OF STRAIN RESPONSE AND ZERO INPUT ANGLE SIGNAL

2. Gravity Correction

Because of the thinness of the rocker link, the counterweight and the endmass together caused a certain static deflection of the beam. The resulting strain is of the order of 10-15% of that associated with the normal operation of the mechanism. Since the theory does not account for the influence of gravity, some compensation procedure had to be found. Figure 5.14 lists experimentally determined strains due to gravity as a function of input angle φ_1 for both the bottom and top gage locations. These curves were used to correct all strain gage readings. The base of the mechanism was tilted approximately 11°, see Figure 5.12a, in order to equalize the gravity effect in both directions of motion.

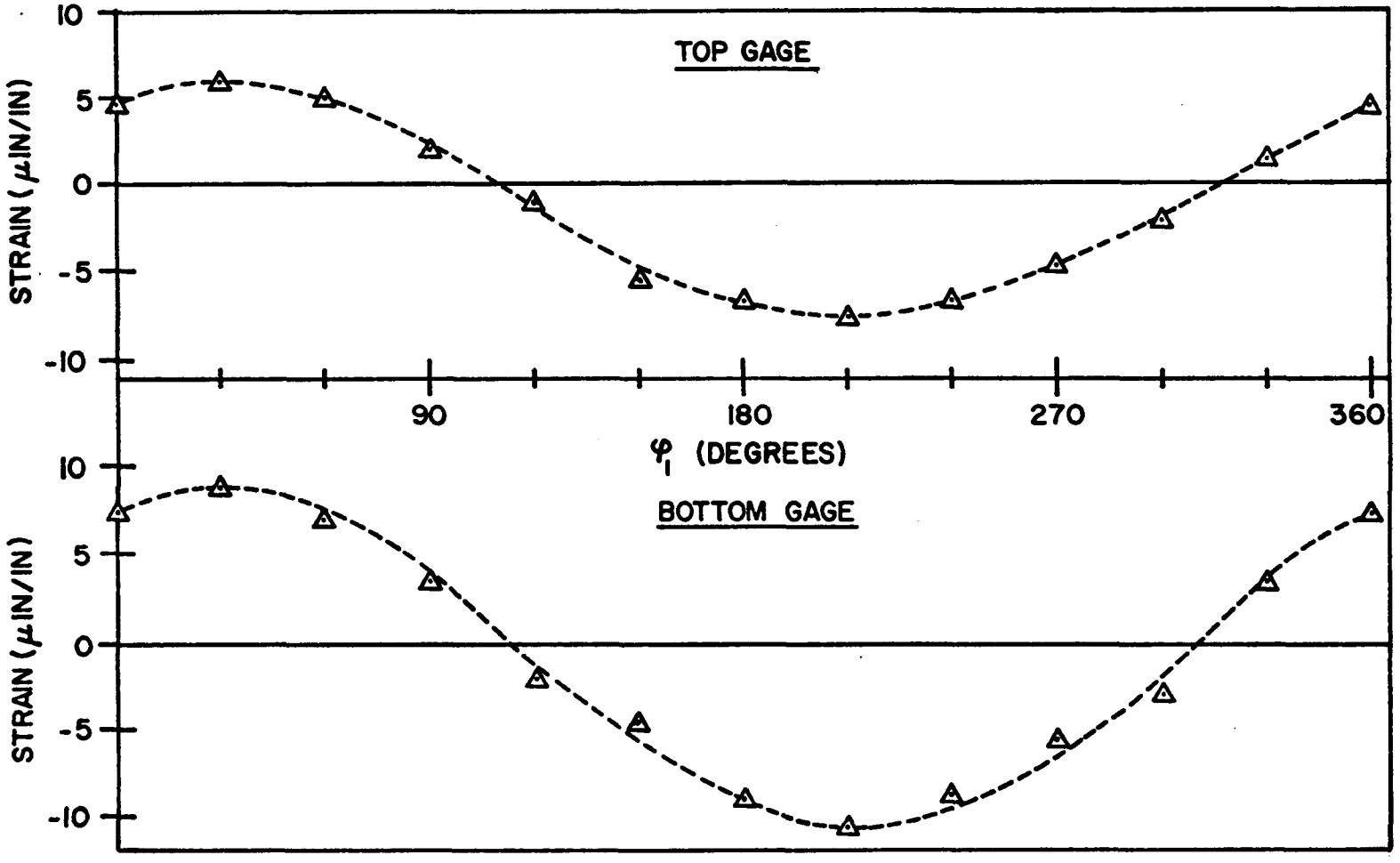

FIGURE 5.14: STRAINS DUE TO GRAVITY FOR CORRECTION

3. Qualitative Experimental Results

Figure 5.15 gives typical uncorrected strain histories at the bottom gage location in the operating range between approximately 110 and 200 rpm. They have been specifically chosen to show the response at 2π-periodic resonance locations of the first mode as well as at locations between these resonances. In all traces, the fundamental harmonic of the wave corresponds to the input speed of the mechanism.

The following conclusions concerning instability, transient and steady state response, as well as resonance locations may be drawn:

a) Stability

The experiment showed that the strain in the operating range never grew without bound and therefore, there are no 2π or 4π-periodic instabilities. This confirms the results of the stability analysis in Section V-F-2, which shows that in the presence of any damping, however small, the system remains stable.

b) Transient and Steady State Response

The responses at 112, 122, 140, 157 and 174 rpm correspond to locations in the stable regions of the first mode, i.e. between resonance locations. It was shown in Section V-E-1 that the presence of a complementary solution would make itself known for these rpm by a superposed "travelling wave", reflecting its non-periodic nature. The absence of

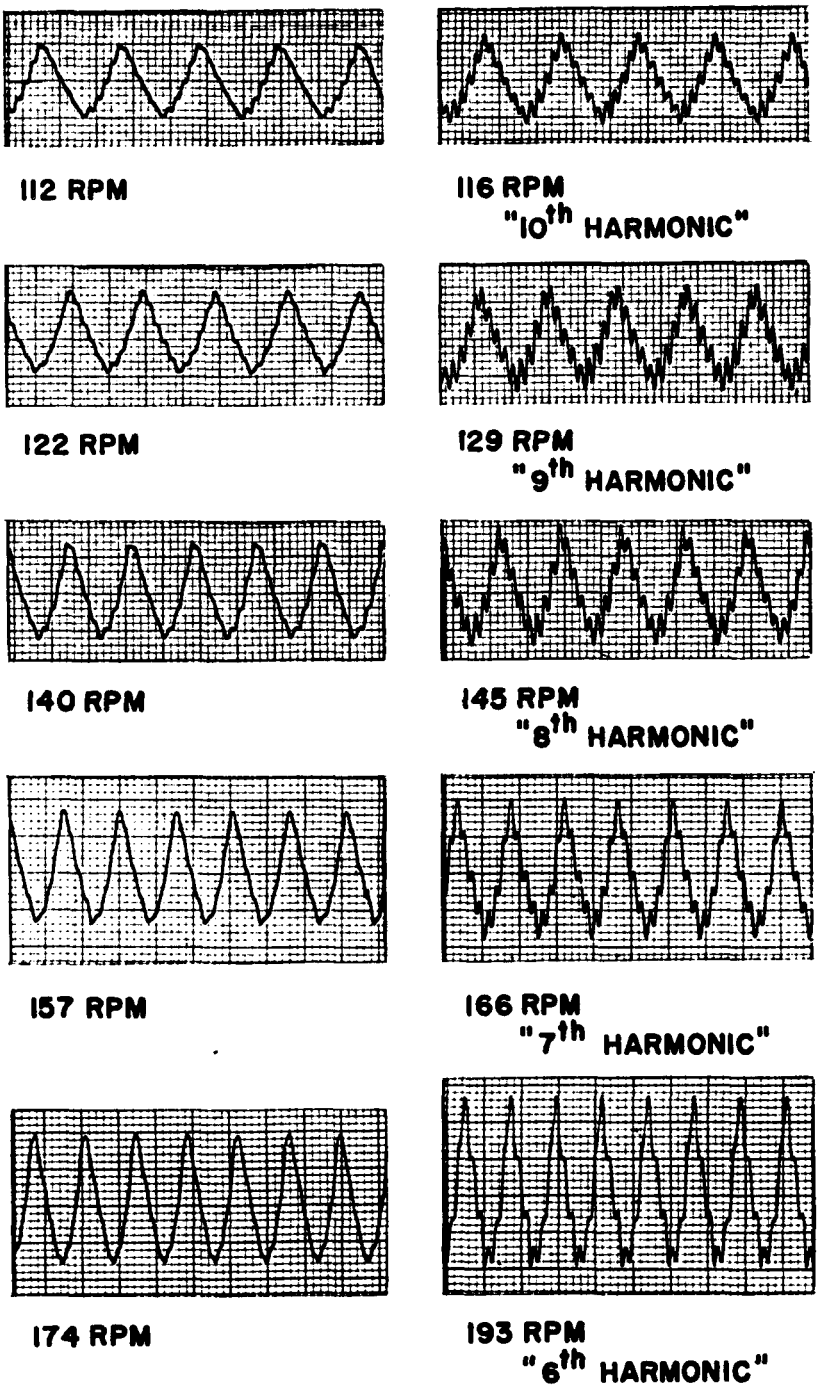

FIGURE 5.15: UNCORRECTED BOTTOM GAGE STRAIN RESPONSE

such a wave indicates that the traces principally reflect the steady state strain, which may be determined with the help of the particular solution.

The high frequency, small amplitude, waves near the maximum strain locations (+ and -) are the responses to bearing impacts caused by clearance in the journal bearings. (This can be more clearly seen in Figures 5.16-5.20.)

c) Resonance Locations

The speeds of 116, 129, 145, 166 and 193 rpm correspond to the resonance locations of the first mode associated with the 2π-periodic stability boundaries of the undamped homogeneous solution. The amplification of certain harmonics of the response is especially to be noted. For example, at 145 rpm, which represents the eighth subharmonic of the natural frequency, the presence of the eighth harmonic of the response, which has the frequency of the natural frequency, can clearly be seen (see Section V-G-3). Figure 5.15 indicates at each of the resonance locations the number of the amplified harmonic. In each case its frequency corresponds to that of the first natural frequency.

It should be pointed out that it was difficult to maintain a constant motor speed in the experiment. With the aid of a tach-generator and an oscilloscope, it was determined that the crank speed varied between five and eight percent of the nominal speed within a single cycle, with the larger variations taking place at lower speeds. This variation must

make itself felt in the traces of both on-resonance and off-resonance locations. For example, the presence of the small in-phase higher harmonics in certain portions of the traces at 112, 122, 140, 157 and 174 rpm can be explained by the approach to resonant speed at those positions within the cycle.

4. Quantitative Experimental Results

The following gives quantitative comparisons between gravity corrected experimental results at selected off as well as on-resonance locations and theory. Good agreement was found at all off-resonance locations where theory predicts identical responses for values of ζ between 0 and 0.0025. In order to get agreement at the resonance locations, it was necessary to adjust ζ in each case.

a) Comparison with Theory at Typical Off-Resonance Locations

Figures 5.16 to 5.18 show comparisons for the off-resonance locations of 160, 190 and 201 rpm, both for top as well as bottom gage locations. In each case, oscilloscope traces are juxtaposed for the sake of completeness. In general, agreement between the corrected experimental traces and theory is very good, with the experimental peak strains being approximately 10% larger than those predicted by theory.(*) The phase agreement of the fundamental mode is excellent. The agreement is somewhat better for the top gage location than for the bottom one because of the generally greater importance of the first mode at the bottom gage location. A variation of speed in the direction of resonance during any cycle causes the appearance of the prevalent higher harmonic of the first mode. This speed variation has less influence at the top gage since the influence of the second mode is just as strong there, and the second mode does not approach

(*) This difference is discussed in Section VI.

VERTICAL SCALE: 25 μIN/IN/DIV
HORIZONTAL SCALE: 0.1 SEC/DIV

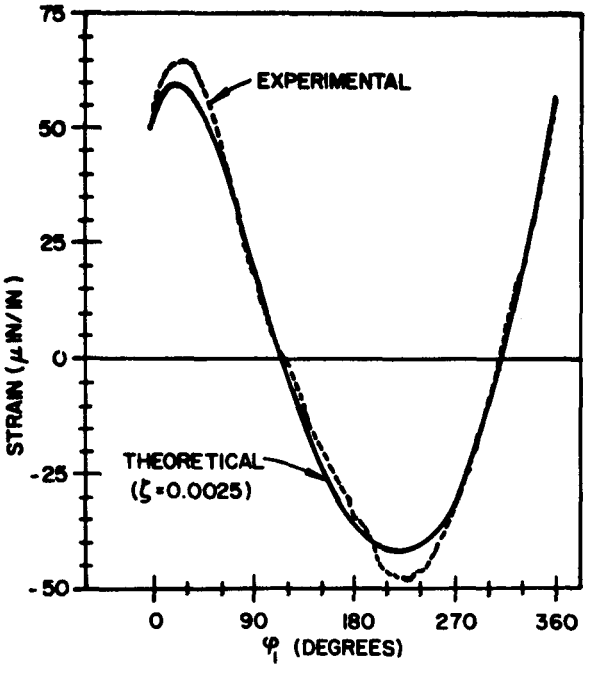

a) TOP GAGE LOCATION

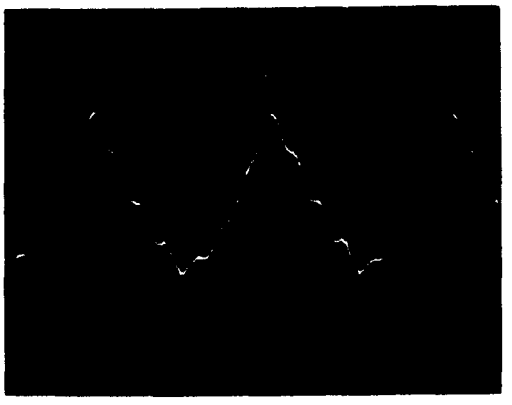

VERTICAL SCALE: 25 μIN/IN/DIV
HORIZONTAL SCALE: 0.1 SEC/DIV

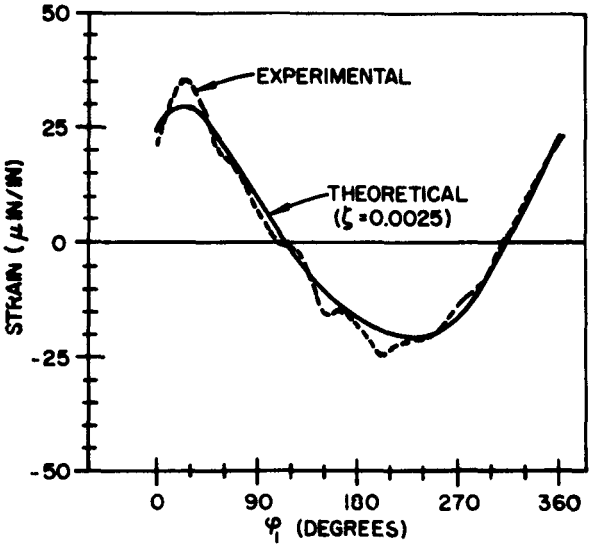

b) BOTTOM GAGE LOCATION

FIGURE 5.16: RESPONSE COMPARISON AT 160 RPM (GRAVITY CORRECTED)

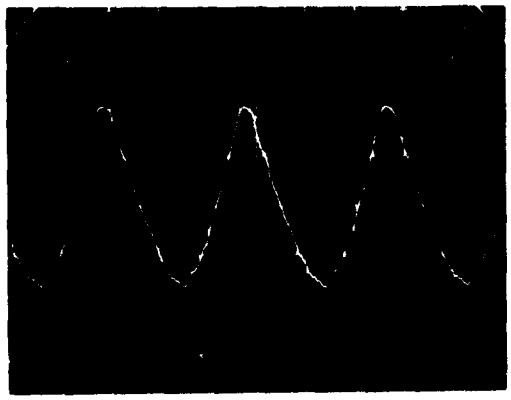

VERTICAL SCALE: 50 μIN/IN/DIV
HORIZONTAL SCALE: 0.1 SEC/DIV

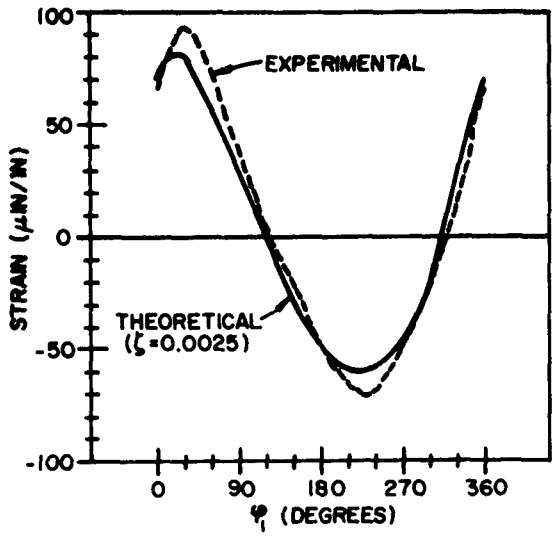

a) TOP GAGE LOCATION

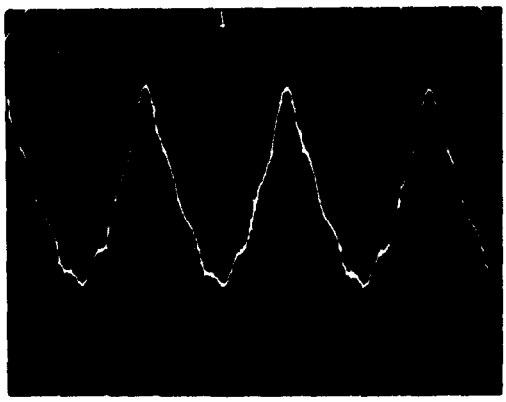

VERTICAL SCALE: 25 μIN/IN/DIV
HORIZONTAL SCALE: 0.1 SEC/DIV

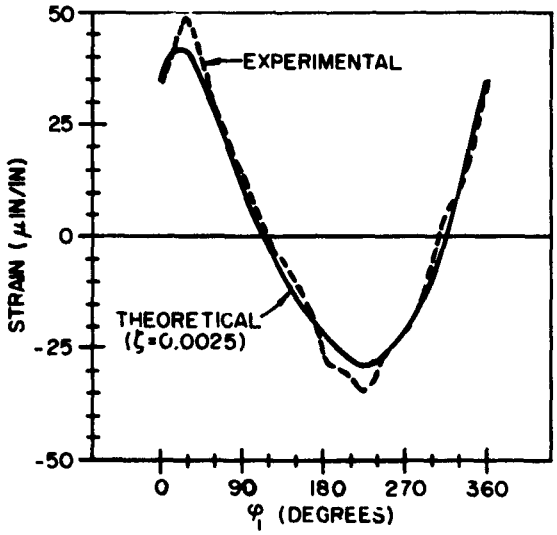

b) BOTTOM GAGE LOCATION

FIGURE 5.17: RESPONSE COMPARISON AT 190 RPM (GRAVITY CORRECTED)

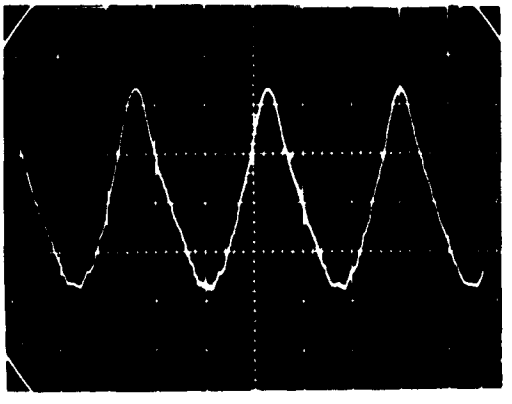

VERTICAL SCALE: 50 μIN/IN/DIV
HORIZONTAL SCALE: 0.1 SEC/DIV

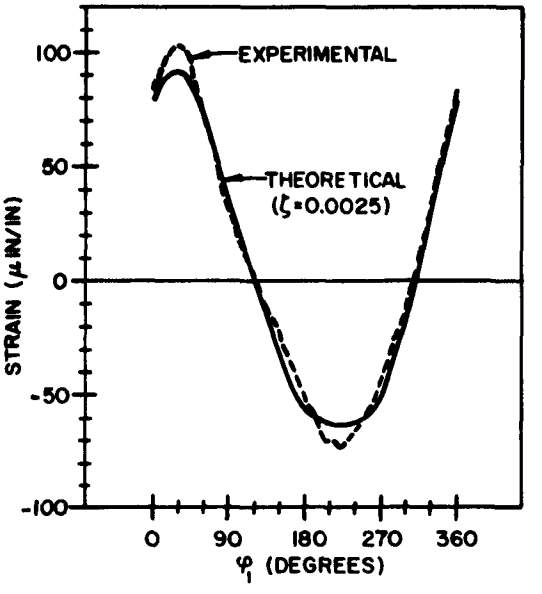

a) TOP GAGE LOCATION

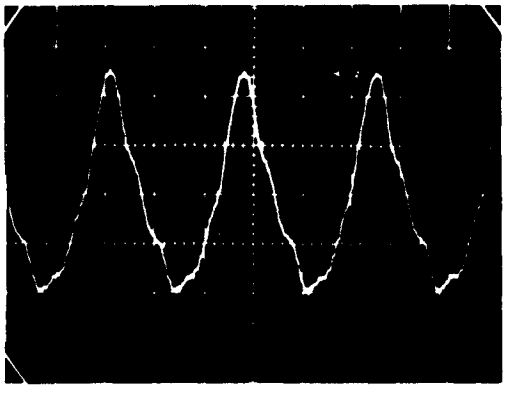

VERTICAL SCALE: 25 μIN/IN/DIV
HORIZONTAL SCALE: 0.1 SEC/DIV

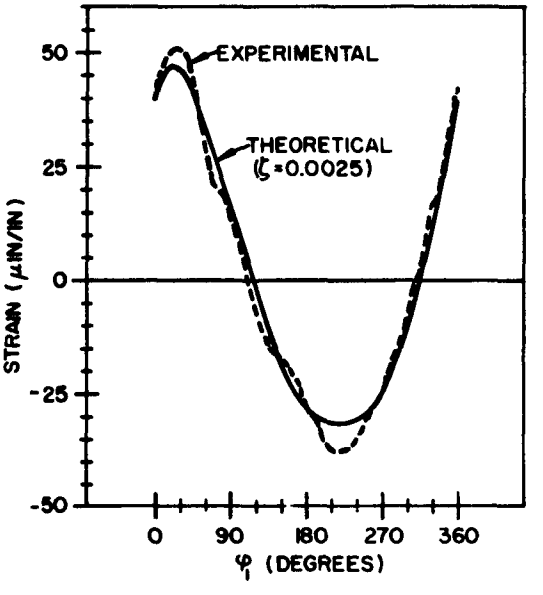

b) BOTTOM GAGE LOCATION

FIGURE 5.18: RESPONSE COMPARISON AT 201 RPM (GRAVITY CORRECTED)

a resonance.

b) Comparison with Theory at Typical On-Resonance Locations

Figures 5.19 and 5.20 show comparisons for the on-resonance locations of 166 and 193 rpm. The same format is followed as in Figures 5.16 to 5.18. To obtain the indicated agreement, it was necessary to manipulate ζ. The ζ used for 166 rpm was 0.00015 and ζ was 0.0025 at 193 rpm. At 145 rpm, which is not shown here but in Figures 5.21 and 5.22, the "matching" ζ was 0.3×10^{-4}.

Some attempt at an explanation for this increase of ζ with speed is in order. While the damping properties of the rocker material are most likely independent of speed, the bearing forces, and with that the friction induced moments in the bearings, are a function of mechanism speed. These bearing moments dissipate energy and may be thought of as increasing the damping ratio with speed. The particular solution section shows that while in a range of ζ from 0 to 0.0025, the response off-resonance is independent of ζ, at resonance it depends very much on the value of ζ. It is believed that the experimental results reflect a continuously increasing ζ.

When reasonable agreement in magnitude is obtained for the bottom gage, the top gage shows a slightly larger discrepancy. The phase agreement for the higher harmonics seems somewhat better for 193 rpm than for 166 rpm. The phase agreement of the fundamental harmonic is very good.

VERTICAL SCALE: 25 μIN/IN/DIV
HORIZONTAL SCALE: 0.1 SEC/DIV

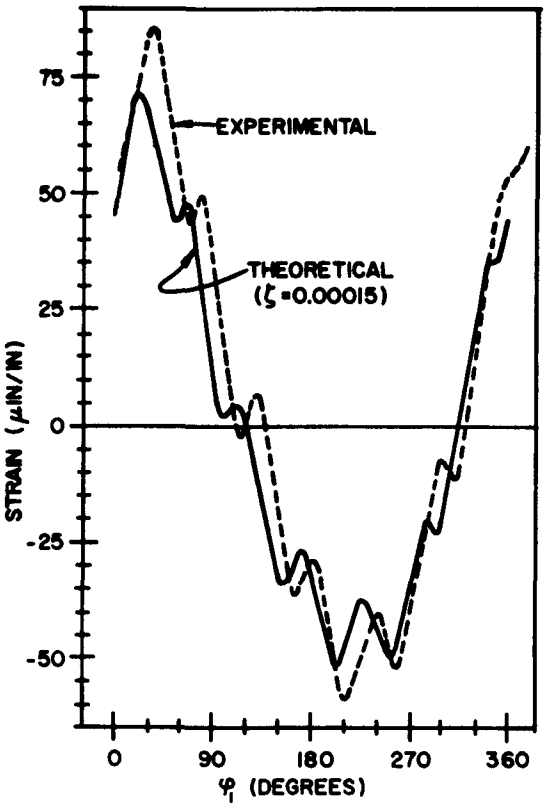

a) TOP GAGE LOCATION

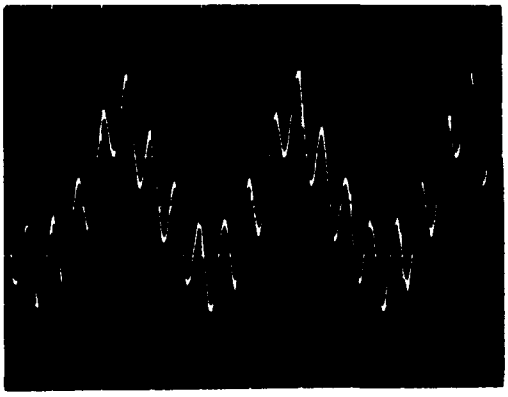

VERTICAL SCALE: 25 μIN/IN/DIV
HORIZONTAL SCALE: 0.1 SEC/DIV

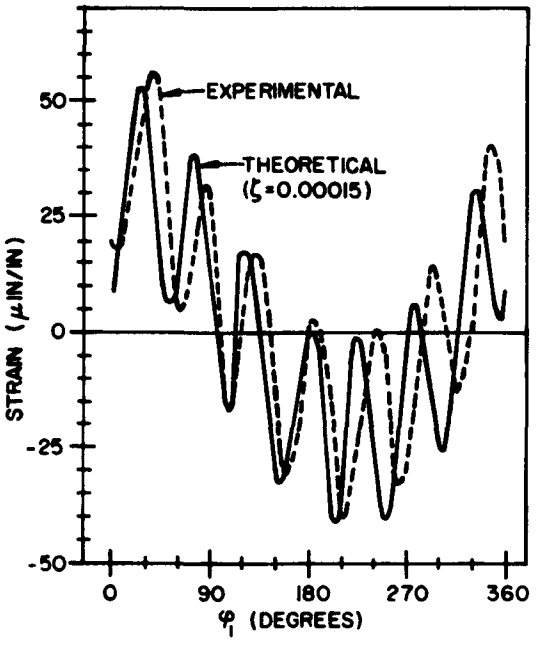

b) BOTTOM GAGE LOCATION

FIGURE 5.19: RESPONSE COMPARISON AT 166 RPM (GRAVITY CORRECTED)

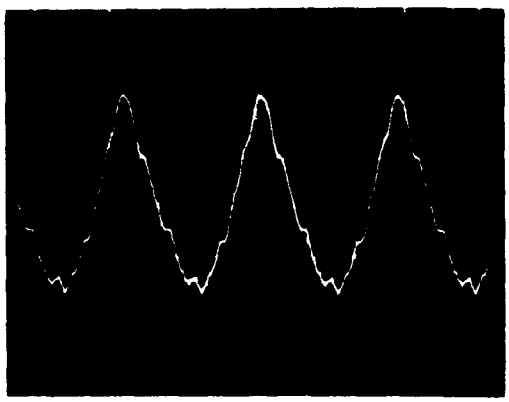

VERTICAL SCALE: 50 μIN/IN/DIV
HORIZONTAL SCALE: 0.1 SEC/DIV

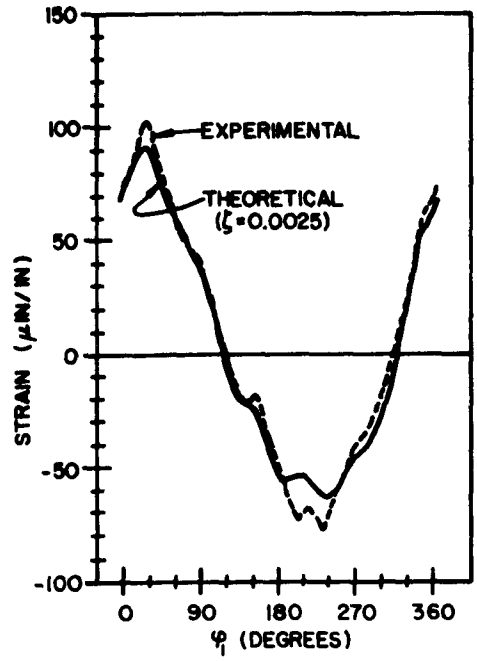

a) TOP GAGE LOCATION

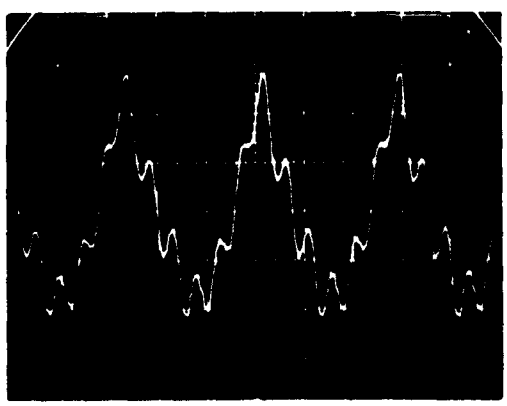

VERTICAL SCALE: 25 μIN/IN/DIV
HORIZONTAL SCALE: 0.1 SEC/DIV

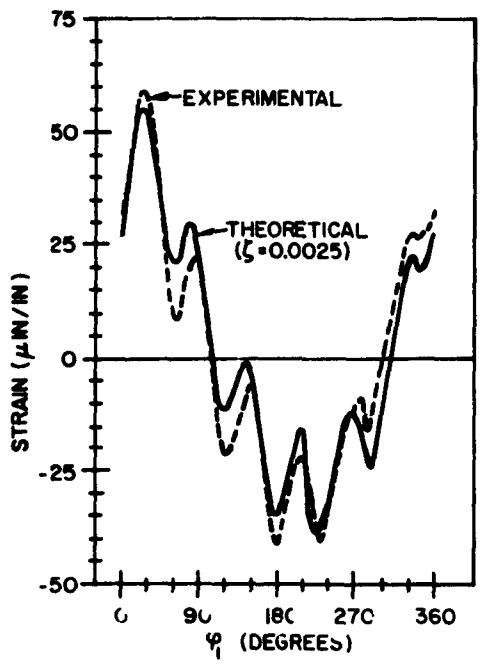

b) BOTTOM GAGE LOCATION

FIGURE 5.20: RESPONSE COMPARISON AT 193 RPM (GRAVITY CORRECTED)

c) Peak Strains Throughout Operating Range

Figures 5.21 and 5.22 show the corrected experimental peak strains at bottom gage and top gage locations throughout the operating range and compare them to the theoretical results. The latter were obtained for all off-resonance locations with $\zeta = 0.0025$. The values of ζ used on-resonance are different at each location and are listed in the figure. The off-resonance strain values of the experiment are between 10-15% larger than those predicted by theory. This difference is discussed in the next section.

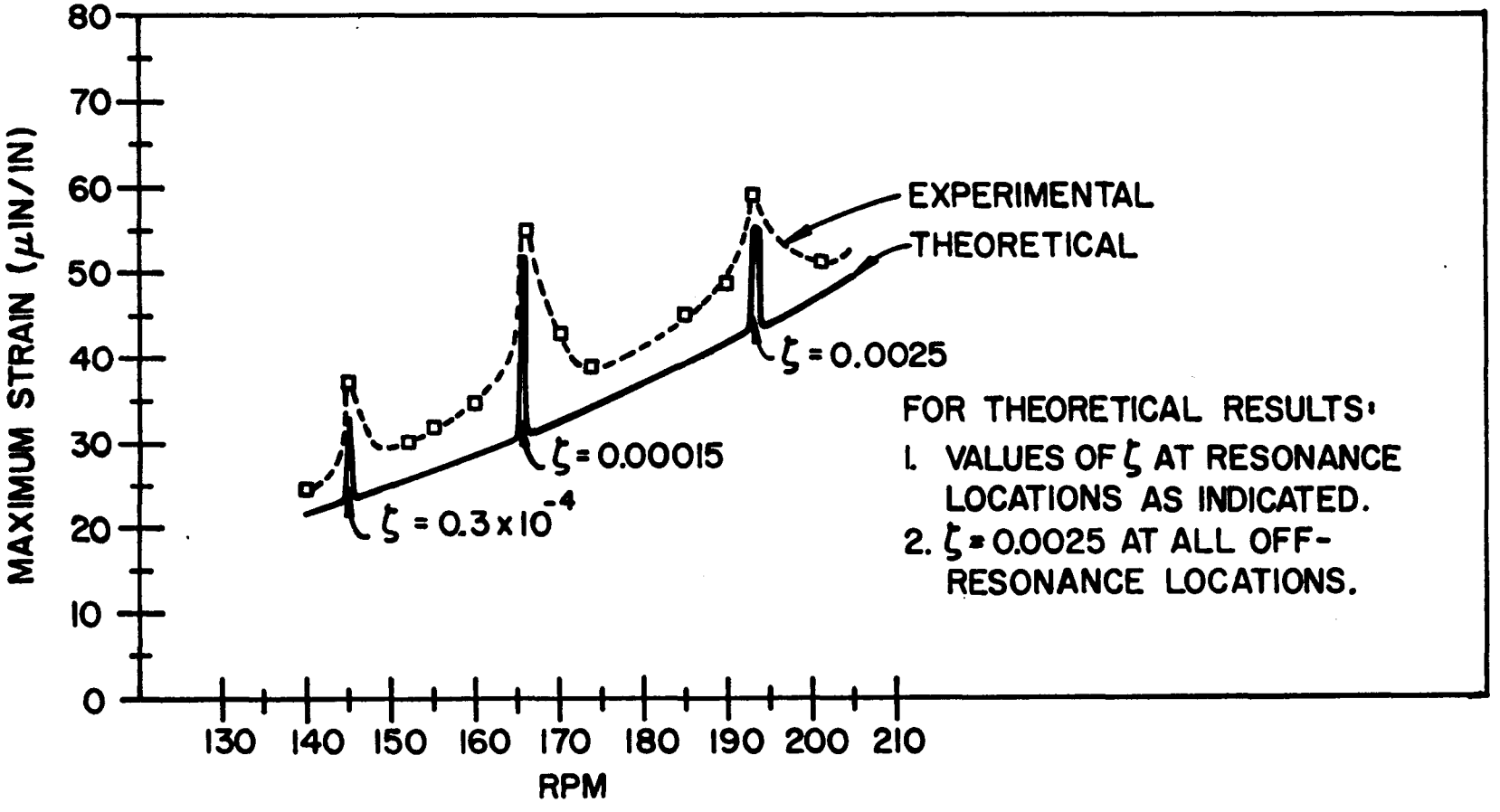

FIGURE 5.21: COMPARISON BETWEEN EXPERIMENTAL AND THEORETICAL RESULTS: CORRECTED MAXIMUM STRAIN AT BOTTOM GAGE LOCATION

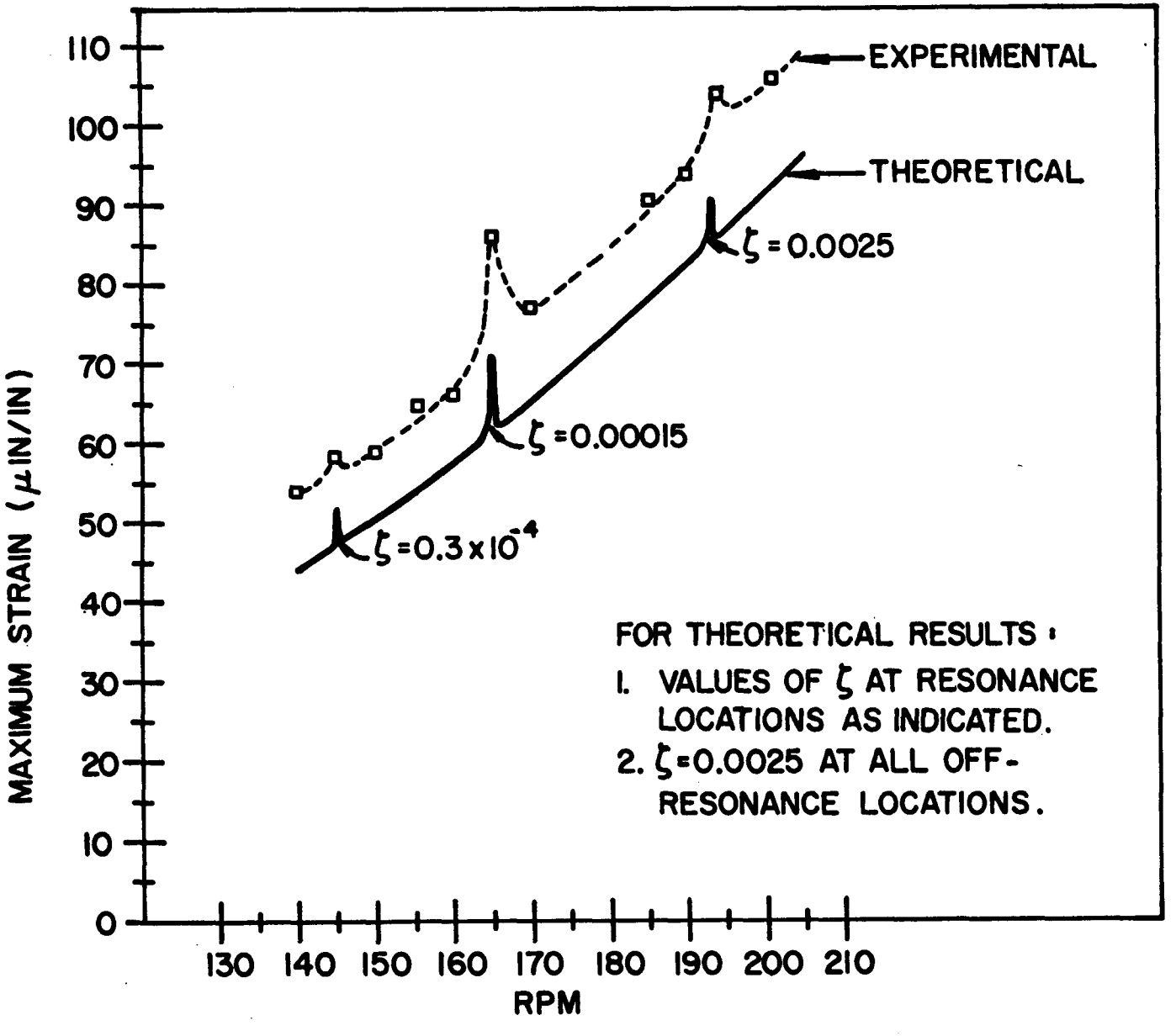

FIGURE 5.22: COMPARISON BETWEEN EXPERIMENTAL AND THEORETICAL RESULTS: CORRECTED MAXIMUM STRAIN AT TOP GAGE LOCATION

VI. DISCUSSION OF RESULTS

While from an engineering point of view the agreement between the experimentally obtained and theoretically predicted strains is very good, it is desirable to discuss some of the possible reasons for the existing discrepancies. These reasons may be found in certain simplifications in the mathematical modeling of the system, in the approximations of the solution method, as well as in some inaccuracies of the experiment.

A. Simplifications in System Modeling

The following lists simplifications in the mathematical modeling of the system:

1) Euler-Bernoulli bending theory, which neglects shear deformations, was used, and the influence of axial deformation was neglected.

2) Constant input angular velocity was assumed. (See Sources of Inaccuracy in Experiment below.)

3) The effect of gravity, which proved to be very important in the example mechanism, was neglected.(*)

(*) While the gravity correction brings the experimental results closer to the theoretically expected ones, one might have obtained better agreement if the static effects had been accounted for in the theory. This was omitted because it was felt that in realistic mechanisms, with comparable endmass and counterweights but vastly stiffer beams, the gravity effects would be negligible.

4) The frictional moments in the journal bearings are not accounted for.

5) The enlargements at the bearing locations, which influence both the frequency and the mass of the beam, were neglected.

6) A viscous damping mechanism was assumed for the beam.

7) The rotational inertia of the beam cross-section was disregarded.

B. Mathematical Approximations

The following lists the assumptions made in the solution of the mathematical model:

1) The solution technique represents an approximation with the assumption of shape functions belonging to an associated problem. Even though the geometric boundary conditions of this subproblem are identical to those of the actual problem, the dependency of the shape functions on the actual time portions of the solution, which should be obtained from a dispersion relationship, is not satisfied.

2) All non-linear terms are dropped without regard to their magnitude, and possible integro-differential portions of the differential equations are avoided by approximating the elastic angles by their rigid body counterparts.

3) The Hill's equations were decoupled.

4) Only the first three solution modes were superposed.

C. Sources of Inaccuracy in Experiment

1) Even though it was assumed that the contribution of the axial strains is small, a somewhat greater accuracy could have been obtained by using compensating strain gages.

2) The inability to maintain constant motor speed throughout a cycle introduced acceleration effects which were not reflected in the constant speed theory. Undoubtedly, this contributes to the larger than expected peak experimental strains.

VII. APPENDICES

APPENDIX A

PLANAR KINEMATICS OF ELASTIC LINK WITH COUNTERWEIGHT AND ENDMASS

1. Elastic Deformations of Beam According to Euler-Bernoulli Theory [32]

Figure A.1 shows a typical section of an elastic link. Its deformations are assumed to be those given by Euler-Bernoulli beam theory, i.e.

$$\left.\begin{aligned} U_P &= u - y\sin\psi \\ V_P &= v - y(1-\cos\psi) \end{aligned}\right\}, \tag{A.1}$$

where U_P represents the axial and V_P the transverse displacement of an arbitrary point P. The points P and P_c lie on the same cross-section, and P_c is a point on the centroidal locus. The components u and v are the axial and transverse displacements of the point P_c, respectively. The component u is due only to the foreshortening of the beam, i.e.

$$u = -\frac{1}{2}\int_0^x \left(\frac{\partial \tilde{v}}{\partial \xi}\right)^2 d\xi, \tag{A.2}$$

(*)

while tension or compression is neglected.

2. Position Vectors

The following section furnishes expressions for the position vectors of an arbitrary point on the link and of the centers of mass of the masses m* and M for the elastic link shown in Figure A.2. The origin of the space fixed coordinate system

(*) $v = v(x,t)$ and $\tilde{v} = v(\xi,t)$.

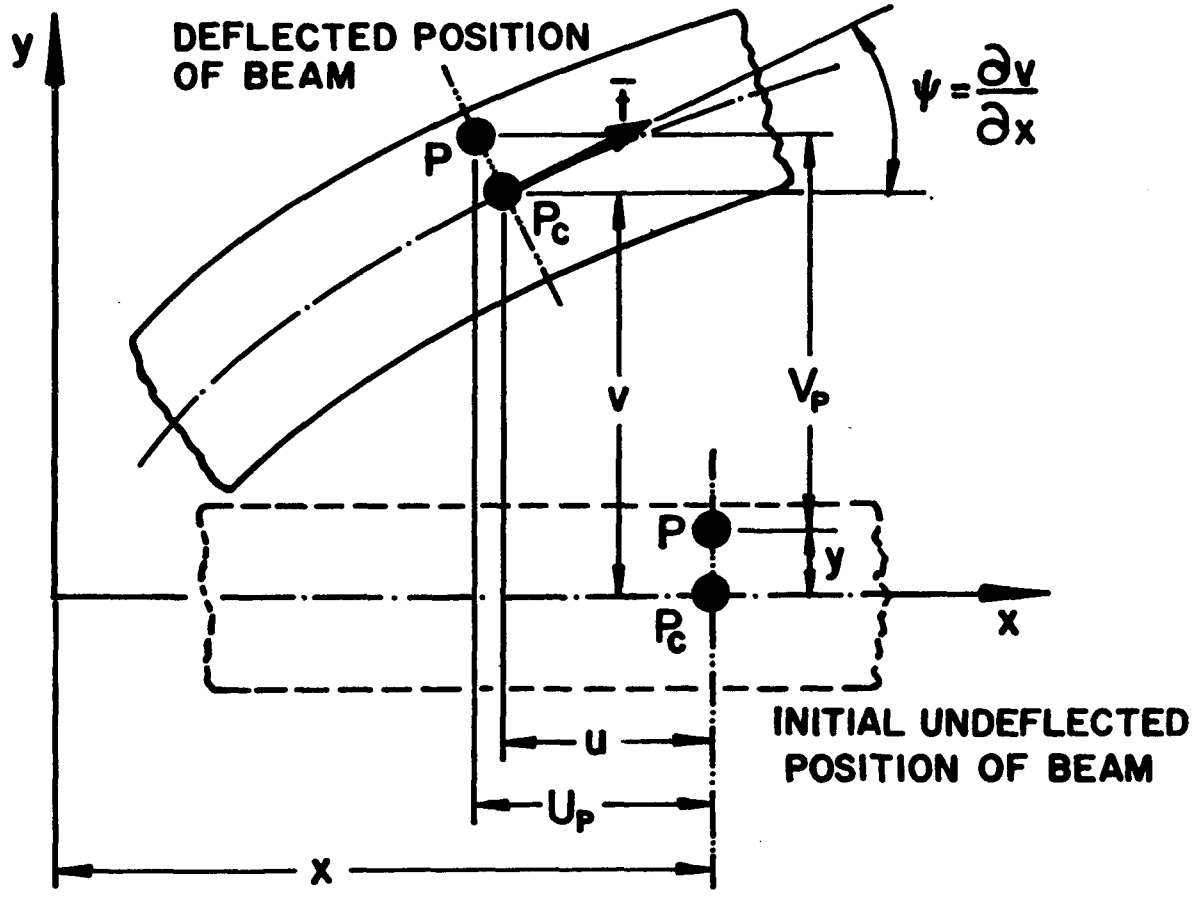

FIGURE A.1: DISPLACEMENT OF POINT ON BEAM

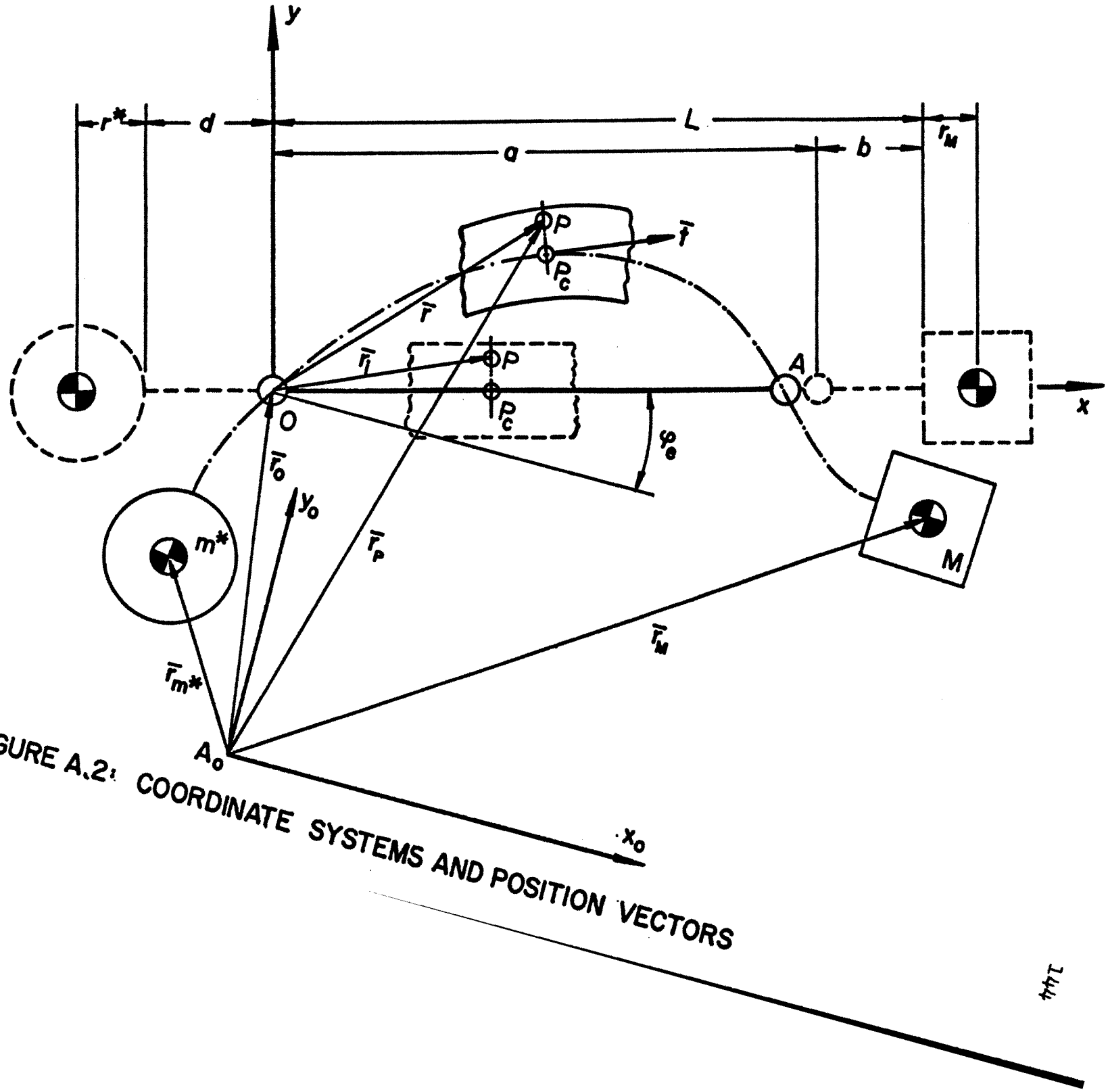

FIGURE A.2: COORDINATE SYSTEMS AND POSITION VECTORS

(x_0,y_0,z_0) is located at point A_0. The body fixed coordinate system (x,y,z) originates at point 0 and is located in such a manner that the x-axis connects the pivot points.

a) Position Vector to Arbitrary Point on Link

The position vector $\bar{r}_P$ of an arbitrary point P is given by:

$$\bar{r}_P = \bar{r}_0 + \bar{r}, \tag{A.3}$$

where $\bar{r}_0$ defines the position of point 0 with respect to point A_0. $\bar{r}$ is the position vector of point P with respect to point 0:

$$\bar{r} = \bar{r}_i + U_P\bar{i} + V_P\bar{j}. \tag{A.4}$$

In the above,

$$\bar{r}_i = x\bar{i} + y\bar{j}, \tag{A.5}$$

the vector from point 0 to the undeflected position of point P.

Substitution of equations (A.1) and (A.5) into (A.4) furnishes the complete expression for the body fixed vector $\bar{r}$:

$$\bar{r} = \left(x+u-y\sin\Psi\right)\bar{i} + \left(v+y\cos\Psi\right)\bar{j}. \tag{A.6}$$

b) Position Vector to Center of Mass of Counterweight m*

In order to describe the position vector $\bar{r}_{m*}$ to the counterweight m*, it is necessary to define the unit tangent vector $\bar{t}$ to the centroidal locus at an arbitrary point (see Figure A.1):

$$\bar{t} = \cos\Psi\bar{i} + \sin\Psi\bar{j}. \tag{A.7}$$

Then

$$\bar{r}_{m*} = \bar{r}_P(-d,0) - r^*\bar{t}(-d), \tag{A.8}$$

where $\bar{r}_P(-d,0)$ is the position vector of the point of attachment of the counterweight m*. With equations (A.3) and (A.7) this becomes:

$$\bar{r}_{m^*} = \bar{r}_0 + \left(-d+u(-d)-r^*\cos\psi(-d)\right)\bar{i} + \left(v(-d,t)-r^*\sin\psi(-d)\right)\bar{j}. \qquad (A.9)$$

c) Position Vector to Center of Mass of Endmass M

The position vector $\bar{r}_M$ to the center of mass of endmass M is shown in Figure A.2:

$$\bar{r}_M = \bar{r}_P(L,0) + r_M\bar{t}(L), \qquad (A.10)$$

or, with equations (A.3) and (A.7),

$$\bar{r}_M = \bar{r}_0 + \left(L+u(L)+r_M\cos\psi(L)\right)\bar{i} + \left(v(L,t)+r_M\sin\psi(L)\right)\bar{j}. \qquad (A.11)$$

3. Velocity Vectors

a) Velocity Vector of Arbitrary Point on Link

The velocity of point P is obtained by appropriate differentiation of equation (A.3):

$$\dot{\bar{r}}_P = \dot{\bar{r}}_0 + \frac{\partial\bar{r}}{\partial t} + \bar{\varphi}_e\times\bar{r}, \qquad (A.12)$$

where $\dot{\bar{r}}_0$ is the velocity of point O. The second and third terms represent the differentiation of the body fixed quantity $\bar{r}$ with respect to the space fixed system. $\bar{\varphi}_e = \dot{\varphi}_e\bar{k}$ is the absolute angular velocity of the coordinate system (x,y,z). Substitution of equation (A.6) leads to:

$$\dot{\bar{r}}_P = \dot{\bar{r}}_0 + \left(\dot{u}-\dot{\varphi}_e v - y(\dot{\varphi}_e+\dot{\psi})\cos\psi\right)\bar{i} + \left(\dot{v}+\dot{\varphi}_e(x+u)-y(\dot{\varphi}_e+\dot{\psi})\sin\psi\right)\bar{j}. \qquad (A.13)$$

b) Velocity Vector of the Center of Mass of Counterweight m*

Differentiation of equation (A.8) furnishes the velocity vector of the center of mass of the counterweight:

$$\dot{\bar{r}}_{m*} = \dot{\bar{r}}_p(-d,0) + \frac{\partial}{\partial t}\left(-r^*\bar{t}(-d)\right) + \dot{\bar{\varphi}}_e \times \left(-r^*\bar{t}(-d)\right) . \tag{A.14}$$

This becomes, with equations (A.7) and (A.13),

$$\dot{\bar{r}}_{m*} = \dot{\bar{r}}_0 + \left[\dot{u}(-d) - \dot{\varphi}_e v(-d,t) + r^*\left(\dot{\varphi}_e + \dot{\psi}(-d)\right)\sin\psi(-d)\right]\bar{i}$$
$$+ \left[\dot{v}(-d,t) + \dot{\varphi}_e\left(-d + u(-d)\right) - r^*\left(\dot{\varphi}_e + \dot{\psi}(-d)\right)\cos\psi(-d)\right]\bar{j} . \tag{A.15}$$

c) Velocity Vector of Center of Mass of Endmass M

Differentiation of equation (A.10) furnishes the velocity vector of endmass M:

$$\dot{\bar{r}}_M = \dot{\bar{r}}_p(L,0) + \frac{\partial}{\partial t}\left(r_M\bar{t}(L)\right) + \dot{\bar{\varphi}}_e \times \left(r_M\bar{t}(L)\right) . \tag{A.16}$$

This leads to:

$$\dot{\bar{r}}_M = \dot{\bar{r}}_0 + \left[\dot{u}(L) - \dot{\varphi}_e v(L,t) - r_M\left(\dot{\varphi}_e + \dot{\psi}(L)\right)\sin\psi(L)\right]\bar{i}$$
$$+ \left[\dot{v}(L,t) + \dot{\varphi}_e\left(L + u(L)\right) + r_M\left(\dot{\varphi}_e + \dot{\psi}(L)\right)\cos\psi(L)\right]\bar{j} . \tag{A.17}$$

d) Angular Velocities of Masses m* and M

The angular velocity $\dot{\bar{\theta}}_{m*}$ of the counterweight m* is given by:

$$\dot{\bar{\theta}}_{m*} = \left(\dot{\varphi}_e + \dot{\psi}(-d)\right)\bar{k} . \tag{A.18}$$

Similarly, the angular velocity $\dot{\bar{\theta}}_M$ of the endmass M is given by:

$$\dot{\bar{\theta}}_M = \left(\dot{\varphi}_e + \dot{\psi}(L)\right)\bar{k} . \tag{A.19}$$

4. Acceleration Vectors

a) Acceleration Vector of Arbitrary Point on Link

The acceleration of point P is obtained by double differentiation of equation (A.3), i.e.

$$\ddot{\bar{r}}_P = \ddot{\bar{r}}_0 + \frac{\partial^2 \bar{r}}{\partial t^2} + \ddot{\bar{\varphi}}_e \times \bar{r} - \dot{\varphi}_e^2 \bar{r} + 2\dot{\bar{\varphi}}_e \times \frac{\partial \bar{r}}{\partial t} \quad , \tag{A.20}$$

where $\ddot{\bar{r}}_0$ is the acceleration of point O, and the rest of the terms represent the second derivative of the body fixed quantity $\bar{r}$ with respect to the space fixed system. $\ddot{\bar{\varphi}}_e = \ddot{\varphi}_e \bar{k}$ is the angular acceleration of the coordinate system (x,y,z).

Substitution of equation (A.6) into the above and subsequent differentiation gives:

$$\ddot{\bar{r}}_P = \left[\ddot{R}_x + y\left(-(\ddot{\varphi}_e+\ddot{\psi})\cos\psi + (\dot{\varphi}_e+\dot{\psi})^2 \sin\psi\right)\right] \bar{i} + \left[\ddot{R}_y - y\left((\ddot{\varphi}_e+\ddot{\psi})\sin\psi + (\dot{\varphi}_e+\dot{\psi})^2\cos\psi\right)\right] \bar{j} \quad , \tag{A.21}$$

where

$$\ddot{R}_x = \ddot{\alpha} + \ddot{u} - v\ddot{\varphi}_e - u\dot{\varphi}_e^2 - 2\dot{v}\dot{\varphi}_e \quad , \tag{A.22}$$

$$\ddot{R}_y = \ddot{\beta} + \ddot{v} + u\ddot{\varphi}_e - v\dot{\varphi}_e^2 + 2\dot{u}\dot{\varphi}_e \quad , \tag{A.23}$$

are the x and y components of the acceleration of a point on the centroidal locus respectively, and

$$\ddot{\alpha} = \ddot{r}_{0x} - x\dot{\varphi}_e^2 \quad , \tag{A.24}$$

$$\ddot{\beta} = \ddot{r}_{0y} + x\ddot{\varphi}_e \quad , \tag{A.25}$$

are the x and y components of the acceleration of a point on

the x-axis and $\ddot{r}_{Ox}$, $\ddot{r}_{Oy}$ are the x and y components of the acceleration $\bar{\ddot{r}}_O$ of the origin of the body fixed coordinate system.

b) Acceleration Vector of the Center of Mass of Counterweight m*

The acceleration of the center of mass of counterweight m* is obtained by double differentiation of equation (A.8):

$$\bar{\ddot{r}}_{m^*} = \bar{\ddot{r}}(-d,0) + \frac{\partial^2\left(-r^*\bar{t}(-d)\right)}{\partial t^2} + \bar{\ddot{\varphi}}_e \times \left(-r^*\bar{t}(-d)\right) - \dot{\varphi}_e^2\left(-r^*\bar{t}(-d)\right) + 2\bar{\dot{\varphi}}_e \times \frac{\partial\left(-r^*\bar{t}(-d)\right)}{\partial t} \tag{A.26}$$

and, with equations (A.7) and (A.21), becomes:

$$\bar{\ddot{r}}_{m^*} = \left[\ddot{R}_x(-d) + r^*\left(\left(\ddot{\varphi}_e + \ddot{\psi}(-d)\right)\sin\psi(-d) + \left(\dot{\varphi}_e + \dot{\psi}(-d)\right)^2\cos\psi(-d)\right)\right]\bar{i} + \left[\ddot{R}_y(-d) - r^*\left(\left(\ddot{\varphi}_e + \ddot{\psi}(-d)\right)\cos\psi(-d) - \left(\dot{\varphi}_e + \dot{\psi}(-d)\right)^2\sin\psi(-d)\right)\right]\bar{j}\,. \tag{A.27}$$

c) Acceleration Vector of the Center of Mass of Endmass M

The acceleration of the center of mass of endmass M is obtained by double differentiation of equation (A.10):

$$\bar{\ddot{r}}_M = \bar{\ddot{r}}_p(L,0) + \frac{\partial^2\left(r_M\bar{t}(L)\right)}{\partial t^2} + \bar{\ddot{\varphi}}_e \times \left(r_M\bar{t}(L)\right) - \dot{\varphi}_e^2\left(r_M\bar{t}(L)\right) + 2\bar{\dot{\varphi}}_e \times \frac{\partial\left(r_M\bar{t}(L)\right)}{\partial t}\,, \tag{A.28}$$

and, with equations (A.7) and (A.21), becomes:

$$\bar{\ddot{r}}_M = \left[\ddot{R}_x(L) - r_M\left(\left(\ddot{\varphi}_e + \ddot{\psi}(L)\right)\sin\psi(L) + \left(\dot{\varphi}_e + \dot{\psi}(L)\right)^2\cos\psi(L)\right)\right]\bar{i} + \left[\ddot{R}_y(L) + r_M\left(\left(\ddot{\varphi}_e + \ddot{\psi}(L)\right)\cos\psi(L) - \left(\dot{\varphi}_e + \dot{\psi}(L)\right)^2\sin\psi(L)\right)\right]\bar{j}\,. \tag{A.29}$$

APPENDIX B

VIRTUAL DISPLACEMENTS

1. Virtual Displacement of Arbitrary Point on Link

The virtual displacement $\delta\bar{r}_P$ of an arbitrary point P is obtained by taking the variation of equation (A.3):

$$\delta\bar{r}_P = \delta\bar{r}_0 + \frac{\partial\bar{r}}{\partial u}\delta u + \frac{\partial\bar{r}}{\partial v}\delta v + \frac{\partial\bar{r}}{\partial\psi}\delta\psi + \overline{\delta\varphi}_e \times \bar{r}. \tag{B.1}$$

In this, $\delta\bar{r}_0$ represents the virtual displacement of point O (see Figure A.2), which must be defined in each case, and $\overline{\delta\varphi}_e = \delta\varphi_e \bar{k}$ is the virtual rotation of the body fixed coordinate system. Performing the indicated differentiations on $\bar{r}$ leads to:

$$\delta\bar{r}_P = \delta\bar{r}_0 + \bar{i}\,\delta u + \bar{j}\,\delta v - y(\cos\psi\,\bar{i} + \sin\psi\,\bar{j})\,\delta\psi + \left[-(v + y\cos\psi)\bar{i} + (x + u - y\sin\psi)\bar{j}\right]\delta\varphi_e . \tag{B.2}$$

2. Virtual Displacement of the Center of Mass of Counterweight m*

Subsequent to the substitution of equation (A.3) into equation (A.8), the virtual displacement $\delta\bar{r}_{m*}$ of the center of mass of the counterweight m* is obtained:

$$\delta\bar{r}_{m*} = \delta\bar{r}_0 + \frac{\partial\left(\bar{r}(-d,0) - r^*\bar{t}(-d)\right)}{\partial u(-d)}\delta u(-d) + \frac{\partial\left(\bar{r}(-d,0) - r^*\bar{t}(-d)\right)}{\partial v(-d)}\delta v(-d) + \frac{\partial\left(\bar{r}(-d,0) - r^*\bar{t}(-d)\right)}{\partial\psi(-d)}\delta\psi(-d) + \overline{\delta\varphi}_e \times \left(\bar{r}(-d,0) - r^*\bar{t}(-d)\right). \tag{B.3}$$

Thus,

$$\delta\bar{r}_{m*} = \delta\bar{r}_0 + \bar{i}\,\delta u(-d) + \bar{j}\,\delta v(-d,t) + r^*\left(\sin\psi(-d)\bar{i} - \cos\psi(-d)\bar{j}\right)\delta\psi(-d) + \left[\left(-v(-d,t) + r^*\sin\psi(-d)\right)\bar{i} + \left(-d + u(-d) - r^*\cos\psi(-d)\right)\bar{j}\right]\delta\varphi_e . \tag{B.4}$$

3. Virtual Displacement of the Center of Mass of Endmass M

Similarly, after the substitution of equation (A.3) into equation (A.10), the virtual displacement $\delta\bar{r}_M$ of the center of mass of the endmass M is given by:

$$\delta\bar{r}_M = \delta\bar{r}_0 + \frac{\partial\left(\bar{r}(L,0) + r_M\bar{t}(L)\right)}{\partial u(L)}\delta u(L) + \frac{\partial\left(\bar{r}(L,0)+r_M\bar{t}(L)\right)}{\partial v(L,t)}\delta v(L,t) + \frac{\partial\left(\bar{r}(L,0)+r_M\bar{t}(L)\right)}{\partial\Psi(L)}\delta\Psi(L) + \overline{\delta\varphi}_e \times \left(\bar{r}(L,0)+r_M\bar{t}(L)\right) . \quad (B.5)$$

Performing the indicated differentiations on the body fixed quantities leads to:

$$\delta\bar{r}_M = \delta\bar{r}_0 + \bar{i}\,\delta u(L) + \bar{j}\,\delta v(L,t) + r_M\left(-\sin\Psi(L)\,\bar{i} + \cos\Psi(L)\bar{j}\right)\delta\Psi(L) + \left[-\left(v(L,t) + r_M\sin\Psi(L)\right)\bar{i} + \left(L+u(L) + r_M\cos\Psi(L)\right)\bar{j}\right]\delta\varphi_e . \quad (B.6)$$

4. Virtual Rotation of Counterweight m*

The virtual rotation of the counterweight m*, with the help of equation (A.18), is given by:

$$\overline{\delta\theta}_{m^*} = \left(\delta\varphi_e + \delta\Psi(-d)\right)\bar{k} . \quad (B.7)$$

5. Virtual Rotation of Endmass M

The virtual rotation of the endmass M, with the help of equation (A.19), is given by:

$$\overline{\delta\theta}_M = \left(\delta\varphi_e + \delta\Psi(L)\right)\bar{k} . \quad (B.8)$$

APPENDIX C

DERIVATION OF EQUATIONS OF MOTION FOR BOTH ELASTIC LINKS WITH HELP OF LAGRANGE MULTIPLIERS

1. Working Form of Hamilton's Equation with Lagrange Multipliers

The working form of Hamilton's equation is obtained from the substitution of equation (3.9) to (3.13), (3.15) and (3.16) into equation (3.1) (after appropriate variation):

$$
\begin{aligned}
&-\int_{t_0}^{t_1}\int_{0}^{a_2}\int_{A_2}\rho_2\,\ddot{\bar{r}}_{P_2}\cdot\delta\bar{r}_{P_2}\,dA_2\,dx_2\,dt-\int_{t_0}^{t_1}\int_{-d}^{L}\int_{A_3}\rho_3\,\ddot{\bar{r}}_{P_3}\cdot\delta\bar{r}_{P_3}\,dA_3\,dx_3\,dt-\int_{t_0}^{t_1}m^*\,\ddot{\bar{r}}_{m^*}\cdot\delta\bar{r}_{m^*}\,dt\\
&-\int_{t_0}^{t_1}J_{m^*}\,\ddot{\bar{\theta}}_{m^*}\cdot\delta\bar{\theta}_{m^*}\,dt-\int_{t_0}^{t_1}M\,\ddot{\bar{r}}_{M}\cdot\delta\bar{r}_{M}\,dt-\int_{t_0}^{t_1}J_{M}\,\ddot{\bar{\theta}}_{M}\cdot\delta\bar{\theta}_{M}\,dt-\int_{t_0}^{t_1}\int_{0}^{a_2}E_2I_2\frac{\partial^4v_2}{\partial x_2^4}\,\delta v_2\,dx_2\,dt\\
&-\int_{t_0}^{t_1}\int_{-d}^{0}E_3I_3\frac{\partial^4v_3}{\partial x_3^4}\,\delta v_3\,dx_3\,dt-\int_{t_0}^{t_1}\int_{0}^{a_3}E_3I_3\frac{\partial^4v_3}{\partial x_3^4}\,\delta v_3\,dx_3\,dt-\int_{t_0}^{t_1}\int_{a_3}^{L}E_3I_3\frac{\partial^4v_3}{\partial x_3^4}\,\delta v_3\,dx_3\,dt\\
&-\int_{t_0}^{t_1}\left[E_2I_2\frac{\partial^2v_2}{\partial x_2^2}\,\delta\frac{\partial v_2}{\partial x_2}-E_2I_2\frac{\partial^3v_2}{\partial x_2^3}\,\delta v_2\right]_0^{a_2}dt-\int_{t_0}^{t_1}\left\{\left[E_3I_3\frac{\partial^2v_3}{\partial x_3^2}\,\delta\frac{\partial v_3}{\partial x_3}-E_3I_3\frac{\partial^3v_3}{\partial x_3^3}\,\delta v_3\right]_{-d}^{0^-}\right.\\
&\left.+\left[E_3I_3\frac{\partial^2v_3}{\partial x_3^2}\,\delta\frac{\partial v_3}{\partial x_3}-E_3I_3\frac{\partial^3v_3}{\partial x_3^3}\,\delta v_3\right]_{0}^{a_3}+\left[E_3I_3\frac{\partial^2v_3}{\partial x_3^2}\,\delta\frac{\partial v_3}{\partial x_3}-E_3I_3\frac{\partial^3v_3}{\partial x_3^3}\,\delta v_3\right]_{a_3^+}^{L}\right\}dt\\
&+\int_{t_0}^{t_1}\int_{0}^{a_2}\lambda_1\delta f_1\,dx_2\,dt+\int_{t_0}^{t_1}\int_{-d}^{L}\lambda_2\delta f_2\,dx_3\,dt+\int_{t_0}^{t_1}\sum_{i=3}^{8}\lambda_i\delta f_i\,dt=0. \qquad \text{(C.1)}
\end{aligned}
$$

2. Substitution into Hamilton's Equation

The following substitutions are now made in equation (C.1):

a) The accelerations of the various points according to Appendix A-4, introducing the appropriate subscripts referring to links 2 and 3.

While not expanded, the coupler link terms $\ddot{R}_{x2}$ and $\ddot{R}_{y2}$ contain

$$\left.\begin{aligned} \ddot{r}_{Ox_2} &= -\dot{\varphi}_1^2 a_1 \cos(\varphi_1-\varphi_{2e}) - \ddot{\varphi}_1 a_1 \sin(\varphi_1-\varphi_{2e}) \\ \text{and} \\ \ddot{r}_{Oy_2} &= -\dot{\varphi}_1^2 a_1 \sin(\varphi_1-\varphi_{2e}) + \ddot{\varphi}_1 a_1 \cos(\varphi_1-\varphi_{2e}) . \end{aligned}\right\} \qquad (C.2a)$$

Similarly, for the terms $\ddot{R}_{x3}$ and $\ddot{R}_{y3}$, which are associated with the rocker,

$$\left.\begin{aligned} \ddot{r}_{Ox_3} &= 0 \\ \text{and} \\ \ddot{r}_{Oy_3} &= 0 . \end{aligned}\right\} \qquad (C.2b)$$

b) The virtual displacements according to Appendix B.

c) The variations of the constraint equations according to Section III-E.

Further, the dot products are executed, integrations over the cross-sectional areas A_2 and A_3 are performed, the trigonometric terms involving ψ are combined, and the following abbreviations are made:

$$\left.\begin{aligned} \mu_2 &= \rho_2 A_2 , \\ \mu_3 &= \rho_3 A_3 . \end{aligned}\right\} \qquad (C.2c)$$

This leads to:

$$-\int_{t_0}^{t_1}\int_{0}^{a_2}\left\{\mu_2\ddot{R}_{x_2}\delta u_2+\mu_2\ddot{R}_{y_2}\delta v_2+\rho_2 I_2\left(\ddot{\varphi}_{2e}+\ddot{\psi}_2\right)\delta\psi_2+\left(\mu_2(x_2+u_2)\ddot{R}_{y_2}-\mu_2 v_2\ddot{R}_{x_2}+\rho_2 I_2\left(\ddot{\varphi}_{2e}+\ddot{\psi}_2\right)\right)\delta\varphi_{2e}\right\}dx_2dt$$

$$-\int_{t_0}^{t_1}\int_{-d}^{L}\left\{\mu_3\ddot{R}_{x_3}\delta u_3+\mu_3\ddot{R}_{y_3}\delta v_3+\rho_3 I_3\left(\ddot{\varphi}_{3e}+\ddot{\psi}_3\right)\delta\psi_3+\left(\mu_3(x_3+u_3)\ddot{R}_{y_3}-\mu_3 v_3\ddot{R}_{x_3}+\rho_3 I_3\left(\ddot{\varphi}_{3e}+\ddot{\psi}_3\right)\right)\delta\varphi_{3e}\right\}dx_3dt$$

$$-\int_{t_0}^{t_1} m^*\left\{\left(\ddot{R}_{x_3}(-d)+r^*\left(\left(\ddot{\varphi}_{3e}+\ddot{\psi}_3(-d)\right)\sin\psi_3(-d)+\left(\dot{\varphi}_{3e}+\dot{\psi}_3(-d)\right)^2\cos\psi_3(-d)\right)\right)\delta u_3(-d)+\left(\ddot{R}_{y_3}(-d)-r^*\left(\left(\ddot{\varphi}_{3e}+\ddot{\psi}_3(-d)\right)\cos\psi_3(-d)\right.\right.\right.$$

$$\left.\left.\left.-\left(\dot{\varphi}_{3e}+\dot{\psi}_3(-d)\right)^2\sin\psi_3(-d)\right)\right)\delta v_3(-d,t)+\left(r^*\ddot{R}_{x_3}(-d)\sin\psi_3(-d)-r^*\ddot{R}_{y_3}(-d)\cos\psi_3(-d)+r^{*2}\left(\ddot{\varphi}_{3e}+\ddot{\psi}_3(-d)\right)\right)\delta\psi_3(-d)+\left(\left(-v_3(-d,t)\right.\right.\right.$$

$$\left.\left.\left.+r^*\sin\psi_3(-d)\right)\ddot{R}_{x_3}(-d)-r^*v_3(-d,t)\left(\left(\ddot{\varphi}_{3e}+\ddot{\psi}_3(-d)\right)\sin\psi_3(-d)+\left(\dot{\varphi}_{3e}+\dot{\psi}_3(-d)\right)^2\cos\psi_3(-d)\right)+\left(-d+u_3(-d)-r^*\cos\psi_3(-d)\right)\ddot{R}_{y_3}(-d)\right.$$

$$\left.-r^*\left(-d+u_3(-d)\right)\left(\left(\ddot{\varphi}_{3e}+\ddot{\psi}_3(-d)\right)\cos\psi_3(-d)-\left(\dot{\varphi}_{3e}+\dot{\psi}_3(-d)\right)^2\sin\psi_3(-d)\right)+r^{*2}\left(\ddot{\varphi}_{3e}+\ddot{\psi}_3(-d)\right)\right\}\delta\varphi_{3e}\Big\}dt-\int_{t_0}^{t_1}\Big\{J_{m^*}\left(\ddot{\varphi}_{3e}+\ddot{\psi}_3(-d)\right)\delta\varphi_{3e}$$

$$+J_{m^*}\left(\ddot{\varphi}_{3e}+\ddot{\psi}_3(-d)\right)\delta\psi_3(-d)\Big\}dt-\int_{t_0}^{t_1}M\left\{\left(\ddot{R}_{x_3}(L)-r_{M}\left(\left(\ddot{\varphi}_{3e}+\ddot{\psi}_3(L)\right)\sin\psi_3(L)+\left(\dot{\varphi}_{3e}+\dot{\psi}_3(L)\right)^2\cos\psi_3(L)\right)\right)\delta u_3(L)+\left(\ddot{R}_{y_3}(L)\right.\right.$$

$$\left.\left.+r_{M}\left(\left(\ddot{\varphi}_{3e}+\ddot{\psi}_3(L)\right)\cos\psi_3(L)-\left(\dot{\varphi}_{3e}+\dot{\psi}_3(-d)\right)^2\sin\psi_3(L)\right)\right)\delta v_3(L,t)+\left(-r_{M}\ddot{R}_{x_3}(L)\sin\psi_3(L)+r_{M}\ddot{R}_{y_3}(L)\cos\psi_3(L)+r_{M}^2\left(\ddot{\varphi}_{3e}+\ddot{\psi}_3(L)\right)\right)\delta\psi_3(L)\right.$$

$$\left.+\left(-\left(v_3(L,t)+r_{M}\sin\psi_3(L)\right)\ddot{R}_{x_3}(L)+r_{M}v_3(L,t)\left(\left(\ddot{\varphi}_{3e}+\ddot{\psi}_3(L)\right)\sin\psi_3(L)+\left(\dot{\varphi}_{3e}+\dot{\psi}_3(L)\right)^2\cos\psi_3(L)\right)+\left(L+u_3(L)+r_{M}\cos\psi_3(L)\right)\ddot{R}_{y_3}(L)\right.\right.$$

$$\left.\left.+r_{M}\left(L+u_3(L)\right)\left(\left(\ddot{\varphi}_{3e}+\ddot{\psi}_3(L)\right)\cos\psi_3(L)-\left(\dot{\varphi}_{3e}+\dot{\psi}_3(L)\right)^2\sin\psi_3(L)\right)+r_{M}^2\left(\ddot{\varphi}_{3e}+\ddot{\psi}_3(L)\right)\right)\delta\varphi_{3e}\right\}dt-\int_{t_0}^{t_1}\left\{J_{M}\left(\ddot{\varphi}_{3e}+\ddot{\psi}_3(L)\right)\delta\varphi_{3e}+\cdots\right.$$

$$+J_{H}\left(\ddot{\varphi}_{3e}+\ddot{\tilde{\varphi}}_{3}(L)\right)\delta\tilde{\varphi}_{3}(L)\Big\}dt-\int_{t_0}^{t_1}\int_{0}^{a_2}E_2I_2\frac{\partial^4 v_2}{\partial x_2^4}\delta v_2\,dx_2dt-\int_{t_0}^{t_1}\int_{-d}^{0}E_3I_3\frac{\partial^4 v_3}{\partial x_3^4}\delta v_3\,dx_3dt-\int_{t_0}^{t_1}\int_{0}^{a_3}E_3I_3\frac{\partial^4 v_3}{\partial x_3^4}\delta v_3\,dx_3dt$$

$$-\int_{t_0}^{t_1}\int_{a_3}^{L}E_3I_3\frac{\partial^4 v_2}{\partial x_3^4}\delta v_3\,dx_3dt-\int_{t_0}^{t_1}\left[E_2I_2\frac{\partial^2 v_2}{\partial x_2^2}\,\delta\frac{\partial v_2}{\partial x_2}-E_2I_2\frac{\partial^3 v_2}{\partial x_2^3}\delta v_2\right]_0^{a_2}dt-\int_{t_0}^{t_1}\Big\{\left[E_3I_3\frac{\partial^2 v_3}{\partial x_3^2}\,\delta\frac{\partial v_3}{\partial x_3}-E_3I_3\frac{\partial^3 v_3}{\partial x_3^3}\delta v_3\right]_{-d}^{0^-}$$

$$+\left[E_3I_3\frac{\partial^2 v_3}{\partial x_3^2}\,\delta\frac{\partial v_3}{\partial x_3}-E_3I_3\frac{\partial^3 v_3}{\partial x_3^3}\delta v_3\right]_0^{a_3}+\left[E_3I_3\frac{\partial^2 v_3}{\partial x_3^2}\,\delta\frac{\partial v_3}{\partial x_3}-E_3I_3\frac{\partial^3 v_3}{\partial x_3^3}\delta v_3\right]_{a_3^+}^{L}\Big\}dt+\int_{t_0}^{t_1}\int_{0}^{a_2}\lambda_1\Big(\delta u_2+\frac{\partial v_2}{\partial x_2}\delta v_2-\frac{\partial v_2(0,t)}{\partial x_2}\delta v_2(0,t)$$

$$-\int_0^{x_2}\frac{\partial^2\tilde{v}_2}{\partial\xi_2^2}\,\delta\tilde{v}_2\,d\xi_2\Big)dx_2dt+\int_{t_0}^{t_1}\int_{-d}^{L}\lambda_2\Big(\delta u_3+\frac{\partial v_3}{\partial x_3}\delta v_3-\frac{\partial v_3(0,t)}{\partial x_3}\delta v_3(0,t)\Big)dx_3dt-\int_{t_0}^{t_1}\int_{-d}^{0}\lambda_2\int_0^{x_3}\frac{\partial^2\tilde{v}_2}{\partial\xi_3^2}\,\delta\tilde{v}_3\,d\xi_3dx_3dt$$

$$-\int_{t_0}^{t_1}\int_0^{a_3}\lambda_2\int_0^{x_3}\frac{\partial^2\tilde{v}_3}{\partial\xi_3^2}\,\delta\tilde{v}_3\,d\xi_3dx_3dt-\int_{t_0}^{t_1}\int_{a_3}^{L}\lambda_2\Big(\int_0^{a_3}\frac{\partial^2\tilde{v}_3}{\partial\xi_3^2}\,\delta\tilde{v}_3\,d\xi_3+\int_{a_3}^{x_3}\frac{\partial^2\tilde{v}_3}{\partial\xi_3^2}\,\delta\tilde{v}_3d\xi_3\Big)dx_3dt+\int_{t_0}^{t_1}\Big\{\lambda_3\Big(\delta u_2(a_2)$$

$$+\frac{\partial v_2(a_2,t)}{\partial x_2}\,\delta v_2(a_2,t)-\frac{\partial v_2(0,t)}{\partial x_2}\,\delta v_2(0,t)-\int_0^{a_2}\frac{\partial^2 v_2}{\partial x_2^2}\,\delta v_2dx_2\Big)+\lambda_4\Big(\delta u_3(a_3)+\frac{\partial v_3(a_3,t)}{\partial x_3}\,\delta v_3(a_3,t)-\frac{\partial v_3(a,t)}{\partial x_3}\,\delta v_3(a,t)$$

$$-\int_0^{a_3}\frac{\partial^2 v_3}{\partial x_3^2}\,\delta v_3dx_3\Big)+\lambda_5\Big(\delta u_3(-d)+\frac{\partial v_3(-d,t)}{\partial x_3}\,\delta v_3(-d,t)-\frac{\partial v_3(0,t)}{\partial x_3}\,\delta v_3(a,t)-\int_0^{-d}\frac{\partial^2 v_3}{\partial x_3^2}\,\delta v_3dx_3\Big)+\lambda_6\Big(\delta u_3(L)$$

$$+\frac{\partial v_3(L,t)}{\partial x_3}\,\delta v_3(L,t)-\frac{\partial v_3(0,t)}{\partial x_3}\,\delta v_3(0,t)-\int_0^{a_3}\frac{\partial^2 v_3}{\partial x_3^2}\,\delta v_3dx_3-\int_{a^3}^{L}\frac{\partial^2 v_3}{\partial x_3^2}\,\delta v_3dx_3\Big)+\lambda_7\Big(\cos\varphi_{2e}\,\delta u_2(a_2)$$

$$-(a_2+u_2(a_2))\sin\varphi_{2e}\,\delta\varphi_{2e}-\cos\varphi_{3e}\,\delta u_3(a_3)+(a_3+u_3(a_3))\sin\varphi_{3e}\,\delta\varphi_{3e}\Big)+\lambda_8\Big(\sin\varphi_{2e}\,\delta u_2(a_2)$$

$$+(a_2+u_2(a_2))\cos\varphi_{2e}\,\delta\varphi_{2e}-\sin\varphi_{3e}\,\delta u_3(a_3)-(a_3+u_3(a_3))\cos\varphi_{3e}\,\delta\varphi_{3e}\Big)\Big\}dt=0 \qquad (C.3)$$

3. Final Form of Hamilton's Equation

Before proceeding, the following simplifications and transformations are introduced:

Since small deflection theory is used:

$$\cos\psi \approx 1,$$

$$\sin\psi \approx \psi = \frac{\partial v}{\partial x}\,.$$

In addition,

$$\delta\psi = \delta\frac{\partial v}{\partial x}\,,$$

and all terms containing this expression are integrated by parts.

In order to be able to collect all terms in δv, such expressions as

$$\int_0^{a_1} \lambda_1 \int_0^{x_1} \frac{\partial^2 \tilde{v}_1}{\partial \xi_1^2}\, \delta\tilde{v}_1\, d\xi_1\, dx_1\,,$$

which contain variable limits are transformed according to:

$$\int_\alpha^\beta F(x)\int_\alpha^x G(\xi)\,d\xi\,dx = \int_\alpha^\beta G(x)\int_x^\beta F(\xi)\,d\xi\,dx\,.^{(*)} \qquad (C.4)$$

When the limits are constant, one uses:

$$\int_{a_2}^{L} F(x)\int_0^{a_2} G(\xi)\,d\xi\,dx = \int_0^{a_2} G(x)\int_{a_2}^{L} F(\xi)\,d\xi\,dx\,. \qquad (C.5)$$

The above leads to the final form of Hamilton's integral, which consists of two parts. The first part gives rise to the associated Euler-Lagrange equations, while the second one, after consideration of the geometric boundary conditions, leads to the natural or dynamic boundary conditions. Both parts contain the Lagrange multipliers.

(*) Based on Leibnitz's rule of differentiation under the integral sign and subsequent integration by parts.

$$\int_{t_0}^{t_1}\int_0^{a_2}\left(\mu_2\ddot{R}_{y_2}+E_2I_2\frac{\partial^4 v_2}{\partial x_2^4}-\lambda_1\frac{\partial v_2}{\partial x_2}-\frac{\partial}{\partial x_2}\left(\rho_2 I_2\left(\ddot{\varphi}_{3e}+\frac{\partial^3 v_2}{\partial x_2\partial t^2}\right)\right)+\frac{\partial^2 v_2}{\partial x_2^2}\left(\int_{x_2}^{a_2}\lambda_1 d\xi_2+\lambda_3\right)\right)\delta v_2 dx_2 dt+\int_{t_0}^{t_1}\int_{-d}^{0}\left(\mu_3\ddot{R}_{y_3}-\lambda_2\frac{\partial v_3}{\partial x_3}\right.$$

$$\left.+E_3I_3\frac{\partial^4 v_3}{\partial x_3^4}-\frac{\partial}{\partial x_3}\left(\rho_3 I_3\left(\ddot{\varphi}_{3e}+\frac{\partial^3 v_3}{\partial x_3\partial t^2}\right)\right)+\frac{\partial^2 v_3}{\partial x_3^2}\left(\int_{x_3}^{-d}\lambda_2 d\xi_3-\lambda_5\right)\right)\delta v_3 dx_3 dt+\int_{t_0}^{t_1}\int_0^{a_2}\left(\mu_3\ddot{R}_{y_3}-\lambda_2\frac{\partial v_3}{\partial x_3}+E_3I_3\frac{\partial^4 v_3}{\partial x_3^4}-\frac{\partial}{\partial x_3}\left(\rho_3 I_3\left(\ddot{\varphi}_{3e}\right.\right.\right.$$

$$\left.\left.\left.+\frac{\partial^3 v_3}{\partial x_3\partial t^2}\right)\right)+\frac{\partial^2 v_3}{\partial x_3^2}\left(\int_{x_3}^{L}\lambda_2 d\xi_3+\lambda_4+\lambda_6\right)\right)\delta v_3 dx_3 dt+\int_{t_0}^{t_1}\int_{a_3}^{L}\left(\mu_3\ddot{R}_{y_3}-\lambda_2\frac{\partial v_3}{\partial x_3}+E_3I_3\frac{\partial^4 v_3}{\partial x_3^4}-\frac{\partial}{\partial x_3}\left(\rho_3 I_3\left(\ddot{\varphi}_{3e}+\frac{\partial^3 v_3}{\partial x_3\partial t^2}\right)\right)+\frac{\partial^2 v_3}{\partial x_3^2}\left(\int_{x_3}^{L}\lambda_2 d\xi_3\right.\right.$$

$$\left.\left.+\lambda_6\right)\right)\delta v_3 dx_3 dt+\int_{t_0}^{t_1}\int_0^{a_2}\left(\mu_2\ddot{R}_{x_2}-\lambda_1\right)\delta u_2 dx_2 dt+\int_{t_0}^{t_1}\left\{\int_0^{a_2}\left(\mu_2(x_2+u_2)\ddot{R}_{y_2}-\mu_2 v_2\ddot{R}_{x_2}+\rho_2 I_2\left(\ddot{\varphi}_{3e}+\frac{\partial^3 v_2}{\partial x_2\partial t^2}\right)\right)dx_2+\lambda_7(a_2+u_2(a_2))\sin\varphi_{3e}\right.$$

$$\left.+\lambda_8(a_2+u_2(a_2))\cos\varphi_{3e}\right\}\delta\varphi_{3e}dt+\int_{t_0}^{t_1}\int_{-d}^{L}\left(\mu_3\ddot{R}_{x_3}-\lambda_2\right)\delta u_3 dx_3 dt+\int_{t_0}^{t_1}\left\{\int_{-d}^{L}\left[\left(\mu_3(x_3+u_3)\ddot{R}_{y_3}-\mu_3 v_3\ddot{R}_{x_3}+\rho_3 I_3\left(\ddot{\varphi}_{3e}+\frac{\partial^3 v_3}{\partial x_3\partial t^2}\right)\right)dx_3\right.\right.$$

$$+m^*\left(-v_3(-d,t)+r^{*x}\frac{\partial v_3(-d,t)}{\partial x_3}\right)\ddot{R}_{x_3}(-d)-m^*r^{*x}v_3(-d,t)\left(\left(\ddot{\varphi}_{3e}+\frac{\partial^3 v_3(-d,t)}{\partial x_3\partial t^2}\right)\frac{\partial v_3(-d,t)}{\partial x_3}+\left(\dot{\varphi}_{3e}+\frac{\partial^2 v_3(-d,t)}{\partial x_3\partial t}\right)^2\right)+m^*\left(-d+u_3(-d)-r^{*x}\right)\ddot{R}_{y_3}(-d)$$

$$-m^*r^{*x}\left(-d+u_3(-d)\right)\left(\left(\ddot{\varphi}_{3e}+\frac{\partial^3 v_3(-d,t)}{\partial x_3\partial t^2}\right)-\left(\dot{\varphi}_{3e}+\frac{\partial^2 v_3(-d,t)}{\partial x_3\partial t}\right)^2\frac{\partial v_3(-d,t)}{\partial x_3}\right)+\left(J_{m^*}+m^*r^{*2}\right)\left(\ddot{\varphi}_{3e}+\frac{\partial^3 v_3(-d,t)}{\partial x_3\partial t^2}\right)-M\left(v_3(L,t)\right.$$

$$\left.+r_M\frac{\partial v_3(L,t)}{\partial x_3}\right)\ddot{R}_{x_3}(L)+Mr_M v_3(L,t)\left(\left(\ddot{\varphi}_{3e}+\frac{\partial^3 v_3(L,t)}{\partial x_3\partial t^2}\right)\frac{\partial v_3(L,t)}{\partial x_3}+\left(\dot{\varphi}_{3e}+\frac{\partial^2 v_3(L,t)}{\partial x_3\partial t}\right)^2\right)+M\left(L+u_3(L)+r_M\right)\ddot{R}_{y_3}(L)$$

$$+Mr_M\left(L+u_3(L)\right)\left(\left(\ddot{\varphi}_{3e}+\frac{\partial^3 v_3(L,t)}{\partial x_3\partial t^2}\right)-\left(\dot{\varphi}_{3e}+\frac{\partial^2 v_3(L,t)}{\partial x_3\partial t}\right)^2\frac{\partial v_3(L,t)}{\partial x_3}\right)+\left(J_M+Mr_M^2\right)\left(\ddot{\varphi}_{3e}+\frac{\partial^3 v_3(L,t)}{\partial x_3\partial t^2}\right)-\lambda_7\left(a_3+u_3(a_3)\right)\sin\varphi_{3e}$$

$$+\lambda_8\left(a_3+u_3(a_3)\right)\cos\varphi_{3e}\Big]\delta\varphi_{3e}+\left(-\lambda_3-\lambda_7\cos\varphi_{2e}-\lambda_8\sin\varphi_{2e}\right)\delta u_2(a_2)+\left(m^*\ddot{R}_{x_3}(-d)+m^*r^{*x}\left(\left(\ddot{\varphi}_{3e}+\frac{\partial^3 v_3(-d,t)}{\partial x_3\partial t^2}\right)\frac{\partial v_3(-d,t)}{\partial x_3}\right.\right.$$

$$\left.\left.+\left(\dot{\varphi}_{3e}+\frac{\partial^2 v_3(-d,t)}{\partial x_3\partial t}\right)^2\right)-\lambda_5\right)\delta u_3(-d)+\left(-\lambda_4+\lambda_7\cos\varphi_{3e}+\lambda_8\sin\varphi_{3e}\right)\delta u_3(a_3)+\left(M\ddot{R}_{x_3}(L)-Mr_M\left(\left(\ddot{\varphi}_{3e}+\frac{\partial^3 v_3(L,t)}{\partial x_3\partial t^2}\right)\frac{\partial v_3(L,t)}{\partial x_3}\right.\right.$$

$$\left.\left.\left.+\left(\dot{\varphi}_{3e}+\frac{\partial^2 v_3(L,t)}{\partial x_3\partial t}\right)^2\right)-\lambda_6\right)\delta u_3(L)\right\}dt+\cdots \qquad (C.6a)$$

$$+\int_{t_0}^{t_1}\Bigg\{\left[E_2I_2\frac{\partial^2 v_2}{\partial x_2^2}\,\delta\frac{\partial v_2}{\partial x_2}-\left(E_2I_2\frac{\partial^3 v_2}{\partial x_2^3}+\lambda_3\frac{\partial v_2}{\partial x_2}-\rho_2I_2\left(\ddot{\varphi}_{3e}+\frac{\partial^3 v_2}{\partial x_2\partial t^2}\right)\right)\delta v_2\right]_0^{a_2}+\int_0^{a_2}\lambda_1 dx_2\frac{\partial v_2(0,t)}{\partial x_2}\,\delta v_1(0,t)$$

$$+\left[E_3I_3\frac{\partial^2 v_3}{\partial x_3^2}\,\delta\frac{\partial v_3}{\partial x_3}-E_3I_3\frac{\partial^3 v_3}{\partial x_3^3}\,\delta v_3\right]_{-d}^{0^-}+\left[E_3I_3\frac{\partial^2 v_3}{\partial x_3^2}\,\delta\frac{\partial v_3}{\partial x_3}-E_3I_3\frac{\partial^3 v_3}{\partial x_3^3}\,\delta v_3\right]_{0^+}^{a_3}+\left[E_3I_3\frac{\partial^2 v_3}{\partial x_3^2}\,\delta\frac{\partial v_3}{\partial x_3}-E_3I_3\frac{\partial^3 v_3}{\partial x_3^3}\,\delta v_3\right]_{a_3^+}^{L}$$

$$+\int_{-d}^{L}\lambda_2 dx_3\frac{\partial v_3(0,t)}{\partial x_3}\,\delta v_3(0,t)-\lambda_5\left[\frac{\partial v_2}{\partial x_3}\,\delta v_3\right]_0^{-d}-\lambda_4\left[\frac{\partial v_2}{\partial x_3}\,\delta v_3\right]_0^{a_3}-\lambda_6\left[\frac{\partial v_3}{\partial x_3}\,\delta v_3\right]_0^{L}+\left[\rho_3I_3\left(\ddot{\varphi}_{3e}+\frac{\partial^3 v_3}{\partial x_3\partial t^2}\right)\delta v_3\right]_{-d}^{L}$$

$$+\left[m^{*}\ddot{R}_{y_3}(-d)-m^{*}r^{*}\left(\left(\ddot{\varphi}_{3e}+\frac{\partial^3 v_3(-d,t)}{\partial x_3\partial t^2}\right)-\left(\dot{\varphi}_{3e}+\frac{\partial^2 v_3(-d,t)}{\partial x_3\partial t}\right)^2\frac{\partial v_3(-d,t)}{\partial x_3}\right)\right]\delta v_3(-d,t)+\left[M\ddot{R}_{y_3}(L)+Mr_M\left(\left(\ddot{\varphi}_{3e}+\frac{\partial^3 v_3(L,t)}{\partial x_3\partial t^2}\right)\right.\right.$$

$$\left.\left.-\left(\dot{\varphi}_{3e}+\frac{\partial^2 v_3(L,t)}{\partial x_3\partial t}\right)^2\frac{\partial v_3(L,t)}{\partial x_3}\right)\right]\delta v_3(L,t)+\left[m^{*}r^{*}\left(\ddot{R}_{x_3}(-d)\frac{\partial v_3(-d,t)}{\partial x_3}-\ddot{R}_{y_3}(-d)\right)+\left(J_{m^{*}}+m^{*}r^{*2}\right)\left(\ddot{\varphi}_{3e}+\frac{\partial^3 v_3(-d,t)}{\partial x_3\partial t^2}\right)\right]\frac{\delta\partial v_3(-d,t)}{\partial x_3}$$

$$+\left[-Mr_M\left(\ddot{R}_{x_3}(L)\frac{\partial v_3(L,t)}{\partial x_3}-\ddot{R}_{y_3}(L)\right)+\left(J_M+Mr_M^2\right)\left(\ddot{\varphi}_{3e}+\frac{\partial^3 v_3(L,t)}{\partial x_3\partial t^2}\right)\right]\delta\frac{\partial v_3(L,t)}{\partial x_3}\Bigg\}dt=0 \qquad (C.6b)$$

4. Euler-Lagrange Equations and Natural Boundary Conditions

Hamilton's integral will have a stationary value when both sets of terms in equation (C.6) vanish.

The Euler-Lagrange equations are obtained by applying the Fundamental Lemma of the Calculus of Variations to the first part of equation (C.6). (Since δu_2, $\delta u_2(a_2)$, δu_3, $\delta u_3(-d)$, $\delta u_3(a_3)$, $\delta u_3(L)$, δv_2, δv_3, $\delta \Phi_{2e}$, $\delta \Phi_{3e}$ are arbitrary variations, their respective coefficients must vanish).

In order to obtain the dynamic boundary conditions, one first considers the geometric boundary conditions:

$$v_2(0,t) = 0, \tag{C.7}$$

$$v_2(a_2,t) = 0, \tag{C.8}$$

$$v_3(0^-,t) = v_3(0,t) = 0, \tag{C.9}$$

$$\frac{\partial v_3(0^-,t)}{\partial x_3} = \frac{\partial v_3(0,t)}{\partial x_3}, \tag{C.10}$$

$$v_3(a_3,t) = v_3(a_3^+,t) = 0, \tag{C.11}$$

$$\frac{\partial v_3(a_3,t)}{\partial x_3} = \frac{\partial v_3(a_3^+,t)}{\partial x_3}, \tag{C.12}$$

This implies, concerning their associated variations, that:

$$\delta v_2(0,t) = 0, \tag{C.13}$$

$$\delta v_2(a_2,t) = 0, \tag{C.14}$$

$$\delta v_3(0^-,t) = \delta v_3(0,t), \tag{C.15}$$

$$\delta \frac{\partial v_3(0^-,t)}{\partial x_3} = \delta \frac{\partial v_3(0,t)}{\partial x_3}, \tag{C.16}$$

$$\delta v_3(a_3,t) = \delta v_3(a_3^+,t) = 0, \tag{C.17}$$

$$\delta \frac{\partial v_3(a_3,t)}{\partial x_3} = \delta \frac{\partial v_3(a_3^+,t)}{\partial x_3}. \tag{C.18}$$

The above expressions are substituted into equation (C.6b). The remaining variations at the boundaries, such as $\delta v_3(L,t)$, etc., are again arbitrary, and their coefficients must vanish.

The Euler-Lagrange equations consist of two groups. The first group represents the partial differential equations in $v_2(x_2,t)$ and the three parts of $v_3(x_3,t)$ respectively. The second group of eight equations allows for the solution of the Lagrange multipliers.

a) Euler-Lagrange Equations

Group 1

$0 \le x_2 \le a_2$:

$$E_2 I_2 \frac{\partial^4 v_2}{\partial x_2^4} - \rho_2 I_2 \frac{\partial^4 v_2}{\partial x_2^2 \partial t^2} + \frac{\partial^2 v_2}{\partial x_2^2}\left(\int_{x_2}^{a_2} \lambda_1 d\xi_{12} + \lambda_3\right) - \lambda_1 \frac{\partial v_2}{\partial x_2} + \mu_2 \ddot{R}_{y_2} = 0 . \quad (C.19)$$

$-d \le x_3 \le 0^-$:

$$E_3 I_3 \frac{\partial^4 v_3}{\partial x_3^4} - \rho_3 I_3 \frac{\partial^4 v_3}{\partial x_3^2 \partial t^2} + \frac{\partial^2 v_3}{\partial x_3^2}\left(\int_{x_3}^{-d} \lambda_2 d\xi_{13} - \lambda_5\right) - \lambda_2 \frac{\partial v_3}{\partial x_3} + \mu_3 \ddot{R}_{y_3} = 0 . \quad (C.20)$$

$0 \le x_3 \le a_3$:

$$E_3 I_3 \frac{\partial^4 v_3}{\partial x_3^4} - \rho_3 I_3 \frac{\partial^4 v_3}{\partial x_3^2 \partial t^2} + \frac{\partial^2 v_3}{\partial x_3^2}\left(\int_{x_3}^{L} \lambda_2 d\xi_{13} + \lambda_4 + \lambda_6\right) - \lambda_2 \frac{\partial v_3}{\partial x_3} + \mu_3 \ddot{R}_{y_3} = 0 . \quad (C.21)$$

$a_3^+ \le x_3 \le L$:

$$E_3 I_3 \frac{\partial^4 v_3}{\partial x_3^4} - \rho_3 I_3 \frac{\partial^4 v_3}{\partial x_3^2 \partial t^2} + \frac{\partial^2 v_3}{\partial x_3^2}\left(\int_{x_3}^{L} \lambda_2 d\xi_{13} + \lambda_6\right) - \lambda_2 \frac{\partial v_3}{\partial x_3} + \mu_3 \ddot{R}_{y_3} = 0 . \quad (C.22)$$

Group 2

$$\mu_2 \ddot{R}_{x_2} - \lambda_1 = 0 . \quad (C.23)$$

$$\int_0^{a_2} \left[\mu_2 (x_2 + u_2) \ddot{R}_{y_2} - \mu_2 v_2 \ddot{R}_{x_2} + \rho_2 I_2 \left(\ddot{\varphi}_{2e} + \frac{\partial^3 v_2}{\partial x_2 \partial t^2}\right)\right] dx_2 + \lambda_7 (a_2 + u_2(a_2)) \sin\varphi_{2e}$$

$$- \lambda_8 (a_2 + u_2(a_2)) \cos\varphi_{2e} = 0 . \quad (C.24)$$

$$\mu_3 \ddot{R}_{x_3} - \lambda_2 = 0 . \quad (C.25)$$

$$- \lambda_3 - \lambda_7 \cos\varphi_{2e} - \lambda_8 \sin\varphi_{2e} = 0 . \quad (C.26)$$

$$m^* \ddot{R}_{x_3}(-d) + m^* r^* \left[\left(\ddot{\varphi}_{3e} + \frac{\partial^3 v_3(-d,t)}{\partial x_3 \partial t^2}\right) \frac{\partial v_3(-d,t)}{\partial x_3} + \left(\dot{\varphi}_{3e} + \frac{\partial^2 v_3(-d,t)}{\partial x_3 \partial t}\right)^2\right] - \lambda_5 = 0 . \quad (C.27)$$

$$- \lambda_4 + \lambda_7 \cos\varphi_{3e} + \lambda_8 \sin\varphi_{3e} = 0 . \quad (C.28)$$

$$M \ddot{R}_{x_3}(L) - M r_{M_1} \left[\left(\ddot{\varphi}_{3e} + \frac{\partial^3 v_3(L,t)}{\partial x_3 \partial t^2}\right) \frac{\partial v_3(L,t)}{\partial x_3} + \left(\dot{\varphi}_{3e} + \frac{\partial^2 v_3(L,t)}{\partial x_3 \partial t}\right)^2\right] - \lambda_6 = 0 . \quad (C.29)$$

$$\int_{-d}^{L}\left(\mu_3(x_3+u_3)\ddot{R}_{y_3}-\mu_3 v_3\ddot{R}_{x_3}+\rho_3 I_3\left(\ddot{\varphi}_{3e}+\frac{\partial^3 v_3}{\partial x_3\partial t^2}\right)\right)dx_3+m^*\left(-v_3(-d,t)+r^*\frac{\partial v_3(-d,t)}{\partial x_3}\right)\ddot{R}_{x_3}(-d)$$

$$-m^*r^*v_3(-d,t)\left(\left(\ddot{\varphi}_{3e}+\frac{\partial^3 v_3(-d,t)}{\partial x_3\partial t^2}\right)\frac{\partial v_3(-d,t)}{\partial x_3}+\left(\dot{\varphi}_{3e}+\frac{\partial^2 v_3(-d,t)}{\partial x_3\partial t}\right)^2\right)+m^*\left(-d+u_3(-d)-r^*\right)\ddot{R}_{y_3}(-d)$$

$$-m^*r^*\left(-d+u_3(-d)\right)\left(\left(\ddot{\varphi}_{3e}+\frac{\partial^3 v_3(-d,t)}{\partial x_3\partial t^2}\right)-\left(\dot{\varphi}_{3e}+\frac{\partial^2 v_3(-d,t)}{\partial x_3\partial t}\right)^2\frac{\partial v_3(-d,t)}{\partial x_3}\right)+\left(J_{m^*}+m^*r^{*2}\right)\left(\ddot{\varphi}_{3e}\right.$$

$$\left.+\frac{\partial^3 v_3(-d,t)}{\partial x_3\partial t^2}\right)-M\left(v_3(L,t)+r_M\frac{\partial v_3(L,t)}{\partial x_3}\right)\ddot{R}_{x_3}(L)+Mr_M v_3(L,t)\left(\left(\ddot{\varphi}_{3e}+\frac{\partial^3 v_3(L,t)}{\partial x_3\partial t^2}\right)\frac{\partial v_3(L,t)}{\partial x_3}\right.$$

$$\left.+\left(\dot{\varphi}_{3e}+\frac{\partial^2 v_3(L,t)}{\partial x_3\partial t}\right)^2\right)+M\left(L+u_3(L)+r_M\right)\ddot{R}_{y_3}(L)+Mr_M\left(L+u_3(L)\right)\left(\left(\ddot{\varphi}_{3e}+\frac{\partial^3 v_3(L,t)}{\partial x_3\partial t^2}\right)\right.$$

$$\left.-\left(\dot{\varphi}_{3e}+\frac{\partial^2 v_3(L,t)}{\partial x_3\partial t}\right)^2\frac{\partial v_3(L,t)}{\partial x_3}\right)+\left(J_M+Mr_M^2\right)\left(\ddot{\varphi}_{3e}+\frac{\partial^3 v_3(L,t)}{\partial x_3\partial t^2}\right)-\lambda_7\left(a_3+u_3(a_3)\right)\sin\varphi_{3e}$$

$$-\lambda_8\left(a_3+u_3(a_3)\right)\cos\varphi_{3e}=0. \qquad \text{(C.30)}$$

b) Natural Boundary Conditions

$$E_2I_2\frac{\partial^2 v_2(0,t)}{\partial x_2^2}=0. \qquad \text{(C.31)}$$

$$E_2I_2\frac{\partial^2 v_2(a_2,t)}{\partial x_2^2}=0. \qquad \text{(C.32)}$$

$$m^*r^*\left(\ddot{R}_{x_3}(-d)\frac{\partial v_3(-d,t)}{\partial x_3}-\ddot{R}_{y_3}(-d)\right)+\left(J_{m^*}+m^*r^{*2}\right)\left(\ddot{\varphi}_{3e}+\frac{\partial^3 v_3(-d,t)}{\partial x_3\partial t^2}\right)-E_3I_3\frac{\partial^2 v_3(-d,t)}{\partial x_3^2}=0. \qquad \text{(C.33)}$$

$$E_3I_3\frac{\partial^3 v_3(-d,t)}{\partial x_3^3}-\rho_3I_3\left(\ddot{\varphi}_{3e}+\frac{\partial^3 v_3(-d,t)}{\partial x_3\partial t^2}\right)-m^*r^*\left(\left(\ddot{\varphi}_{3e}+\frac{\partial^3 v_3(-d,t)}{\partial x_3\partial t^2}\right)-\left(\dot{\varphi}_{3e}\right.\right.$$

$$\left.\left.+\frac{\partial^2 v_3(-d,t)}{\partial x_3\partial t}\right)^2\frac{\partial v_3(-d,t)}{\partial x_3}\right)-\lambda_5\frac{\partial v_3(-d,t)}{\partial x_3}+m^*\ddot{R}_{y_3}(-d)=0. \qquad \text{(C.34)}$$

$$E_3 I_3 \frac{\partial^2 v_3(0^-,t)}{\partial x_3^2} = E_3 I_3 \frac{\partial^2 v_3(0,t)}{\partial x_3^2} . \qquad (C.35)$$

$$E_3 I_3 \frac{\partial^2 v_3(a_3,t)}{\partial x_3^2} = E_3 I_3 \frac{\partial^2 v_3(a_3^+,t)}{\partial x_3^2} . \qquad (C.36)$$

$$E_3 I_3 \frac{\partial^2 v_3(L,t)}{\partial x_3^2} + (J_M + M r_M^2)\left(\ddot{\varphi}_{3e} + \frac{\partial^3 v_3(L,t)}{\partial x_3 \partial t^2}\right) - M r_M \left(\ddot{R}_{x_3}(L)\frac{\partial v_3(L,t)}{\partial x_3} - \ddot{R}_{y_3}(L)\right) = 0. \qquad (C.37)$$

$$-E_3 I_3 \frac{\partial^3 v_3(L,t)}{\partial x_3^3} + \rho_3 I_3 \left(\ddot{\varphi}_{3e} + \frac{\partial^3 v_3(L,t)}{\partial x_3 \partial t^2}\right) + M r_M \left(\left(\ddot{\varphi}_{3e} + \frac{\partial^3 v_3(L,t)}{\partial x_3 \partial t^2}\right) - \left(\dot{\varphi}_{3e} + \frac{\partial^2 v_3(L,t)}{\partial x_3 \partial t}\right)^2 \frac{\partial v_3(L,t)}{\partial x_3}\right) - \lambda_6 \frac{\partial v_3(L,t)}{\partial x_3} + M \ddot{R}_{y_3}(L) = 0. \qquad (C.38)$$

5. Determination of Lagrange Multipliers

In order to express the partial differential equations of Group 1 of the previous section in terms of $v_2(x_2,t)$ and $v_3(x_3,t)$ only, it is first necessary to solve Group 2 of the Euler-Lagrange equations for the eight Lagrange multipliers. This results in:

$$\lambda_1 = \mu_2 \ddot{R}_{x_2} , \tag{C.39}$$

$$\lambda_2 = \mu_3 \ddot{R}_{x_3} , \tag{C.40}$$

$$\lambda_3 = -\frac{\cot(\varphi_{3e}-\varphi_{2e})}{(a_2+u_2(a_2))}\int_0^{a_2} K_2(x_2,t)\,dx_2 - \frac{\csc(\varphi_{3e}-\varphi_{2e})}{(a_3+u_3(a_3))}\left[\int_{-d}^{L} K_3(x_3,t)dx_3 + \mathfrak{M}_3^* + \mathfrak{M}_{3M}\right], \tag{C.41}$$

$$\lambda_4 = \frac{\csc(\varphi_{3e}-\varphi_{2e})}{(a_2+u_2(a_2))}\int_0^{a_2} K_2(x_2,t)dx_2 + \frac{\cot(\varphi_{3e}-\varphi_{2e})}{(a_3+u_3(a_3))}\left[\int_{-d}^{L} K_3(x_3,t)dx_3 + \mathfrak{M}_3^* + \mathfrak{M}_{3M}\right], \tag{C.42}$$

$$\lambda_5 = m^*\ddot{R}_{x_3}(-d) + m^*r^*\left(\left(\ddot{\varphi}_{3e} + \frac{\partial^3 v_3(-d,t)}{\partial x_3 \partial t^2}\right)\frac{\partial v_3(-d,t)}{\partial x_3} + \left(\dot{\varphi}_{3e} + \frac{\partial^2 v_3(-d,t)}{\partial x_3 \partial t}\right)^2\right), \tag{C.43}$$

$$\lambda_6 = M\ddot{R}_{x_3}(L) - M r_H\left(\left(\ddot{\varphi}_{3e} + \frac{\partial^3 v_3(L,t)}{\partial x_3 \partial t^2}\right)\frac{\partial v_3(L,t)}{\partial x_3} + \left(\dot{\varphi}_{3e} + \frac{\partial^2 v_3(L,t)}{\partial x_3 \partial t}\right)^2\right), \tag{C.44}$$

$$\lambda_7 = \frac{\cos\varphi_{3e}}{(a_2+u_2(a_2))\sin(\varphi_{3e}-\varphi_{2e})}\int_0^{a_2} K_2(x_2,t)dx_2 + \frac{\cos\varphi_{2e}}{(a_3+u_3(a_3))\sin(\varphi_{3e}-\varphi_{2e})}\left[\int_{-d}^{L} K_3(x_3,t)dx_3 + \mathfrak{M}_3^* + \mathfrak{M}_{3M}\right], \tag{C.45}$$

$$\lambda_8 = \frac{\sin\varphi_{2e}}{(a_3+u_3(a_3))\sin(\varphi_{3e}-\varphi_{2e})}\left[\int_{-d}^{L} K_3(x_3,t)dx_3 + \mathfrak{M}_3^* + \mathfrak{M}_{3M}\right] + \frac{\sin\varphi_{3e}}{(a_2+u_2(a_2))\sin(\varphi_{3e}-\varphi_{2e})}\int_0^{a_2} K_2(x_2,t)dx_2 , \tag{C.46}$$

where

$$K_2(x_2,t) = \mu_2(x_2+u_2)\ddot{R}_{y_2} - \mu_2 v_2 \ddot{R}_{x_2} + \rho_2 I_2\left(\ddot{\varphi}_{2e} + \frac{\partial^3 v_2}{\partial x_2 \partial t^2}\right), \qquad (C.47)$$

$$K_3(x_3,t) = \mu_3(x_3+u_3)\ddot{R}_{y_3} - \mu_3 v_3 \ddot{R}_{x_3} + \rho_3 I_3\left(\ddot{\varphi}_{3e} + \frac{\partial^3 v_3}{\partial x_3 \partial t^2}\right), \qquad (C.48)$$

$$\begin{aligned} M_3^* = {} & m^*\left(-v_3(-d,t) + r^*\frac{\partial v_3(-d,t)}{\partial x_3}\right)\ddot{R}_{x_3}(-d) - m^* r^* v_3(-d,t)\left(\left(\ddot{\varphi}_{3e} + \frac{\partial^3 v_3(-d,t)}{\partial x_3 \partial t^2}\right)\frac{\partial v_3(-d,t)}{\partial x_3}\right. \\ & \left. + \left(\dot{\varphi}_{3e} + \frac{\partial^2 v_3(-d,t)}{\partial x_3 \partial t}\right)^2\right) + m^*\left(-d + u_3(-d) - r^*\right)\ddot{R}_{y_3}(-d) - m^* r^*(-d+u_3(-d))\left(\left(\ddot{\varphi}_{3e}\right.\right. \\ & \left.\left. + \frac{\partial^3 v_3(-d,t)}{\partial x_3 \partial t^2}\right) - \left(\dot{\varphi}_{3e} + \frac{\partial^2 v_3(-d,t)}{\partial x_3 \partial t}\right)^2 \frac{\partial v_3(-d,t)}{\partial x_3}\right) + \left(J_{M^*} + m^* r^{*2}\right)\left(\ddot{\varphi}_{3e} + \frac{\partial^3 v_3(-d,t)}{\partial x_3 \partial t^2}\right), \end{aligned} \qquad (C.49)$$

$$\begin{aligned} M_{3M} = {} & -M\left(v_3(L,t) + r_M\frac{\partial v_3(L,t)}{\partial x_3}\right)\ddot{R}_{x_3}(L) + M r_M\left(\left(\ddot{\varphi}_{3e} + \frac{\partial^3 v_3(L,t)}{\partial x_3 \partial t^2}\right)\frac{\partial v_3(L,t)}{\partial x_3}\right. \\ & \left. + \left(\dot{\varphi}_{3e} + \frac{\partial^2 v_3(L,t)}{\partial x_3 \partial t}\right)^2\right) + M\left(L + u_3(L) + r_M\right)\ddot{R}_{y_3}(L) + M r_M\left(L + u_3(L)\right)\left(\left(\ddot{\varphi}_{3e}\right.\right. \\ & \left.\left. + \frac{\partial^3 v_3(L,t)}{\partial x_3 \partial t^2}\right) - \left(\dot{\varphi}_{3e} + \frac{\partial^2 v_3(L,t)}{\partial x_3 \partial t}\right)^2 \frac{\partial v_3(L,t)}{\partial x_3}\right) + \left(J_M + M r_M^2\right)\left(\ddot{\varphi}_{3e} + \frac{\partial^3 v_3(L,t)}{\partial x_3 \partial t^2}\right). \end{aligned} \qquad (C.50)$$

To express the Lagrange multipliers in terms of the appropriate v's, the constraint equations (3.17) to (3.22) are used to obtain the various u's. The derivatives of the u's are obtained by appropriate differentiation.

The elastic angles φ_{2e} and φ_{3e} must be solved for with the help of equations (3.25) and (3.26) by a method similar to that employed in rigid body kinematics (see Appendix I). The u's in these expressions come again from the constraint equations (3.19) and (3.20). Once φ_{2e} and φ_{3e} are known, their associated angular velocities and angular accelerations may be found by differentiation.

The resulting expressions for the λ's are not shown here since subsequent linearization and the approximation of the elastic angles by the rigid mechanism angles makes this unnecessary.

6. Partial Differential Equations and Boundary Conditions for both Elastic Links

The partial differential equations of motion and the associated boundary conditions for each link are now obtained by the substitution of the Lagrange multipliers into the differential equations as well as the boundary conditions. For the sake of completeness, the geometric boundary conditions are also shown. Even though the resulting expressions are shown in terms of the λ's, $\ddot{R}_x$, $\ddot{R}_y$ as well as the elastic angles, it must be kept in mind that, for solution they must be transformed by means of the appropriate constraint equations and their derivatives into functions of the v's only. Because of the above, non-linear partial integro-differential equations result.

a) Link 2:

Differential Equation

$$E_2 I_2 \frac{\partial^4 v_2}{\partial x_2^4} - \rho_2 I_2 \frac{\partial^4 v_2}{\partial x_2^2 \partial t^2} + N_1(x_2,t) \frac{\partial^2 v_2}{\partial x_2^2} + \mu_2 \ddot{R}_{y_2} - \mu_2 \ddot{R}_{x_2} \frac{\partial v_2}{\partial x_2} = 0 , \qquad (C.51)$$

where

$$N_1(x_2,t) = \int_{x_2}^{a_2} \lambda_1 d\xi_2 + \lambda_3 . \qquad (C.52)$$

Natural Boundary Conditions

$$E_2 I_2 \frac{\partial^2 v_2(0,t)}{\partial x_2^2} = 0 . \qquad (C.53)$$

$$E_2 I_2 \frac{\partial^2 v_2(a_2,t)}{\partial x_2^2} = 0 . \qquad (C.54)$$

Geometric Boundary Conditions

$$V_2(0,t) = 0 \quad . \tag{C.55}$$

$$V_2(a_2,t) = 0 \quad . \tag{C.56}$$

b) Link 3:

Differential Equations

Beam Section 1: $-d \leq x_3 \leq 0^-$

$$E_3 I_3 \frac{\partial^4 v_3}{\partial x_3^4} - \rho_3 I \frac{\partial^4 v_3}{\partial x_3^2 \partial t^2} + N_2(x_3,t)\frac{\partial^2 v_3}{\partial x_3^2} + \mu_3 \ddot{R}_{y_3} - \mu_3 \ddot{R}_{x_3}\frac{\partial v_3}{\partial x_3} = 0, \tag{C.57}$$

where

$$N_2(x_3,t) = \int_{x_3}^{-d} \lambda_2 d\xi_3 - \lambda_5 \cdot \tag{C.58}$$

Beam Section 2: $0 \leq x_3 \leq a_3$

$$E_3 I_3 \frac{\partial^4 v_3}{\partial x_3^4} - \rho_3 I_3 \frac{\partial^4 v_3}{\partial x_3^2 \partial t^2} + N_3(x_3,t)\frac{\partial^2 v_3}{\partial x_3^2} + \mu_3 \ddot{R}_{y_3} - \mu_3 \ddot{R}_{x_3}\frac{\partial v_3}{\partial x_3} = 0, \tag{C.59}$$

where

$$N_3(x_3,t) = \int_{x_3}^{L} \lambda_2 d\xi_3 + \lambda_4 + \lambda_6 \cdot \tag{C.60}$$

Beam Section 3: $a_3^+ \leq x_3 \leq L$

$$E_3 I_3 \frac{\partial^4 v_3}{\partial x_3^4} - \rho_3 I_3 \frac{\partial^4 v_3}{\partial x_3^2 \partial t^2} + N_4(x_3,t)\frac{\partial^2 v_3}{\partial x_3^2} + \mu_3 \ddot{R}_{y_3} - \mu_3 \ddot{R}_{x_3}\frac{\partial v_3}{\partial x_3} = 0, \tag{C.61}$$

where

$$N_4(x_3,t) = \int_{x_3}^{L} \lambda_2 d\xi_2 + \lambda_6 \quad \cdot \tag{C.62}$$

Natural Boundary Conditions

$$-E_3I_3\frac{\partial^2 v_3(-d,t)}{\partial x_3^2}+m^*r^*\left(\ddot{R}_{x_3}(-d)\frac{\partial v_3(-d,t)}{\partial x_3}-\ddot{R}_{y_3}(-d)\right)+\left(J_{m^*}+m^*r^{*2}\right)\left(\ddot{\varphi}_{3e}+\frac{\partial^3 v_3(-d,t)}{\partial x_3\partial t^2}\right)=0. \tag{C.63}$$

$$E_3I_3\frac{\partial^3 v_3(-d,t)}{\partial x_3^3}+m^*\ddot{R}_{y_3}(-d)-m^*r^*\left(\left(\ddot{\varphi}_{3e}+\frac{\partial^3 v_3(-d,t)}{\partial x_3\partial t^2}\right)-\left(\dot{\varphi}_{3e}+\frac{\partial^2 v_3(-d,t)}{\partial x_3\partial t}\right)^2\frac{\partial v_3(-d,t)}{\partial x_3}\right)$$

$$-\beta_3I_3\left(\ddot{\varphi}_{3e}+\frac{\partial^3 v_3(-d,t)}{\partial x_3\partial t^2}\right)-\left[m^*\ddot{R}_{x_3}(-d)+m^*r^*\left(\left(\ddot{\varphi}_{3e}+\frac{\partial^3 v_3(-d,t)}{\partial x_3\partial t^2}\right)\frac{\partial v_3(-d,t)}{\partial x_3}\right.\right.$$

$$\left.\left.+\left(\dot{\varphi}_{3e}+\frac{\partial^2 v_3(-d,t)}{\partial x_3\partial t}\right)^2\right)\right]\frac{\partial v_3(-d,t)}{\partial x_3}=0. \tag{C.64}$$

$$E_3I_3\frac{\partial^2 v_3(0^-,t)}{\partial x_3^2}=E_3I_3\frac{\partial^2 v_3(0,t)}{\partial x_3^2}. \tag{C.65}$$

$$E_3I_3\frac{\partial^2 v_3(a_3,t)}{\partial x_3^2}=E_3I_3\frac{\partial^2 v_3(a_3^+,t)}{\partial x_3^2}. \tag{C.66}$$

$$E_3I_3\frac{\partial^2 v_3(L,t)}{\partial x_3^2}-Mr_M\left(\ddot{R}_{x_3}(L)\frac{\partial v_3(L,t)}{\partial x_3}-\ddot{R}_{y_3}(L)\right)+\left(J_M+Mr_M^2\right)\left(\ddot{\varphi}_{3e}+\frac{\partial^3 v_3(L,t)}{\partial x_3\partial t^2}\right)=0. \tag{C.67}$$

$$-E_3I_3\frac{\partial^3 v_3(L,t)}{\partial x_3^3}+M\ddot{R}_{y_3}(L)+Mr_M\left(\left(\ddot{\varphi}_{3e}+\frac{\partial^3 v_3(L,t)}{\partial x_3\partial t^2}\right)-\left(\dot{\varphi}_{3e}+\frac{\partial^2 v_3(L,t)}{\partial x_3\partial t}\right)^2\frac{\partial v_3(L,t)}{\partial x_3}\right)$$

$$+\beta_3I_3\left(\ddot{\varphi}_{3e}+\frac{\partial^3 v_3(L,t)}{\partial x_3\partial t^2}\right)-\left[M\ddot{R}_{x_3}(L)-Mr_M\left(\left(\ddot{\varphi}_{3e}+\frac{\partial^3 v_3(L,t)}{\partial x_3\partial t^2}\right)\frac{\partial v_3(L,t)}{\partial x_3}\right.\right.$$

$$\left.\left.+\left(\dot{\varphi}_{3e}+\frac{\partial^2 v_3(L,t)}{\partial x_3\partial t}\right)^2\right)\right]\frac{\partial v_3(L,t)}{\partial x_3}=0. \tag{C.68}$$

Geometric Boundary Conditions

$$v_3(0^-,t) = 0. \tag{C.69}$$

$$v_3(0,t) = 0. \tag{C.70}$$

$$\frac{\partial v_3(0^-,t)}{\partial x_3} = \frac{\partial v_3(0,t)}{\partial x_3}. \tag{C.71}$$

$$v_3(a_3,t) = 0. \tag{C.72}$$

$$v_3(a_3^+,t) = 0. \tag{C.73}$$

$$\frac{\partial v_3(a_3,t)}{\partial x_3} = \frac{\partial v_3(a_3^+,t)}{\partial x_3}. \tag{C.74}$$

APPENDIX D

DERIVATION OF EQUATION OF MOTION FOR ELASTIC ROCKER WITH COUNTERWEIGHT AND ENDMASS BY METHOD OF SUBSTITUTION OF CONSTRAINT EQUATIONS (ASSUMPTION OF RIGID COUPLER)

This appendix concerns itself with the derivation of the equations of motion for the rocker of a balanced shaker mechanism where the counterweight is tangent to the pivot point D (see Figure D.1). Instead of using the Lagrange multipliers for incorporating the constraint equations, their variations are substituted in terms of δv_3.

1. Hamilton's Principle

Since the auxiliary conditions are not used in the present derivation, equation (3.1) reduces to:

$$\delta\int_{t_0}^{t_1}(T-\Pi)\,dt = 0. \qquad \text{(D.1)}$$

2. Working Form of Hamilton's Equation

The working form of Hamilton's equation is obtained from the substitution of the appropriate energy variations into equation (D.1). Since the coupler of the mechanism is now rigid, it has no potential energy, and the variation of the kinetic energy integral of equation (3.9) reduces to:

$$\delta\int_{t_0}^{t_1} T_2\,dt = -\int_{t_0}^{t_1} M_2\,\ddot{\bar{r}}_{2c}\cdot\delta\bar{r}_{2c}\,dt - \int_{t_0}^{t_1} J_{2c}\,\ddot{\varphi}_{2e}\,\delta\varphi_{2e}\,dt, \qquad \text{(D.2)}$$

where

$\ddot{\bar{r}}_{2c}$ is obtained according to equation (A.21) with $u_2, v_2 = 0$, $x_2 = a_2/2$, $y_2 = 0$,

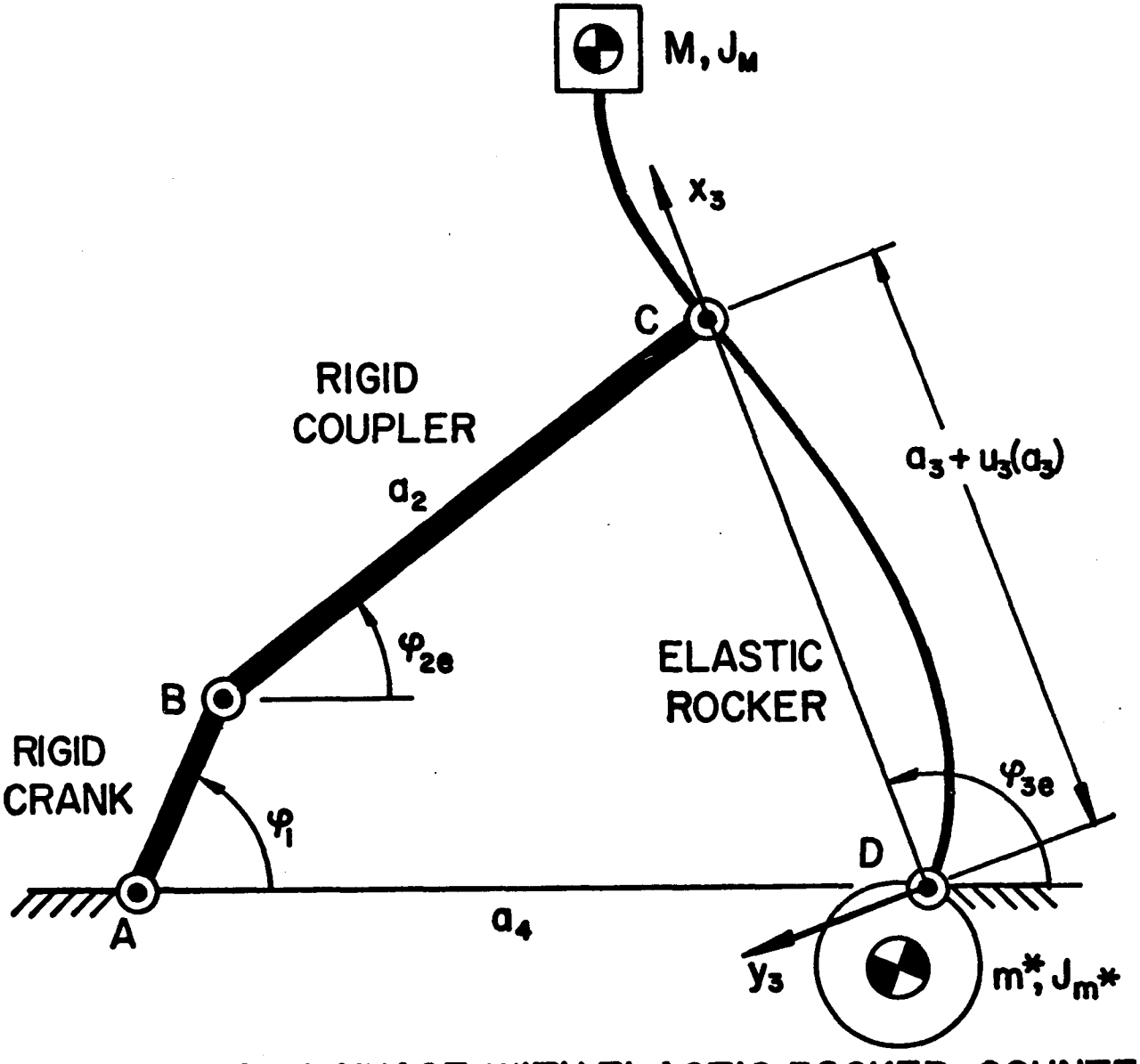

FIGURE D.1: FOUR-BAR LINKAGE WITH ELASTIC ROCKER, COUNTERWEIGHT AND ENDMASS.

$\delta\bar{r}_{2c}$ is obtained according to equation (B.2) with

$u_2, v_2 = 0$, $x_2 = a_2/2$, $y_2 = 0$,

M_2 = the total mass of the coupler.

J_{2c} = the mass moment of inertia of the coupler about its center of mass.

$\ddot{\varphi}_{2e}$ = the absolute angular acceleration of the coupler.

Because the counterweight is tangent to the pivot point at D, the length d = 0.

When the above modifications are included into equations (3.9) to (3.13) and (3.16), and the results substituted into equation (D.1), one obtains the working form of Hamilton's integral:

$$\int_{t_o}^{t_1} M_2 \ddot{\bar{r}}_{2c} \cdot \delta\bar{r}_{2c}\, dt + \int_{t_o}^{t_1} J_{2c} \ddot{\varphi}_{2e} \delta\varphi_{2e}\, dt + \int_{t_o}^{t_1}\int_{0}^{L}\int_{A_3} \rho_3 \ddot{\bar{r}}_{P_3} \cdot \delta\bar{r}_{P_3}\, dA_3\, dx_3\, dt$$

$$+ \int_{t_o}^{t_1} m^* \ddot{\bar{r}}_{m^*} \cdot \delta\bar{r}_{m^*}\, dt + \int_{t_o}^{t_1} J_{m^*} \ddot{\bar{\theta}}_{m^*} \cdot \delta\bar{\theta}_{m^*} dt + \int_{t_o}^{t_1} M \ddot{\bar{r}}_{M} \cdot \delta\bar{r}_{M} dt$$

$$+ \int_{t_o}^{t_1} J_M \ddot{\bar{\theta}}_{M} \cdot \delta\bar{\theta}_{M} dt + \int_{t_o}^{t_1}\int_{0}^{a_3} E_3 I_3 \frac{\partial^4 v_3}{\partial x_3^4} \delta v_3\, dx_3\, dt + \int_{t_o}^{t_1}\int_{a_3}^{L} E_3 I_3 \frac{\partial^4 v_3}{\partial x_3^4} \delta v_3\, dx_3\, dt$$

$$+ \int_{t_o}^{t_1} \left\{ \left[E_3 I_3 \frac{\partial^2 v_3}{\partial x_3^2} \frac{\delta \partial v_3}{\partial x_3} - E_3 I_3 \frac{\partial^3 v_3}{\partial x_3^3} \delta v_3 \right]_0^{a_3} + \left[E_3 I_3 \frac{\partial^2 v_3}{\partial x_3^2} \frac{\delta \partial v_3}{\partial x_3} \right.\right.$$

$$\left.\left. - E_3 I_3 \frac{\partial^3 v_3}{\partial x_3^3} \delta v_3 \right]_{a_3^+}^{L} \right\} dt = 0. \qquad \text{(D.3)}$$

3. Substitution into Hamilton's Equation

The following substitutions are now made in equation (D.3):

a) Accelerations and virtual displacements are substituted according to Appendices A and B respectively, and the dot products are performed.

b) Integration over the cross-sectional area A_3 is carried out.

c) Trigonometric terms involving ψ_3 are combined.

d) Small deflection is assumed and therefore,

$$\cos \psi_3 \approx 1,$$
$$\sin \psi_3 \approx \psi_3 = \frac{\partial v_3}{\partial x_3} .$$

e) The term containing $\partial v_3/\partial x_3$ is integrated by parts.

f) The abbreviation

$$\mu_3 = \rho_3 A_3$$

is made.

With the above one obtains:

$$\int_{t_0}^{t_1}\left(\frac{M_2 a_2}{2}\ddot{\beta}_2\left(\frac{a_2}{2}\right)+J_{2C}\ddot{\varphi}_{2e}\right)\delta\varphi_{2e}dt+\int_{t_0}^{t_1}\int_0^L\left\{\mu_3\ddot{R}_{x_3}\delta u_3+\left(\mu_3\ddot{R}_{y_3}\right.\right.$$

$$\left.-\frac{\partial}{\partial x_3}\left(\rho_3 I_3\left(\ddot{\varphi}_{3e}+\frac{\partial^3 v_3}{\partial x_3\partial t^2}\right)\right)\right)\delta v_3+\left(\mu_3(x_3+u_3)\ddot{R}_{y_3}-\mu_3 v_3\ddot{R}_{x_3}+\rho_3 I_3\left(\ddot{\varphi}_{3e}\right.\right.$$

$$\left.\left.+\frac{\partial^3 v_3}{\partial x_3\partial t^2}\right)\right)\delta\varphi_{3e}\Big\}dx_3dt+\int_{t_0}^{t_1}\Big[\left(J_m^*+m^*r^{*2}\right)\left(\ddot{\varphi}_{3e}+\frac{\partial^3 v_3(0,t)}{\partial x_3\partial t^2}\right)-M\Big(v_3(L,t)$$

$$+r_M\frac{\partial v_3(L,t)}{\partial x_3}\Big)\ddot{R}_{x_3}(L)+Mr_M v_3(L,t)\left(\left(\ddot{\varphi}_{3e}+\frac{\partial^3 v_3(L,t)}{\partial x_3\partial t^2}\right)\frac{\partial v_3(L,t)}{\partial x_3}+\left(\dot{\varphi}_{3e}+\frac{\partial^2 v_3(L,t)}{\partial x_3\partial t}\right)^2\right)$$

$$+M(L+u_3(L)+r_M)\ddot{R}_{y_3}(L)+Mr_M(L+u_3(L))\left(\left(\ddot{\varphi}_{3e}+\frac{\partial^3 v_3(L,t)}{\partial x_3\partial t^2}\right)-\left(\dot{\varphi}_{3e}+\frac{\partial^2 v_3(L,t)}{\partial x_3\partial t}\right)^2\frac{\partial v_3(L,t)}{\partial x_3}\right)$$

$$+\left(J_M+Mr_M^2\right)\left(\ddot{\varphi}_{3e}+\frac{\partial^3 v_3(L,t)}{\partial x_3\partial t^2}\right)\Big]\delta\varphi_{3e}dt+\int_{t_0}^{t_1}\left[\left(J_m^*+m^*r^{*2}\right)\left(\ddot{\varphi}_{3e}+\frac{\partial^3 v_3(0,t)}{\partial x_3\partial t^2}\right)\right]\delta\frac{\partial v_3(0,t)}{\partial x_3}$$

$$+\int_{t_0}^{t_1}\left[-Mr_M\ddot{R}_{x_3}(L)\frac{\partial v_3(L,t)}{\partial x_3}+Mr_M\ddot{R}_y(L)+\left(J_M+Mr_M^2\right)\left(\ddot{\varphi}_{3e}+\frac{\partial^3 v_3(L,t)}{\partial x_3\partial t^2}\right)\right]\delta\frac{\partial v_3(L,t)}{\partial x_3}dt$$

$$+\int_{t_0}^{t_1}\left[M\ddot{R}_{x_3}(L)-Mr_M\left(\left(\ddot{\varphi}_{3e}+\frac{\partial^3 v_3(L,t)}{\partial x_3\partial t^2}\right)\frac{\partial v_3(L,t)}{\partial x_3}+\left(\dot{\varphi}_{3e}+\frac{\partial^2 v_3(L,t)}{\partial x_3\partial t}\right)^2\right)\right]\delta u_3(L)dt$$

$$+\int_{t_0}^{t_1}\left[M\ddot{R}_{y_3}(L)+Mr_M\left(\left(\ddot{\varphi}_{3e}+\frac{\partial^3 v_3(L,t)}{\partial x_3\partial t^2}\right)-\left(\dot{\varphi}_{3e}+\frac{\partial^2 v_3(L,t)}{\partial x_3\partial t}\right)^2\frac{\partial v_3(L,t)}{\partial x_3}\right)\right]\delta v_3(L,t)$$

$$+\int_{t_0}^{t_1}\int_0^{a_3}E_3I_3\frac{\partial^4 v_3}{\partial x_3^4}\delta v_3dx_3dt+\int_{t_0}^{t_1}\int_{a_3}^{L}E_3I_3\frac{\partial^4 v_3}{\partial x_3^4}\delta v_3dx_3dt+\int_{t_0}^{t_1}\Big\{\Big[\rho_8 I_3\left(\ddot{\varphi}_{3e}+\frac{\partial^3 v_3}{\partial x_3\partial t^2}\right)\delta v_3\Big]_0^L$$

$$+\Big[E_3I_3\frac{\partial^2 v_3}{\partial x_3^2}\delta\frac{\partial v_3}{\partial x_3}-E_3I_3\frac{\partial^3 v_3}{\partial x_3^3}\delta v_3\Big]_0^{a_3}+\Big[E_3I_3\frac{\partial^2 v_3}{\partial x_3^2}\delta\frac{\partial v_3}{\partial x_3}-E_3I_3\frac{\partial^3 v_3}{\partial x_3^3}\delta v_3\Big]_{a_3^+}^L\Big\}dt=0.$$

(D. 4a)

The above expression is now modified in the following way:

a) To express the differential equations and boundary conditions in terms of $v_3(x_3,t)$ only, the terms $\delta\varphi_{2e}$, $\delta\varphi_{3e}$, δu_3 and $\delta u_3(L)$, derived in Appendix E, are substituted. (This represents the essential part of the substitution method.)

b) The elastic angles φ_{2e} and φ_{3e} and their derivatives must now be accounted for. While, as in Section 5 of Appendix C, these expressions are approximated by the corresponding rigid body ones given in Appendix I, their exact determination will be briefly outlined. With a rigid coupler, φ_{2e} and φ_{3e} are only functions of $v_3(x_3,t)$ and may be obtained by the solution of the elastic loop equations (3.25) and (3.26) with $u_2(a_2) = 0$ and $u_3(a_3)$ obtained according to equation (3.20). The elastic angular velocities and angular accelerations can then be found by appropriate differentiation.

c) In order to collect terms in δv_3, such expressions as:

$$\int_0^{a_3} \mu_3 \ddot{R}_{x_3} \int_0^{x_3} \frac{\partial^2 \tilde{v}_3}{\partial \xi_3^2} \delta\tilde{v}_3 d\chi_3 ,$$

which contain variable limits, are transformed according to:

$$\int_\alpha^\beta F(\chi) \int_\alpha^\chi G(\xi) d\xi d\chi = \int_\alpha^\beta G(\chi) \int_\chi^\beta F(\xi) d\xi d\chi .$$

When the limits are constant, one uses

$$\int_{a_3}^{L} F(\chi)\int_{0}^{a_3} G(\xi)\,d\xi\,d\chi = \int_{0}^{a_3} G(\chi)\int_{a_3}^{L} F(\xi)\,d\xi\,d\chi\,.$$

With the above operations equation (D.4a) becomes:

$$\int_{t_0}^{t_1}\int_0^{a_3}\Big\{\mu_3\ddot{R}_{y_3}-\mu_3\ddot{R}_{x_3}\frac{\partial v_3}{\partial x_3}+E_3I_3\frac{\partial^4 v_3}{\partial x_3^4}-\rho_3I_3\frac{\partial^4 v_3}{\partial x_3^2\partial t^2}+\frac{\partial^2 v_3}{\partial x_3^2}\Big[\Big[\int_{x_3}^{L}\mu_3\ddot{R}_{x_3}(\xi_3)d\xi_3+\frac{\csc(\varphi_3-\varphi_2)}{a_2}\Big(\frac{M_2a_2}{2}\ddot{\beta}_2\Big(\frac{a_2}{2}\Big)+J_{2c}\ddot{\varphi}_2\Big)$$

$$+\frac{\cot(\varphi_3-\varphi_2)}{(a_3+u_3(a_3))}\Big(\int_0^{L}\Big[\mu_3(\xi_3+u_3(\xi_3))\ddot{R}_{y_3}(\xi_3)-\mu_3v_3(\xi_3,t)\ddot{R}_{x_3}(\xi_3)+\rho_3I_3\Big(\ddot{\varphi}_3+\frac{\partial^3 v_3(\xi_3,t)}{\partial\xi_3\partial t^2}\Big)\Big]d\xi_3+(J_m^*+m^*r^{*2})\Big(\ddot{\varphi}_3+\frac{\partial^3 v_3(0,t)}{\partial x_3\partial t^2}\Big)$$

$$-M\Big(v_3(L,t)+r_M\frac{\partial v_3(L,t)}{\partial x_3}\Big)\ddot{R}_{x_3}(L)+Mr_Mv_3(L,t)\Big(\Big(\ddot{\varphi}_3+\frac{\partial^3 v_3(L,t)}{\partial x_3\partial t^2}\Big)\frac{\partial v_3(L,t)}{\partial x_3}+\Big(\dot{\varphi}_3+\frac{\partial^2 v_3(L,t)}{\partial x_3\partial t}\Big)^2\Big)+M(L+u_3(L)+r_M)\ddot{R}_{y_3}(L)$$

$$+Mr_M(L+u_3(L))\Big(\Big(\ddot{\varphi}_3+\frac{\partial^3 v_3(L,t)}{\partial x_3\partial t^2}\Big)-\Big(\dot{\varphi}_3+\frac{\partial^2 v_3(L,t)}{\partial x_3\partial t}\Big)^2\frac{\partial v_3(L,t)}{\partial x_3}\Big)+(J_M+Mr_M^2)\Big(\ddot{\varphi}_3+\frac{\partial^3 v_3(L,t)}{\partial x_3\partial t^2}\Big)\Big]+M\ddot{R}_{x_3}(L)-Mr_M\Big(\Big(\ddot{\varphi}_3$$

$$+\frac{\partial^3 v_3(L,t)}{\partial x_3\partial t^2}\Big)\frac{\partial v_3(L,t)}{\partial x_3}+\Big(\dot{\varphi}_3+\frac{\partial^2 v_3(L,t)}{\partial x_3\partial t}\Big)^2\Big)\Big]\Big]\delta v_3dx_3dt+\int_{t_0}^{t_1}\int_{a_3}^{L}\Big\{\mu_3\ddot{R}_{y_3}-\mu_3\ddot{R}_{x_3}\frac{\partial v_3}{\partial x_3}+E_3I_3\frac{\partial^4 v_3}{\partial x_3^4}-\rho_3I_3\frac{\partial^4 v_3}{\partial x_3^2\partial t^2}$$

$$+\frac{\partial^2 v_3}{\partial x_3^2}\Big[\Big[\int_{x_3}^{L}\mu_3\ddot{R}_{x_3}(\xi_3)d\xi_3+M\ddot{R}_{x_3}(L)-Mr_M\Big(\Big(\ddot{\varphi}_3+\frac{\partial^3 v_3(L,t)}{\partial x_3\partial t^2}\Big)\frac{\partial v_3(L,t)}{\partial x_3}+\Big(\dot{\varphi}_3+\frac{\partial^2 v_3(L,t)}{\partial x_3\partial t}\Big)^2\Big)\Big]\Big]\delta v_3dx_3dt$$

$$+\int_{t_0}^{t_1}\Big\{\Big[\Big[-\frac{\csc(\varphi_3-\varphi_2)}{a_2}\Big(\frac{M_2a_2}{2}\ddot{\beta}_2\Big(\frac{a_2}{2}\Big)+J_{2c}\ddot{\varphi}_2\Big)-\frac{\cot(\varphi_3-\varphi_2)}{(a_3+u_3(a_3))}\Big(\int_0^{L}\Big[\mu_3(x_3+u_3)\ddot{R}_{y_3}-\mu_3v_3\ddot{R}_{x_3}+\rho_3I_3\Big(\ddot{\varphi}_3+\frac{\partial^3 v_3}{\partial x_3\partial t^2}\Big)\Big]dx_3$$

$$+(J_m^*+m^*r^{*2})\Big(\ddot{\varphi}_3+\frac{\partial^3 v_3(0,t)}{\partial x_3\partial t^2}\Big)-M\Big(v_3(L,t)+r_M\frac{\partial v_3(L,t)}{\partial x_3}\Big)\ddot{R}_{x_3}(L)+Mr_Mv_3(L,t)\Big(\Big(\ddot{\varphi}_3+\frac{\partial^3 v_3(L,t)}{\partial x_3\partial t^2}\Big)\frac{\partial v_3(L,t)}{\partial x_3}+\Big(\dot{\varphi}_3+\frac{\partial^2 v_3(L,t)}{\partial x_3\partial t}\Big)^2\Big)$$

$$+Mr_M(L+u_3(L))\Big(\Big(\ddot{\varphi}_3+\frac{\partial^3 v_3(L,t)}{\partial x_3\partial t^2}\Big)-\Big(\dot{\varphi}_3+\frac{\partial^2 v_3(L,t)}{\partial x_3\partial t}\Big)^2\frac{\partial v_3(L,t)}{\partial x_3}\Big)+(J_M+Mr_M^2)\Big(\ddot{\varphi}_3+\frac{\partial^3 v_3(L,t)}{\partial x_3\partial t^2}\Big)\Big]\Big]\Big[\frac{\partial v_3}{\partial x_3}\delta v_3\Big]_0^{a_3}$$

$$+\int_0^{L}\mu_3\ddot{R}_{x_3}dx_3\frac{\partial v_3(0,t)}{\partial x_3}\delta v_3(0,t)+(J_m^*+m^*r^{*2})\Big(\ddot{\varphi}_3+\frac{\partial^3 v_3(0,t)}{\partial x_3\partial t^2}\Big)\delta\frac{\partial v_3(0,t)}{\partial x_3}+\Big[-Mr_M\ddot{R}_{x_3}(L)\frac{\partial v_3(L,t)}{\partial x_3}+Mr_M\ddot{R}_{y_3}(L)$$

$$+(J_M+Mr_M^2)\Big(\ddot{\varphi}_3+\frac{\partial^3 v_3(L,t)}{\partial x_3\partial t^2}\Big)\Big]\delta\frac{\partial v_3(L,t)}{\partial x_3}+\Big[M\ddot{R}_{y_3}(L)+Mr_M\Big(\Big(\ddot{\varphi}_3+\frac{\partial^3 v_3(L,t)}{\partial x_3\partial t^2}\Big)-\Big(\dot{\varphi}_3+\frac{\partial^2 v_3(L,t)}{\partial x_3\partial t}\Big)^2\frac{\partial v_3(L,t)}{\partial x_3}\Big]\delta v_3(L,t)$$

$$+\Big[\rho_3I_3\Big(\ddot{\varphi}_3+\frac{\partial^3 v_3}{\partial x_3\partial t^2}\Big)\delta v_3\Big]_0^{L}+\Big[E_3I_3\frac{\partial^2 v_3}{\partial x_3^2}\delta\frac{\partial v_3}{\partial x_3}-E_3I_3\frac{\partial^3 v_3}{\partial x_3^3}\delta v_3\Big]_0^{a_3}+\Big[E_3I_3\frac{\partial^2 v_3}{\partial x_3^2}\delta\frac{\partial v_3}{\partial x_3}-E_3I_3\frac{\partial^3 v_3}{\partial x_3^3}\delta v_3\Big]_{a_3}^{L}$$

$$+\Big[-M\ddot{R}_{x_3}(L)+Mr_M\Big(\Big(\ddot{\varphi}_3+\frac{\partial^3 v_3(L,t)}{\partial x_3\partial t^2}\Big)\frac{\partial v_3(L,t)}{\partial x_3}+\Big(\dot{\varphi}_3+\frac{\partial^2 v_3(L,t)}{\partial x_3\partial t}\Big)^2\Big)\Big]\Big[\frac{\partial v_3}{\partial x_3}\delta v_3\Big]_0^{L}\Big\}dt=0. \qquad \text{(D.4b)}$$

4. Linearization of Hamilton's Equation

The non-linear terms of equation (D.4b) are now dropped and terms involving the rotational inertia $\rho_3 I_3$ are neglected because they are small. Further, damping is included, and the terms $C_D \partial v/\partial t$ are introduced into the two integrals which will give rise to the Euler-Lagrange equations.

The terms $\ddot{R}_{x3}$ and $\ddot{R}_{y3}$ are expanded according to equations (A.22) and (A.23) with

$$\ddot{\alpha}_3 = -\chi_3 \dot{\varphi}_3^2 , \tag{D.5}$$

$$\ddot{\beta}_3 = \chi_3 \ddot{\varphi}_3 . \tag{D.6}$$

Integrals involving these expressions may be evaluated. Thus,

$$\int_{\chi_3}^{L} \mu_3 \ddot{\alpha}_3(\xi_3) d\xi_3 = -\mu_3 \dot{\varphi}_3^2 \int_{\chi_3}^{L} \xi_3 \, d\xi_3 = -\mu_3 \dot{\varphi}_3^2 \frac{(L^2 - \chi_3^2)}{2} , \tag{D.7}$$

and

$$\int_0^L \mu_3 \xi_3 \ddot{\beta}_3(\xi_3) d\xi_3 = \ddot{\varphi}_3 \int_0^L \mu_3 \xi_3^2 d\xi_3 = \ddot{\varphi}_3 J_{3D} , \tag{D.8}$$

where

J_{3D} = the total mass moment of inertia of link 3 with respect to the ground pivot point D. (Recall that the rotational inertia of the cross-section is being neglected.)

Similarly, the term $\ddot{\beta}_2(a_2/2)$, which arises for the rigid body coupler, is given by:

$$\ddot{\beta}_2\left(\frac{a_2}{2}\right) = -\dot{\varphi}_1^2 a_1 \sin(\varphi_1 - \varphi_2) + \ddot{\varphi}_1 a_1 \cos(\varphi_1 - \varphi_2) + \frac{a_2}{2} \ddot{\varphi}_2 . \tag{D.9}$$

(*)

With the above, equation (D.4b) becomes:

(*) For kinematics see Appendix I.

$$\int_{t_0}^{t_1}\int_{0}^{a_3}\left\{C_1\frac{\partial^4 v_3}{\partial x_3^4}+G_1(x_3,t)\frac{\partial^2 v_3}{\partial x_3^2}+C_2\frac{\partial^2 v_3}{\partial t^2}+G_2(x_3,t)\frac{\partial v_3}{\partial x_3}+C_{D3}\frac{\partial v_3}{\partial t}-C_2G_5(t)v_3\right.$$

$$\left.+G_3(x_3,t)\right\}\delta v_3\,dx_3\,dt+\int_{t_0}^{t_1}\int_{a_3}^{L}\left\{C_1\frac{\partial^4 v_3}{\partial x_3^4}+G_4(x_3,t)\frac{\partial^2 v_3}{\partial x_3^2}+C_2\frac{\partial^2 v_3}{\partial t^2}+G_2(x_3,t)\frac{\partial v_3}{\partial x_3}\right.$$

$$\left.+C_{D3}\frac{\partial v_3}{\partial t}-C_2G_5(t)v_3+G_3(x_3,t)\right\}\delta v_3\,dx_3\,dt$$

$$+\int_{t_0}^{t_1}\left\{\left[-C_1\frac{\partial^3 v_3}{\partial x_3^3}\delta v_3+G_1(L,t)\frac{\partial v_3}{\partial x_3}\delta v_3\right]_0^{a_3}+G_4(0,t)\frac{\partial v_3(0,t)}{\partial x_3}\delta v_3(0,t)\right.$$

$$+C_1\frac{\partial^3 v_3(a_3^+,t)}{\partial x_3^3}\delta v_3(a_3^+,t)+\left[-C_1\frac{\partial^2 v_3(0,t)}{\partial x_3^2}+C_3\frac{\partial^3 v_3(0,t)}{\partial x_3\partial t^2}+C_3G_6(t)\right]\delta\frac{\partial v_3(0,t)}{\partial x_3}$$

$$+C_1\left[\frac{\partial^2 v_3(a_3,t)}{\partial x_3^2}-\frac{\partial^2 v_3(a_3^+,t)}{\partial x_3^2}\right]\delta\frac{\partial v_3(a_3,t)}{\partial x_3}+\left[C_1\frac{\partial^2 v_3(L,t)}{\partial x_3^2}+C_4\frac{\partial^3 v_3(L,t)}{\partial x_3\partial t^2}\right.$$

$$\left.+C_5\frac{\partial^2 v_3(L,t)}{\partial t^2}+C_6G_5(t)\frac{\partial v_3(L,t)}{\partial x_3}-C_5G_5(t)v_3(L,t)+C_9G_6(t)\right]\delta\frac{\partial v_3(L,t)}{\partial x_3}$$

$$+\left[-C_1\frac{\partial^3 v_3(L,t)}{\partial x_3^3}+C_5\frac{\partial^3 v_3(L,t)}{\partial x_3\partial t^2}+C_7\frac{\partial^2 v_3(L,t)}{\partial t^2}+C_8G_5(t)\frac{\partial v_3(L,t)}{\partial x_3}\right.$$

$$\left.\left.-C_7G_5(t)v_3(L,t)+C_{10}G_6(t)\right]\delta v_3(L,t)\right\}dt=0, \qquad (D.10)$$

where

$$\left.\begin{aligned} C_1 &= E_3 I_3 & C_6 &= M r_M L \\ C_2 &= \mu_3 & C_7 &= M \\ C_3 &= J_{M^*} + m^* r^{*2} = J^* & C_8 &= ML \\ C_4 &= J_M + M r_M^2 = \tilde{J} & C_9 &= \tilde{J} + M r_M L = C_4 + C_6 \\ C_5 &= M r_M & C_{10} &= ML + M r_M = C_5 + C_8 \end{aligned}\right\} \quad (D.11)$$

$$G_1(x_3,t) = -\frac{\mu_3}{2}(L^2-x_3^2)\dot{\varphi}_3^2 + \frac{\csc(\varphi_3-\varphi_2)}{a_2}\left[\frac{M_2 a_2}{2}\left(-\dot{\varphi}_1^2 a_1 \sin(\varphi_1-\varphi_2) + \ddot{\varphi}_1 a_1 \cos(\varphi_1-\varphi_2) + \frac{a_2}{2}\ddot{\varphi}_2\right) + J_{2C}\ddot{\varphi}_2\right] + \ddot{\varphi}_3 \frac{\cot(\varphi_3-\varphi_2)}{a_3}\left[J_{3O} + J^* + J_M + M(L+r_M)^2\right] - M(L+r_M)\dot{\varphi}_3^2, \quad (D.12)$$

$$G_2(x_3,t) = \mu_3 x_3 \dot{\varphi}_3^2, \quad (D.13)$$

$$G_3(x_3,t) = \mu_3 x_3 \ddot{\varphi}_3, \quad (D.14)$$

$$G_4(x_3,t) = -\frac{\mu_3}{2}(L^2-x_3^2)\dot{\varphi}_3^2 - M(L+r_M)\dot{\varphi}_3^2, \quad (D.15)$$

$$G_5(t) = \dot{\varphi}_3^2, \quad (D.16)$$

$$G_6(t) = \ddot{\varphi}_3. \quad (D.17)$$

This form of Hamilton's integral represents the basis for Kantorovich's method shown in Appendix G.

5. Partial Differential Equations and Boundary Conditions

The Euler-Lagrange equations are obtained by applying the Fundamental Lemma of the Calculus of Variations to the first part of equation (D.10). In order to obtain the dynamic boundary conditions, one first considers the geometric boundary conditions:

$$v_3(0,t) = 0 \ , \tag{D.18}$$

$$v_3(a_3,t) = 0 \ , \tag{D.19}$$

$$v_3(a_3^+,t) = 0 \ , \tag{D.20}$$

$$\frac{\partial v_3(a_3,t)}{\partial x_3} = \frac{\partial v_3(a_3^+,t)}{\partial x_3} \ . \tag{D.21}$$

This implies, concerning their variations, that:

$$\delta v_3(0,t) = 0 \ , \tag{D.22}$$

$$\delta v_3(a_3,t) = 0 \ , \tag{D.23}$$

$$\delta v_3(a_3^+,t) = 0 \ , \tag{D.24}$$

$$\delta\frac{\partial v_3(a_3,t)}{\partial x_3} = \delta\frac{\partial v_3(a_3^+,t)}{\partial x_3} \ . \tag{D.25}$$

The remaining variations at the boundaries, such as $\delta v_3(L,t)$, $\delta\partial v_3(0,t)/\partial x_3$, etc., are arbitrary and their coefficients must vanish in order to make Hamilton's integral vanish.

The resulting partial differential equation and associated boundary conditions become:

Differential Equations

Beam Section 1: $0 \le x_3 \le a_3$

$$C_1 \frac{\partial^4 v_3}{\partial x_3^4} + G_1(x_3,t)\frac{\partial^2 v_3}{\partial x_3^2} + C_2 \frac{\partial^2 v_3}{\partial t^2} + G_2(x_3,t)\frac{\partial v_3}{\partial x_3} - C_2 G_5(t) v_3 + G_3(x_3,t) = 0. \tag{D.26}$$

Beam Section 2: $a_3^+ \le x_3 \le L$

$$C_1 \frac{\partial^4 v_3}{\partial x_3^4} + G_4(x_3,t)\frac{\partial^2 v_3}{\partial x_3^2} + C_2 \frac{\partial^2 v_3}{\partial t^2} + G_2(x_3,t)\frac{\partial v_3}{\partial x_3} - C_2 G_5(t) v_3 + G_3(x_3,t) = 0. \tag{D.27}$$

Natural Boundary Conditions

$$-C_1 \frac{\partial^2 v_3(0,t)}{\partial x_3^2} + C_3 \frac{\partial^3 v_3(0,t)}{\partial x_3 \partial t^2} + C_3 G_6(t) = 0 . \tag{D.28}$$

$$C_1 \left(\frac{\partial^2 v_3(a_3,t)}{\partial x_3^2} - \frac{\partial^2 v_3(a_3^+,t)}{\partial x_3^2} \right) = 0. \tag{D.29}$$

$$C_1 \frac{\partial^2 v_3(L,t)}{\partial x_3^2} + C_4 \frac{\partial^3 v_3(L,t)}{\partial x_3 \partial t^2} + C_5 \frac{\partial^2 v_3(L,t)}{\partial t^2} + C_6 G_5(t) \frac{\partial v_3(L,t)}{\partial x_3}$$

$$- C_5 G_5(t) v_3(L,t) + C_9 G_6(t) = 0. \tag{D.30}$$

$$-C_1 \frac{\partial^3 v_3(L,t)}{\partial x_3^3} + C_5 \frac{\partial^3 v_3(L,t)}{\partial x_3 \partial t^2} + C_7 \frac{\partial^2 v_3(L,t)}{\partial t^2} + C_8 G_5(t) \frac{\partial v_3(L,t)}{\partial x_3}$$

$$- C_7 G_5(t) v_3(L,t) + C_{10} G_6(t) = 0 . \tag{D.31}$$

Equations (D.18) to (D.21) gave the geometric boundary conditions already.

APPENDIX E

DETERMINATION OF δu_3, $\delta\varphi_{2e}$ AND $\delta\varphi_{3e}$ WITH ASSUMPTION OF RIGID COUPLER

When setting up the differential equation for an elastic link by the method of substitution, it is necessary to know the expressions for the various δu's and $\delta\varphi_e$'s. For a rigid coupler (see Appendix D) it is only necessary to know δu_3, $\delta u_3(a_3)$, $\delta u_3(L)$ as well as $\delta\varphi_{2e}$ and $\delta\varphi_{3e}$.

The δu's are obtained from equations (3.29), (3.31) and (3.33):

$$\delta u_3 = -\left[\frac{\partial v_3}{\partial x_3}\,\delta v_3\right]_0^{x_3} + \int_0^{x_3} \frac{\partial^2 \tilde{v}_3}{\partial \xi_{33}^2}\,\delta \tilde{v}_3\, d\xi_{33} \,, \tag{E.1}$$

$$\delta u_3(a_3) = -\left[\frac{\partial v_3}{\partial x_3}\,\delta v_3\right]_0^{a_3} + \int_0^{a_3} \frac{\partial^2 v_3}{\partial x_3^2}\,\delta v_3\, dx_3 \,, \tag{E.2}$$

$$\delta u_3(L) = -\left[\frac{\partial v_3}{\partial x_3}\,\delta v_3\right]_0^{L} + \int_0^{a_3} \frac{\partial^2 v_3}{\partial x_3^2}\,\delta v_3\, dx_3 + \int_{a_3}^{L} \frac{\partial^2 v_3}{\partial x_3^2}\,\delta v_3\, dx_3 . \tag{E.3}$$

$\delta\varphi_{2e}$ and $\delta\varphi_{3e}$ are solved for simultaneously from equations (3.34) and (3.35). Since link 2 is assumed rigid in the shaker mechanism, $\delta u_2(a_2) = 0$. Then:

$$-a_2 \sin\varphi_{2e}\,\delta\varphi_{2e} + (a_3 + u_3(a_3))\sin\varphi_{3e}\,\delta\varphi_{3e} = \cos\varphi_{3e}\,\delta u_3(a_3) \,, \tag{E.4}$$

$$a_2 \cos\varphi_{2e}\,\delta\varphi_{2e} - (a_3 + u_3(a_3))\cos\varphi_{3e}\,\delta\varphi_{3e} = \sin\varphi_{3e}\,\delta u_3(a_3) \,. \tag{E.5}$$

Cramer's rule leads to:

$$\delta\varphi_{2e} = \frac{\delta u_3(a_3)}{a_2 \sin(\varphi_{3e}-\varphi_{2e})} \quad , \tag{E.6}$$

and

$$\delta\varphi_{3e} = \frac{\cot(\varphi_{3e}-\varphi_{2e})\,\delta u_3(a_3)}{a_3 + u_3(a_3)} \quad . \tag{E.7}$$

Finally, with equation (E.2), the above becomes:

$$\delta\varphi_{2e} = \frac{\csc(\varphi_{3e}-\varphi_{2e})}{a_2}\int_0^{a_3} \frac{\partial^2 v_3}{\partial x_3^2}\,\delta v_3\, dx_3 - \frac{\csc(\varphi_{3e}-\varphi_{2e})}{a_2}\left[\frac{\partial v_3}{\partial x_3}\,\delta v_3\right]_0^{a_3} , \tag{E.8}$$

and

$$\delta\varphi_{3e} = \frac{\cot(\varphi_{3e}-\varphi_{2e})}{a_3+u_3(a_3)}\int_0^{a_3} \frac{\partial^2 v_3}{\partial x_3^2}\,\delta v_3\, dx_3 - \frac{\cot(\varphi_{3e}-\varphi_{2e})}{a_3+u_3(a_3)}\left[\frac{\partial v_3}{\partial x_3}\,\delta v_3\right]_0^{a_3} . \tag{E.9}$$

APPENDIX F

SUBPROBLEM: DYNAMICS OF SIMPLY SUPPORTED BEAM WITH OVERHANG, ENDMASS AND COUNTERWEIGHT

1. Statement of Problem

In order to solve the equations of motion of the elastic rocker by the method of Kantorovich, it is necessary to determine an appropriate shape function and its associated eigenvalues and orthogonality condition. This is accomplished by the solution of the free vibration problem of the beam shown in Figure F.1. (The work of J. C. Maltbaek [22] has been helpful for this purpose.)

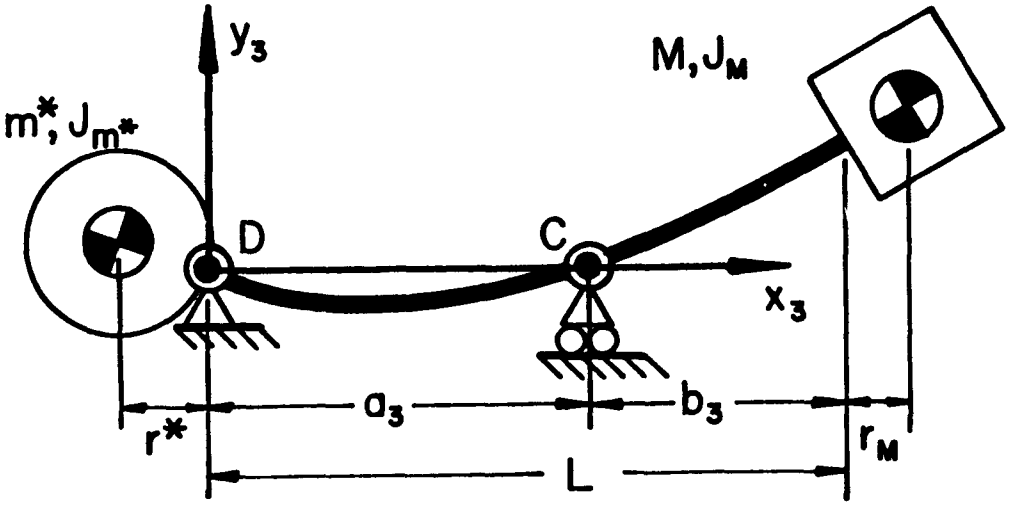

Figure F.1 Subproblem

2. Equations of Motion and Boundary Conditions

The differential equations of motion and the natural boundary conditions for the two sections of the beam are obtained with the help of Hamilton's integral, i.e.

$$\delta\int_{t_0}^{t_1}(T-\Pi)\,dt = 0 \qquad \text{(F.1)}$$

In the above the components of the kinetic energy are given by:

$\frac{1}{2}\int_0^L \mu_3\left(\frac{\partial v}{\partial t}\right)^2 dx_3$ = kinetic energy of beam,

$\frac{1}{2}m^*r^{*2}\left(\frac{\partial^2 v(0,t)}{\partial x_3\partial t}\right)^2 + \frac{1}{2}J_m^*\left(\frac{\partial^2 v(0,t)}{\partial x_3\partial t}\right)^2$ = kinetic energy of counterweight,

$\frac{1}{2}M\left(\frac{\partial v(L,t)}{\partial t} + r_M\frac{\partial^2 v(L,t)}{\partial x_3\partial t}\right)^2 + \frac{1}{2}J_M\left(\frac{\partial^2 v(L,t)}{\partial x_3\partial t}\right)^2$ = kinetic energy of endmass,

$\frac{1}{2}\int_0^{a_3} E_3I_3\left(\frac{\partial^2 v}{\partial x_3^2}\right)^2 dx_3 + \frac{1}{2}\int_{a_3}^{L} E_3I_3\left(\frac{\partial^2 v}{\partial x_3^2}\right)^2 dx_3$ = potential energy of two-section beam.

Substitution of the above energy terms into equation (F.1) and subsequent variation as well as integration by parts furnishes:

$$-\int_{t_0}^{t_1}\int_0^{a_3}\left(\mu_3\frac{\partial^2 v}{\partial t^2} + E_3I_3\frac{\partial^4 v}{\partial x_3^4}\right)\delta v\,dx_3\,dt - \int_{t_0}^{t_1}\int_{a_3}^{L}\left(\mu_3\frac{\partial^2 v}{\partial t^2} + E_3I_3\frac{\partial^4 v}{\partial x_3^4}\right)\delta v\,dx_3\,dt$$

$$-\int_{t_0}^{t_1}\left\{\left[\left(J_m^* + m^*r^{*2}\right)\frac{\partial^3 v(0,t)}{\partial x_3\partial t^2} - E_3I_3\frac{\partial^2 v(0,t)}{\partial x_3^2}\right]\delta\frac{\partial v(0,t)}{\partial x_3} + E_3I_3\frac{\partial^3 v(0,t)}{\partial x_3^3}\,\delta v(0,t)\right.$$

$$+E_3I_3\left(\frac{\partial^2 v(a_3,t)}{\partial x_3^2}\,\delta\frac{\partial v(a_3,t)}{\partial x_3} - \frac{\partial^2 v(a_3^+,t)}{\partial x_3^2}\,\delta\frac{\partial v(a_3^+,t)}{\partial x_3} - \frac{\partial^3 v(a_3,t)}{\partial x_3^3}\,\delta v(a_3,t) + \frac{\partial^3 v(a_3^+,t)}{\partial x_3^3}\,\delta v(a_3^+,t)\right)$$

$$+\left(\left(J_M + Mr_M^2\right)\frac{\partial^3 v(L,t)}{\partial x_3\partial t^2} + Mr_M\frac{\partial^2 v(L,t)}{\partial t^2} + E_3I_3\frac{\partial^2 v(L,t)}{\partial x_3^2}\right)\delta\frac{\partial v(L,t)}{\partial x_3} + \left(M\frac{\partial^2 v(L,t)}{\partial t^2}\right.$$

$$\left.\left.+Mr_M\frac{\partial^3 v(L,t)}{\partial x_3\partial t^2} - E_3I_3\frac{\partial^3 v(L,t)}{\partial x_3^3}\right)\delta v(L,t)\right\}dt = 0. \qquad \text{(F.2)}$$

Since the geometric boundary conditions are given by:

$$\left.\begin{aligned} &v_3(0,t) = 0 \\ &v_3(a_3,t) = 0 \\ &v_3(a_3^+,t) = 0 \\ &\frac{\partial v_3(a_3,t)}{\partial x_3} = \frac{\partial v_3(a_3^+,t)}{\partial x_3} \end{aligned}\right\}, \tag{F.3}$$

one obtains:

$$\left.\begin{aligned} &\delta v_3(0,t) = 0 \\ &\delta v_3(a_3,t) = 0 \\ &\delta v_3(a_3^+,t) = 0 \\ &\delta\frac{\partial v_3(a_3,t)}{\partial x_3} = \delta\frac{\partial v_3(a_3^+,t)}{\partial x_3} \end{aligned}\right\}. \tag{F.4}$$

Use of the above and application of the Fundamental Lemma leads to the following differential equations and associated natural boundary conditions:

For $0 \le x_3 \le a_3$:

$$C_2\frac{\partial^2 v}{\partial t^2} + C_1\frac{\partial^4 v}{\partial x_3^4} = 0, \tag{F.5}$$

for $a_3^+ \le x_3 \le L$:

$$C_2\frac{\partial^2 v}{\partial t^2} + C_1\frac{\partial^4 v}{\partial x_3^4} = 0, \tag{F.6}$$

and

$$-C_1\frac{\partial^2 v(0,t)}{\partial x_3^2} + C_3\frac{\partial^3 v(0,t)}{\partial x_3 \partial t^2} = 0, \tag{F.7}$$

$$\frac{\partial^2 v(a_3,t)}{\partial x_3^2} = \frac{\partial^2 v(a_3^+,t)}{\partial x_3^2} \quad , \tag{F.8}$$

$$C_1 \frac{\partial^2 v(L,t)}{\partial x_3^2} + C_5 \frac{\partial^2 v(L,t)}{\partial t^2} + C_4 \frac{\partial^3 v(L,t)}{\partial x_3 \partial t^2} = 0 \quad , \tag{F.9}$$

$$-C_1 \frac{\partial^3 v(L,t)}{\partial x_3^3} + C_7 \frac{\partial^2 v(L,t)}{\partial t^2} + C_5 \frac{\partial^3 v(L,t)}{\partial x_3 \partial t^2} = 0, \tag{F.10}$$

where the constants C_1, C_2, etc., are identical to those given in equation (D.11) of Appendix D.

3. Shape Function and Characteristic Equation

The partial differential equations (F. 5) and (F. 6) are solved by means of separation of variables, i.e.

$$v(x_3,t) = V(x_3) e^{i\omega t} . \tag{F.11}$$

Substitution of the above leads to:

For $0 \le x_3 \le a_3$:

$$\frac{d^4V}{dx_3^4} - \lambda^4 V = 0 \quad , \tag{F.12}$$

for $a_3^+ \le x_3 \le L$:

$$\frac{d^4V}{dx_3^4} - \lambda^4 V = 0 \quad , \tag{F.13}$$

where

$$\lambda^4 = \omega^2 \frac{C_2}{C_1} \quad , \tag{F.14}$$

and the boundary conditions:

$$V(0) = 0 \ , \tag{F.15}$$

$$V''(0) + \lambda^4 C_{11} V'(0) = 0 \ , \tag{F.16}$$

$$V(a_3) = 0 \ , \tag{F.17}$$

$$V'(a_3) = V'(a_3^+) \ , \tag{F.18}$$

$$V''(a_3) = V''(a_3^+) \ , \tag{F.19}$$

$$V(a_3^+) = 0 \ , \tag{F.20}$$

$$V''(L) - \lambda^4 C_{14} V'(L) - \lambda^4 C_{13} V(L) = 0 \ , \tag{F.21}$$

$$V'''(L) + \lambda^4 C_{13} V'(L) + \lambda^4 C_{12} V(L) = 0 \ , \tag{F.22}$$

where

$$C_{11} = \frac{C_3}{C_2} \ , \tag{F.23}$$

$$C_{12} = \frac{C_1}{C_2} \ , \tag{F.24}$$

$$C_{13} = \frac{C_5}{C_2} \ , \tag{F.25}$$

$$C_{14} = \frac{C_4}{C_2} \ . \tag{F.26}$$

The solutions to equations (F.13) and (F.14) are given by:

For $0 \le x_3 \le a_3$:

$$V(x_3) = A_{11} \sin \lambda x_3 + A_{12} \cos \lambda x_3 + A_{13} \sinh \lambda x_3 + A_{14} \cosh \lambda x_3 \ , \tag{F.27}$$

and for $a_3^+ \leq x_3 \leq L$:

$$V(x_3) = A_{21} \sin\lambda x_3 + A_{22} \cos\lambda x_3 + A_{23} \sinh\lambda x_3 + A_{24} \cosh\lambda x_3 . \tag{F.28}$$

The portion of the shape function $V(x_3)$ for $0 \leq x_3 \leq a_3$ (up to the constant A_{11} which is arbitarily chosen to be unity) is determined with the boundary conditions (F.15), (F.16) and (F.17):

$$V_n(x_3) = \sin\lambda_n x_3 + \Gamma_{1n} \sinh\lambda_n x_3 + \Gamma_{2n}(\cos\lambda_n x_3 - \cosh\lambda_n x_3), \tag{F.29}$$

where

$$\Gamma_{1n} = \frac{-\sin\lambda_n a_3 - \frac{\lambda_n^3 C_{11}}{2}(\cos\lambda_n a_3 - \cosh\lambda_n a_3)}{\sinh\lambda_n a_3 + \frac{\lambda_n^3 C_{11}}{2}(\cos\lambda_n a_3 - \cosh\lambda_n a_3)} , \tag{F.30}$$

$$\Gamma_{2n} = \frac{\lambda_n^3 C_{11}}{2}\left(\frac{\sinh\lambda_n a_3 - \sin\lambda_n a_3}{\sinh\lambda_n a_3 + \frac{\lambda_n^3 C_{11}}{2}(\cos\lambda_n a_3 - \cosh\lambda_n a_3)}\right). \tag{F.31}$$

Similarly, the portion of the shape function $V(x_3)$ for $a_3^+ \leq x_3 \leq L$ is determined with the boundary conditions (F.19), (F.20), (F.21) and (F.22):

$$V_n(x_3) = \Gamma_{5n}\Big[\sin\lambda_n(x_3-a_3) + \Gamma_{3n}\sinh\lambda_n(x_3-a_3) + \Gamma_{4n}\big(\cosh\lambda_n(x_3-a_3) - \cos\lambda_n(x_3-a_3)\big)\Big] , \tag{F.32}$$

where

$$\Gamma_{3n} = \frac{\Delta_{2n}\Delta_{4n} + \Delta_{1n}\Delta_{5n}}{\Delta_{3n}\Delta_{4n} + \Delta_{1n}\Delta_{6n}} , \tag{F.33}$$

$$\Gamma_{4n} = \frac{\Delta_{2n} - \Delta_{3n}\Gamma_{3n}}{\Delta_{1n}} , \tag{F.34}$$

$$\Gamma_{5n} = \frac{1}{2\Gamma_{4n}}\left\{-\sin\lambda_n a_3 - \frac{1}{\Delta_{7n}}\left[\sin\lambda_n a_3 \sinh\lambda_n a_3 + \frac{\lambda_n^3 C_{11}}{2}\left(2\cos\lambda_n a_3 \sinh\lambda_n a_3 - \sin\lambda_n a_3\left(\cos\lambda_n a_3 + \cosh\lambda_n a_3\right)\right)\right]\right\}, \tag{F.35}$$

and

$$\Delta_{1n} = (1+\lambda_n^2 C_{13})\cos\lambda_n b_3 + (1-\lambda_n^2 C_{13})\cosh\lambda_n b_3 - \lambda_n^3 C_{14}(\sin\lambda_n b_3 + \sinh\lambda_n b_3) , \tag{F.36}$$

$$\Delta_{2n} = (1+\lambda_n^2 C_{13})\sin\lambda_n b_3 + \lambda_n^3 C_{14}\cos\lambda_n b_3 , \tag{F.37}$$

$$\Delta_{3n} = (1-\lambda_n^2 C_{13})\sinh\lambda_n b_3 - \lambda_n^3 C_{14}\cosh\lambda_n b_3 , \tag{F.38}$$

$$\Delta_{4n} = \lambda_n C_{12}(\cos\lambda_n b_3 - \cosh\lambda_n b_3) - (1+\lambda_n^2 C_{13})\sinh\lambda_n b_3 + (1-\lambda_n^2 C_{13})\sin\lambda_n b_3 , \tag{F.39}$$

$$\Delta_{5n} = (1-\lambda_n^2 C_{13})\cos\lambda_n b_3 - \lambda_n C_{12}\sin\lambda_n b_3 , \tag{F.40}$$

$$\Delta_{6n} = (1+\lambda_n^2 C_{13})\cosh\lambda_n b_3 + \lambda_n C_{12}\sinh\lambda_n b_3 , \tag{F.41}$$

$$\Delta_{7n} = \sinh\lambda_n a_3 + \frac{\lambda_n^3 C_{11}}{2}\left(\cos\lambda_n a_3 - \cosh\lambda_n a_3\right) . \tag{F.42}$$

The characteristic equation is obtained from the remaining boundary condition (F.18), i.e. $V'(a_3) = V'(a_3^+)$. Thus,

$$\frac{-2\sin\lambda_n a_3 \sinh\lambda_n a_3 - \lambda_n^3 C_{11}(\cos\lambda_n a_3 \sinh\lambda_n a_3 - \sin\lambda_n a_3 \cosh\lambda_n a_3)}{\cos\lambda_n a_3 \sinh\lambda_n a_3 - \sin\lambda_n a_3 \cosh\lambda_n a_3 + \lambda_n^3 C_{11}(1 - \cos\lambda_n a_3 \cosh\lambda_n a_3)} = \frac{2(\Delta_{2n}\Delta_{6n} - \Delta_{3n}\Delta_{5n})}{\Delta_{1n}(\Delta_{5n} + \Delta_{6n}) + \Delta_{4n}(\Delta_{2n} + \Delta_{3n})} . \quad \text{(F.43)}$$

In order to compute slopes and moments in the vibration problem, the first and second derivatives of the shape function are given:

For $0 \le x_3 \le a_3$:

$$V_n'(x_3) = \left[\lambda_n \cos\lambda_n x_3 + \Gamma_{1n}\cosh\lambda_n x_3 - \Gamma_{2n}(\sin\lambda_n x_3 + \sinh\lambda_n x_3)\right], \quad \text{(F.44)}$$

$$V_n''(x_3) = \lambda_n^2\left[-\sin\lambda_n x_3 + \Gamma_{1n}\sinh\lambda_n x_3 - \Gamma_{2n}(\cos\lambda_n x_3 + \cosh\lambda_n x_3)\right], \quad \text{(F.45)}$$

and for $a_3^+ \le x_3 \le L$:

$$V_n'(x_3) = \lambda_n\Gamma_{5n}\left[\cos\lambda_n(x_3 - a_3) + \Gamma_{3n}\cosh\lambda_n(x_3 - a_3) + \Gamma_{4n}\left(\sinh\lambda_n(x_3 - a_3) + \sin\lambda_n(x_3 - a_3)\right)\right], \quad \text{(F.46)}$$

$$V_n''(x_3) = \lambda_n^2\Gamma_{5n}\left[-\sin\lambda_n(x_3 - a_3) + \Gamma_{3n}\sinh\lambda_n(x_3 - a_3) + \Gamma_{4n}\left(\cosh\lambda_n(x_3 - a_3) + \cos\lambda_n(x_3 - a_3)\right)\right]. \quad \text{(F.47)}$$

4. Orthogonality Condition

To determine the orthogonality condition, let λ_m and λ_n be two distinct eigenvalues and V_m and V_n be corresponding sets of eigenfunctions resulting from the solution of the eigenvalue problem.(*) Then, according to equations (F.13) and (F.14), one obtains:

$$\frac{d^4V_m}{dx_3^4} = \lambda_m^4 V_m \tag{F.48}$$

and

$$\frac{d^4V_n}{dx_3^4} = \lambda_n^4 V_n \ . \tag{F.49}$$

Now one multiplies equation (F.48) by V_n and equation (F.49) by V_m respectively, subtracts the individual results from each other, and finally integrates the result over the full span of the beam:

$$\int_0^{a_3}\left[V_n\frac{d^4V_m}{dx_3^4} - V_m\frac{d^4V_n}{dx_3^4}\right]dx_3 + \int_{a_3}^{L}\left[V_n\frac{d^4V_m}{dx_3^4} - V_m\frac{d^4V_n}{dx_3^4}\right]dx_3$$

$$= (\lambda_m^4-\lambda_n^4)\left\{\int_0^{a_3} V_m V_n\,dx_3 + \int_{a_3}^{L} V_m V_n\,dx_3\right\} \ . \tag{F.50}$$

Integration of the left hand side of equation (F.50) by parts twice and the substitution of the required boundary terms according to equations (F.15) through (F.22) leads to the following condition:

(*) This approach is successful because the problem is self-adjoint.

$$(\lambda_m^4 - \lambda_n^4)\left\{\int_0^{a_3} V_m V_n \, dx_3 + \int_{a_3}^{L} V_m V_n \, dx_3 + C_{11} V_m'(0) V_n'(0) + C_{12} V_m(L) V_n(L)\right.$$

$$\left. + C_{13}\left(V_m(L) V_n'(L) + V_m'(L) V_n(L)\right) + C_{14} V_m'(L) V_n'(L)\right\} = 0. \qquad \text{(F.51)}$$

Since $\lambda_m \neq \lambda_n$, then

$$\int_0^{a_3} V_m V_n \, dx_3 + \int_{a_3}^{L} V_m V_n \, dx_3 + C_{11} V_m'(0) V_n'(0) + C_{12} V_m(L) V_n(L)$$

$$+ C_{13}\left(V_m(L) V_n'(L) + V_m'(L) V_n(L)\right) + C_{14} V_m'(L) V_n'(L) = 0. \qquad \text{(F.52)}$$

Substitution for C_{11}, C_{12}, C_{13} and C_{14} according to equations (F.23) through (F.26) leads to the final form of the orthogonality condition:

$$C_2 \int_0^{a_3} V_m V_n \, dx_3 + C_2 \int_{a_3}^{L} V_m V_n \, dx_3 + C_3 V_m'(0) V_n'(0) + C_1 V_m(L) V_n(L)$$

$$+ C_5\left(V_m(L) V_n'(L) + V_m'(L) V_n(L)\right) + C_4 V_m'(L) V_n'(L) = \mathcal{N}_m \delta_{nm}, \qquad \text{(F.53)}$$

where $\mathcal{N}_m$ is the value of the expression when n = m and δ_{nm} is the Kronecker delta.

APPENDIX G

DETERMINATION OF HILL-TYPE DIFFERENTIAL EQUATIONS BY METHOD OF KANTOROVICH

1. Method of Kantorovich

To obtain Hill's equations in $q_n(t)$, the solution form

$$v_3(x_3,t) = \sum_n V_n(x_3)\, q_n(t) , \qquad (G.1)$$

as well as its various derivatives are substituted into Hamilton's integral as represented by equation (D.10). The $V_n(x_3)$ are those of Appendix F.

Since the shape function is prescribed, only the time portion of the solution form can be varied. Thus, for example,

$$\delta \frac{\partial v_3(0,t)}{\partial x_3} = \sum_m V_m'(0)\, \delta q_m ,$$

where the primes denote differentiation with respect to x_3. Because this subproblem satisfies the geometric boundary conditions,

$$\delta v_3(0,t) = \sum_m V_m(0)\, \delta q_m = 0$$

and

$$\delta v_3(a_3,t) = \sum_m V_m(a_3)\, \delta q_m = 0 .$$

Substitution into equation (D.10) leads to:

$$\int_{t_0}^{t_1}\int_{0}^{a_3}\Big\{C_1\sum_n V_n^{IV}q_n + G_1(x_3,t)\sum_n V_n''q_n + C_2\sum_n V_n\ddot{q}_n + G_2(x_3,t)\sum_n V_n'q_n$$

$$+ C_{D3}\sum_n V_n\dot{q}_n - C_2G_5(t)\sum_n V_nq_n + G_3(x_3,t)\Big\}\sum_m V_m\,\delta q_m\,dx_3\,dt$$

$$+\int_{t_0}^{t_1}\int_{a_3}^{L}\Big\{C_1\sum_n V_n^{IV}q_n + G_4(x_3,t)\sum_n V_n''q_n + C_2\sum_n V_n\ddot{q}_n + G_2(x_3,t)\sum_n V_n'q_n$$

$$+C_{D3}\sum_n V_n\dot{q}_n - C_2G_5(t)\sum_n V_nq_n + G_3(x_3,t)\Big\}\sum_m V_m\,\delta q_m\,dx_3\,dt$$

$$+\int_{t_0}^{t_1}\Big\{\Big[-C_1\sum_n V_n''(0)q_n + C_3\sum_n V_n'(0)\ddot{q}_n + C_3G_6(t)\Big]\sum_m V_m'(0)\,\delta q_m$$

$$+C_1\Big[\sum_n V_n''(a_3)q_n - \sum_n V_n''(a_3^+)q_n\Big]\sum_m V_m'(a_3)\,\delta q_m + \Big[C_1\sum_n V_n''(L)q_n$$

$$+C_4\sum_n V_n'(L)\ddot{q}_n + C_5\sum_n V_n(L)\ddot{q}_n + C_6G_5(t)\sum_n V_n'(L)q_n - C_5G_5(t)\sum_n V_n(L)q_n$$

$$+C_9G_6(t)\Big]\sum_m V_m'(L)\,\delta q_m + \Big[-C_1\sum_n V_n'''(L)q_n + C_5\sum_n V_n'(L)\ddot{q}_n + C_7\sum_n V_n(L)\ddot{q}_n$$

$$+C_8G_5(t)\sum_n V_n'(L)q_n - C_7G_5(t)\sum_n V_n(L)q_n + C_{10}G_6(t)\Big]\sum_m V_m(L)\,\delta q_m\Big\}\,dt = 0. \qquad (G.2)$$

The coefficients of the various derivatives of $q_n(t)$ are first collected. Then the boundary terms $V_n''(0)$, $V_n''(a_3)$, $V_n''(L)$ and $V_n'''(L)$ are expressed according to the natural boundary conditions (F.16), (F.19), (F.21) and (F.22), respectively. Further, use is made of the following identity:

$$C_1\left[\int_0^{a_3} V_m V_n^{IV}\,dx_3 + \int_{a_3}^{L} V_m V_n^{IV}\,dx_3\right] = \omega_n^2 C_2\left[\int_0^{a_3} V_m V_n\,dx_3 + \int_{a_3}^{L} V_m V_n\,dx_3\right] \quad (G.3)$$

which originates from equations (F.12) and (F.13). Finally terms may be collected with the help of the orthogonality condition (F.53), and one obtains:

$$\int_{t_0}^{t_1}\sum_m\Bigg\{\gamma_m\ddot{q}_m + \sum_n \dot{q}_n C_{D_3}\left[\int_0^{a_3} V_m V_n\,dx_3 + \int_{a_3}^{L} V_m V_n\,dx_3\right] + \left(\omega_m^2 - G_5(t)\right)\gamma_m q_m$$

$$+ \sum_n q_n\Bigg[\int_0^{a_3} G_1(x_3,t)\,V_m V_n''\,dx_3 + \int_{a_3}^{L} G_4(x_3,t)\,V_m V_n''\,dx_3 + \int_0^{a_3} G_2(x_3,t)\,V_m V_n'\,dx_3$$

$$+ \int_{a_3}^{L} G_2(x_3,t)\,V_m V_n'\,dx_3 + G_5(t)\Big((C_4+C_6)V_m'(L)V_n'(L) + (C_5+C_8)V_m(L)V_n'(L)$$

$$+ C_3 V_m'(0)V_n'(0)\Big)\Bigg] + \Bigg[\int_0^{a_3} G_3(x_3,t)\,V_m\,dx_3 + \int_{a_3}^{L} G_3(x_3,t)\,V_m\,dx_3 + G_6(t)\Big(C_3 V_m'(0)$$

$$+ C_9 V_m'(L) + C_{10} V_m(L)\Big)\Bigg]\Bigg\}\delta q_m\,dt = 0\,. \quad (G.4)$$

2. Coupled Hill-Type Equations

Application of the Fundamental Lemma to equation (G.4) furnishes the following infinite set of coupled Hill-type differential equations:

$$\ddot{q}_m + \frac{C_{D3m}}{\mathcal{N}_m}\sum_n \mathcal{J}_{1(m,n)}\dot{q}_n + \left(\omega_m^2 - G_5(t)\right)q_m + \frac{1}{\mathcal{N}_m}\sum_n H_{mn}(t)\,q_n = \frac{F_m(t)}{\mathcal{N}_m} \quad , \tag{G.5}$$

for $m = 1,2,3,\ldots$.

This shows that each natural frequency ω_m has associated with it a damping constant C_{D3m}.

Further,

$$\mathcal{J}_{1(m,n)} = \int_0^{a_3} V_m V_n\,dx_3 + \int_{a_3}^{L} V_m V_n\,dx_3 \quad , \tag{G.6}$$

$$\begin{aligned} H_{mn}(t) = {} & \int_0^{a_3} G_1(x_3,t)V_m V_n''\,dx_3 + \int_{a_3}^{L} G_4(x_3,t)V_m V_n''\,dx_3 \\ & + \int_0^{a_3} G_2(x_3,t)V_m V_n'\,dx_3 + \int_{a_3}^{L} G_2(x_3,t)V_m V_n'\,dx_3 + G_5(t)\Big[(C_4+C_6)V_m'(L)V_n'(L) \\ & + (C_5+C_8)V_m(L)V_n'(L) + C_3 V_m'(0)V_n'(0)\Big] \quad , \end{aligned} \tag{G.7}$$

$$\begin{aligned} F_m(t) = {} & -\int_0^{a_3} G_3(x_3,t)V_m\,dx_3 - \int_{a_3}^{L} G_3(x_3,t)V_3\,dx_3 - G_6(t)\Big[C_3 V_m'(0) \\ & + C_9 V_m'(L) + C_{10}V_m(L)\Big] \quad . \end{aligned} \tag{G.8}$$

APPENDIX H

FORM OF SOLUTION OF DAMPED AND UNDAMPED HILL'S EQUATIONS: REVIEW OF FLOQUET THEORY

1. Homogeneous Equation

a) Floquet Theory Associated with Undamped Homogeneous Hill's Equation

In the absence of damping, the homogeneous portion of an expression of the type of equation (4.42) becomes:

$$\frac{d^2q}{d\varphi_1^2} + B(\varphi_1)q = 0, \tag{H.1}$$

where $B(\varphi_1) = \Lambda + A(\varphi_1)$. $A(\varphi_1)$ is a periodic function and Λ is a system parameter. According to Floquet theory at least one of the two solutions of this second order equation has the form:

$$q(\varphi_1) = e^{\mu\varphi_1}\Phi(\varphi_1) . \tag{H.2}$$

In the above, μ is a complex parameter called the characteristic exponent, and $\Phi(\varphi_1)$ is a periodic function of φ_1 which has the same period as $A(\varphi_1)$. For mechanisms with constant input angular velocity, $A(\varphi_1)$ is 2π-periodic.

The values of the characteristic exponent μ which are generally possible, as well as those which are specifically associated with the stability boundaries (transition points from stable to unstable solutions), are determined from the characteristic equation

$$\rho^2 - \Delta\rho + 1 = 0 , \tag{H.3}$$

where

$$\rho = e^{2\pi\mu} \quad . \tag{H.4}$$

In the above, 2π represents the period of $B(\varphi_1)$, and Δ is a constant for a particular system.

The solution of the characteristic equation,

$$\rho_1, \rho_2 = \frac{\Delta}{2} \pm \sqrt{\frac{\Delta^2}{4} - 1} \quad , \tag{H.5}$$

enables one to find the possible values of the exponent μ. Table H.1 lists values of ρ and μ which are associated with stable and unstable regions, as well as the stability boundaries. The characteristic exponent $\mu_{1,2}$ is obtained from $\rho_{1,2}$ by

$$\mu_{1,2} = \frac{\ln \rho_{1,2}}{2\pi} \quad , \tag{H.6}$$

where

$$\ln \rho = \ln|\rho| + i(\theta + 2k\pi) \; ; \; k = 0, \pm 1, \pm 2, \pm 3, \ldots \tag{H.7}$$

If ρ is complex, i.e.

$$\rho = u + iv \, , \tag{H.8}$$

then

$$\theta = \tan^{-1} \frac{v}{u} \quad . \tag{H.9}$$

Important properties concerning the periodicity of solutions on the boundaries between the stable and unstable regions may be ascertained from Case II of Table H.1. Since $\Phi(\varphi_1)$ is a 2π-periodic function, one obtains from equation (H.2) for the case where $\rho_{1,2} = 1$, the total solution

Value of A		ρ	μ $k = 0, \pm 1, \pm 2, \ldots$	Condition of Stability
Case I $\lvert A \rvert < 2$ Stable Region	$0 < A < 2$	$\lvert \rho_1 \rvert = 1$	$\mu_1 = \frac{(\theta_1 + 2k\pi)i}{2\pi}$ $\theta_1 = \tan^{-1} \sqrt{\frac{4}{A^2} - 1}$	Stable
		$\lvert \rho_2 \rvert = 1$	$\mu_2 = -\mu_1$	Stable
	$-2 < A < 0$	$\lvert \rho_1 \rvert = 1$	$\mu_1 = \frac{(\theta_1 + 2k\pi)i}{2\pi}$ $\theta_1 = \tan^{-1} - \sqrt{\frac{4}{A^2} - 1}$	Stable
		$\lvert \rho_2 \rvert = 1$	$\mu_2 = \mu_1$	Stable
Case II $\lvert A \rvert = 2$ Stability Boundaries	$A = 2$	$\rho_1 = \rho_2 = 1$	$\mu_1 = \mu_2 = ki$	Unstable: presence of secular term.
	$A = -2$	$\rho_1 = \rho_2 = -1$	$\mu_1 = \mu_2 = \frac{(2k + 1)}{2} i$	Unstable: presence of secular term.
Case III $\lvert A \rvert > 2$ Unstable Region	$A > 2$	$\rho_1 > 1$	$\mu_1 = \frac{\ln \lvert \rho_1 \rvert}{2\pi} + ki$	Unstable
		$0 < \rho_2 < 1$	$\mu_2 = -\mu_1$	Stable
	$A < -2$	$-1 < \rho_1 < 0$	$\mu_1 = \frac{\ln \lvert \rho_1 \rvert}{2\pi} + \frac{(2k + 1)}{2} i$	Stable
		$\rho_2 < -1$	$\mu_2 = -\mu_1$	Unstable

Table H.1 Possible Values of μ.

$$q(\varphi_1) = \sum_{-n}^{\infty} a_n e^{in\varphi_1} + \varphi_1 \sum_{-n}^{\infty} b_n e^{in\varphi_1} . \qquad (H.10)$$

Thus, the non-secular portion of the solution is 2π-periodic. Similarly, when $\rho_{1,2} = -1$ the total solution becomes:

$$q(\varphi_1) = \sum_{-n}^{\infty} c_n e^{i\left(\frac{2n+1}{2}\right)\varphi_1} + \varphi_1 \sum_{-n}^{\infty} d_n e^{i\left(\frac{2n+1}{2}\right)\varphi_1} . \qquad (H.11)$$

In this boundary case, the non-secular portion of the solution is 4π-periodic. These particular properties of periodicity are used to determine the stability boundaries. (See Section 1b below.)

To obtain specific characteristic exponents $\mu_{1,2}$, which correspond to certain parameter combinations contained in the coefficient $B(\varphi_1)$ of equation (H.1), the constant Δ of the characteristic equation must be known. According to [5,6] it may be found from:

$$\Delta = q_1(2\pi) + \frac{dq_2(2\pi)}{d\varphi_1} . \qquad (H.12)$$

where $q_1(\varphi_1)$ and $q_2(\varphi_1)$ are two linearly independent solutions to equation (H.1) which satisfy the initial conditions:

$$\left.\begin{aligned} q_1(0) &= 1, \quad \frac{dq_1(0)}{d\varphi_1} = 0, \\ q_2(0) &= 0, \quad \frac{dq_2(0)}{d\varphi_1} = 1 . \end{aligned}\right\} \qquad (H.13)$$

Thus, Δ can be found by way of two appropriate numerical solutions of equation (H.1) [23].

b) Determination of Stability Boundaries for Undamped Homogeneous Hill's Equation

Table H.1 shows that the transition from stable to unstable solutions of the homogeneous equation occurs when

$$\mu_{1,2} = 0,\ \pm i,\ \pm 2i,\ \pm 3i,\ldots \text{(}2\pi\text{-periodic solution)} \qquad \text{(H.14)}$$

or when

$$\mu_{1,2} = \pm\tfrac{1}{2} i,\ \pm\tfrac{3}{2} i,\ \pm\tfrac{5}{2} i,\ldots \text{(}4\pi\text{-periodic solution)} \qquad \text{(H.15)}$$

To find the parameter combinations in $B(\varphi_1)$ of equation (H.1) which correspond to the values of $\mu_{1,2}$ in equations (H.14) and (H.15), one makes use of the following general method.

The 2π-periodic function $\Phi(\varphi_1)$ in the solution equation (H.2) is expanded into a complex Fourier series, i.e.

$$q(\varphi_1) = e^{\mu\varphi_1} \sum_{m=-\infty}^{\infty} \psi_m e^{im\varphi_1}, \qquad \text{(H.16)}$$

where the ψ_m are unknown complex coefficients.(*) Further, $B(\varphi_1)$, a 2π-periodic function which contains the frequency ratio $\Lambda = (\omega/\dot{\varphi}_1)^2$ and all mechanism parameters, is expanded into a Fourier series

$$B(\varphi_1) = \Lambda + \sum_{n=-\infty}^{\infty} \beta_n e^{in\varphi_1}, \qquad \text{(H.17)}$$

where the β_n are complex constants containing the mechanism parameters.

(*) The complex form of the Fourier series is used, because the resulting complex Hill's determinants have the same general form for both the 2π and 4π-periodic boundary cases. This makes it possible to use the same computer program for both.

Substitution of equations (H.16) and (H.17) into (H.1) leads to:

$$e^{\mu\varphi_1}\sum_{-\infty}^{\infty}\left[(\mu+mi)^2+\beta_0+\Lambda\right]\psi_m e^{im\varphi_1}+e^{\mu\varphi_1}\sum_{-\infty}^{\infty}\sum_{-\infty}^{\infty *}\beta_n\psi_m e^{i(m+n)\varphi_1}=0. \quad \text{(H.18)}$$

The * on the summation sign indicates that the term for $n = 0$ is not to be considered. Rearrangement of equation (H.18) leads to:

$$e^{\mu\varphi_1}\sum_{-\infty}^{\infty}\left\{\left[(\mu+mi)^2+\beta_0+\Lambda\right]\psi_m+\sum_{-\infty}^{\infty *}\beta_n\psi_{m-n}\right\}e^{im\varphi_1}=0. \quad \text{(H.19)}$$

Since the $e^{im\varphi_1}$ are linearly independent, each of their coefficients must vanish, and the unknowns ψ_m could be obtained by the solution of the doubly infinite set of homogeneous algebraic equations (for $m = 0, \pm1, \pm2, \pm3, \ldots$):

$$\left[(\mu+mi)^2+\beta_0+\Lambda\right]\psi_m+\sum_{-\infty}^{\infty *}\beta_n\psi_{m-n}=0. \quad \text{(H.20)}$$

A nontrivial solution results if the coefficient determinant of the ψ_m vanishes, i.e.

$$
\begin{vmatrix}
\cdot & \cdot & \cdot & \cdot & \cdot & \cdot & \cdot & \cdot & \cdot & \cdot & \cdot \\
\cdot & (\mu-2i)^2+\beta_0+\Lambda & & \beta_{-1} & \beta_{-2} & & \beta_{-3} & & \beta_{-4} & & \cdot \\
\cdot & & \beta_1 & (\mu-i)^2+\beta_0+\Lambda & \beta_{-1} & & \beta_{-2} & & \beta_{-3} & & \cdot \\
\cdot & & \beta_2 & & \beta_1 & \mu^2+\beta_0+\Lambda & & \beta_{-1} & & \beta_{-2} & \cdot \\
\cdot & & \beta_3 & & \beta_2 & \beta_1 & (\mu+i)^2+\beta_0+\Lambda & & \beta_{-1} & & \cdot \\
\cdot & & \beta_4 & & \beta_3 & \beta_2 & & \beta_1 & (\mu+2i)^2+\beta_0+\Lambda & & \cdot \\
\cdot & \cdot & \cdot & \cdot & \cdot & \cdot & \cdot & \cdot & \cdot & \cdot & \cdot
\end{vmatrix} = 0. \qquad \text{(H.21)}
$$

Table H.2 Hill's Determinant for Undamped Case

This infinite determinant, called Hill's determinant, furnishes a relationship between Λ and the β_n for any given μ, and may therefore be used for determining the stability boundaries as a function of Λ and a specific mechanism parameter contained in the β_n. This eigenvalue problem in $(-\Lambda)$ can be solved if the infinite determinant is approximated by a suitably chosen finite segment.

For the proper choice of such a segment, one must consider that all infinite determinants which are, for example, associated with the 2π-periodic boundaries have the same form and value regardless of the μ which is substituted from equation (H.14). They only differentiate themselves from each other by a shift in rows. Consequently, properly located segments of the infinite determinants must also give identical answers for all μ. To this end, they must contain symmetrical values along their diagonals of $(\mu - i)^2$, μ^2, $(\mu + i)^2$, etc. Thus, for the 2π-periodic boundaries one need only use $\mu = 0$, while for the 4π-periodic boundaries $\mu = 1/2\, i$ will suffice. (Note that for both cases the Hill's determinants are Hermitian.)

c) Form of Solution of Damped Homogeneous Hill's Equation and Associated Stability Boundaries

When damping is added to equation (H.1) it becomes:

$$\frac{d^2q}{d\varphi_1^2} + \Delta \frac{dq}{d\varphi_1} + B(\varphi_1)q = 0 , \tag{H.22}$$

where Δ generally represents a damping constant.

To apply Floquet theory, the following transformation is introduced:

$$q(\varphi_1) = e^{-\frac{\Delta}{2}\varphi_1} z(\varphi_1), \tag{H.23}$$

and equation (H.22) becomes:

$$\frac{d^2z}{d\varphi_1^2} + \left(\bar{\Lambda} + \sum_{-\infty}^{\infty} \beta_n e^{in\varphi_1}\right) z = 0 , \tag{H.24}$$

where

$$\bar{\Lambda} = \Lambda - \frac{\Delta^2}{4} . \tag{H.25}$$

The solution form of the above is given by equation (H.2), i.e.

$$z(\varphi_1) = e^{\mu\varphi_1} \Phi(\varphi_1) . \tag{H.26}$$

Then, according to equation (H.23),

$$q(\varphi_1) = e^{(\mu - \frac{\Delta}{2})\varphi_1} \Phi(\varphi_1) . \tag{H.27}$$

This expression is unstable whenever the real part of the exponent $(\mu - \Delta/2)$ is larger than zero. Therefore, the stability boundary occurs when the quantity $(\mathrm{Re}(\mu) - \Delta/2)$ is

equal to zero. This condition corresponds to Re(μ) is equal to $\Delta/2$.

The forms of the $q(\varphi_1)$ on the stability boundaries are found from the following considerations:

Case III of Table H.1 shows that whenever μ has a real part in the solution of an undamped Hill's equation, such as (H.24), it appears in one of the following two forms:

$$\mu_{1,2} = \pm\left(\frac{\ln|\rho|}{2\pi}\right) + ki \quad ; \quad k = 0, \pm 1, \pm 2, \pm 3, \ldots \tag{H.28}$$

or

$$\mu_{1,2} = \pm\left(\frac{\ln|\rho|}{2\pi}\right) + \left(\frac{2k+1}{2}\right) i \quad ; \quad k = 0, \pm 1, \pm 2, \pm 3, \ldots \tag{H.29}$$

Therefore, for the present case,

$$\mathrm{Im}(\mu_{1,2}) = ki \quad ; \quad k = 0, \pm 1, \pm 2, \pm 3, \ldots \tag{H.30}$$

or

$$\mathrm{Im}(\mu_{1,2}) = \left(\frac{2k+1}{2}\right) i \quad ; \quad k = 0, \pm 1, \pm 2, \pm 3, \ldots \tag{H.31}$$

Since the value of k in the above expressions does not affect the solution form of equation (H.27), the value $k = 0$ may be chosen as representative and the total solutions on both stability boundaries are given by the general forms:

$$q(\varphi_1) = \sum_{n=-\infty}^{\infty} a_n e^{in\varphi_1} + e^{-\Delta\varphi_1} \sum_{n=-\infty}^{\infty} b_n e^{in\varphi_1} , \tag{H.32}$$

or

$$q(\varphi_1) = \sum_{n=-\infty}^{\infty} c_n e^{i\left(\frac{2n+1}{2}\right)\varphi_1} + e^{-\Delta\varphi_1} \sum_{n=-\infty}^{\infty} d_n e^{i\left(\frac{2n+1}{2}\right)\varphi_1} . \tag{H.33}$$

The non-decaying portion of equation (H.32) is 2π-periodic and therefore represents the 2π-periodic boundaries. The non-decaying portion of equation (H.33) is 4π-periodic and represents the 4π-periodic boundaries.

The parameter combinations corresponding to these stability boundaries are obtained by proceeding with equation (H.24) in $z(\varphi_1)$ in the same manner as was done for equation (H.1) in $q(\varphi_1)$. The resulting complex Hill's determinant will be of the form shown in Table H.3.

The eigenvalue problem in $(-\Lambda)$ is then solved using the following values of μ:

$$\mu = \frac{\Delta}{2} + ki; \; k = 0, \pm 1, \pm 2, \ldots \tag{H.35}$$

or

$$\mu = \frac{\Delta}{2} + \left(\frac{2k+1}{2}\right)i, \; k = 0, \pm 1, \pm 2, \ldots \tag{H.36}$$

Again, it is enough to evaluate a segment of the infinite determinant. For the 2π-periodic boundaries one need only use $\mu = \Delta/2$, while for the 4π-periodic boundaries $\mu = \Delta/2 + 1/2$ is sufficient. (See discussion in connection with equation (H.21).)

$$
\begin{vmatrix}
\cdot & \cdot & \cdot & \cdot & \cdot & \cdot & \cdot & \cdot & \cdot & \cdot & \cdot & \cdot & \cdot \\
\cdot & (\mu-2i)^2+\beta_0-\frac{\Delta^2}{4}+\Lambda & & \beta_{-1} & & \beta_{-2} & & \beta_{-3} & & \beta_{-4} & & & \cdot \\
\cdot & & \beta_1 & & (\mu-i)^2+\beta_0-\frac{\Delta^2}{4}+\Lambda & & \beta_{-1} & & \beta_{-2} & & \beta_{-3} & & \cdot \\
\cdot & & \beta_2 & & \beta_1 & & u^2+\beta_0-\frac{\Delta^2}{4}+\Lambda & & \beta_{-1} & & \beta_{-2} & & \cdot \\
\cdot & & \beta_3 & & \beta_2 & & \beta_1 & & (\mu+i)^2+\beta_0-\frac{\Delta^2}{4}+\Lambda & & \beta_{-1} & & \cdot \\
\cdot & & \beta_4 & & \beta_3 & & \beta_2 & & \beta_1 & & (\mu+2i)^2+\beta_0-\frac{\Delta^2}{4}+\Lambda & & \cdot \\
\cdot & \cdot & \cdot & \cdot & \cdot & \cdot & \cdot & \cdot & \cdot & \cdot & \cdot & \cdot & \cdot
\end{vmatrix} = 0. \qquad (H.34)
$$

Table H.3 Hill's Determinant for Damped Case

2. Particular Solution in Stable Regions

The general form of a nonhomogeneous damped Hill's equation, as in equation (4.42), is given by:

$$\frac{d^2q}{d\varphi_1^2} + \Delta \frac{dq}{d\varphi_1} + B(\varphi_1)q = \mathcal{F}(\varphi_1) , \tag{H.37}$$

(in equation (4.42) $\mathcal{F}(\varphi_1) = \hat{F}_m(\varphi_1)/\mathcal{K}_m$), and Δ is again a damping constant.

The technique of Variation of Parameters indicates that, at all points in the stable regions, the particular solution is given by a 2π-periodic Fourier series [19]:

$$q_p(\varphi_1) = \frac{p_0}{2} + \sum_1^\infty (p_{cm}\cos m\varphi_1 + p_{sm}\sin\varphi_1) . \tag{H.38}$$

It will now be shown how the coefficients p_0, p_{cm} and p_{sm} are obtained:

The 2π-periodic functions $B(\varphi_1)$ (see equation (4.44)) and $\mathcal{F}(\varphi_1)$ are expressed in terms of Fourier series of this periodicity, i.e.

$$B(\varphi_1) = \Lambda + \frac{b_0}{2} + \sum_1^\infty (b_{cn}\cos n\varphi_1 + b_{sn}\sin n\varphi_1), \tag{H.39}$$

where

$$b_{cn} = \frac{1}{\pi}\int_0^{2\pi} A(\varphi_1)\cos n\varphi_1\, d\varphi_1 \; ; \; n = 0,1,2,\ldots \tag{H.40}$$

$$b_{c0} = b_0 \tag{H.41}$$

$$b_{sn} = \frac{1}{\pi}\int_0^{2\pi} A(\varphi_1)\sin n\varphi_1\, d\varphi_1 \; ; \; n = 1,2,\ldots \tag{H.42}$$

and

$$\mathcal{F}(\varphi_1) = \frac{f_0}{2} + \sum_{m}^{\infty} \left(f_{cm} \cos m\varphi_1 + f_{sm} \sin m\varphi_1 \right), \tag{H.43}$$

where

$$f_{cm} = \frac{1}{\pi} \int_0^{2\pi} \mathcal{F}(\varphi_1) \cos m\varphi_1 \, d\varphi_1 \; ; \; m = 0, 1, 2, \ldots \tag{H.44}$$

$$f_{co} = f_0 \tag{H.45}$$

$$f_{sm} = \frac{1}{\pi} \int_0^{2\pi} \mathcal{F}(\varphi_1) \sin m\varphi_1 \, d\varphi_1 \; ; \; m = 1, 2, \ldots \tag{H.46}$$

Substitution of equations (H.38), (H.39) and (H.43) into the differential equation (H.37) leads to:

$$\sum_{m}^{\infty} m^2 \left(-p_{cm} \cos m\varphi_1 - p_{sm} \sin m\varphi_1 \right) + \Delta \sum_{m}^{\infty} m \left(-p_{cm} \sin m\varphi_1 + p_{sm} \cos m\varphi_1 \right)$$

$$+ \left(\Lambda + \frac{b_0}{2} + \sum_{n}^{\infty} \left(b_{cn} \cos n\varphi_1 + b_{sn} \sin n\varphi_1 \right) \right) \left(\frac{p_0}{2} + \sum_{m}^{\infty} \left(p_{cm} \cos m\varphi_1 + p_{sm} \sin m\varphi_1 \right) \right)$$

$$= \frac{f_0}{2} + \sum_{m}^{\infty} \left(f_{cm} \cos m\varphi_1 + f_{sm} \sin m\varphi_1 \right). \tag{H.47a}$$

The product indicated in the above expression is treated according to the procedure given by G.P. Tolstov [31]. After collecting the results into groups of like terms, one obtains:

$$\sum_{m=1}^{\infty}\left\{\left[\sum_{\substack{n=1\\n\neq m}}^{\infty}\left(\frac{b_{c(n-m)}+b_{c(n+m)}}{2}\right)p_{cn}+\left(-m^2+\Lambda+\frac{b_0+b_{c(m+m)}}{2}\right)p_{cm}+\frac{b_{cm}}{2}p_0\right.\right.$$

$$\left.+\left(m\Delta+\frac{b_{s(m+m)}}{2}\right)p_{sm}+\sum_{\substack{n=1\\n\neq m}}^{\infty}\left(\frac{b_{s(n-m)}+b_{s(n+m)}}{2}\right)p_{sn}\right]\cos m\varphi_1$$

$$+\frac{1}{2}\sum_{n=1}^{\infty}\left(b_{cn}p_{cn}+b_{sn}p_{sn}\right)+\left(\frac{\Lambda}{2}+\frac{b_0}{4}\right)p_0$$

$$+\left[\sum_{\substack{n=1\\n\neq m}}^{\infty}\left(\frac{b_{s(n+m)}-b_{s(n-m)}}{2}\right)p_{cn}+\left(-m\Delta+\frac{b_{s(m+m)}}{2}\right)p_{cm}+\frac{b_{sm}}{2}p_0\right.$$

$$\left.\left.+\left(-m^2+\Lambda+\frac{b_0-b_{c(m+m)}}{2}\right)p_{sm}+\sum_{\substack{n=1\\n\neq m}}^{\infty}\left(\frac{b_{c(n-m)}-b_{c(n+m)}}{2}\right)p_{sn}\right]\sin m\varphi_1\right\}$$

$$=\frac{f_0}{2}+\sum_{m=1}^{\infty}\left(f_{cm}\cos m\varphi_1+f_{sm}\sin m\varphi_1\right), \qquad \text{(H.47b)}$$

where

$$b_{c(-k)}=b_{c(k)} \qquad \text{(H.48)}$$

and

$$b_{s(-k)}=-b_{s(k)} \qquad \text{(H.49)}$$

must be applied when needed.

Comparison of the coefficients of like terms in the above leads to the infinite set of nonhomogeneous algebraic equations in the unknowns p_0, p_{cm} and p_{sm} $(m = 1,2,3,\ldots)$:

$$\sum_{\substack{n=1\\ n\neq m}}^{\infty}\left(\frac{b_{c(n-m)}+b_{c(n+m)}}{2}\right)p_{cn}+\left(-m^2+\Lambda+\frac{b_0+b_{c(m+m)}}{2}\right)p_{cm}+\frac{b_{cm}}{2}p_0$$

$$+\left(m\Delta+\frac{b_{s(m+m)}}{2}\right)p_{sm}+\sum_{\substack{n=1\\ n\neq m}}^{\infty}\left(\frac{b_{s(n-m)}+b_{s(n+m)}}{2}\right)p_{sn}=f_{cm}\,, \qquad \text{(H.50)}$$

$$\sum_{1}^{\infty} b_{cn}p_{cn}+\left(\Lambda+\frac{b_0}{2}\right)p_0+\sum_{1}^{\infty} b_{sn}p_{sn}=f_0\,, \qquad \text{(H.51)}$$

$$\sum_{\substack{n=1\\ n\neq m}}^{\infty}\left(\frac{b_{s(n+m)}-b_{s(n-m)}}{2}\right)p_{cn}+\left(-m\Delta+\frac{b_{s(m+m)}}{2}\right)p_{cm}+\frac{b_{sm}}{2}p_0$$

$$+\left(-m^2+\Lambda+\frac{b_0-b_{c(m+m)}}{2}\right)p_{sm}+\sum_{\substack{n=1\\ n\neq m}}^{\infty}\left(\frac{b_{c(n-m)}-b_{c(n+m)}}{2}\right)p_{sn}=f_{sm}\,. \qquad \text{(H.52)}$$

These equations may be expressed in matrix form as

$$\mathbb{B}\,\mathbb{P}=\mathbf{F}, \qquad \text{(H.53)}$$

where the coefficients matrix $\mathbb{B}$ as well as the column vectors $\mathbb{P}$ and $\mathbf{F}$ are defined as follows:

$$
\begin{bmatrix}
\cdot & \cdot & \cdot & \cdot & \cdot & \cdot & \cdot & \cdot \\
\cdot & -9+\frac{b_0+b_{c6}}{2}+\Lambda & \frac{b_{c1}+b_{c5}}{2} & \frac{b_{c2}+b_{c4}}{2} & \frac{b_{c3}}{2} & \frac{b_{s4}-b_{s2}}{2} & \frac{b_{s5}-b_{s1}}{2} & 3\Delta+\frac{b_{s6}}{2} \\
\cdot & \frac{b_{c1}+b_{c5}}{2} & -4+\frac{b_0+b_{c4}}{2}+\Lambda & \frac{b_{c1}+b_{c3}}{2} & \frac{b_{c2}}{2} & \frac{b_{s3}-b_{s1}}{2} & 2\Delta+\frac{b_{s4}}{2} & \frac{b_{s1}+b_{s5}}{2} \\
\cdot & \frac{b_{c2}+b_{c4}}{2} & \frac{b_{c1}+b_{c3}}{2} & -1+\frac{b_0+b_{c2}}{2}+\Lambda & \frac{b_{c1}}{2} & \Delta+\frac{b_{s2}}{2} & \frac{b_{s1}+b_{s3}}{2} & \frac{b_{s2}+b_{s4}}{2} \\
\cdot & b_{c3} & b_{c2} & b_{c1} & b_0+\Lambda & b_{s1} & b_{s2} & b_{s3} \\
\cdot & \frac{b_{s4}-b_{s2}}{2} & \frac{b_{s3}-b_{s1}}{2} & -\Delta+\frac{b_{s2}}{2} & \frac{b_{s1}}{2} & -1+\frac{b_0+b_{c2}}{2}+\Lambda & \frac{b_{c1}-b_{c3}}{2} & \frac{b_{c2}-b_{c4}}{2} \\
\cdot & \frac{b_{s5}-b_{s1}}{2} & -\Delta 2+\frac{b_{s4}}{2} & \frac{b_{s1}+b_{s3}}{2} & \frac{b_{s2}}{2} & \frac{b_{c1}-b_{c3}}{2} & -4+\frac{b_0-b_{c4}}{2}+\Lambda & \frac{b_{c1}-b_{c5}}{2} \\
\cdot & -3\Delta+\frac{b_{s6}}{2} & \frac{b_{s5}+b_{s1}}{2} & \frac{b_{s4}-b_{s2}}{2} & \frac{b_{s3}}{2} & \frac{b_{c2}-b_{c4}}{2} & \frac{b_{c1}-b_{c5}}{2} & -9+\frac{b_0-b_{c6}}{2}+\Lambda \\
\cdot & \cdot & \cdot & \cdot & \cdot & \cdot & \cdot & \cdot
\end{bmatrix}
\begin{bmatrix} \cdot \\ p_{c3} \\ p_{c2} \\ p_{c1} \\ p_0 \\ p_{s1} \\ p_{s2} \\ p_{s3} \\ \cdot \end{bmatrix}
=
\begin{bmatrix} \cdot \\ f_{c3} \\ f_{c2} \\ f_{c1} \\ f_0 \\ f_{s1} \\ f_{s2} \\ f_{s3} \\ \cdot \end{bmatrix}
$$

(H.54)

For a solution of a finite number of the coefficients p_0, p_{cm} and p_{sm}, the infinite set of equations is reduced to one by choosing a coefficient matrix $\mathbb{B}$ symmetrical in rows and columns with respect to the central element $\Lambda + \frac{b_0}{2}$.

APPENDIX I

KINEMATICS OF FOUR-BAR LINKAGE

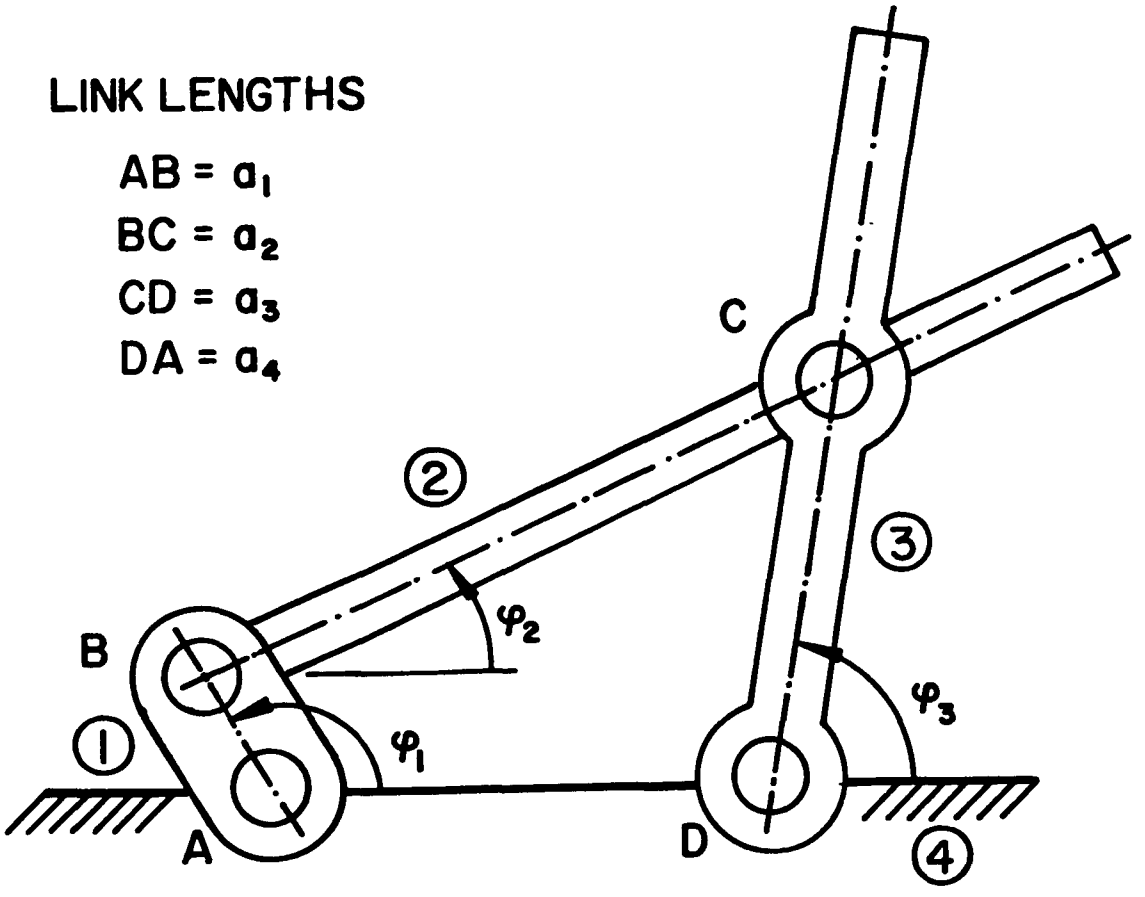

Figure I.1: Four-Bar Linkage

1. Definitions

$$\lambda = \frac{a_1}{a_2} \; ; \quad \mu = \frac{a_3}{a_2} \; ; \quad \nu = \frac{a_4}{a_2} \; . \tag{I.1}$$

$$\tau_1 = \mu \sin(\varphi_1 - \varphi_3) + \nu \sin \varphi_1 \; . \tag{I.2}$$

$$\tau_3 = \lambda \sin(\varphi_1 - \varphi_3) + \nu \sin \varphi_3 \; . \tag{I.3}$$

2. Link Angles

a) Output Link

$$\varphi_3 = 2\tan^{-1}\left(\frac{A-\sqrt{A^2+B^2-C^2}}{B+C}\right), \tag{I.4}$$

where

$$\left.\begin{aligned} A &= \sin\varphi_1 \ , \\ B &= \cos\varphi_1 - \nu/\lambda \ , \\ C &= \frac{\lambda^2+\mu^2+\nu^2-1}{2\mu\lambda} - \frac{\nu}{\mu}\cos\varphi_1 \ . \end{aligned}\right\} \tag{I.5}$$

b) Coupler Link

$$\varphi_2 = \tan^{-1}\left(\frac{\lambda\sin\varphi_1 - \mu\sin\varphi_3}{\lambda\cos\varphi_1 - \mu\cos\varphi_3 - \nu}\right) . \tag{I.6}$$

3. Link Angular Velocities

a) Output Link

$$\dot{\varphi}_3 = \frac{\lambda\tau_1}{\mu\tau_3}\,\dot{\varphi}_1 \ . \tag{I.7}$$

b) Coupler Link

$$\dot{\varphi}_2 = \frac{\lambda}{\tau_3}\sin(\varphi_1-\varphi_3)\,\dot{\varphi}_1 \ . \tag{I.8}$$

4. Link Angular Accelerations

a) Output Link

$$\ddot{\varphi}_3 = \left(\frac{\dot{\varphi}_2}{\dot{\varphi}_1}\right)\ddot{\varphi}_1 + \frac{\lambda}{\tau_3}\cos(\varphi_1-\varphi_3)(\dot{\varphi}_1-\dot{\varphi}_3)^2 + \frac{\nu}{\mu\tau_3}\left(\lambda\cos\varphi_1\,\dot{\varphi}_1^2 - \mu\cos\varphi_3\,\dot{\varphi}_3^2\right) . \tag{I.9}$$

b) Coupler Link

$$\ddot{\varphi}_2 = \left(\frac{\dot{\varphi}_2}{\dot{\varphi}_1}\right)\ddot{\varphi}_1 + \frac{\nu\lambda}{\tau_3^2}\left(\dot{\varphi}_1 \cos(\varphi_1-\varphi_3)\sin\varphi_3 - \dot{\varphi}_3 \sin\varphi_1\right)\dot{\varphi}_1 \qquad \text{(I.10)}$$

VIII. REFERENCES

1. R. M. Alexander and K. L. Lawrence, "An Experimental Investigation of the Dynamic Response of an Elastic Mechanism", Journal of Engineering for Industry, Trans. ASME, Vol. 96, Series B, February 1974, pp. 268-274.

2. R. M. Alexander and K. L. Lawrence, "Dynamic Strain in a Four-Bar Mechanism", Proceedings of the Third Applied Mechanism Conference, Oklahoma State University, Stillwater, November 1973.

3. R. M. Alexander and K. L. Lawrence, "Experimentally Determined Dynamic Strains in an Elastic Mechanism", ASME Paper No. 74-DET-33.

4. R. S. Berkof, "On the Optimization of Mass Distribution in Mechanisms", PhD Dissertation, City University of New York, University Microfilms, Ann Arbor, Michigan, 1969 (No. 69-19052).

5. V. V. Bolotin, The Dynamic Stability of Elastic Systems, Holden Day, San Francisco, 1964.

6. L. Cesari, Asymptotic Behavior and Stability Problems in Ordinary Differential Equations, Springer-Verlag, New York, 1971.

7. J. Chakraborty and A. K. Khare, "Kineto-Elastodynamic Analysis of Slider-Crank Mechanisms with a Flexibly Attached Slider", ASME Paper No. 74-DET-5.

8. S. C. Chu and K. C. Pan, "Dynamic Behavior of a High-Speed Slider-Crank Mechanism", ASME Paper No. 74-DET-36.

9. E. A. Coddington and N. Levinson, Theory of Ordinary Differential Equations, McGraw-Hill Book Company, New York, 1955.

10. A. G. Erdman, G. N. Sandor and R. G. Oakberg, "A General Method for Kineto-Elastodynamic Analysis and Synthesis of Mechanisms", Journal of Engineering for Industry, Trans. ASME, Vol. 94, Series B, November 1972, pp. 1193-1205.

11. A. G. Erdman and G. N. Sandor, "Kineto-Elastodynamics-A Review of the State of the Art and Trends", Mechanism and Machine Theory, Vol. 7, 1972, pp. 19-33.

12. H. Goldstein, Classical Mechanics, Addison-Wesley Publishing Company, Reading, Massachusetts, April 1965.

13. H. Houben, "Untersuchungen über die Stabilität elastischer Bewegungen in der Koppel eines Viergelenkgetriebes", PhD Dissertation, TH Aachen, 1965.

14. C. S. Hsu, "On the Parametric Excitation of a Dynamic System Having Multiple Degrees of Freedom", Journal of Applied Mechanics, Trans. ASME, Vol. 85, Series E, 1973, pp. 367-372.

15. I. Imam, G. N. Sandor and S. N. Kramer, "Deflection and Stress Analysis in High Speed Planar Mechanisms With Elastic Links", Journal of Engineering for Industry, Trans. ASME, Vol. 95, Series B, May 1973, pp. 541-548.

16. I. Imam and G. N. Sandor, "A General Method of Kineto-Elastodynamic Design of High Speed Mechanisms", Mechanism and Machine Theory, Vol. 8, 1973, pp. 497-516.

17. I. Imam and G. N. Sandor, "High-Speed Mechanism Design-A General Analytical Approach", ASME Paper No. 74-DET-50.

18. T. R. Kane, Dynamics, Holt, Rinehart and Winston, Inc., New York, 1968.

19. G. Kotowski, "Lösungen der inhomogenen Mathieuschen Differtialgleichung mit periodischer Störfunktion beliebiger Frequenz (mit besonderer Berücksichtigung der Resonanzlosungen", Zeitschrift für augewandte Mathematik und Mechanik, Vol. 23, No. 4, 1943, pp. 213-229.

20. C. Lanczos, The Variational Principles of Mechanics, University of Toronto Press, Toronto, 1966.

21. G. G. Lowen and W. G. Jandrasits, "Survey of Investigations into the Dynamic Behavior of Mechanisms Containing Links with Distributed Mass and Elasticity", Mechanism and Machine Theory, Vol. 7, 1972, pp. 3-17.

22. J. C. Maltbaek, "Free Vibrations of Three-Span Uniform Beams and Related Systems", International Journal of Mechanical Sciences, Vol. 5, 1963, pp.321-333.

23. E. Massa, "On the Instability of Parametrically Excited Two Degrees of Freedom Vibration Systems with Viscous Damping", Meccanica, Vol. 2, No. 4, December 1967, pp. 243-255.

24. E. Mettler, "Kinetische Instabilität eines elastischen Trägers unter Parametererregung durch rotierende Unwuchten", Ingenieur-Archiv, Vol. 39, 1970, pp. 171-186.

25. P. M. Nossal, "A Mechanical Cell Disintegrator", Australian Journal of Experimental Biology, Vol. 31, 1953, pp. 583-590.

26. H. Parkus, "Beanspruchung und Schwingungen von Pleuelstangen", Österreichisches Ingenieur-Archiv., Vol. 3, No. 3, 1949, pp. 222-253.

27. J. P. Sadler and G. N. Sandor, "A Lumped Parameter Approach to Vibration and Stress Analysis of Elastic Linkages", Journal of Engineering for Industry, Trans. ASME, Vol. 95, Series B, May 1973, pp. 549-557.

28. J. P. Sadler and G. N. Sandor, "Nonlinear Vibration Analysis of Elastic Four-Bar Linkages", Journal of Engineering for Industry, Trans. ASME, Vol. 96, Series B, May 1974, pp. 411-414.

29. J. P. Sadler, "On the Analytical Lumped Mass Model of an Elastic Four-Bar Mechanism", ASME Paper No. 74-DET-38.

30. M. J. O. Strutt, Lamesché-Mathieusche und verwandte Funktionen in Physik und Technik, Chelsea Publishing Company, New York, 1967.

31. G. P. Tolstov, Fourier Series, Prentice-Hall, Englewood Cliffs, New Jersey, March 1965.

32. K. Washizu, Variational Methods in Elasticity and Plasticity, Pergamon Press, New York, 1968.

33. R. C. Winfrey, "Dynamic Analysis of Elastic Link Mechanisms by Reduction of Coordinates", Journal of Engineering for Industry, Trans. ASME, Vol. 94, Series B, May 1972, pp. 577-582.

IX. AUTOBIOGRAPHICAL STATEMENT

Walter Gottfried Jandrasits was born on April 22, 1942 in Brooklyn, New York. He attended Bronx Public School No. 102, Henry Hudson Junior High School, and James Monroe High School, graduating from the latter with an academic diploma in June 1959.

He attended Hunter College for one year, and then the City College of New York, from which he received a Bachelor of Mechanical Engineering degree in January 1965.

In February 1965, he entered the doctoral program at the City University of New York. From 1965 to 1974, while continuing his studies, he was a Teaching Fellow, a NASA Trainee and a Lecturer in the Mechanical Engineering Department of the City College of New York, teaching Thermodynamics, Theory of Engineering Experimentation, and Engineering Graphics. In January 1967 he received a Master of Engineering (Mechanical) degree.

On January 13, 1975, he successfully defended his dissertation, thus completing the requirements for the degree of Doctor of Philosophy.

In 1971 he published a survey of investigations into the dynamic behavior of mechanisms containing elastic links together with Dr. Gerard G. Lowen.

He presently resides in the Bronx, New York, with his wife and daughter.